



Università degli Studi di Milano
Dipartimento di Chimica

Doctorate School in Chemical Sciences and Technologies
Doctorate in Chemical Sciences
XXV cycle

ELECTROCHEMISTRY FOR THE DEVELOPMENT OF
INNOVATIVE THREE-DIMENSIONAL AND CHIRAL
THIOPHENE-BASED ORGANIC SEMICONDUCTORS

CHIM-02

Ph. D. Thesis

VALENTINA BONOMETTI

R08776

Supervisor: Prof. Patrizia Romana Mussini

Co-supervisor: Prof. Francesco Sannicolò

School Director: Prof. Silvia Ardizzone

Academic Year 2011/2012

	<i>Index</i>	
1	Introduction	1
	1.1 Conducting polymers: concept and applications	1
	1.2 Electrochemistry of conducting polymers	12
	1.3 Spider-like oligothiophenes	20
	1.4 Chirality in Conducting polymers	28
	1.5 Aim of the present PhD thesis	32
2	Experimental	33
	2.1 Cyclic voltammetry	33
	2.2.1 <i>An introduction to CV</i>	33
	2.1.2 <i>The voltammetric cell and the electrodes</i>	41
	2.1.3 <i>The experimental setup and the analysis protocol</i>	43
	2.1.4 <i>The reagents</i>	47
	2.2 Electrochemical Quartz Crystal Microbalance	48
	2.2.1 An introduction to EQCM	48
	2.3 Circular dichroism	54
	2.3.1 <i>An introduction to CD spectroscopy</i>	54
	2.3.2 <i>The experimental setup and the analysis protocol</i>	57
	2.4 Electrochemical Impedance Spectroscopy	59
	2.4.1 <i>An introduction to EIS</i>	59
	2.4.2 <i>The experimental setup and the analysis protocol</i>	70
	2.4 Other experimental techniques	70
3	Results and Discussion	73
	3.1 The genetically-modified spider-like oligothiophenes	73
	3.1.1 <i>red-FHexT6, FHexT6 and FHexT6C₆₀</i>	91
	3.2 The Inherently Chiral molecules	97
	3.2.1 <i>T*8₃ and T*14₅: Inherently Chiral Spider-like oligothiophenes</i>	97
	3.2.2 <i>T4-BT2</i>	104
	3.2.3 <i>Other cases of inherently chiral molecules</i>	125
4	Conclusions	144
5	Side-works:	
	Poly-CPDT films decorated with dinuclear Re(I) complex chromophore pendants: electrochemical and spectroscopic properties	147
	Chirality on account of residual stereoisomerism	160

List of formulae and abbreviations

AFM	Atomic Force Microscopy
BMIMPF ₆	1-butyl-3-methylimidazolium hexafluorophosphate
Cc ⁺	Bis(cyclopentadienyl)cobalt(III) hexafluorophosphate
CD	Circular Dichroism
CE	Counter electrode
CP	Conducting polymers
CV	Cyclic voltammetry
EPR, ESR	Electron Paramagnetic Resonance, Electron Spin Resonance
Fc	Ferrocene
Fc [*]	(S)-(-)- or (R)-(+)-N,N-dimethyl-1-ferrocenylethylamine
GC	Glassy Carbon
IL	Ionic Liquid
MeCN	Acetonitrile
Me ₂ Fc	Dimethylferrocene
Me ₁₀ Fc	Decamethylferrocene
r.d.s.	Rate-determining step
Ref	Reference electrode
SCE	Saturated Calomel Electrode
SEM	Scanning Electron Microscopy
TBA ⁽⁺⁾	Tetrabutylammonium ⁽⁺⁾
CS ⁽⁻⁾	Canphorsulfonate
P ⁽⁻⁾	Perchlorate
PF ₆ ⁽⁻⁾	Hexafluorophosphate
<i>p</i> -TS ⁽⁻⁾	Paratoluenesulfonate
WE	Working electrode

1. Introduction

When asked to explain the importance of the discovery of conducting polymers, I offer two basic answers. First, they did not (could not?) exist, and second, they offer a unique combination of properties not available from other known materials. The first expresses an intellectual challenge; the second expresses a promise for utility in a wide variety of applications.

A.J. Heeger

© The Nobel Foundation

1.1 Conducting polymers: concept and applications ¹

The first example of conducting polymer dates back 1862, when Letheby reported the anodic oxidation of aniline in a solution of diluted sulphuric acid, but it was only in the seventies of the XX century that the phenomenon of conducting polymers was really discovered, thanks to the pioneering works of Shirakawa, Heeger and MacDiarmid on the doping of polyacetylene films: when treated with iodine vapours, the conductivity of the polyacetylene increased more than ten million times (from $10^{-5} \text{ S}\cdot\text{cm}^{-1}$ to $\sim 10^3 \text{ S}\cdot\text{cm}^{-1}$). Polyacetylene is considered the archetype of conducting polymers, and the discovery of its conductive properties represented a great breakthrough in the fields of chemistry and material chemistry, so that the Heeger, MacDiarmid and Shirakawa were awarded the Nobel Prize in Chemistry in 2000.

In fact, while common plastics are saturated polymers where all the four valence electrons of the carbon atoms are used up in covalent bonds, polyacetylene is a conjugated system, with one unpaired electron (the π electron) per carbon atom.

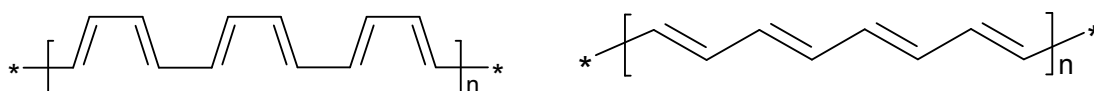


Figure 1: Chemical structures of *trans*-polyacetylene (left) and *cis*-polyacetylene (right)

Moreover, it is characterized by a π bonding system, where carbon orbitals are in the sp^2p_z configuration and where the orbitals of successive carbon atoms along the conjugated backbone overlap, leading to an electron delocalization along the conjugated chain, thus providing a sort of highway for charge mobility along the backbone. Thus, it is the chain symmetry that determines the electronic structure. In the case of polyacetylene $(-\text{CH})_n$, each carbon atom is σ bonded to two neighbouring carbons and one hydrogen atom with one π electron on each carbon. There could be two limiting cases:

¹ A.J. Heeger, *Rev. Mod. Phys.*, **2001**, 73 (3), 681-700

I.F. Perepichka, D.F. Perepichka, *Handbook of Thiophene-based materials: Applications in Organic Electronics and Photonics*, 2009, Wiley, Chichester, ISBN 978-0-470-05732-2

J. Heinze, B.A. Frontana-Urbe, S. Ludwigs, *Chem. Rev.*, **2010**, 110, 4724-4771

Editorial of *Polym. Int.*, **2012**, 61, 337-341

J. L. Brédas, G. B. Street, *Acc. Chem. Res.*, **1985**, 18, 309-315

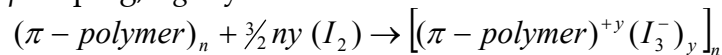
- if the carbon-carbon bond lengths were equal, the formula $(-CH)_n$ would imply a metallic state, having one unpaired electron per formula unit. Each carbon contributes a single p_z electron to the π band, that would be half-filled, mimicking the behaviour of a one-dimensional (1D) metal.
- if the electron-electron interactions were too strong, $(-CH)_n$ would be an antiferromagnetic Mott insulator.

Experimentally, it was observed an easy conversion to the metallic state upon doping, thus eliminating the second alternative. However, neutral polyacetylene is a semiconductor, with a 1.5 eV energy gap, because of the so-called Peierls instability. It was demonstrated that 1D metals are unstable with respect to a structural distortion which opens the energy gap at the Fermi level, thus rendering semiconductors this kind of conjugated systems. Consequently, in polyacetylene, the structure is dimerized on account of Peierls instability, resulting in the formula unit $(-CH=CH)_n$. The π band is divided into π and π^* bands, the former being filled by two electrons per atom, the last being empty. The energy difference between the highest occupied state in the π band and the lowest unoccupied state in the π^* band is the π - π^* energy gap E_g ; it is worthwhile noticing that, since E_g depends on the molecular structure of the repeat unit, it could be modulated quite easily upon an appropriate molecular design.

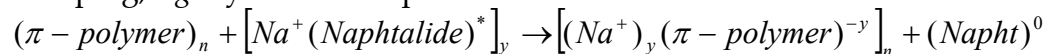
Increasing the conjugated chain length to infinite, the E_g should tend to zero, at least in principle. Actually, the presence of defects and distortion limits the effective conjugation, which, alone, is not enough to ensure the conductivity to the level of a metal. Other charge carriers are then introduced by a *doping* process, which is a completely different phenomenon with respect to the case of traditional inorganic semiconductors.

In fact, while inorganic semiconductors are doped by addition of elements from the III or V group, the doping in the case of conducting polymers corresponds to redox reactions in the polymer network, always accompanied by rather complex counter-ion dynamics, necessary to ensure the electroneutrality: in this sense, conductive polymers are actually salts. The electrical conductivity then results from the existence of charge carriers, which are mobile on the highway provided by the conjugated system. Conducting polymers can be doped chemically:

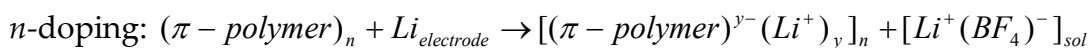
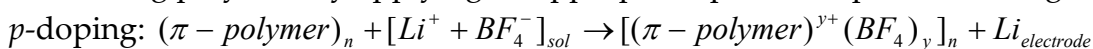
p-doping, e.g. by iodine:



n-doping, e.g. by sodium naphthalide:



However, the chemical doping is sometimes difficult to control, especially if intermediate doping levels are required. The electrochemical route could be the solution to this problem, because it is the electrode that supplies the required redox charge to the conducting polymer, by applying an appropriate potential, positive or negative:



Polyacetylene was the first highly conducting organic polymer, but it was never commercialized, being too much sensitive to humidity and oxygen. Starting from this first

structure, many other conjugated system were then studied and employed as conducting polymers: some examples are reported in Figure 2.

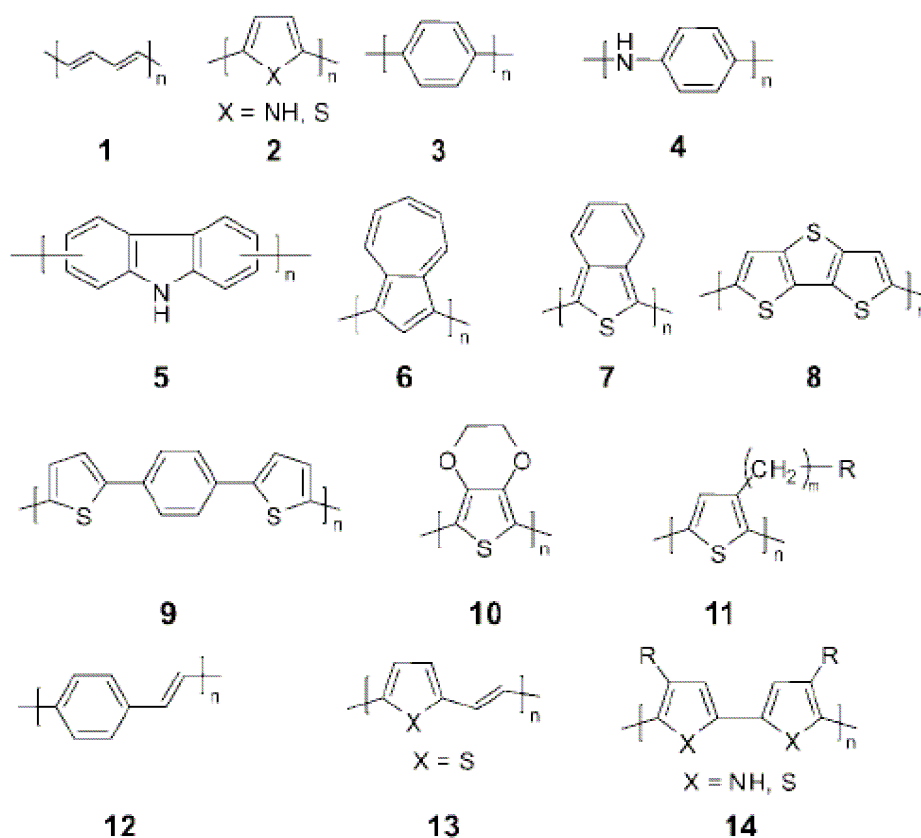


Figure 2: Some examples of conducting polymers:

1, polyacetylene (PA), 2 polypyrrole (PPy), polythiophene (PTh); 3, poly-p-phenylene (PPP); 4, polyaniline (PANI); 5, polycarbazole; 6, polyazulene; 7, poly(isothionaphthalene); 8, poly(dithienothiophene); 9, poly(dithienylbenzene); 10, poly(ethylenedioxythiophene) (PEDOT); 11, poly(3-alkylthiophene); 12, poly(phenylenevinylene) (PPV); 13, poly(thienylenevinylene); 14, poly(bipyrrole), poly(bithiophene).

Organic conducting polymers are efficient materials for a wide range of applications, from energetics, electronics (bulk-heterojunction solar cells, dye-sensitized solar cells, organic light-emitting diodes, and organic field effect transistors) to sensoristics, offering the advantage of being light-weight, flexible, low-cost compounds, thus providing a valid and interesting alternative to traditional inorganic semiconductors. In addition, their synthetic versatility is such that it is possible to design and synthesize molecules for specific targets and applications, by changing the length of the conjugated chain, by adding substituent able to modify some physico-chemical properties (colour, solubility, additional redox centres, mechanical properties...). Conducting polymers are *functional smart materials*: they are able to recognize particular environmental stimuli (*i.e.*, an electrical stimulus, or the presence of a chiral analyte, in case of chiral conducting polymers, as it will be discussed more in detail in this PhD work), to process and transfer the information, thanks to their conductivity, and to respond to the stimulus sufficiently fast. They have a dynamic character, that has to be properly controlled, so it is important to control the response time. Conducting polymers appear to be suitable for applications in optics and electronics for the development of many devices: displays, light-emitting diodes, antistatic and

anticorrosion coatings, supercapacitors, organic photovoltaics, separation membranes, sensors, and rechargeable batteries, thanks to their charge/discharge properties. Other interesting applications concern their electrochromism, *i.e.* their change of colour upon polarization. Polythiophene films, for example, are red when oxidized, and blue when reduced, while polyaniline films have a complete range of shades. Applications in sensoristics have been developed thanks to the modulable physico-chemical properties combined with the conductivity, as in the so-called electronic noses: these devices are constituted by an array of conducting polymers, each of them is sensitive to a particular chemical substance (*i.e.*, electron donating or withdrawing compounds, NO₂, H₂S, NH₃,...) interacts with the polymer, by causing some changes in its conformation or modifying its resistance. Such changes are often reversible, so these sensors can be recovered after use. Other interesting applications concern the photovoltaics: this kind of application sounds particularly important in the frame of the actual energetic panorama, and provides a valid alternative to conventional silicon-based photovoltaic systems, that requires ultra-high purity silicon, and difficult processing techniques, resulting in high costs while the conversion efficiencies are no more than 15-25%. Conductive polymer-based solar cells² presents many advantages: light weight, high absorption coefficients (even above 10⁷ m⁻¹), that allow to use a very small thickness (100-300 nm) of active material for a good absorption yield, processability on flexible substrates, easy solution processing (spin-coating, ink-jet printing), semitransparency, tunability of physico-chemical properties by structure modifications, low material amount needed for the fabrication, in contrast with traditional inorganic semiconductor-based solar cells, that require thicker active layers (few micrometers for CuInSe₂ cells, around 100 μm for crystalline Si ones). The major drawbacks are the rather narrow absorption width of organic materials (while Si and CuInSe₂, for example, cover the whole visible spectrum of the sun light and beyond, to more than 1000 nm, corresponding to an optical band gap of 1.1 eV), lower efficiency and stability. However this technology is improving faster and faster, and many devices are currently used for the production of energy from sunlight.

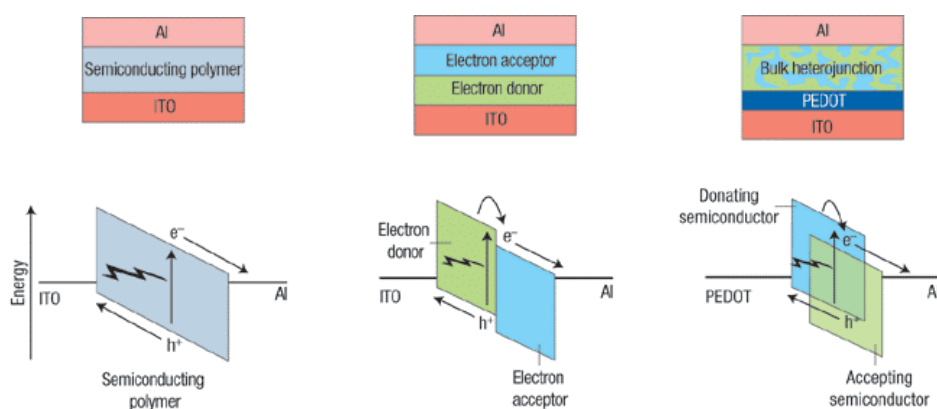


Figure 3a: Schematic representation of polymer solar cells

² Michael D. McGehee & Mark A. Topinka, *Nature Materials*, 2006, 5, 675 - 676

The mechanism of polymer solar cell is based essentially on four steps

- absorption of light and generation of excitons within the active layer
- diffusion of the exciton to the interface between a donor and an acceptor materials
- dissociation of the exciton and generation of charges
- charge transport and collection at the electrodes

Only the first step expressly requires a low band gap (*i.e.*, large absorption range) active material, while the others concern an interplay between molecular structure and properties. The first class of organic solar cells were based on a thin layer of conducting polymer sandwiched between the anode and the cathode: the efficiencies of this kind of cell were lower than 1%, but they pointed out that polythiophene systems were good candidates for this kind of applications. These single-layer cells then evolved into double layer cells, having two layers, one electron-donor material, typically a regioregular poly(3-hexyl)thiophene, P3HT (having HOMO and LUMO at -5.0 and -3.3 eV)³ and one electron-acceptor material, typically a phenyl-C₆₁-butyric acid methyl ester, PCBM (having HOMO and LUMO at -6.1 and -3.7 eV)³; however, the exciton diffusion length is only 5-20 nm, thus only the excitons generated next to the interface could reach it and dissociate before recombination. The solution to this problem was to increase the contact interface between the donor and the acceptor material, making a blend: the bulk-heterojunction solar cells, with efficiencies ranging from 5 to 15%.

The functioning mechanism of a bulk-heterojunction solar cell is described below, and illustrated in Figure 3b.^{4, 5}

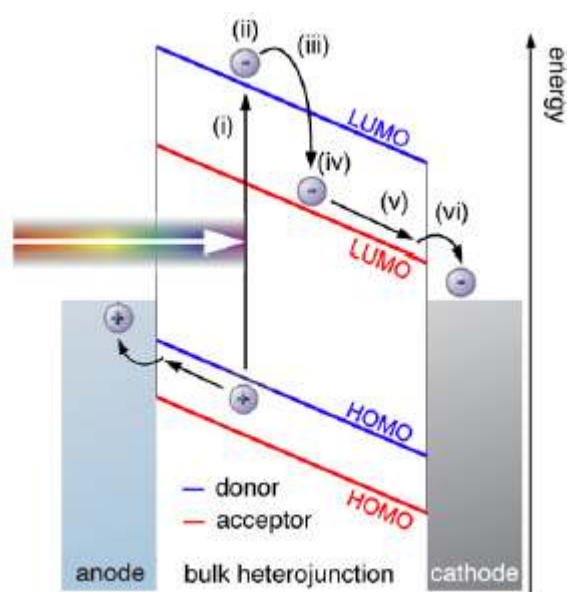


Figure 3b: Functioning mechanism of a bulk-heterojunction solar cell.

The sun light is absorbed by the active layer (i), causes the excitation of a donor's electron from its valence band (HOMO in blue) to its conduction band (LUMO in blue), leaving an hole in the valence band. This is the excitonic state (ii) and indicates the presence of interacting electron and hole by coulombic attraction. Then, the electron is transferred on the acceptor's LUMO (in red) by hopping (iii), and then transferred to the cathode (v, vi). In the same way, the hole is transferred to the anode.

The energy gap of the donor material has to be sufficiently small in order to absorb most part of the solar spectrum, and the donor's LUMO has to be higher of at least 0.3 eV than the acceptor's LUMO, which has to receive the electron and transfer it

³ Sigma-Aldrich catalogue *Materials Science Products*

⁴ Renzo Graziosi, *M.Sc. Thesis*, Università degli Studi di Milano, 2012

⁵ C. Deibel, V.Dyakonov, *Rep. Prog. Phys.*, **2010**, 73, 1

to the cathode. This constitutes the driving force for the charge dissociation in the donor material and it is necessary to overcome the charge aggregation energy in the excitons. The difference between the HOMOs of the donor and the acceptor materials is then responsible of the exciton dissociation and affords a good charge transfer and a good charge separation at the donor-acceptor interface: in fact, if the HOMO of the donor is too low, the dissociation of the electron-hole pair at the interface between the donor and the acceptor becomes difficult. The difference between the donor's HOMO and the acceptor's LUMO is characteristic of the cell and it is defined as *open circuit voltage* (V_{oc})

The most common donor-acceptor couple in bulk-heterojunction solar cell is P3HT and PCBM. Unfortunately, the low value of the PCBM's LUMO limits the open circuit voltage to a value around 0.6 eV, thus limiting the efficiency of the device.

However, the technology of the bulk-heterojunction solar cells appears to be promising, and many materials are under investigation to find the most suitable for this kind of applications; in this frame, PCBM remains the most promising compound, in spite of its faible absorbance in the visible region, such that only the donor is able to absorb sunlight, because its LUMO is well positioned with respect to the combination with many possible donor materials, and it can efficiently stabilize the negative charge, up to six successive electrons, with good charge transport ability. Many modifications of the fullerene have been proposed⁶, as reported, for example, in Figure 4a

A different approach⁷ is to employ non-fullerene acceptors (Figure 4b), based on conjugated systems, bearing electron-donor and electron-withdrawing subunits, that show interesting absorption properties in the visible region and lower LUMO values, but their performance in the devices are, at the moment, lower than PCBM ones.

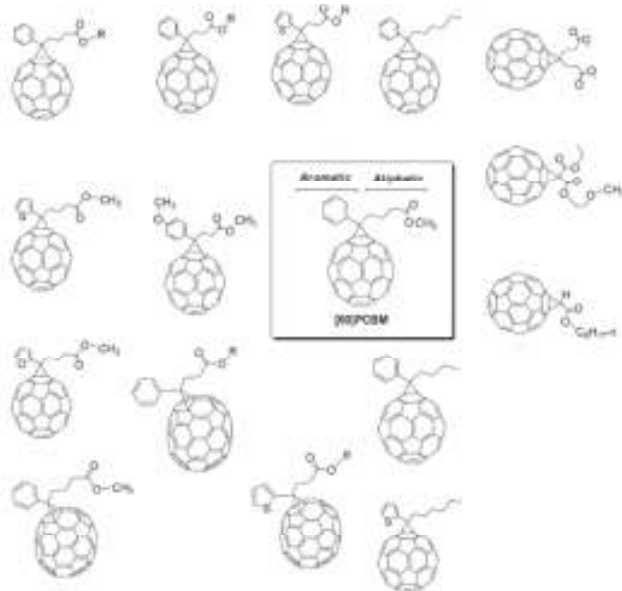


Figure 4a: Examples of new fullerene derivatives

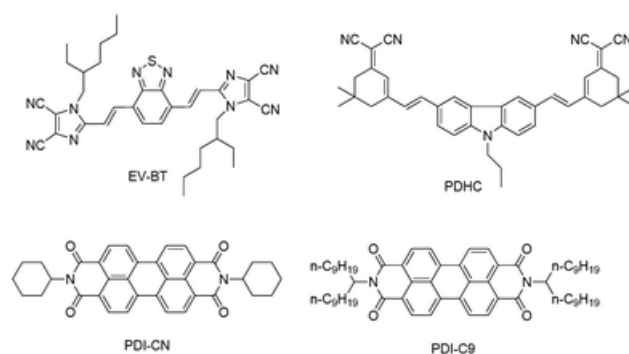


Figure 4 b: Examples of non-fullerene acceptors

⁶ M.M. Wienk, J.M. Kroon, W.J.H. Verhees, J. Knol, J.C. Hummelen, P.A.V. Hal, R.A.J. Janssen, *Angew. Chem. Int. Ed.*, **2003**, 42, 3371; P.A. Troshin, H. Hoppe, J. Renz, M. Egginger, J.Y. Mayorova, A.E. Goryachev, A.S. Peregodov, R.N. Lyubovskaya, G. Gobsch, N.S. Sariciftci, V.F. Razumov, *Adv. Funct. Mat.*, **2009**, 19, 779.

⁷ Y. Li, Q. Guo, Z. Li, J. Pei, W. Tian, *Energy Environ. Sci.*, **2010**, 3, 1427

A great breakthrough in organic photovoltaics was the discovery of the dye-sensitized solar cells⁸, by Michael Graetzel, at the beginning of the nineties of the XX century, showing enhanced performance under real outdoor conditions, even suitable for indoor applications, light-weight, coloured and semitransparent, so that they could adsorb light from both faces and angles.

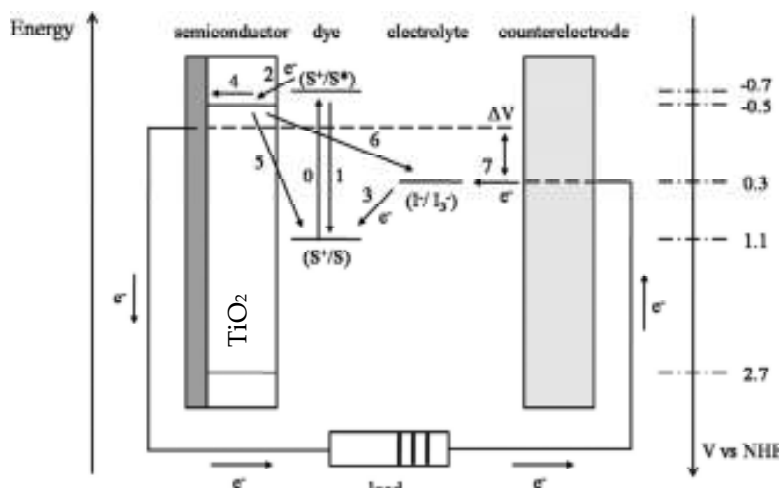


Figure 5: Scheme of a dye-sensitized solar cell

The numbers in the figure indicates the steps of the functioning of the cell:

0 = photoexcitation of the sensitizer

2 = electron injection into the mesoporous oxide film (typically, TiO₂)

4 = electron transfer through the film to the ITO or FTO electrode, and transfer through an external circuit to the counterelectrode

7 = reduction of redox mediator in the electrolyte at the counterelectrode

8 = regeneration of the oxidized sensitizer in the pristine form (reduction by redox mediator).

There are some parasite processes, to be avoided:

1 = decay of the excited sensitizer

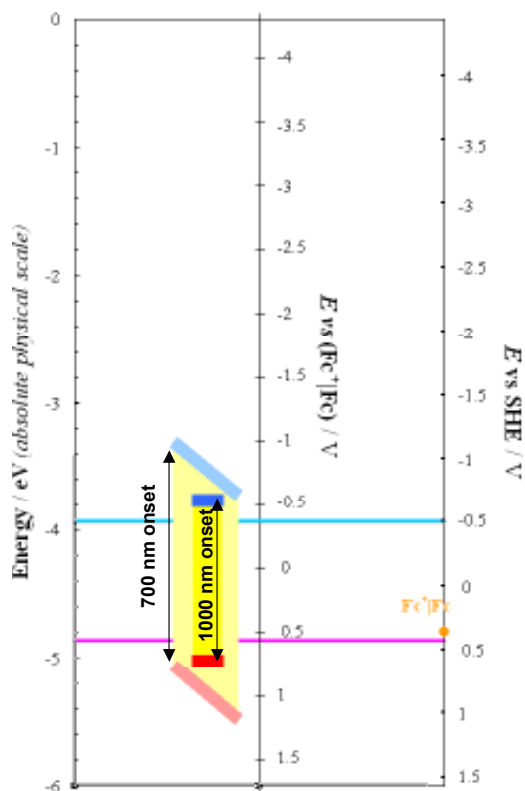
5 = recombination of electrons in the semiconductor with the oxidized sensitizer

6 = recombination of electrons in the semiconductor with the oxidized redox mediator.

⁸ A. Hagfeldt, G. Boschloo, L. Sun, L. Kloo, H. Pettersson, *Chem. Rev.*, **2010**, 110, 11, 6595-6663;

B. O'Regan, M. Grätzel, *Nature*, **1991**, 353, 737-740; Y. Ooyama, Y. Harima, *ChemPhysChem*, published online 16 Jul 2012, DOI: 10.1002/cphc.201200218

To achieve efficient electron injection from the excited dye to the conduction band of TiO₂, the energy level of the LUMO of the dye must be higher (more negative) than that of the conduction band (-0.5 V vs NHE) of the TiO₂ electrode (some researchers have proposed that an energy gap of over 0.2 eV is necessary for efficient electron injection). On the other



hand, to achieve efficient regeneration of the oxidized state by electron transfer from the I₃⁻/I⁻ redox couple in the electrolyte, the sensitizer has to fulfil some energetic requirements: first, the HOMO-LUMO gap of the sensitizer should be narrow enough to allow the dye absorption spectrum to cover most of the solar light spectrum (vis + NIR) (possibly, the sensitizer should have high molar absorption coefficients). This could be improved by increasing conjugation and/or inserting favourable localized reduction and/or oxidation sites. Second, also the position of the HOMO and LUMO levels of the sensitizer is important; in particular the energy level of the LUMO must be higher than that of the conduction band of the TiO₂ electrode (possibly, by at least 0.2 eV).

The energy level of the HOMO must be lower than that of the I₃⁻/I⁻ redox potential (possibly, by at least 0.2-0.3 eV), this could be modulated by inductive

effects of suitable substituents.

Then, other structural requirements have to be taken into account: the molecule must have at least one anchoring group for adsorption onto TiO₂, the directionality of electrons should be designed to provide efficient electron injection from the LUMO to TiO₂ while avoiding electron recombination from TiO₂ to HOMO. Moreover, dye aggregation on the TiO₂ should be avoided since it results in intermolecular energy transfer and reduced yield of electron injection in TiO₂, and there should be some hydrophobic substituents on the dye skeleton to act as barriers to prevent hydrophilic I₃⁻ ions from approaching the TiO₂ surface, thereby retarding charge recombination, and, finally, the molecule must have excellent stability even after prolonged redox cycling.

The most common dyes are metal complexes, especially ruthenium-based ones, but metal-free organic dye sensitizers present many advantages: synthetic versatility, lower cost of starting materials, less environmental issues, high molar extinction coefficients. The most common structure of organic dyes is composed by a sequence of donor-bridge-acceptor subunits. When the dye absorbs light, intramolecular charge transfer occurs from subunit acceptor to donor through the π -bridge.

Both these technologies present many advantages, and still many drawbacks, but the research in this field is very active and challenging, and performances of these organic photovoltaic cells are improving faster and faster.

In particular, this PhD thesis concerns polythiophene systems. The structure of polyheterocycles recalls the structure of *cis*-polyacetylene, but it is more stabilized by the

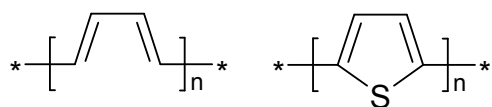


Figure 6: Structures of *cis*-polyacetylene and polythiophene

presence of the heteroatom. Among all the possible derived structures, polythiophenes have emerged as optimum candidates for many applications, thanks to their efficient electronic conjugation, good stability, and great chemical versatility.

Concerning their structure, polyheterocycles significantly differ from the polyacetylene system, since they have a non-degenerate ground state, with two possible limiting mesomeric structures, aromatic and quinoid, the latter having higher energy.

In the case of polyacetylene (*i.e.*, a polymer with a degenerate ground state), the potential curve shows two minima, at the same energy, corresponding to the A and B possible structures, with alternated single and double bonds, as illustrated in Figure 7: a defect that converts A into B generates a maximum in energy.

In chemistry, this corresponds to the formation of an highly reactive radical, while in physics, the domain boundary between two degenerate ground states is defined soliton, as illustrated in Figure 8a.

However, experimental evidence indicates that the structural relaxation in the vicinity of the domain boundary is extended over 14 carbon atoms, as illustrated in Figure 8b.

Concerning the polythiophene case, taken as example for the great majority of conducting polymers, the explanation is more complicated, due to the presence of a relative and an absolute minima in the potential curve, due, respectively, to the non-degenerate quinoid and aromatic structures. The description of charging in conducting polymers is generally explained by the bipolaron model introduced by Brédas in the 1980s.⁹ The model was originally referred to characterize defects in inorganic crystalline solids, and then extended to the field of conducting polymers; this model is nowadays generally accepted.

In a polymer, just as in a crystal, the interaction of a polymer unit cell with all its neighbors leads to the formation of electronic bands: the valence band (VB, highest occupied

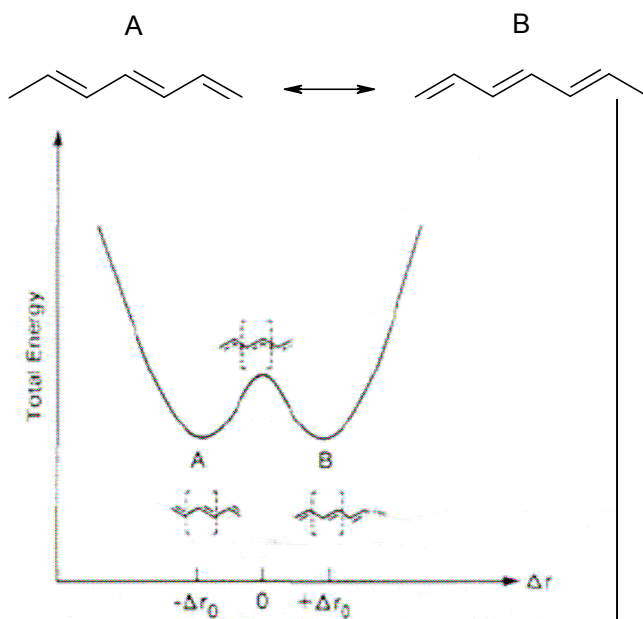


Figure 7: Potential energy curve for polyacetylene

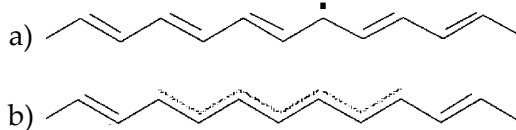


Figure 8: a) soliton in *trans*-polyacetylene, b) structural relaxation in vicinity of a domain boundary

⁹ J. L. Brédas, R. R. Chance, R. Silbey, *Phys. Rev. B*, **1982**, 26, 5843; J. L. Brédas, G. B. Street, *Acc. Chem. Res.* **1985**, 18, 308

electronic levels) and the conduction band (CB, lowest unoccupied levels). The bandgap (E_g) between the VB and CB determines the intrinsic electrical properties of the material. For organic conjugated polymers, it is normally larger than 1.5 eV so that these materials are intrinsically insulating.

In an organic polymer chain, it can be energetically favorable to localize the charge that appears on the chain and to have, around the charge, a local distortion (relaxation) of the lattice. This process causes the presence of localized electronic states in the gap due to a local upward shift $\Delta\varepsilon$ of the HOMO and downward shift of the LUMO.

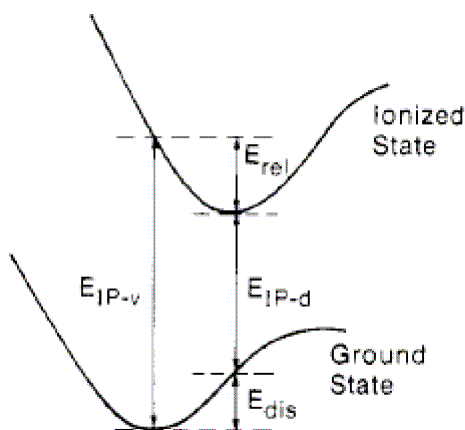


Figure 9: Illustration of the energies involved in a molecular ionization process. E_{IP-v} is the vertical ionization energy, E_{rel} the relaxation energy gained in the ionized state, E_{dis} the distortion energy to be paid in the ground state in order that the molecule adopts the equilibrium geometry of the ionized state, and E_{IP-d} the ionization energy of the distorted molecule.

Considering the case of oxidation, the ionization energy is lowered by an amount $\Delta\varepsilon$. If $\Delta\varepsilon$ is larger than the energy E_{dis} necessary to distort the lattice locally around the charge, this charge localization process is favorable relative to the band process. This corresponds to the formation of a polaron.

A polaron could be thought as the state between a neutral and a charged solitons, whose energetic states hybridize and form bonding and antibonding orbitals. The neutral soliton contributes with zero charge and one single spin, while the charged soliton brings a charge corresponding to $\pm e$

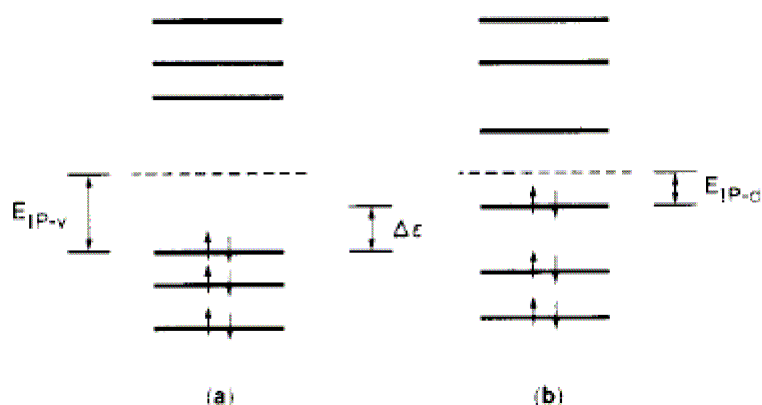


Figure 10: Schematic illustration of the one-electron energy levels for an organic molecule (e.g., biphenyl) in its ground-state electronic configuration adopting: (a) the equilibrium geometry of the ground state; (b) the equilibrium geometry of the first ionized state.

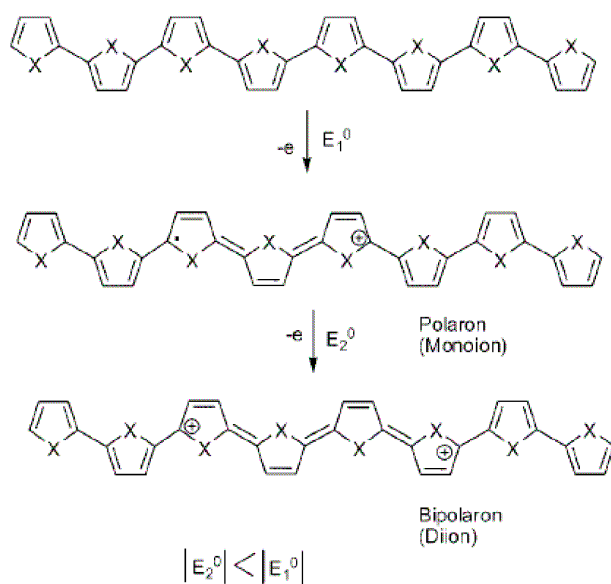


Figure 11: Formation of the bipolaron state in polythiophene upon oxidation. The ionized states are stabilized by a local distortion in a quinoid structure.

and no spin. Consequently, the resulting polaron has $q = \pm e$ and $s = 1/2$, and exhibit an ESR signal, as well as two bands in the UV-Vis-NIR spectrum. In other words, a polaron is a radical ion with spin $1/2$ associated to a distortion in the polymer: it is a charge carrier and it is shown by a localization of the charge itself in correspondance with a distortion in the chain. It must be stressed that in the case of polaron formation, the VB remains full and the CB empty. There is no appearance of metallic character since the half-occupied level is localized in the gap. When a second electron is removed from the polaron, the so-called bipolaron is formed. The transition from the neutral state to the bipolaron takes place via the polaron state, and, thus, corresponds sequentially to redox transitions observed in two-step redox systems. In contrast to normal redox processes, however, additional local distortions occur in the chain during the charging of the polymer. Already in the first step, the formation of polarons, there is a gain of relaxation energy E_{rel} , that corresponds to the bonding energy of the polaron.

If the creation energy of a bipolaron relative to that of two polarons are compared, the distortion energy E_{dis} to form one bipolaron is roughly equal to that to form two polarons. On the other hand, the decrease in ionization energy is much more important in the bipolaron case ($2\Delta\varepsilon^{bip}$) than for two polarons ($2\Delta\varepsilon^{pol}$), as shown in Figure 9. This is the reason why one bipolaron is thermodynamically more stable than two polarons in these systems despite the Coulomb repulsion between two similar charges. Furthermore, the latter is also largely screened by the presence of dopants (counterions) with opposite charge. In case of p - (n -) type doping, the bipolaron levels in the gap are empty (fully occupied). The bipolarons are thus spinless, and show no ESR signal and only one absorption band in the UV-Vis-NIR spectrum. Also the polaron pair is a spinless state, and, consequently, shows no ESR signal, but has two absorptions in the UV-Vis-NIR spectrum.

The case of polyacetylene is significantly different: as a result of the degeneracy, the two charges forming a would-be bipolaron in *trans*-PA can readily separate. This process is favorable because there is no increase in distortion energy when the two charges separate, since the geometric structure that appears between them has the same energy as the geometric structure on the other sides of the charges. In physics terminology, such a charge associated with a boundary or domain wall is called a soliton, because it has the properties of a solitary wave which can propagate without deformation and dissipation. Starting from one side of the soliton, the double bonds become gradually longer and the single bonds shorter, so that arriving at the other side, the alternation has completely reversed. This implies that the bond lengths do equalize in the middle of a soliton. The presence of a soliton leads to the appearance of a localized electronic level at mid-gap, which is half-occupied in the case of a neutral soliton and empty (doubly occupied) in the case of a positively (negatively) charged soliton.

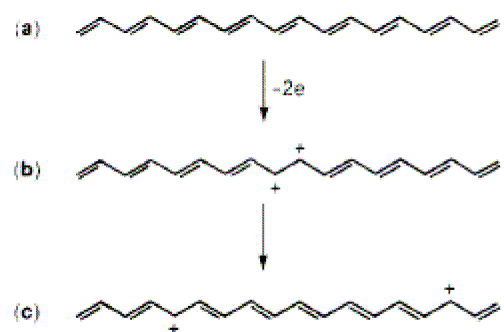


Figure 12: Illustration of the formation of two charged solitons on a chain of *trans*-polyacetylene.

1.2 Electrochemistry of conductive polymers¹⁰

After this general description of what conjugated polymers are and on their possible applications, it is important to explain now the mechanisms of synthesis.

In particular, this work is focused on the electrochemistry of polythiophene systems: in our case, the production of conducting polymers is obtained by electrooxidation of the corresponding monomer, by applying a suitable potential.

The generally accepted electropolymerization mechanism involves the formation of radical cations, that couple together or with the starting monomer, as illustrated in the Figure 14:

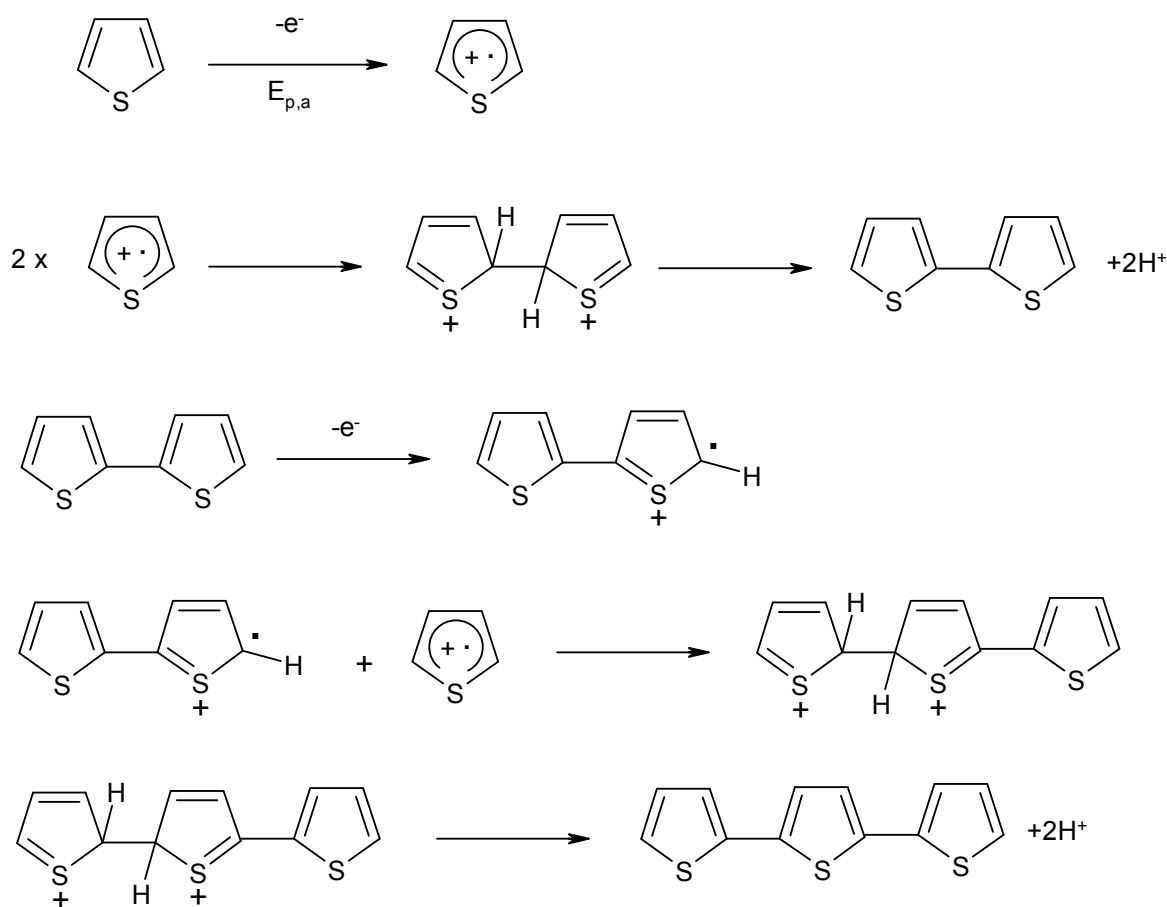


Figure 14: Accepted mechanism for the electropolymerization of thiophene: E(CCE)_n sequence.

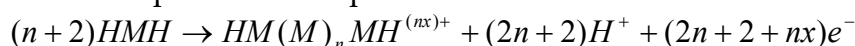
The oxidation of the monomer in the α position generates a radical cation, that couples with another radical cation, generating a doubly charged σ-dimer. The elimination of two protons (which is the rate determining step) and the consequent rearomatization of the system (which is the driving force of the reaction) generate a neutral dimer. As it is more conjugated than the monomer, it is immediately oxidized and its cation undergoes a next

¹⁰ J. Heinze, B.A. Frontana-Urbe, S. Ludwigs, *Chem. Rev.*, **2010**, *110*, 4724-4771

I.F. Perepichka, D.F. Perepichka, *Handbook of Thiophene-based materials: Applications in Organic Electronics and Photonics*, 2009, Wiley, Chichester, ISBN 978-0-470-05732-2

coupling step, and so on. The mechanism is essentially a sort of chain propagation reaction, with a series of E(CCE)_n steps.

Each coupling step has to be activated by two species; the calculated electrochemical stoichiometry is 2.07-2.6 F·mol⁻¹ of reacting monomer¹¹. The film-forming process needs two electrons per molecule, that requires 2 F·mol⁻¹ and the additional charge normally serves the partial reversible oxidation of the conjugated polymer. It is worthwhile noticing that, since the polymer is longer than the monomer, and thus its conjugation is more extended, its oxidation occurs at less positive potential than the monomer, so the two processes, the polymer formation and its doping, occur simultaneously. The complete reaction equation of the process is:



(2n+2) electrons are used for the polymerization process itself, while the remaining nx electrons are required for the doping process. Generally, x is between 0.25 and 0.4, *i.e.*, every third to fourth monomeric subunit has been charged at the end of polymerization. Higher levels of doping could be forced, by applying a more positive potential, but this extra energy could lead to overoxidation of thiophenes, and consequently a degradation of the physico-chemical and mechanical properties of the polymer film.

However, this mechanism is still under debate, particularly concerning the rate determining step and the role of the protons. It seems that the addition of small quantities of water to the working solutions could help the polymerization process, because the σ -intermediates are weak acids and water could act as a sufficiently strong base to initiate the proton elimination process. The existence of σ -dimers itself has been questioned, especially in those cases where the active α -position of the monomers is blocked by a substituent, thus preventing coupling reactions. In such cases, the formation of π -mers is more likely. In all cases, cyclic voltammetry shows the reversible formation of radical cations without chemical follow-up steps.

Another criticism moved to this mechanism concerned the radical cation-radical cation coupling, on account of the strong Coulombic repulsions between two cations, and a radical-substrate coupling was considered to be more likely. However, it has been shown that even small molecules that are equally charged are able to dimerize at a diffusion-controlled rate, as then confirmed by a theoretical analysis and careful quantitative kinetic studies of the coupling steps of oligomeric pyrroles and thiophenes¹²

In summary, a simple chain propagation mechanism is unlikely. Rather, the electropolymerization involves three different stages:

- oxidation of the monomer at the electrode, formation of soluble oligomers in the diffusion layer (preferably by successive dimerization steps)
- deposition of oligomers involving nucleation and growth processes

¹¹ A. F. Diaz, J. I. Castillo, J. A. Logan, W. Y. J. Lee, *Electroanal. Chem.*, **1981**, 129, 115;

E. M. Genies, G. Bidan, A. F. Diaz, *J. Electroanal. Chem.*, **1983**, 149, 101

¹² C.P. Andrieux, P. Audebert, P. Hapiot, J.M. Savéant, *J. Phys. Chem.*, **1991**, 95, 10158.

J.C. Lacroix, F. Maurel, P.C. Lacaze, *J. Am. Chem. Soc.*, **2001**, 123, 1989.

P. Audebert, J.M. Catel, G. Le Costumer, V. Duchenet, P. Hapiot, *J. Phys. Chem. B*, **1995**, 99, 11923.

P. Audebert, J.M. Catel, G. Le Costumer, V. Duchenet, P. Hapiot, *J. Phys. Chem. B*, **1998**, 102, 8661.

- solid state polymerization, producing longer chains and cross-linked materials

To understand the properties of the conducting polymers, it is important to estimate the length of the conjugated chain that can be obtained by electropolymerization. It seems more likely to get oligomers, instead of polymers, *e.g.* the poly-T4-BT2 described in the present PhD thesis is composed mainly by dimers, trimers, and could reach the degree of pentamer, as it will be shown in Chapter 3.2.2.

The efficiency of electropolymerization could change a lot with the experimental parameters, for example by changing the starting molecule: this is typically a monomer, but starting with a short oligomer, for instance, changes two essential parameters: the oxidation potential gets lower for increasing the chain length, and the kinetics of the process is slowed down. The lowering of the oxidation potential has, in addition, the advantage of facilitating a defect-free polymerization, because nucleophilic reactions of solvents with growing oligomers do not take place. Another interesting modification of monomer is the introduction of electron-withdrawing or electron-donor substituents: the oxidation potential is shifted to higher or lower potentials, respectively, and also the position of the substituent has effects on the electropolymerization.

However, it is a hard task to control the electropolymerization process, and it is really difficult to obtain perfectly reproducible polymer films, featuring identical electrochemical and structural properties: even small variations in temperature, formation potential, concentration of the starting monomer affect the physical and chemical characteristics of the resulting film. In the present PhD thesis, one of the most ambitious aim was to obtain perfectly reproducible films from enantiopure thiophene-based monomers, in order to verify the performance of our *inherently chiral* monomers as surface-modified electrodes for enantiomer discrimination and asymmetric electrocatalysis: most of the experimental difficulties were overcome by employing ionic liquids and screen-printed electrodes, as it will be discussed more in detail in Chapter 2 and 3.

Even the polymerization technique influences the properties of the resulting polymer films: potentiodynamic (cyclic voltammetry), potentiostatic and galvanostatic polymerization are the three most important techniques. In cyclic voltammetry the potential changes cyclically and regularly during the deposition of the conducting polymer onto the electrode. The growing polymer undergoes cyclic changes between its neutral (insulating) and its doped (conducting) states; this process is accompanied by a continuous exchange of electrolyte and solvent through the freshly deposited polymer, affecting the morphology of the polymer matrix, that has to be elastic enough to allow subsequent compaction and opening of the structure. At the end of the experiment, conducting polymers are generally obtained in their neutral state (but it is always possible to stop the experiment at a potential different from the neutral state), while galvanostatic and potentiostatic methods give polymers in their conducting state; in addition, the polymerization at low potentials ends in the formation of well-ordered σ -dimers.

In galvanostatic experiment, the overall polymerization rate is constant, due to the current control. In this case, the resulting potential during the galvanostatic experiment is temperature dependent and shifts to lower values at decreasing temperatures, on account of changes in the volume of solvents with temperature, that lead to changes in the concentration of the monomer. Furthermore, at the beginning of the electropolymerization, the potential initially increases and then decreases after a few seconds, possibly because the first period of oligomerization involves the consumption of the starting polymer which leads to an increase of the potential. Almost simultaneously redox-active charged oligomers are formed in front of the electrode. They catalyze the oxidation of monomeric species which leads to a decrease of the potential after a few seconds. The potentiostatic method is characterized by strong changes in the current and the polymerization rate. Nevertheless, the results are in principle similar to those of the galvanostatic technique because the material that has been deposited is not discharged during polymerization. So, for each monomer, the best conditions for electropolymerization should be carefully tested. Other factors that influence the properties of conducting polymers are the type of solvent, the presence of any additives, and the type of supporting electrolyte. Concerning the type of solvent, it should possess high polarity in order to minimize the coulombic repulsions during the cationic coupling step, and its nucleophilicity should be low, in order to avoid nucleophilic attacks on the

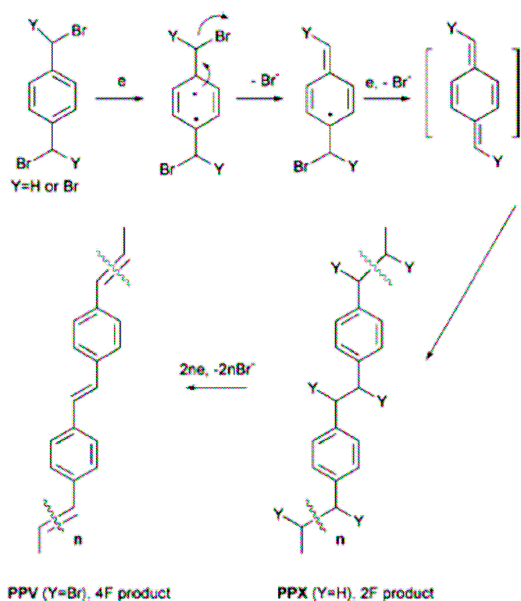


Figure 15: Electrochemical reductive electropolymerization of $\alpha, \alpha', \alpha''$ -tetrabromo-*p*-xylylene (TBPX) to produce PPVs, from J. H. P. Utley, J.J. Gruber, *J. Mater. Chem.*, 2002, 12, 1613.

cationic intermediates: in the case of the most commonly used solvents, it rises in the following order: $CH_3NO_2 < CH_2Cl_2 < \text{propylene carbonate PC} < CH_3CN < H_2O$. The supporting electrolyte, in particular its size and shape, have considerable influence on the polymerization process, *e.g.* on the morphology, on the charging/discharging process and on the conductivity of the resulting film. For example, *in situ* conductivity of PEDOT films decreases with the anion sequence $ClO_4^- > BF_4^- > CF_3SO_3^- > PF_6^-$.¹³ It is worthwhile citing that some conducting polymers, *i.e.* poly(*p*-phenylenevinylens) (PPVs), *via* the poly(*p*-xylylenes) (PPXs) are prepared by cathodic electropolymerization, as shown in Figure 15.

¹³ P. H. Aubert, L. Groenendaal, F. Louwet, L. Lutsen, D. Vanderzande, G. Zotti, *Synth. Met.*, 2002, 126, 193

In the present PhD thesis, cyclic voltammetry has been extensively used not only to deposit polymer films, but also to study the charging/discharging phenomena of conducting polymers, also in combination with electrochemical quartz crystal microbalance. As before mentioned, the doping process correspond to an oxidation or reduction, and ions from the supporting electrolyte play an active role, in order to maintain the electroneutrality.

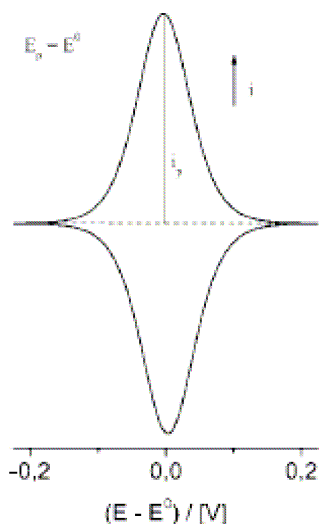


Figure 16: Theoretical cyclic voltammogram for a thin layer film with one redox centre.

In the case of a simple one-electron transfer for a thin layer film, reversible cyclic voltammograms (CVs) should show completely symmetrical and mirror-image anodic and cathodic waves, with identical peak potentials and current levels (Figure 16).

The current in the reversible case is then

$$i = \frac{n^2 F^2 A \Gamma_T v \exp \theta}{RT(1 + \exp \theta)^2}, \text{ where } \theta = \frac{nF}{RT}(E - E^0) \text{ and}$$

$\Gamma_T = \Gamma_{ox} + \Gamma_{red}$ correspond to the total surface covered with reduced and oxidized states.

It is worthwhile noticing the linearity between the current i and the potential scan rate v . In principle, this is valid only for monomolecular layers. When increasing the film thickness,

diffusion sets in during electrochemical charging/discharging and, as a consequence, the voltammetric response gradually shifts from mirror symmetrical diagrams to the classic, asymmetrical shape with i proportional to $v^{1/2}$. Characteristic features of voltammetry of conducting polymers are a steep anodic wave at the start of charging, followed by a broad and flat plateau as the potential increases. In the reverse scan a potential-shifted cathodic wave appears at the negative end of the capacity-like plateau (Figure 17).

The number of accessible redox states increases with increasing chain length of the system, resulting in the superposition of redox states over a broad potential range for long chain lengths. Therefore, the capacity-like plateau is referred to faradaic redox processes. Moreover, the voltammetric signal of the steep anodic wave at the beginning of the charging certainly belongs to a close superposition of several redox states. The fact that the polymeric material is normally polydisperse additionally favors the superposition of redox states. So, the electrochemical charging process of conducting polymers should be described by

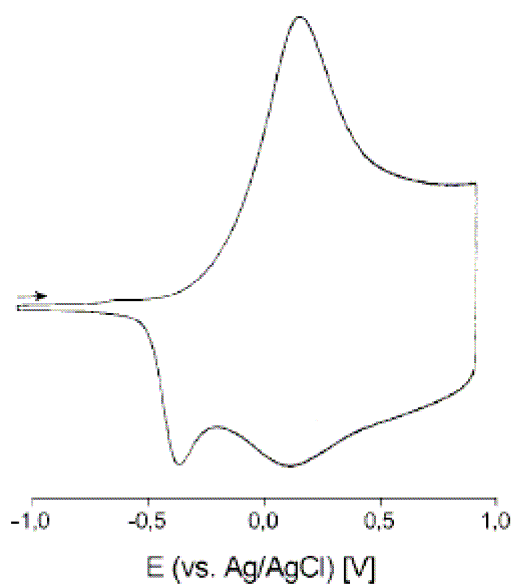


Figure 17: Cyclic voltammogram of the oxidation of poly(4,4'-dimethoxybithiophene) in $\text{CH}_2\text{Cl}_2 + \text{TBAPF}_6$ 0.1 M, $T = 273\text{K}$, $v = 200 \text{ mV/s}$

a sequence of discrete but overlapping redox steps.

At increasing chain lengths for chainlike conjugated oligomers and polymers, the following general trends have been established:

- Redox states of identical charge (*e.g.*, mono- or di-ion) shift toward lower energies. For long chains, the energies of low redox states gradually approach a common convergence limit.
- Adding successive monomeric subunits in the molecular chain enlarges the number of accessible redox states.
- The energy gap widens considerably between the lowest and the highest charged states.
- The number of redox states is limited and does not exceed the number of monomeric subunits in a chain.
- The chemical stability of charged species related to the same redox states increases, and therefore, the tendency for follow-up reactions decreases.

A further characteristic of voltammetric experiments with CPs is the conspicuous separation between the wave of anodic charging and cathodic discharging (hysteresis) (Figure 16 *vs* Figure 17). It was initially interpreted as a kinetic effect of slow heterogeneous charge transfer or conformational changes during charging. As the potentials of the anodic and cathodic peaks are virtually independent of the scan rate, the hysteresis could not be due to a classical square scheme involving heterogeneous and homogeneous kinetics but due to N-shaped free energy curves as a consequence of phase transitions in the polymer¹⁴.

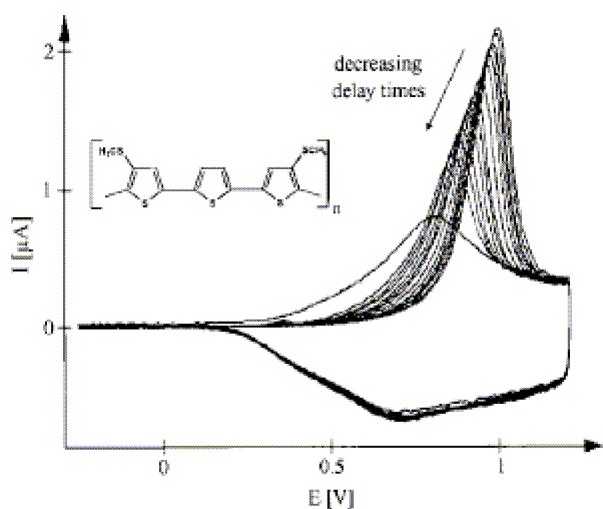


Figure 18: Memory effect of poly(4,4''-dithiomethyl-2,2',2''-terthiophene) in CH₃CN + TBAPF₆ 0.1 M for different waiting times τ (top down): 30, 15, 10, 8, 6, 4, 2, and 1 min; 45, 30, 15, 10, and 5 s; V = 60 V/s, T = 298 K, Pt disk electrode ($r = 12.5 \mu\text{m}$).

Another unusual phenomenon shown by conducting polymers is the so-called *first cycle* or *memory effect*: after a waiting time in the discharged state of a polymeric film, the first voltammetric cycle differs markedly in shape and peak position from subsequent cycles. While the anodic wave of the very first cycle appears at relatively positive potentials and is normally both steep and

sharp, all subsequent anodic scans show broadened waves which are significantly shifted toward negative potentials (Figure 18). The phrase *memory effect* is related to the fact that the electrochemical response during charging of polymeric films depends on the history of

¹⁴ S. W. Feldberg, I. Rubinstein, *J. Electroanal. Chem.*, **1988**, *240*, 1–15

foregoing electrochemical events. During charging/discharging of CPs, a rearrangement of the chain configuration took place, which was followed by the incorporation and extraction of counterions. Thus, during reduction, expulsion of counterions occurs from opened channels that get closed slowly as a function of waiting time, and then the reoxidation requires increasing extra energy to reopen the channels.

It is worthwhile remembering that during charging and discharging, the electroneutrality must be ensured: both ions from the supporting electrolyte are likely to be involved. During discharging from the *p*-doped state, anions are expelled from the polymer matrix, and cations may be incorporated; also the solvent plays an important role. The ion dynamics can be followed by electrochemical quartz crystal microbalance.

In principle, the *n*-doping process is analogous to the *p*-doping process. However, the *n*-doping results to be less important, since in most cases the reduction processes of conducting polymers are out of the potential window allowed by commonly used organic solvents. A peculiar phenomenon that concerns the *n*-doping is the so-called *charge trapping*. The negative charge, injected at a given potential, is released only at much more

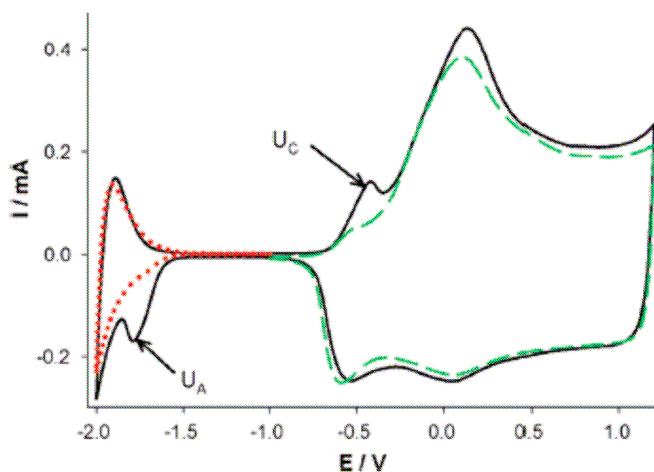


Figure 19: Cyclic voltammetry of a PEDOT film in 0.1 M TEABF₄/CH₃CN: responses of film cycled through both *n*- and *p*-doping regions (black line), through the *p*-doping region (green line) and through the *n*-doping region (red line). From A. R. Hillman, S. J. Daisley, S. Bruckenstein, *Electrochim. Acta* 2008, 53, 3763

positive potentials in the reverse scan. This effect could be attributed to structural modifications in the polymer network (*i.e.*, the generation of quinone-like redox states), that, analogously as the memory effect, requires more energy to restore the initial conformation.

It is likely that the discharging processes of this polymer are incomplete and regions of conducting material and associated anions/cations are isolated within an insulating matrix of undoped polymer. With this model, kinetic control at the completion of the undoping process must be assumed, which may be caused by changes in the polymer structure.

The charging of the conducting polymer is an essential process to make it show its conductive properties. Under *in situ* conditions, conductivity increases sigmoidally as a function of the applied potential (*i.e.*, the doping level), and then reaches a plateau, as illustrated in Figure 20. It is always important to remember that conducting polymers are actually semiconductors, with conductivities ranging between 100 and 300 S·cm⁻¹, with some cases that reach values higher than 1000 S·cm⁻¹: these values were obtained with the four probe technique. This technique consists in applying a current between the two

In the case of PEDOT charging, here illustrated in Figure 19, ion trapping occurs during consecutive *p*- and *n*-

external probes and measuring the potential difference between the two internal probes. Zotti *et al.*¹⁵ proposed to use a twin-band electrode to measure the conductivity of conductivity in conjugated organic polymers. The twin-band electrode is constituted by two platinum sheets; between them a thin layer of insulating material is inserted. Auxiliary reference and counter electrodes allow the electrodeposition of the conducting polymer to be investigated on the two platinum electrodes (used together as working electrode), that, being very near, result to be bridged by the conducting polymer layer. In this case, it is possible, with a second circuit, to measure in direct current the ohmic resistance of the conducting bridge. With the first circuit, it is possible to polarize the conducting polymer, and with the second circuit it is possible to measure *in situ* the resistance at the different doping levels.

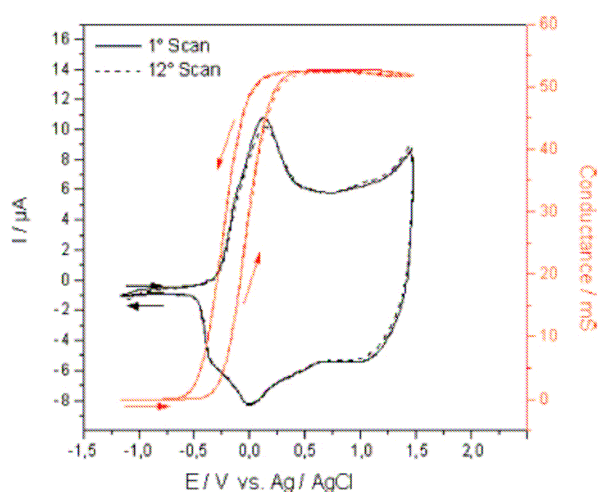


Figure 20: Cyclic voltammogram and typical sigmoidal change of the relative conductivity of poly(4,4'-bithiophene) in CH_2Cl_2 + TBAPF_6 0.1 M, $v = 5$ mV/s.

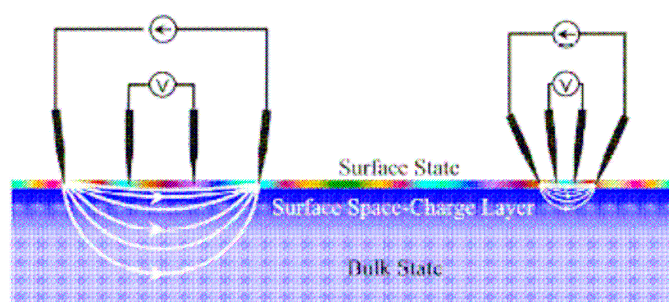


Figure 21: Macro (left) and micro (right) four-point-probe method for measuring electrical conductance. The distribution of current flowing through a semiconductor specimen is schematically drawn.

The mechanism of charge transport is still under debate. For simple redox polymers, a mixed-valence conduction based on charge hopping between oxidized and reduced sites of a redox state is accepted. In the case of conducting polymers, according to the bipolaron model, one mechanism of charge transport is along the conjugated chain. Being the conjugated chains relatively short, the rate determining transport step is likely to be an intermolecular hopping.

¹⁵ G. Schiavon, S. Sitran, G. Zotti, *Synthetic metals*, 1989, 32, 209

1.3 Spider-like oligothiophenes

One of the aims of the present PhD work, concerning the electrochemistry of three-dimensional thiophene-based semiconductors, is to develop predictive criteria for target-oriented molecular design, on the basis of a systematic study of different molecule families, starting from our previous results on the series of the branched spider-like oligothiophenes.¹⁶ In such papers we focused on finding a rationalization between structure and electronic properties in branched multithiophene systems, since the literature in this field was rich of examples of appealing structures, for example swivel cruciform (Figure 21, in blue), X-shaped (Figure 21, in red) and star-shaped ones (Figure 21, in magenta), and dendrimers, (up to 30 thiophene units, **30T**, by Advincula¹⁷, (Figure 21 in green), and up to 90 thiophenes, **G4,a-16-mer**, by Bauerle¹⁸, (Figure 21 in orange) that generally required important synthetic efforts but in many cases lead only to poor improvement in their performances as organic semiconductors.

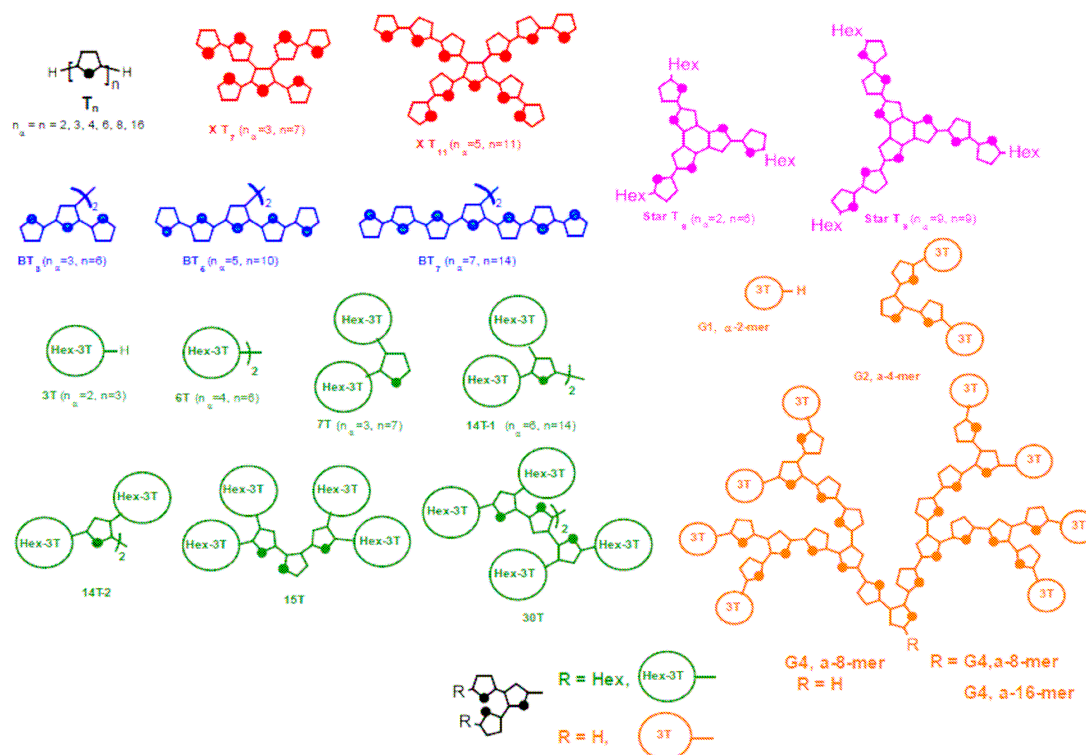


Figure 21: Classification of linear and branched oligothiophenes.

¹⁶ T. Benincori, M. Capaccio, F. De Angelis, L. Falciola, M. Muccini, P. Mussini, A. Ponti, S. Toffanin, P. Traldi, F. Sannicolò, *Chem. Eur. J.*, **2008**, *14*, 459; T. Benincori, V. Bonometti, F. De Angelis, L. Falciola, M. Muccini, P. R. Mussini, T. Pilati, G. Rampinini, S. Rizzo, S. Toffanin, F. Sannicolò, *Chem. Eur. J.*, **2010**, *16*, 9086

¹⁷ C. Xia, X. Fan, J. Locklin, R. C. Advincula, *Org. Lett.*, **2002**, *4*, 2067; C. Xia, X. Fan, J. Locklin, R. C. Advincula, A. Gies, W. Nonidez, *J. Am. Chem. Soc.*, **2004**, *126*, 8735; R. C. Advincula, *Dalton Trans.*, **2006**, 2778

¹⁸ C. Ma, E. Mena-Osteriz, T. Debaerdemaeker, M. M. Wienk, R. A. J. Janssen, P. Bauerle, *Angew. Chem.*, **2007**, *119*, 1709; *Angew. Chem. Int. Ed.*, **2007**, *46*, 1679

In order to understand which are the parameters to take into account to find a compromise between synthetic feasibility and properties, the basic properties of these molecules were compared to those of linear α -oligothiophenes, taken as reference substrates because of their planarity, leading to the highest effective conjugation and narrowest energy gap possible for all-thiophene systems.

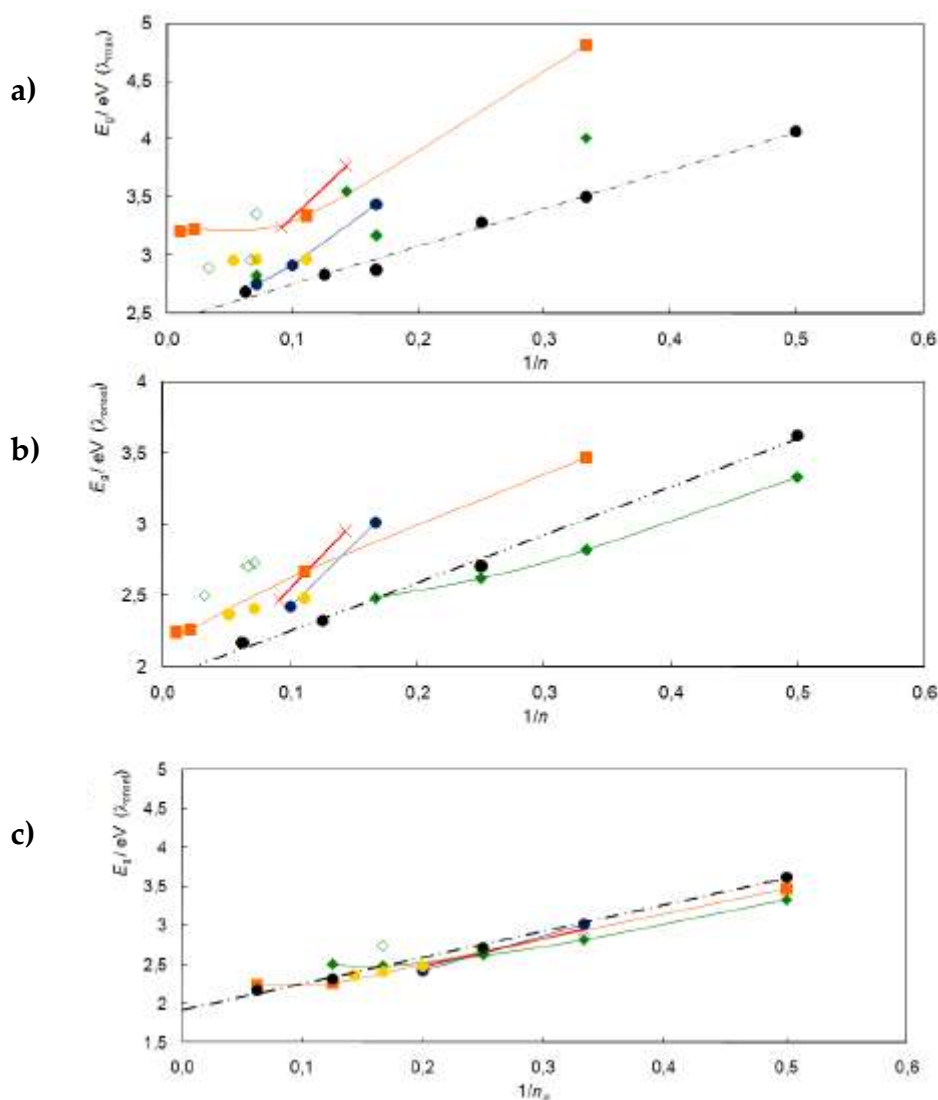


Figure 22: Optical band-gaps for the compounds reported in Figure 21:

a) $E_g(\lambda)$ calculated from λ_{max} and plotted as a function of the reciprocal of the overall number of thiophene units n ;

b) $E_g(\lambda)$ calculated from λ_{max} and plotted as a function of the reciprocal of the number of thiophene units in the longest α -conjugated chain, n_α ;

c) $E_g^*(\lambda)$ calculated from λ_{onset} and plotted as a function of $1/n_\alpha$.

Different colors refer to different families of literature compounds in Figure 21; the empty green diamond corresponds to Advincula's 14 T-2.

Yellow circles refer to the spider-like compounds having bithiophenes as side chains.

The comparison of these molecules (which was not an easy task to achieve, since the experimental conditions, in which the characterizations were performed, were different and in some cases not clearly reported) evidenced interesting trends: in general, at increasing overall number of thiophenes, n , the energy gap values tend to shrink, up to a limit of 7-8 thiophene units, then the energy gap values tend to flatten. In addition, all the series are lying over the linear α -oligothiophene one. When considering not the overall number of thiophenes, n , but the number of α,α -linked ones, n_α , in the longest conjugated chain the normalization improves, and all the series lay together with the planar oligothiophene systems; thus it is clear that what is important in terms of effective conjugation is only the number of α,α -linked units. So, even big dendritic molecules having many α -conjugated branches with different lengths display an optical gap close to that exhibited by the unsubstituted α -oligothiophenes T_n , with n corresponding to the longest α -conjugated branch of the dendrimer. Large multi-thiophene molecules display, however, energy gaps generally higher than expected due to some distortion from coplanarity of the main α -conjugated chain produced by branching. In conclusion, the synthetic engagement required to prepare molecules consisting of a very large number of thiophene rings is not always accompanied by the acquisition of extraordinary conjugation properties, even though other very interesting physical features are acquired, like the high chemical stability and solubility in non-polar organic solvents. In this frame, two families of spider-like oligothiophenes were designed and synthesised by the group of Prof. F. Sannicolò of the Università degli Studi di Milano, focusing on the number of α -linked thiophene units, here illustrated in Figure 23:

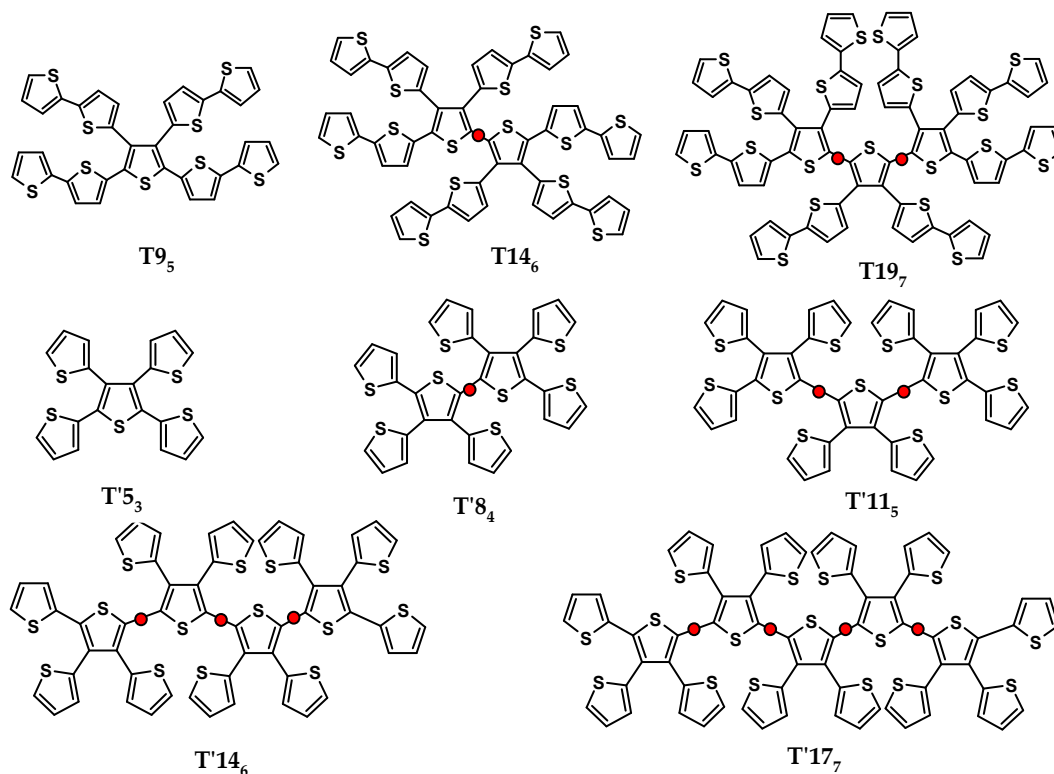


Figure 23: T and T' series of spider-like oligothiophenes

They are composed by an α -conjugated chain constituting the “body” of the spider; the T series is characterized by bithiophene pendants as “legs” along the α,α -linked chain, the T' series has monothiophene pendants. Branching is a key parameter to be taken into account in molecular design, since it enhances the solubility; however, it creates distortions from planarity, that reduce the conjugation leading to an increase of the HOMO-LUMO gap. In this cases, it appears more correct to speak in terms of *effective conjugation*, *i.e.*, the actual conjugation length of a system distorted by the presence of *nodes* along the main conjugated chain.

The synthetic strategy was based on the following considerations:

- The molecules have structural parameters n and n_α in the critical area ($n = 8-9$; $n_\alpha = 5-6-7$), since it has been observed that greater n and n_α are not accompanied by significant improvements in the optical or electrical properties, in particular relatively to the lowering of the HOMO LUMO gap, even if other interesting physico-chemical properties may be acquired (*i.e.*, stability, solubility...)
- The synthetic pathway has to be relatively easy: these molecules were synthesized *via* a Stille coupling, starting from inexpensive, commercially available materials. A good regioselectivity *via* electrochemical oxidative coupling is expected, since the α -positions of the main conjugated chain are preferred. Furthermore, the high symmetry (*e.g.*, T9₅ (C_{2v}), T14₆ (C_{2h}), T19₇ (C_{2v})), makes the α positions homotopic, so a high constitutional order is expected in the polymerization process.

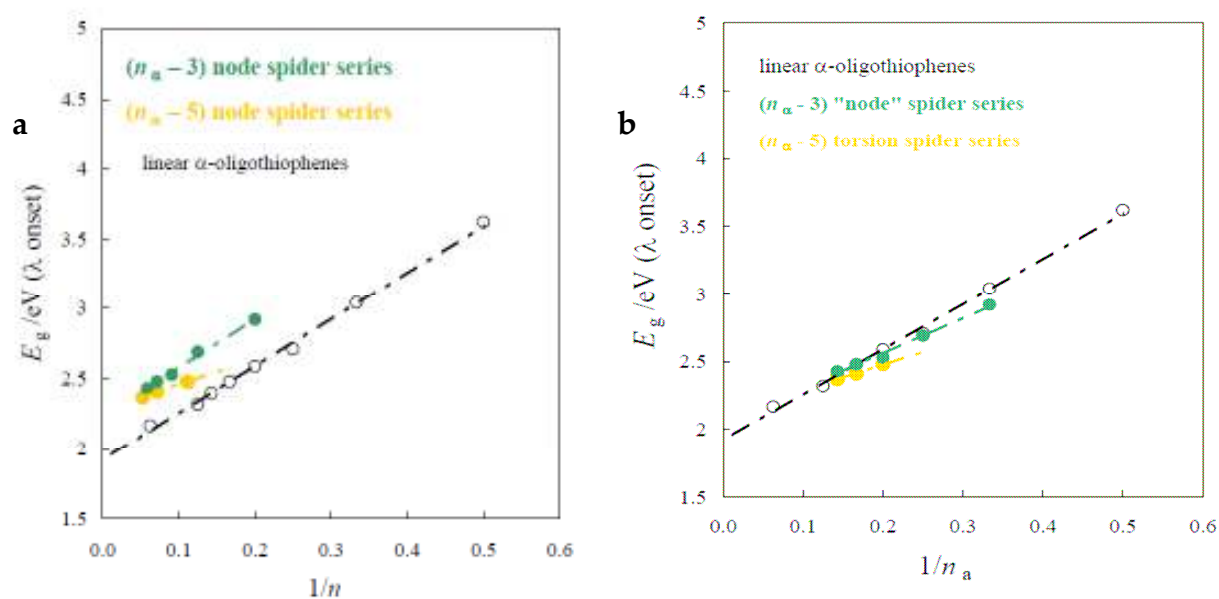


Figure 24: Optical band-gaps for the compounds reported in Figure 19:

a) $E_g(\lambda)$ calculated from λ_{onset} and plotted as a function of the $1/n$;

b) $E_g(\lambda)$ calculated from λ_{onset} and plotted as a function of $1/n_\alpha$;

The yellow dots correspond to the T series (bithiophene side chains), the green dots correspond to the T' series (monothiophene side chains).

It is worthwhile noticing that the T and T' spider-like oligothiophenes are not planar, but are characterized by the presence of *nodes*, indicated in the Figure 23 by circles, arising at every α,α -linked thiophenes bearing pendants on the β -positions. The number of nodes is then $(n_\alpha-5)$ for the T series, and $(n_\alpha-3)$ for the T' series. The spectroscopical energy gap values were compared to the series of α -oligothiophenes, and the hypothesis made for the branched oligothiophenes illustrated before was confirmed also in this case (Figure 24).

Also in this case, the normalization with respect to $1/n$ leads to good linearities, and both lines lie above the reference series; in particular, the T' series, having higher density of nodes, has the highest energy gaps, while considering $1/n_\alpha$, the series are almost overlapping with the planar oligothiophene reference series, with some discrepancies due to the presence of *nodes*. It is worthwhile noticing that, even increasing n_α to infinite, the energy gap will not tend to zero, but to a limiting minimum value. This holds for all-thiophene series where both the oxidation and reduction sites correspond to the main conjugated chain; however, inserting a non-thiophene core, *e.g.*, an electron-withdrawing group, the oxidation and reduction sites will be differentiated, and in particular the LUMO will result to be more stabilized, thus leading to a decrease of the gap. This idea lead to the design of the so-called *genetically-modified* spider-like oligothiophenes, that will be discussed more in detail in Chapter 3.1.

Furthermore, it was found that substituents in the β -positions of thiophene have negligible effect on the effective conjugation, the β substituents being almost perpendicular to the α -conjugated chain.

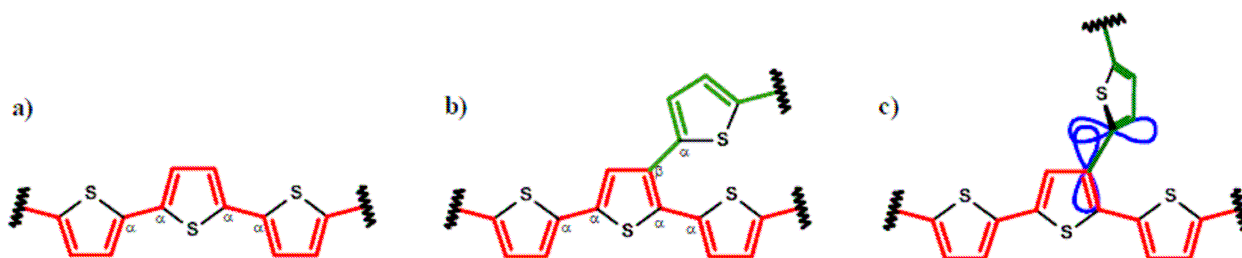


Figure 25: Schematic representation of α,α and α,β connections in oligothiophenes

In Figure 25 the conjugation along the bonds of a chain of thiophenes linked through the α positions is shown in red and, in green, the conjugative sequence of the same α -oligothiophene unit connected with a thiophene substituent in β position. Even in the latter case the communication between the green and the red double bonds could formally occur, since the double bonds of the two thiophene rings are conjugated. However, the more efficient conjugation through α - α junctions with respect to the α - β connections and the steric interactions between the rings maintain the α -conjugated chain coplanar with the sacrifice of the α - β conjugation. The aromatic ring located in β position is distorted from planarity and, therefore, there is just a small overlap of the π orbitals of the carbon atoms involved in the interanular bond.

It is interesting to compare two molecules, T14₆ and T'14₆, having the same overall number of thiophenes, and the same number of α -conjugated thiophenes in the main chain, but a different number of *nodes*.

	$E_{p,a}$ V(SCE)	$E_{p,c}$ V(SCE)	$E_{g,max EC}$ eV	$E_{onset,a}$ V(SCE)	$E_{onset,c}$ V(SCE)	$E_{g onset EC}$ eV	λ_{max} nm	$E_{g,max}$ eV	λ_{onset} nm	$E_{g,onset}$ eV
T14 ₆	1.08	-1.66	2.74	0.95	-1.49	2.44	420	2.96	515	2.41
T'14 ₆	1.11	-1.97	3.08	0.97	-1.80	2.77	370	3.35	500	2.48

It is evident, from these data, that the compound T14₆, having only one *node* instead of three, has significantly lower energy gaps, both electrochemical and spectroscopical.

The voltammetric characteristics reflect the theory of *nodes*.

In the T series, the shortest compound T9₅ is the most efficiently conjugated, and its oxidation potential is the lowest in the series, and, being the less sterically hindered, shows a better attitude to the polymerization than the others.

The most striking features of T9₅, T14₆, and T19₇ and of the polymers obtained from their electrooxidative polymerization are:

- an outstanding stability towards external agents;
- resistance under repetitive electrochemical cycling, even at negative potentials;
- similarity of the spectroscopic properties in solution and in the solid state;
- remarkable solubility in organic non polar solvents.

Starting from these results, the T' series was then developed: the introduction of 2-thienyl units on the β positions of an α -oligothiophene backbone produces effects on solubility that are very similar to those generated by conventional alkyl substitution. Moreover, the thiophene rings connected to the α -conjugated backbone through α,β junctions can also contribute to the spreading and stabilization of the charges injected into the conjugated backbone.

It is interesting to compare the voltammetric characteristics of the molecules of this series: the first oxidation potentials only shows a slight anticipation with increasing n_α . The same anticipation is observed in the case of the first reduction potentials.

Since the inductive effects in this homogeneous series can be considered approximately constant, this restricted trend reflects a limited increase of the conjugation efficiency with

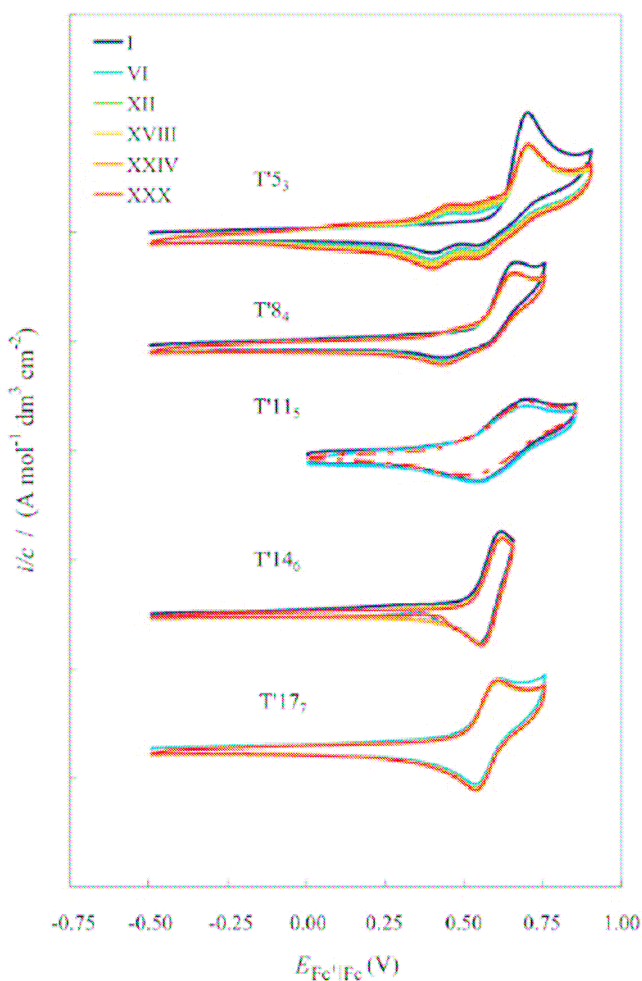
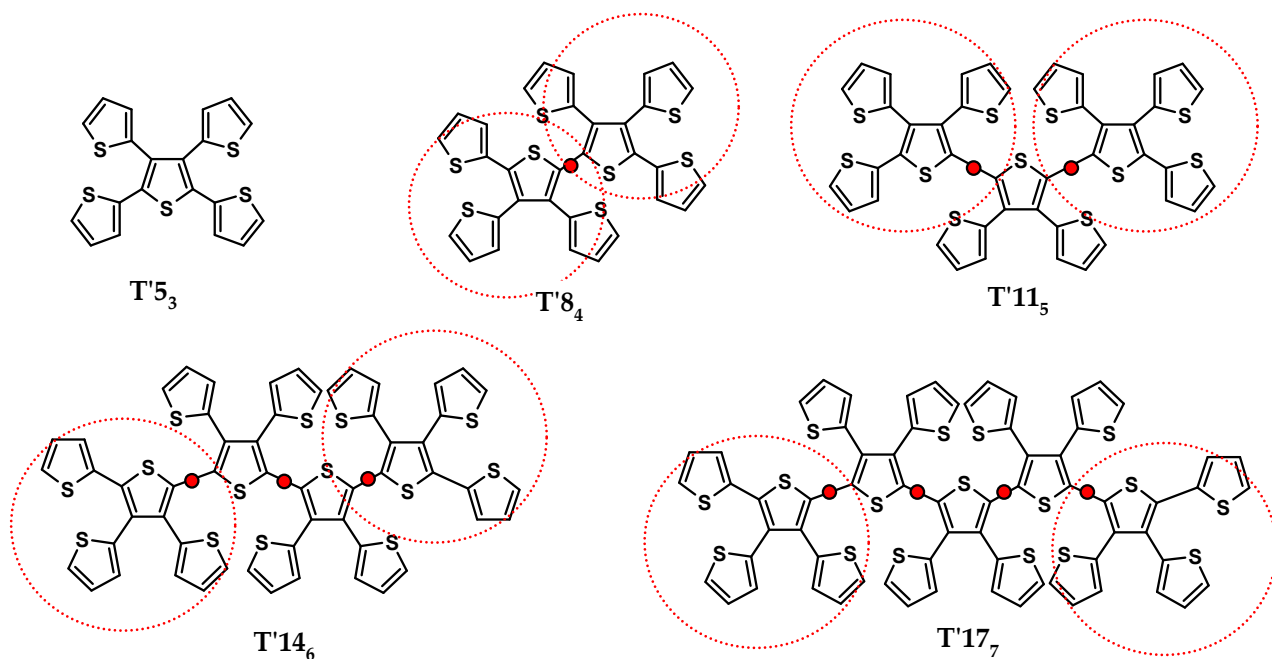


Figure 26: Synopsis of the voltammetric characteristics and polymerization attitude of the spider-like T' series. Data recorded in CH₂Cl₂+TBAP 0.1 M on a GC electrode; potentials referred to the Fc⁺|Fc couple.

the number of thiophenes because of the hampering effect by the *nodes* in the α,α -backbone. In any case, all systems have enough conjugation efficiency to afford both radical cation and radical anion stabilization within the accessible potential window.

From Figure 26, it is evident how the polymerization attitude decreases at increasing size of the molecules, and it is accompanied by an increase in the reversibility of the anodic peaks. In particular, for T'11₅ it is possible to observe two nearly equivalent oxidation peaks, which become completely equivalent in the cases of T'14₆ and T'17₇. This behaviour can be explained in terms of increasing distances between two active redox sites; the longer the distance, the more independent and equivalent the two electron transfer processes. The increasing reversibility of the monomer peaks corresponds to a decrease in the oligomerization ability. In fact, we obtained oligomerization only in T'5₃ and T'8₄, and also in T'11₅ but only increasing the monomer concentration. A possible explanation is that, with increasing steric hindrance, the probability of coupling between two radical cations localized only in the α -positions of terminal thiophenes gradually decreases. The shape of the voltammograms in the last three cases could be explained considering the nodes localization in the molecule:



The molecules have identical terminal moieties, constituted by a tetrathiophene unit, with only two α -linked thiophenes. These units constitute two identical redox centres, connected by a π -system partially hampered by the presence of nodes, at increasing distance. It is likely that, in T'11₅, those redox centres are so close that they are still interacting, giving two nearly equivalent oxidation peaks, while in the successive molecules, the increasing distance and number of nodes make the two redox sites completely independent: in these cases, the $E_p - E_{p/2}$ is about 57 mV, corresponding to a simple monoelectronic peak, but with double height with respect to the former terms of the series.

In conclusion, this work allowed to obtain a deeper understanding of the relationship between structure and electronic properties, pointing out that actually it is the number of α -linked oligothiophenes and the density of possible distortions from planarity (*nodes*) that

determine the effective conjugation and thus the electronic properties of the molecules, which is a very important rule for target-oriented molecular design. The evolution of these systems towards the *genetically-modified spiders* (Chapter 3.1) afforded a more complete picture of the electronic properties in branched oligothiophene systems, in particular in the frame of controlling the HOMO and LUMO positions and gap.

1.4 Chirality in Conducting Polymers

The availability of materials which could couple electroactivity properties and enantio-recognition capability is an ambitious objective of the modern chemical research. It would be a great innovation to find a material which could combine the potentialities of chirality (*i.e.*, the ordered spontaneous chain assembling induced by chirality, the noncentrosymmetry associated to chiral materials, which is a prerequisite for second order nonlinear optics, the ability of chiral enantiomerically enriched molecules to discriminate between antipodes, as required in sensors designed for the detection of chiral analytes, the possibility to be employed in asymmetric synthesis or electrosynthesis) with the advantages of conducting polymers (*i.e.*, electrical conductivity, redox and pH switching capability, electrochromism, relatively low cost and ease of processing, light weight) thus obtaining *chiral conducting polymers*. This kind of functional molecular materials appear to be very promising for applications in many fields, for example in asymmetric electrocatalysis, in optoelectronics, or for the development of chiral electroanalytical sensors.

According to the literature, rare are the examples of exciting results in this area, even though the number of papers and reports in this field is steadily increasing in the years¹⁹ One of the reasons for the limited success in this research area is possibly related to the design of the materials, which is a very complex task since a compromise, not easy to find, between electroactivity properties and chirality manifestations must be realized. According to the literature, the most common strategy is to attach chiral pendants (*i.e.*, sugar, aminoacid, or manmade ones, designed for specific applications) to the conjugated electroactive backbone. The presence of carbon stereocenters invariably characterizes the chiral substituents. The enantiodiscrimination properties transmitted to the backbone by the substituents depend upon the functional groups characterizing them, upon their density and distance from the electroconducting chain and upon the nature of the linker. Only in a few cases, however, significant chirality manifestations have been found in polymers designed according to this strategy, also because the experimental conditions (*i.e.*, solvent, pH, temperature...) strongly affect the chirality manifestations of the obtained polymers. In some cases, the polymers obtained by chemical oxidation by FeCl₃ are characterized by intrinsic constitutional disorder, because of random head-to-head, tail-to-tail, head-to tail junctions, and, in order to obtain regioregular polymers, long and tricky synthetic pathways have to be followed.²⁰ Another approach is to synthesize monomers featuring two identical stereocentres with C₂ symmetry²¹, as the example reported in Figure 27 : in this case, the polymer obtained both by chemical or electrochemical oxidation is regioregular, but, on the other hand, the chirality of the resulting material strongly depends

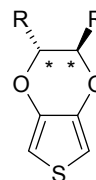


Figure 27: An example of C₂ symmetry monomer bearing two stereocentres

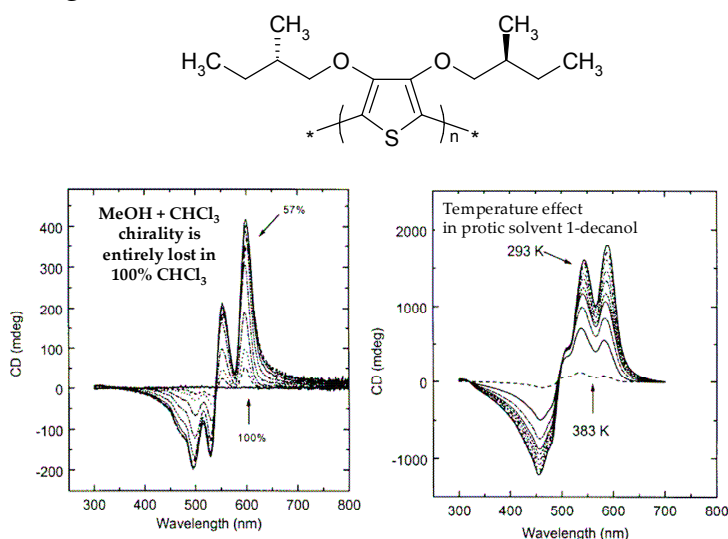
¹⁹ L. A. P. Kane-Maguire, G.G. Wallace, *Chem. Soc. Rev.*, **2010**, 39, 2545

²⁰ G. Bidan, S. Guillerez and V. Sorokin, *Adv. Mater.*, **1996**, 8, 157

²¹ D. Caras-Quintero, P. Bäuerle, *Chem. Comm.*, **2004**, 926-927

on the aggregation state of the chain, as shown by CD, and can be easily lost by passing from an aprotic apolar solvent to a polar and protic one, or by raising the temperature.

The effect of the experimental conditions is also well described in a paper by B. M. W. Langeveld-Voss and coworkers²², where the authors report on the behaviour of the



molecule in Figure 28. The observed optical activity is attributed to intermolecular helical packing of predominantly planar chains, and macroscopical chirality hinges on a supramolecular order that is lost by changing the solvent (as illustrated, with increasing percentage of chloroform in methanol), or by raising the temperature.

Figure 28: Effect of solvent and temperature on the chirality of the C₂ symmetry polymer above.

Other chiral conducting polymers can be obtained by using templating agents, for example by performing electrochemical polymerization in the presence of (+) or (-) camphorsulphonic acid²³, or by exploiting the non-covalent bond between an achiral water-soluble polythiophene and a natural polysaccharide, schizophyllan (SPG)²⁴, or even by molecular imprinting in the presence of aminoacid templates to get chiral selective cavities in the conducting polymer film²⁵.

In this context, with the support of our studies on the relationships between structure and electronic properties in branched (*spider-like*) oligothiophenes, as illustrated in the Introduction, a new strategy was developed by the group of Prof. Sannicolò, in order to accede to chiral polythiophenes (and polypyrroles), starting from chiral oligothiophene monomers in which chirality is not related to the presence of stereogenic centres external to the conjugated sequence, but results from a tailored torsion internally produced in the oligothiophene (or oligopyrrole) backbone (*inherently chiral* monomers)²⁶. This can be achieved by introducing into the monomer structure different typologies of stereogenic elements, which are designed so as to not interrupt the conjugated sequence.

²² B. M. W. Langeveld-Voss, R. A. J. Janssen and E. W. Meijer, *J. Mol. Struct.*, **2000**, 521, 285

²³ L. A. P. Kane-Maguire, G.G. Wallace, *Chem. Soc. Rev.*, **2010**, 39, 2545

²⁴ C. Li, M. Numata, A.-H. Bae, K. Sakurai, S. Shinkai, *J. Am. Chem. Soc.*, **2005**, 127, 4548

²⁵ B. Deore, Z. Chen, T. Nagaoka, *Anal. Chem.*, **2000**, 72, 3989

²⁶ F. Sannicolò, S. Rizzo, T. Benincori, W. Kutner, K. Noworyta, J. W. Sobczak, V. Bonometti, L. Falciola, P. R. Mussini, M. Pierini, *Electrochim. Acta*, **2010**, 55, 8352

The structural design (schematically depicted in Figure 29) was developed along the following guidelines:

1. A stereogenic element which does not interrupt the conjugated sequence, like an atropisomeric bithiophene or bipyrrole scaffold, is introduced into the conjugated backbone of the monomer.

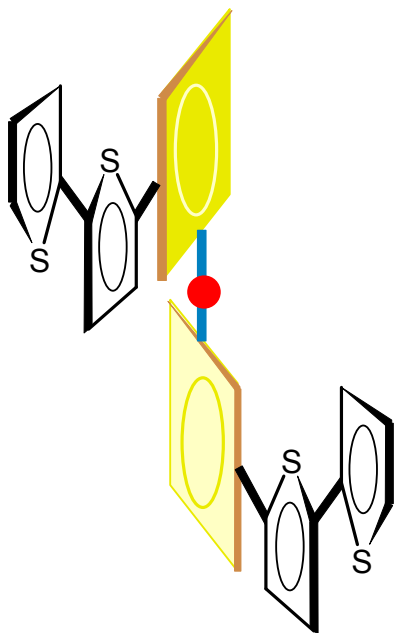


Figure 29: General structure of an inherently chiral monomer

2. The polymerization sites of the monomers must be homotopic, thus granting the perfect constitutional regularity of the polymers. This requirement is satisfied only by molecules belonging to the C_2 (and D_2) point group. In this case, being the positions involved in the polymerization homotopic, all the problems related to head-to-head, tail-to-tail or head-to-tail random couplings are suppressed. Furthermore, all the polymerization products, at any polymerization degree (dimers, trimers, etc.) are C_2 symmetric as well.

3. The synthetic accessibility of the monomers is very important. All the substrates are conceived so as to envisage the possibility of a large scale production in case of success, starting from inexpensive, commercially available materials.

4. The monomers could be properly functionalized in different positions without resorting to sophisticated, complex reactions. The introduction of selected functional

groups is important to attract the analytes into the polymer matrix by establishing specific interaction with them and/or to confer selected physical properties to the materials, solubility in organic solvents in particular, which is a very crucial parameter for processability.

According to this strategy, a complete series of *inherently chiral* monomers, here illustrated in the Figure 30, has been designed, synthesized and then characterized, revealing interesting features both as monomers and as polymers, and even both as racemate and as separated enantiomers. In fact, theoretical calculations revealed high energy barrier of rotation around the central node, as then confirmed by resolution of the products by HPLC on a chiral stationary phase at analytical, and in some cases semi-preparative levels: in all cases enantiomers could be easily separated and stored at room temperature.

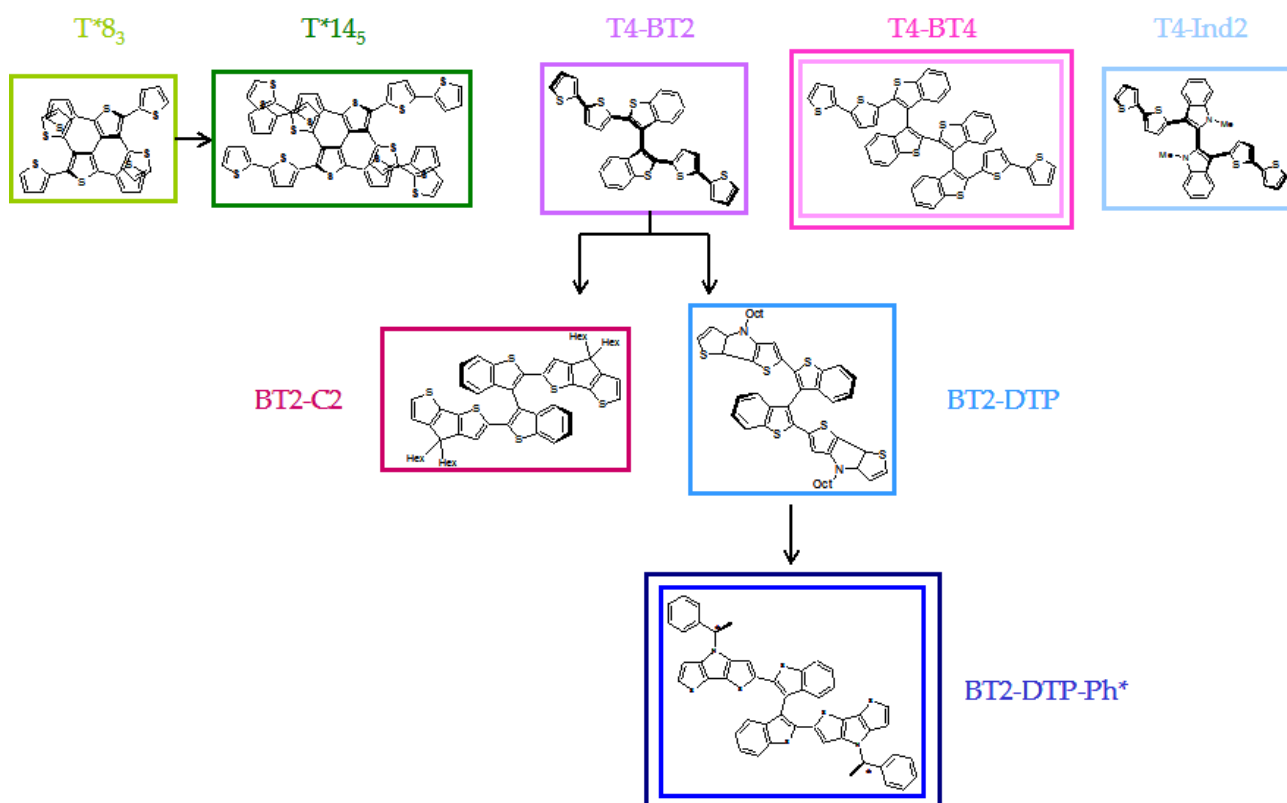


Figure 30: The series of the *inherently chiral* molecules

The acronyms in the names mean:

T = thiophene

BT = benzothiophene

Ind = N-methyl indole

C = 4,4-dihexyl-cyclopenta[3,2-b]bithiophene

DTP = N-octyl dithienopyrrole,

Ph* = (*R*)-phenylethylamine

while the number indicates the number of that kind of units in the monomer.

In the case of T^*8_3 and T^*14_5 , the star is needed to differentiate these chiral molecules from the achiral spider-like molecules belonging to previous series.

In the next sections, the voltammetric features as well as all the characteristics of these molecules, examined by means of various electrochemical, spectroscopical and solid-state techniques, will be discussed in detail.

1.5 Aim of the present PhD thesis

Starting from the very promising results described in the Introduction, the present project was planned aiming to:

- extend the knowledge on the relationship between structure and electronic properties in thiophene-based molecular materials, in particular concerning the modification of branched all-thiophene monomers (*spider-like oligothiophenes*) with a series of suitable electron richer or electron poorer cores (*genetically modified spider-like oligothiophenes*), in order to modulate HOMO and LUMO levels and HOMO-LUMO gaps for target-oriented applications, *e.g.*, in the energetics and electronics fields; as a limiting case, a new fullerene/multithiophene dyad was also developed and characterized;
- study and characterize thiophene-based monomers with high 3-D character and polymerization capability, acting as outstanding copolymer building blocks affording fast, regular and virtually unlimited polymerization of comonomers having important functional properties but poor intrinsic polymerization ability, resulting in conducting copolymer films of excellent properties, fully retaining the functional properties of the refractory comonomer;
- verify the innovative strategy of coupling electroactivity with the concept and potentialities of chirality, leading to the development of the *inherently chiral conducting polymers* family by regularly intercalating, along the conducting backbone of a polyheterocyclic system, some tridimensional stereogenic spacers capable of inducing a tailored distortion though maintaining active the conjugative communication between the different chain units.
- deal with a complete characterization of the molecules, either single molecules, monomers or polymers, in solution or at solid-state, with different techniques and combined techniques: cyclic voltammetry, electrochemical quartz crystal microbalance EQCM, UV-Vis-(NIR) spectroscopy, electron spin resonance ESR, electrochemical impedance spectroscopy EIS, circular dichroism CD, atomic force microscopy AFM and scanning electron microscopy SEM.
- complete the study of two side-works: employ the cyclic voltammetry to evaluate the impact of the electronrichness of the phosphorous centre on the *residual stereoisomerism* in phosphane and phosphane oxide propellers, and to complete the characterization, by CV, EQCM and EIS of a poly(cyclopentadithiophene) film decorated with Re(I) complex chromophore pendants, for promising applications as electrochromic material.

2. Experimental

This new quantum mechanics promised to explain all of chemistry. And though I felt an exuberance at this, I felt a certain threat, too. "Chemistry," wrote Crookes, "will be established upon an entirely new basis... We shall be set free from the need for experiment, knowing a priori what the result of each and every experiment must be." I was not sure I liked the sound of this. Did this mean that chemists of the future (if they existed) would never actually need to handle a chemical; might never see the colors of vanadium salts, never smell a hydrogen selenide, never admire the form of a crystal; might live in a colorless, scentless, mathematical world? This, for me, seemed an awful prospect, for I, at least, needed to smell and touch and feel, to place myself, my senses, in the middle of the perceptual world.

Oliver Sacks, *Uncle Tungsten*, 2001

2.1 Cyclic voltammetry

2.2.1 An introduction to CV

The term *voltammetry* is the class of electroanalytical methods offering the widest spectrum of diagnostic potentialities, providing *at the same time* qualitative, quantitative and mechanistic information concerning *all* electroactive analytes present in the working solution and on the electrode surface, by recording, in a three-electrode cell, the current (\div rate of the electron transfer process) flowing between the working electrode W and a counter electrode C as a function of the potential (\div energy) applied to the working electrode W with respect to a reference electrode R with a regular modulation with time.

The signals can be either step-like, obtained by varying the potential very slowly (*i.e.*, working in stationary conditions), or peak-like, obtained by varying the potential in a faster way (*i.e.*, working in non-stationary conditions), or as a consequence of specific signal treatment (in some highly sensitive methods).

The most common working electrodes are *microelectrodes*, implying superficial areas of about a few square millimeters (with *ultramicroelectrodes* (UME), of smaller dimensions, affording exceptional performances in peculiar cases). As a consequence, during the analysis the analyte consumption is minimal and thus the voltammetry can be considered as a non-destructive technique at macroscopic level. Generally, the working electrodes are solid (metals, graphite, oxides, *etc.*). There are two particular and very important exceptions: the rotating disk electrodes, for kinetic studies, and the mercury electrodes. The latter could be stationary electrodes in hanging mercury drop mode (*hanging drop mercury electrode*, HDME).

In particular, *cyclic voltammetry* is the technique of choice for preliminary investigations of redox active species in solution and/or on the working electrode surface.

In this technique

- a **stationary electrode (metal or non-metal)** is employed as working electrode;
- the potential is **scanned along a triangular waveform, implying the same scan rate in both directions**;
- Since the potential scan rate is usually **very high** (~20-20000 mV/s) **non-stationary waves** (peak-like) are usually obtained working on normal microelectrodes, albeit *convolution* can afford transformation of the peak signal in a stationary-like step one.

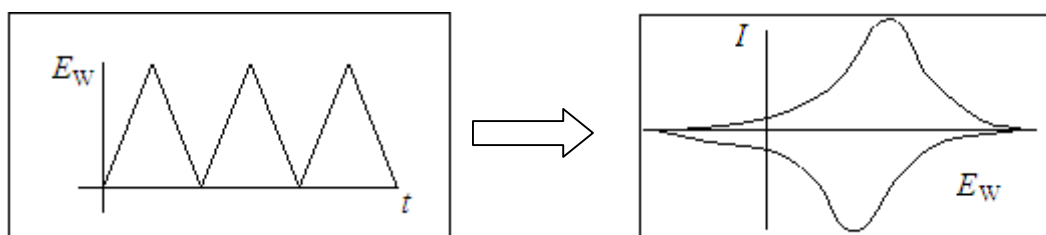


Figure 1a: Perturbation and answer of a typical cyclic voltammetry

Experiments are performed using a potentiostat/galvanostat combined with a function generator managed by a PC, and a three-electrode cell, including, as above mentioned:

- a **working electrode WE**, on which the electron transfer ET processes under study take place, involving any species redox active in the available potential window, either diffusing to the surface from the solution bulk, or present on the electrode surface (*e.g.* as thin films or adsorbed species). In particular, the ET processes are studied monitoring the current I flowing between the working electrode and a counter electrode as a function of the E_w potential measured with respect to a reference electrode;
- a **reference electrode, Ref**, characterized by an invariant potential E_R ;
- a **counter electrode, CE**, completing the electrical circuit in which current I flows. This electrode cannot coincide with the reference electrode because a counter reaction (of opposite sign with respect to the reaction on the working electrode) occurs on it, thus preventing the control of its potential. Albeit the ET process is studied in terms of I vs E_w characteristics, the potential difference between working electrode and counter electrode (in practice between cathode and anode or *vice versa*) is also a significant parameter, particularly for the optimization of the operating circuit in the preparative tests, and is termed *cell voltage*.

The technique answer is, as already mentioned, a current I (y axis) as a function of E_w potential (x axis).

In particular a signal for every charge transfer is obtained with respect to a rectangular-shaped background (corresponding to the capacitive current for double-layer charging). Peak potentials E_p (or, in the case of steps, half-wave potentials $E_{1/2}$) identify the species that are oxidized or reduced and thus allow qualitative analysis; concurrently, peak

currents I_p (or, in the case of steps, limiting currents I_L) are proportional to the reagent concentration and afford quantitative analysis.

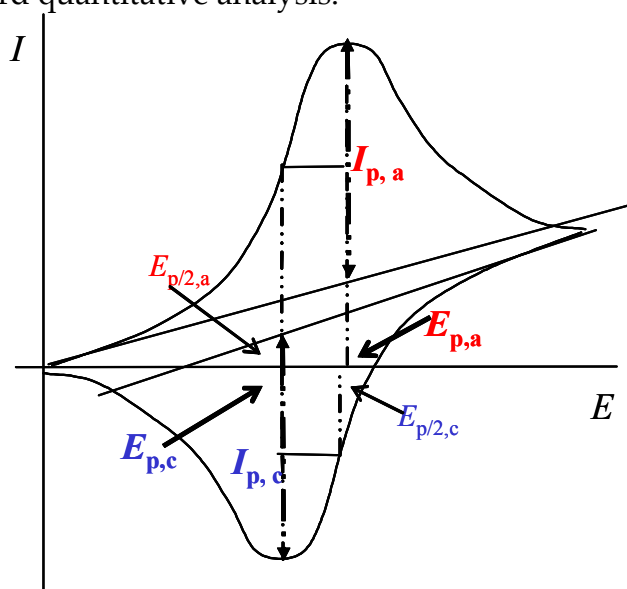


Figure 1b: Most important parameters characterizing a cyclic voltammetry peak

Obviously, with the exception of the mercury (which is easily renewable in a reproducible way), the CV answer is connected to the working electrode previous “story”; in particular, it could have been poisoned or covered by an insulating film. For this reason it is very important to carry out convenient electrode surface pre-treatments (*e.g.* mechanical, ultrasound and electrochemical polishing), ensuring a clean and active surface and, thus, a reproducible answer.

The voltammograms could change upon cycling, tending to a stationary one; in this frame the most important cycles are the first one (implying fresh surface) and the stationary one.

Concerning the analysis of the voltammetric peaks:

- currents are generally normalized with respect to (a) the electrode surface area (b) the substrate concentration (c) the square root of scan rate (in case of faradaic *diffusive* ET processes, *i.e.* involving redox active species diffusing to the surface from the solution bulk) or the scan rate (in case of pseudocapacitive ET processes, involving surface-confined redox active species, as in the case of adsorbed species or electroactive thin layers);
- tests with subsequent reagent additions can be useful to study the peak behavior when varying the analyte concentration, to verify possible modifications on the voltammetric curve and, in particular, to obtain a further criterion to distinguish between adsorptive peaks (tending to an asymptotic current with surface saturation) and diffusive peaks (that grow proportionally with the concentration).

The most important parameters for the interpretation of experimental results are described below:

E_p vs $\log v$. Usually a linear trend is observed; possible deviations at increasingly high scan rates can be associated to (a) uncompensated ohmic drop (see below); (b) changes of ET mechanism. The slope of the linear characteristic gives information about the electrochemical reversibility (*i.e.* facility) of the ET process corresponding to the voltammetric peak. The two extreme cases are complete electrochemical reversibility (negligible activation barrier for ET), resulting in zero slope, and electrochemical irreversibility, with a slope increasing with the irreversibility degree (*i.e.* with the ET activation barrier becoming more and more determining). A possible transition between reversibility and irreversibility results in curvilinear trends.

$(E_p - E_{p/2})$ vs $\log v$ Also this parameter provides a further proof of ET electrochemical reversibility, in particular for a completely reversible monoelectronic peak this difference is 0.057 V at 298 K at any scan rate. Increasing irreversibility results in larger $(E_p - E_{p/2})$ values, increasing with increasing scan rate.

i_p vs. $v^{1/2}$, i_p vs. v :

Faradaic peaks typically show a linear i_p vs $v^{0.5}$ dependence, for either reversible or irreversible processes. In particular:

“Nernstian” faradaic process: $(2.69 \cdot 10^5) n^{3/2} D_o^{1/2} c_0^b v^{1/2}$ at 25°C.

Monoelectronic irreversible faradaic process: $(2.99 \cdot 10^5) \alpha^{1/2} D_o^{1/2} c_0^b v^{1/2}$ at 25°C.

Since α is usually ~ 0.5 , the slope is usually lower in the irreversible case; quasi-reversibility is characterized by a transition between the two limiting conditions.

Adsorption peaks peaks typically follow a linear i_p vs v dependence, as in the following case:

$$i_p = \frac{n^2 F^2 v \Gamma_o^b}{4RT}$$

Superimposing faradaic peaks obtained at different potential scan rates and normalized as previously explained, they have to perfectly coincide for reversible processes (albeit the capacitive background, varying with v , will become increasingly higher with respect to the faradaic signal), while for irreversible processes they have to shift at more extreme potentials, without significant variations in their shape, unless a change in the mechanism occurs.

In the case of specific adsorption of reagents or products, ancillary peaks appear with respect to the main one, with the following peculiar features:

- as mentioned above, they tend to an asymptotic value with increasing substrate concentration, corresponding to saturation of the surface active sites;

- they typically depend on the scan rate v rather than on $v^{0.5}$, just like the capacitive background current, and for this reason they are usually termed "pseudocapacitive" peaks;
- In the case of reagent adsorption, the ancillary peak *follows* the main one (adsorbed reagent molecules are thermodynamically stabilized and thus the reaction ΔG is less favourable); in the case of product adsorption, the ancillary peak precedes the main one (adsorbed product molecules are thermodynamically stabilized and thus the reaction ΔG is more favourable);
- The presence of strong side interactions between adsorbed molecules results in a narrower peak;
- A chemically reversible ET involving adsorbed species typically results in symmetrical forward and backward peaks.

Chemical and electrochemical reversibility: the backward peak. The presence of a backward peak and its relative height with respect to the forward one account for the degree of *chemical* reversibility of the reaction. In particular, the absolute value of the ratio of the i_p related to the two peaks should be close to 1 for a diffusion-controlled process in case of complete chemical reversibility. On the other hand, the E_p forward – E_p backward distance between the peaks provides a further proof of the degree of *electrochemical* reversibility (along with the above mentioned E_p vs $\log v$ and $E_p - E_{p1/2}$ criteria), being constant and equal to 0.057 V at 298 K for an electrochemically reversible monoelectronic process, while being higher and increasing with increasing scan rate for an electrochemically irreversible one.

Peak convolution²⁷. In any case it is possible to convert voltammograms obtained in non-steady state conditions (peak-shaped), into stationary signals (step-shaped) by a mathematical operation called "convolution"

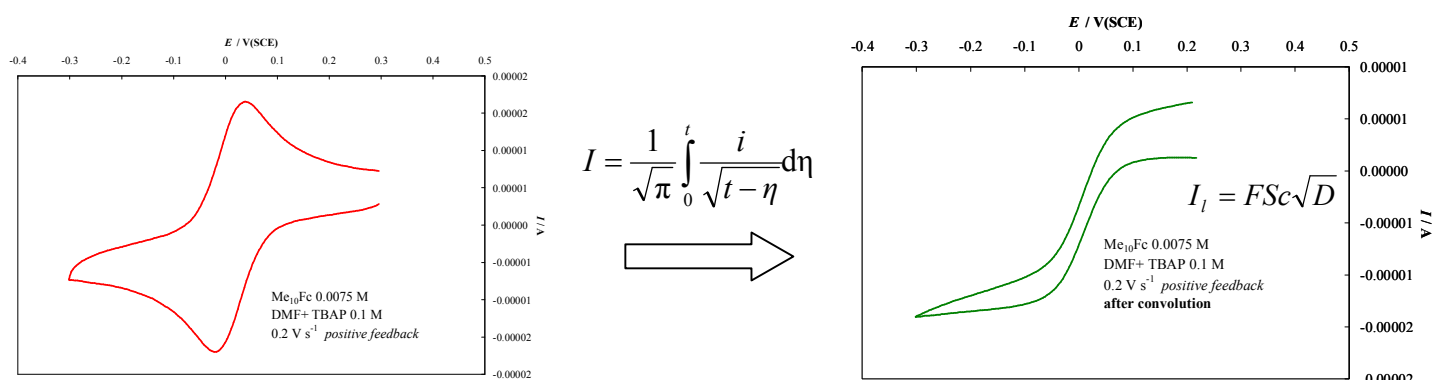


Figure 2: Example of peak convolution

²⁷ A.J. Bard, L.R. Faulkner, *Electrochemical Methods: Fundamentals and Applications*, 2nd ed., Wiley, New York, 247-252, 2001

C.P. Andrieux, J-M. Savéant, *J. Electroanal. Chem.*, **1970**, 25, 147

J. C. Imbeaux, J-M. Savéant, *J. Electroanal. Chem.*, **1973**, 44, 159

Ohmic drop compensation

The aim of voltammetry, as of many other electrochemical experiments, is to correlate the electrodic double layer potential with the current flowing inside it. Although the current is easily measured, the potential is always prone to error, because the measurement cannot be done in direct contact with the solution side of the double layer. The small distance between the measurement point and the ideal measurement point causes a potential drop iR_u (induced by the current flowing through the electrolyte) that is added to the measured potential. In most cases, such potential drop is negligible because the currents are very low (in the order of microampères) and thus, since the resistance is in the order of hundreds of ohms, the potential difference is in the order of millivolts. In other cases, the error is remarkable and methods for the measurement correction are necessary. The most used method is the *positive feedback*, in which the instrument interposes, in the measurement circuit, an IR term, with a smaller and opposite value to the effect to be compensated. This method requires the preliminary evaluation of the system resistance.

The effect of a lack in the ohmic drop compensation is similar to an increase of irreversibility: the peaks are larger, lower in height, and more separated. So the ohmic drop compensation is essential for mechanistic studies based on the morphologic evaluation of the peaks.

If cyclic voltammetry is used for the monomer electropolymerization, as in the cases studied in the present PhD work, it is convenient not to apply the ohmic drop compensation, if not strictly necessary for mechanistic studies, since the reagent concentration variations, on account of possible solvent evaporation during the experiment, can lead to more concentrated working solution, and thus the IR term, set during the *positive feedback* operation, could be too high, causing a short circuit that burns the electrode surface together with the material deposited onto it.

Morfology of CV peaks related to a simple ET

A simple electron transfer, without any successive chemical reaction, could be:

- **[electrochemically] reversible**, if its activation barrier is negligible; when the reagent reaches the electrode, it undergoes facile electron transfer and it is instantaneously transformed into the product. So the current (*i.e.*, the rate of the process) is controlled only by the diffusion, *i.e.*, the current is simply the rate at which the reagent comes to the electrode by diffusion within the diffuse layer δ (*i.e.*, the layer close to the electrode where convection cannot completely renovate the reagents consumed by the reaction). In this case the standard potential E° and the diffusion coefficient D are the main parameters to take into account.
- **[electrochemically] irreversible**, if the activation barrier is significant, and the charge transfer step results to be kinetically determining with respect to diffusion. In this case, the charge transfer constant k_{ET} and the activation barrier symmetry parameter α (that describes the position of activated complex with respect to reagents and products; it can variate between 0 and 1 and when it is equal to 0.5, the reaction intermediate is equidistant from reagents and products) are the main parameters to take into account.

The CV peak morphologic features with the related diagnostic criteria concerning the ET mechanism, are reported in the following Table for both cases (Table 1)

E_{rev}	E_{irr}
$E_{p,c} = E^0 - 1.11 \frac{RT}{F}$ $E_{p,a} = E^0 + 1.11 \frac{RT}{F}$ <p>the distance between E_p and E^0 is equal to 0.0285 V at 25 °C</p>	$E_{p,c} = E^0 - 0.78 \frac{RT}{\alpha F} + \frac{RT}{\alpha F} \ln \left(k_s \sqrt{\frac{RT}{\alpha F v D}} \right)$ $E_{p,a} = E^0 + 0.78 \frac{RT}{\alpha F} + \frac{RT}{(1-\alpha)F} \ln \left(k_s \sqrt{\frac{RT}{(1-\alpha)F v D}} \right)$
<p>E_p constant with both v and c</p>	$\frac{dE_p}{d \log v} = \frac{2.303RT}{2\alpha F} = \frac{0.02958}{\alpha} \text{ V a } 25^\circ\text{C}$ <p>The peak is shifted to more extreme potentials; the higher the process irreversibility, the faster the shift</p>
$ E_{p/2} - E_p = \frac{2.20RT}{F} = 0.0565 \text{ V at } 25^\circ\text{C}$	$ E_{p/2} - E_p = \frac{1.857RT}{\alpha F} = \frac{0.047709}{\alpha} \text{ V a } 25^\circ\text{C}$ <p>The more irreversible the process, the broader the peak distance</p>
$ E_{p,fw} - E_{p,bw} = \frac{2.22RT}{F} = 0.057 \text{ V at } 25^\circ\text{C}$	<p>If the backward peak is present, the more irreversible the process, the greater the separation of the peaks.</p>
$i_p = \frac{I_p}{S} = 0.446Fc\sqrt{D} \sqrt{\frac{Fv}{RT}}$	$i_p = \frac{I_p}{S} = 0.496Fc\sqrt{D} \sqrt{\frac{\alpha Fv}{RT}}$ <p>For E_{irr}, usually $\alpha \sim 0.5$, so the current is lower than in an E_{rev}</p>

Table 1: CV peak characteristics for an ET mechanism, where the electrochemical step is reversible (left side) or irreversible (right side).

It is interesting also to compare the characteristics of a peak corresponding to to a simultaneous reversible transfer of two electrons ($2e^-$)²⁸. In the vacuum the ingress/egress of a second electron is an unfavoured process with respect to the first one because of the coulombic repulsion between charges; accordingly, the second reduction/oxidation peak of a molecule should always be shifted towards more extreme potentials (higher energies) than the first one.

However, by operating in a polar solvent, the free energy of solvation of a dianion (or dication) is generally more than double than that of the monoanion (or monocation), and thus the solvation can result in the second ET approaching the first one, and even, in limiting cases, in the second ET resulting more advantageous than the first one. These molecules show peaks commonly termed as *bielectronic*, having in an electrochemically reversible case the features collected in Table 2.

²⁸ J-M. Savéant, *Elements of Molecular and Biomolecular Electrochemistry. An Electrochemical Approach to Electron Transfer Chemistry*. Wiley, New Jersey, 62-73, 2006

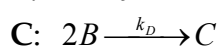
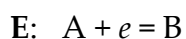
$E_{2 \text{ rev}}$
$E_{p,c} = E^0 - 1.11 \frac{RT}{2F}$ So, the distance between $E_{p,c}$ and E^0 is 0.0143 V at 25°C. In the bielectronic case, the peak potential is closer to the standard potential than in the monoelectronic one.
E_p constant with v and c
$E_{p/2} - E_p = 1.10 \frac{RT}{F}$ (28.3 mV at 25°C) The bielectronic wave has about half width of the monoelectronic one
$E_{p,forward} - E_{p,backward} = 1.11 \frac{RT}{F}$ (28.5 mV at 25°C) In the bielectronic wave, in case of chemical reversibility, the distance between forward and backward peak is half of the monoelectronic one
$i_p = 2\sqrt{2} \times 0.446 FSc\sqrt{D} \sqrt{\frac{Fv}{RT}}$ The bielectronic wave is more than double higher than the monoelectronic one.

Table 2: CV peak characteristics corresponding to an electrochemically reversible two electron simultaneous transfer.

The case of electropolymerization

The generally accepted mechanism of electropolymerization of conducting polymers, particularly for thiophene-based systems, as previously discussed in Chapter 1.2, consists in an $E(CE)_n$ sequence, with an alternation of chemical steps (*i.e.*, deprotonation of cations and rearomatization of the system, that constitutes the *r.d.s.* of mechanism) and electronic transfers, that follow the initial oxidation step. For these reasons, the mechanism could be included in the particular case of the electrodimmerization, in a general scheme of an $E_{rev}C$ system.

In the following Table 3, the criteria to recognize the specific case of an EC process where the chemical step, kinetically determining, is a dimerization, are reported²⁹



²⁹ J-M. Savéant, *Elements of Molecular and Biomolecular Electrochemistry. An Electrochemical Approach to Electron Transfer Chemistry*. Wiley, New Jersey, 2006, p.102-106

$E_{rev}\underline{C}$ Particular case of electrodimerization $A \pm e = B ; 2B \xrightarrow{k_D} C$
$E_{p,c} = E^0 - 0.903 \frac{RT}{F} + \frac{RT}{3F} \ln \left(\frac{RT}{4F} \frac{k_D c}{v} \right)$
$\frac{dE_p}{d \log v} = 0.0197 \text{ V a } 25^\circ\text{C} \quad \frac{dE_p}{d \log c} = 0.0197 \text{ V a } 25^\circ\text{C}$
$ E_{p/2} - E_p = \frac{1.51RT}{F} = 0.0388 \text{ V a } 25^\circ\text{C}$ <p>The peak is narrower with respect to the case of a simple $E_{rev}\underline{C}$ but broader than that of a bielectronic E_{rev}</p>
<p>Lack of the backward peak</p>
$i_p = \frac{I_p}{S} = 0.527 F c \sqrt{D} \sqrt{\frac{Fv}{RT}}$ <p>The current is even higher than the case of simple $E_{rev}\underline{C}$</p>

Table 3: CV peak characteristics in the case of electrodimerization

2.1.2 The voltammetric cell and the electrodes³⁰

Cyclic voltammetry is the main technique employed in our study on oligothiophene systems, and it has been performed in many different conditions (*i.e.*, changing the electrode materials, the solvent, the supporting electrolytes,...) to evaluate the effect of different parameters on the behaviour of the molecules under investigation.

Cyclic voltammetry is a three-electrode technique and employs a working electrode, a counterelectrode and a reference electrode, as explained in Chapter 2.1.

In our experimental protocol, the counter electrode was generally a platinum wire or a platinum sheet, in cases where a more extended surface was needed to afford a more homogeneous electric field between the counterelectrode and the working electrode, thus allowing a better electrodeposition.

The reference electrode was KCl-saturated calomel, in a double bridge filled with the working solution, to avoid as much as possible any leakage of KCl in the electrochemical cell. Overnight, the double bridge was kept in 65% nitric acid and carefully rinsed first with water and then with acetone, and dried in the oven before use. The SCE was kept in a

³⁰ Valentina Bonometti, M.Sc. Thesis, Università degli Studi di Milano, 2009

saturated KCl solution, and rinsed before use. The KCl saturation and bias potentials of the entire laboratory SCE batch were periodically verified. In the CV sessions the SCE potential was regularly tested against the ferrocene/ferricinium redox couple³¹, as recommended by IUPAC, in a fresh monomer-free working solution. Very importantly, referencing CV data to ferrocene also afforded intersolvental normalization of experiments carried out in different solvents and estimation of (approximate) absolute potential and HOMO and LUMO values.

Other reference electrodes were used for specific purposes, e.g. Ag|AgCl or Ag pseudoreferences, in cases where a small-dimension electrode was needed.

Concerning the working electrode, various types have been used:

- *Glassy carbon electrode*: embedded in Teflon[®], having a surface of 0.071 cm²; this actually was the most used electrode in the experimental work of the present PhD thesis, on account of its non-catalyticity, a desirable condition for characterization of the *intrinsic* reactivity of the molecular materials under study.
- *Au tip*: embedded in Teflon, having a surface of 0.0355 cm², it has been used to check possible specific effects in the electrochemistry of oligothiophene systems, on account of the well known specific affinity of sulphur atoms for gold surfaces.
- *Pt disk electrodes*: having a surface of 0.00785 cm², it has been used mainly at the Polish Academy of Science as the routine working electrode in local protocols.

The above mentioned electrodes were activated and polished before every experiment and also during it (every time it was necessary to clean the electrode surface from reaction residuals) with diamond powder (granulometry 1 μm) on a Struers DP Nap wet cloth, followed by rinsing with deionized water.

- *Pt grid*: to perform ESR measurements
- *Pt or Au sheet*: to deposit thick layer of electroactive films, to be collected for MALDI measurements.

All the above mentioned electrodes were kept in 65% nitric acid overnight to remove any traces of organic residuals.

- *ITO (Indium Tin Oxide) electrodes*: these transparent electrodes (having a resistance of 8-12 Ω/sq) were used to perform spectroelectrochemical analysis and circular dichroism. They allowed to appreciate the electrochromism of the oligothiophene films upon oxidation and reduction cycles even at naked eye. The ITO electrodes were rinsed in ethanol or isopropanol in an ultrasonic bath and then dried before use, and considered as monouse electrodes.
- *Au-coated glass slides*: this kind of electrodes were used at the Institute of Physical Chemistry of the Polish Academy of Sciences, being a good substrate for deposition of films for AFM imaging

³¹ G. Gritzner, J. Kuta, *Pure Appl. Chem.*, **1984**, 56, 461; G. Gritzner, *Pure Appl. Chem.*, **1990**, 62, 1839

- Au-coated AT-cut quartz crystals, 10 MHz and 5 MHz: these are the electrodes employed in EQCM experiments. The crystals were rinsed before use in water and ethanol, and considered as monouse electrodes, since the removal of the polymeric film may damage the sputtered gold layer. It is possible, however, to remove thin polymer layers with *piranha* solution ($\text{H}_2\text{SO}_4 : \text{H}_2\text{O}_2 = 3 : 1$ v/v) for about five minutes, or with diluted sulphuric acid.
- Recently, with the aim of optimizing the reproducibility of the electrodepositions, screen-printed electrodes by DropSens® have been used (Figure 3). Actually these electrodes are a complete electrochemical cell, consisting in a ceramic support with the three electrodes: the working electrode (carbon, platinum or gold), the counterelectrode (platinum or the same material as the working electrode) and a reference electrode (actually, a silver pseudoreference). These electrodes are monouse but the perfectly reproducible geometry of the system makes all the screen-printed electrodes equivalent, thus the reproducibility of the electrodeposited films was guaranteed, in spite of employing a pseudoreference (in any case, normalization with the Fc couple was carried out).

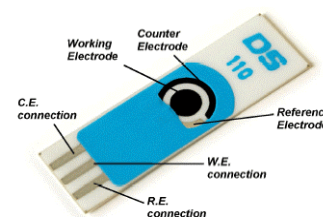


Figure 3: An example of a DropSens® screen printed electrode.

2.1.3 The experimental setup and the analysis protocol

For the voltammetric experiments, potentiostats AUTOLAB PGSTAT12, AUTOLAB PGSTAT128, AUTOLAB PGSTAT101 and PGSTAT302N equipped with the FRA2 module for the EIS measurements, by Metrohm (Switzerland), equipped with the GPES 4.9 or NOVA 1.7 softwares for experimental data elaboration were used. The technique was a staircase voltammetry, with potential step variations. The ohmic drop compensation was applied with the positive feedback technique only for the monomer characterization and for the stability tests on the electrodeposited polymer films in monomer-free solution, but not for the electrodepositions, to avoid possible burning of the growing film and/or electrode due to possible variation in the supporting electrolyte concentration on account of organic solvent evaporation.

The analysis protocol concerned:

- the voltammetric characterization of the monomer, generally at $5 \cdot 10^{-4}$ M concentration in a 4 cm³ working solution (dichloromethane or acetonitrile and 0.1 M supporting electrolyte, either tetrabutylammonium perchlorate, TBAP or hexafluorophosphate, TBAPF₆), scanning the potential in the anodic-cathodic direction in the whole available potential window, and then, after polishing the working electrode, in the opposite direction, in order to evaluate the anodic and cathodic peaks of the molecule under investigation without interferences due to previous reduction or oxidation reactions.

From the distance between the first anodic and the first cathodic peak, it is possible to evaluate the HOMO-LUMO gap, and the position of the peaks can be correlated to the HOMO and LUMO levels by the following equations³²:

$$E_{HOMO}(eV) = -1e \cdot [E_{p,a}(V \text{ vs } Fc^+ | Fc) + 4.8 (V \text{ } Fc^+ | Fc \text{ vs zero})],$$

$$E_{LUMO}(eV) = -1e \cdot [E_{p,c}(V \text{ vs } Fc^+ | Fc) + 4.8 (V \text{ } Fc^+ | Fc \text{ vs zero})].$$

These equations are consistent with the absolute value for the normal hydrogen electrode (NHE) critically assessed in the fundamental review paper by S. Trasatti³³.

In literature, many possible approaches to the calculation of the HOMO and LUMO levels are adopted³⁴, often without specifying the adopted criteria and protocols, thus resulting in a misleading confusion in this field. In this work, the same working conditions were used, so the calculated values, eventually referred to the Fc⁺/Fc couple, are comparable. More detailed considerations of the meaning of these different approaches are reported in a very recent paper by A. Tacca and coworkers³⁵: concerning the calculation of the HOMO LUMO levels and gap, the most popular calculation criteria are the *onset* one (based on onset absorption wavelengths and onset peak potentials) and the *maxima* one (based on maxima absorption wavelengths and peak potentials). Actually, considering both the responses of both UV-vis and CV methods in terms of intensities (either absorption or current ones) observed as a function of applied energies:

- (i) in both cases the *onset* criterion corresponds to the minimum energy required to obtain minimum detectable intensity (either absorption or current one);
- (ii) in both cases the *maximum* criterion corresponds to the energy related to observation of maximum intensity (either absorption or current one).

However, in the simpler case of UV-vis absorption, involving electron promotion between intramolecular energy levels, the significance of the two approaches is much more straightforward:

- (i) the *onset* criterion provides estimation of the energy required for the process by the molecule in the most favourable conformation (*i.e.*, the one having the most effective conjugation), albeit not the most populated one; the electrochemical onset was calculated, for well-defined peaks, according to the formula $E_p - 2E_{p/2}$ and verified on the voltammogram. In case of ill-defined peaks, the onset was estimated graphically with the tangent lines.
- (ii) the maximum criterion provides estimation of the energy required for the process by the molecule in its most populated conformation, albeit not the most favourable one.

The electrochemical case, while providing essential additional information with respect to the spectroscopic one (in particular, HOMO and LUMO levels besides the HOMO-LUMO gaps), corresponds to a much more complex process, *i.e.* heterogeneous electron transfer.

³² W.-Y. Wong, X.-Z. Wang, Z. He, A.B. Djuricic, C.-T. Yip, K.-Y. Cheung, H. Wang, C.S.K. Mak, W.-K. Chan, *Nat. Mater.*, **2007**, 6, 521.

R.S. Ashraf, M. Shahid, E. Klemm, M. Al-Ibrahim, S. Sensfuss, *Macromol. Rapid Commun.*, **2006**, 27, 1454

³³ S. Trasatti, *Pure Appl. Chem.*, **1986**, 58, 955-966

³⁴ C. M., Cardona, W, Li, A. E. Kaifer, D. Stockdale, G.C. Bazan, *Adv. Mater.*, **2011**, 23(20), 2367-2371

³⁵ A. Tacca, R. Po, M. Caldararo, S. Chiaberge, L. Gila, L. Longo, P. R. Mussini, A. Pellegrino, N. Perin, M. Salvalaggio, A. Savoini, S. Spera, *Electrochim. Acta*, **2011**, 56, 6638– 6653

Therefore in the electrochemical case the onset and maxima conditions are related to a much more complex bundle of parameters, which depend on the specific reaction mechanism and can be significantly influenced by the experimental conditions. A particularly critical case is when the electron transfer processes are electrochemically irreversible (*i.e.* they involve a significantly high electron barrier), since in this case the peak potentials E_{max} exhibit high ($dE_{max}/d\log v$) slopes. This can result in scarce reproducibility of the estimated HOMO and LUMO levels and gaps, albeit relative comparison at constant scan rate could be acceptable in a systematic molecule series, provided that all other conditions be kept constant.

However, in the electrochemical case a third approach is possible besides the above E_{max} and E_{onset} ones, hinging on the standard potentials E° for the considered electron transfers (or better formal potentials $E^{\circ'}$). This criterion, being independent on both scan rate and concentration, and directly related to the process ΔG° , is obviously the safest, most reproducible, best defined, and therefore most significant one. However, it is often not applicable since the E° parameter can be easily evaluated without further mechanistic analysis only when electrochemically and chemically reversible peaks are observed, *i.e.*:

- having low activation barrier and therefore low or null $dE_{max}/d\log v$, and
- resulting in a stable product, affording the back ET process), for which $E^\circ \gg (E_{max,forward} + E_{max,backward})/2 \gg E_{1/2}$ (from peak convolution). This is unfortunately seldom the case when dealing with monomers having high polymerization aptitude.

Therefore, considering that it is necessary to compare all systems along the same criterion, in our case only the *onset* and *maxima* criteria can be applied.

In our case both these criteria can be considered well defined and reproducible, because the peak potentials generally do not vary very much with scan rate; furthermore, since we are not dealing with a thermodynamic calculation but with an extrathermodynamic estimation, which *inter alia* involves as the key parameter the ferrocene couple absolute energy level, whose reliability is still under discussion, the HOMO and LUMO levels estimated by the first two criteria could be considered significant, both taken *per se* and, even more so, in relative terms.

In any case it is evident that it is very important to try to maintain the same working conditions in the case of estimating values to be compared.

In particular, the working protocol included the following steps:

- the anodic and cathodic peaks of the molecule under investigation were characterized one by one, at different scan rates;
- the electropolymerization was then performed, by cycling the potential in a potential window, whose amplitude was determined on the basis of the preliminar monomer characterization (generally, including the anodic peak corresponding to the α -positions of the terminal thiophenes, that are the active positions for the coupling process, as explained in Chapter 1.2);
- the electrodeposited polymer film underwent repeated potential cycling in a monomer-free solution, even at different scan rate, in order to achieve a sort of film *conditioning* (*e.g.*, equilibrating it with the monomer free medium, while also possibly activating and linking to the growing oligomer some monomer molecules,

entrapped in the polymer network, and let it rearrange its three-dimensional structure after the growing process) and to evaluate peculiar film behaviours, *e.g.*, the charge trapping effect (as described in Chapter 1.2)

In general, it is a really hard task to obtain perfectly reproducible polymer films, in terms of their physico-chemical properties, working with traditional volatile organic solvents, on account of their possible evaporation during the experiment, that leads to significant changes in the concentration of the working solution, besides implying safety problems and requiring addition of high amounts of supporting electrolyte to obtain the necessary conductivity. These problems could be overcome by shifting to non-conventional media such as room temperature ionic liquids (RTILs). In fact, RTILs present various desirable advantages over molecular solvents, including negligible vapour pressure, high intrinsic conductivity without addition of supporting electrolyte and easy recyclability³⁶.

Moreover, specifically dealing with electropolymerizations, preliminary studies³⁷ point to ionic liquids, both as such and as cosolvents, significantly improving the regularity and the mechanical and morphological properties of the conducting films to be employed, *e.g.* in the energetic, optoelectronic, and sensoristic domains. Furthermore, ILs are polar, a feature that could help the stabilization of the charged polymerization intermediates, the polymer doping level can be significantly higher, on account of the much higher ion availability in ILs, the degree of solvent swelling of the polymer films (which should be lower in ILs), significantly impacts on the ion mobility within the polymer, and thus on the latter's electrochemical activity, and, finally, ILs allow better oligomer solubility, on account of their polar nature, and control the extent to which they diffuse away from the electrode, on account of their high viscosity. Also the reconditioning of the conducting film network after storage should be less critical, since there would be no solvent evaporation and electrolyte concentration within the film.

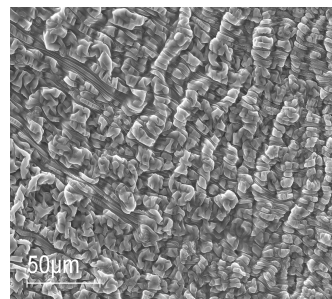
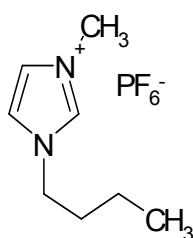


Figure 4: (left) Molecular structure of BMIMPF₆ and (right) SEM image of a layer of BMIMPF₆ on a GC screen printed electrode

In particular, 1-butyl-3-methylimidazolium hexafluorophosphate BMIMPF₆, was chosen for our first experiments in ionic liquids, since it showed good performance in thiophene-based monomer electropolymerizations³⁸, it has the same counter anion as for the former

³⁶ F. Endres, A.P. Abbott, D.R. MacFarlane, *Electrodeposition from Ionic Liquids*, 2008, Wiley-VCH, ISBN 978-3-527-31565-9

³⁷ F. Endres, A.P. Abbott, D.R. MacFarlane, *Electrodeposition from Ionic Liquids*, 2008, Wiley-VCH, ISBN 978-3-527-31565-9, A.Pietrzyk, W.Kutner, R.Chitta, M. E. Zandler, F. D'Souza, F. Sannicolò, P.R. Mussini, *Anal. Chem.*, 2009, 81(24), 10061

³⁸ F. Endres, A.P. Abbott, D.R. MacFarlane, *Electrodeposition from Ionic Liquids*, 2008, Wiley-VCH, ISBN 978-3-527-31565-9

and parallel studies in molecular solvents (CH_2Cl_2 and MeCN), and is commercially available at reasonable price (~150 € / 50 g).

2.1.4 The reagents

<i>Reagent</i>	<i>Producer and characteristics</i>
Acetonitrile, MeCN	Sigma-Aldrich, $\geq 99.5\%$ over molecular sieves
Bis(cyclopentadienyl)cobalt(III)hexafluorophosphate, CpPF_6	Aldrich, $>98\%$
Diamond powder, mono- and polycrystalline	Sigma-Aldrich, 99.9% , particle size $1\ \mu\text{m}$,
1,1'-dimethylferrocene Me_2Fc	Sigma-Aldrich, $>97\%$
Decamethylferrocene Me_{10}Fc	Fluka, $\geq 95\%$
Dichloromethane, CH_2Cl_2	Sigma-Aldrich, puriss., $\geq 99.9\%$; contains 25 mg/l of amylene as stabilizer
Ferrocene, Fc	Fluka, $> 98\%$
Tetrabutylammonium hexafluorophosphate, TBAPF_6	Fluka, $>99\%$
Tetrabutylammonium perchlorate, TBAP	Sigma-Aldrich, $\geq 99\%$, for electrochemical analysis

2.2 The electrochemical quartz crystal microbalance

2.2.1 An introduction to EQCM

The electrochemical quartz crystal microbalance is a tool that belongs to the wide family of the acoustic wave devices, based on a piezoelectric material (typically, quartz), that, under a given electrical stimulus, emits an acoustic wave that interacts with the adjacent medium. The acoustic wave generally propagates within a small distance in that medium, and, consequently, the answer (*i.e.*, a frequency) recorded by the instrument is determined by the interphase properties. This feature makes the applications of the EQCM interesting in many fields, *e.g.*, in analytical chemistry, for the study of the electrochemical processes coupled with mass transfers between electrode and solution, and also for kinetics and mechanistic studies.

The piezoelectric effect, discovered at the end of the XIX century by Jacques and Pierre Curie, is the principle on which the EQCM functioning is based³⁹:

A mechanical stress applied on the surface of some crystals, *e.g.* quartz, results in an electrical potential across the crystal, whose amplitude is proportional to the applied stress. This peculiar phenomenon is generally found in acentric materials, *i.e.*, materials that crystallize in noncentrosymmetric space groups: a single crystal of an acentric material has a polar axis, due to electric dipoles associated to the arrangement of the atoms in the crystal lattice. Consequently, a mechanical stress applied on the surface of this kind of materials generates a net change in the dipole moment, and, thus, a charge: a net change of electrical charge on the crystal faces occurs, whose entity and direction depend on the relative orientations of the dipoles and of the crystal faces.

Vice versa, it is possible to find a converse piezoelectric effect, whenever the application of a potential results in a mechanical strain, proportional to the applied voltage.

In the quartz, such a deformation is elastic.

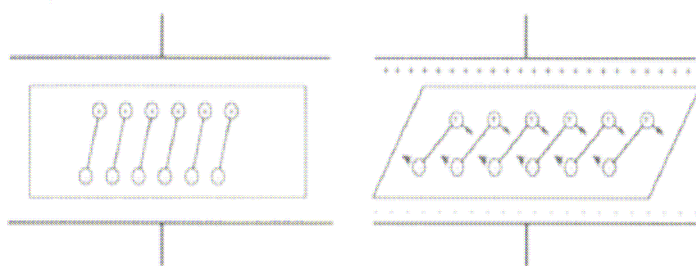


Figure 1: Schematic representation of the inverted piezoelectric effect, where the applied electric field induces a new orientation of the dipoles and causes a mechanical distortions

³⁹ M.D. Ward, Principles and applications of the electrochemical quartz crystal microbalance, *Monographs in Electroanalytical Chemistry and Electrochemistry: Physical Electrochemistry, Principles, Methods, and Applications*; edited by I. Rubinstein, Marcel Dekker, New York, **1995**, 293-338

D.A. Buttry, M.D.Ward, *Chem. Rev.*, **1992**, 1355

V. Bonometti, M.Sc. Thesis, Università degli Studi di Milano, 2009

An alternated potential applied across the crystal (e.g. quartz, of having a thickness t_q) causes a vibrational motion of the crystal itself, that results in an acoustic wave propagating, forward and backward, between the crystal faces. When the wavelength of the acoustic wave is equal to twice the crystal thickness (taking into account also the electrode thickness) the resonance condition of the stationary wave can be established.

In such resonance condition, the acoustic wave frequency is

$$f_0 = \frac{v_{tr}}{2t_q}, \text{ where } v_{tr} \text{ is the transverse velocity of sound in the crystal } (3.34 \cdot 10^4 \text{ m}\cdot\text{s}^{-1} \text{ for the}$$

AT-cut quartz crystal, *i.e.* a thin quartz wafer prepared by slicing through a quartz rod at an angle of 35° with respect to the x axis, commonly used for applications in EQCM).

Thus, it is the crystal thickness that defines the operating frequency.

Assuming that the acoustic properties and the density of the deposited films are equal to those of the quartz, the change in thickness happening during a deposition process is considered as a kind of extension of the quartz crystal itself, and the resonance frequency changes accordingly:

$$\Delta f = \frac{-2f_0^2 \Delta m}{A\sqrt{\mu_q \rho_q}}$$

This relation is better known as *Sauerbrey's equation*, where:

Δf = measured change of frequency

Δm = mass change

A = piezoelectrically active area

ρ_q = quartz density = 2.648 g/cm^3

μ_q = shear modulus of the AT-cut quartz crystal = $2.947 \cdot 10^{11} \text{ g/cm s}^2$

Being some terms of the relation constant, the Sauerbrey's equation can be simplified as:

$$\Delta f = -C_f \Delta m$$

However, it is important to remember that the Sauerbrey's equation is derived from the approximation according to which the deposited material is treated as an extension of the quartz itself⁴⁰: this can be considered valid when the deposited layer is thin, elastic and has the same acoustic impedance as the quartz. The approximation still holds for mass changes concerning rigid films, that are less than 1% of the quartz crystal mass, *i.e.* the majority of cases for the deposition of rigid films, where rigid means thin and elastic.

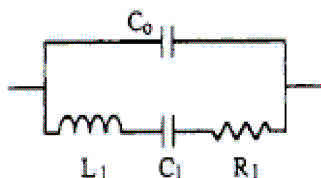


Figure 2: Butterworth-Van Dyke circuit, corresponding to the EQCM system

⁴⁰ A.J. Bard, M. Stratmann, P.R. Unwin, *Encyclopedia of Electrochemistry, Vol.3 Instrumentation and Electroanalytical Chemistry*, Wiley, 2003, ISBN 978-3-527-30395-3, pp. 230-289

The EQCM system can be represented by an equivalent circuit, better known as *Butterworth-Van Dyke* circuit, constituted by a capacitor C_0 in parallel with a series of inductor L_1 , a capacitor C_1 and a resistor R_1 . This series is defined motional branch, and represents the vibrational behaviour of the crystal.

In particular, C_0 constitutes the static capacitance of the quartz plate with the electrodes, and takes into account possible parasite capacitances, L_1 represents the mass moved during the oscillation, C_1 the energy acquired during the oscillation and R_1 the energy dissipation due to internal frictions.

When the capacitor discharges on the inductor, a magnetic field around the latter is formed, and opposes to the current flowing; when the discharge of the capacitor is complete, and the current tends to zero, the electromotive force in L creates an opposite current and the capacitor gets charged again. The repetition of this circuit determines electric oscillations, modulated by a factor proportional to R , which is very small, for the quartz crystal. The *Butterworth-Van Dyke* circuit describes very well the EQCM behaviour in the vacuum or in the gas phase, but, in solution, it is necessary to consider the variations in the resonator characteristics due to the liquid density (that increases the mass) and to its viscosity (that provokes energy dissipations). In a Newtonian liquid the circuit can be modified by adding a further inductor L_2 , and a further resistor R_2 in the motional branch, corresponding to the above mentioned liquid density and viscosity. It is important to underline that a greater density or viscosity leads to a decrease of the resonance frequency, and, in particular, a greater viscosity could lead to a significant loss in accuracy. Such effects are particularly important for the study of polymer films that could undergo

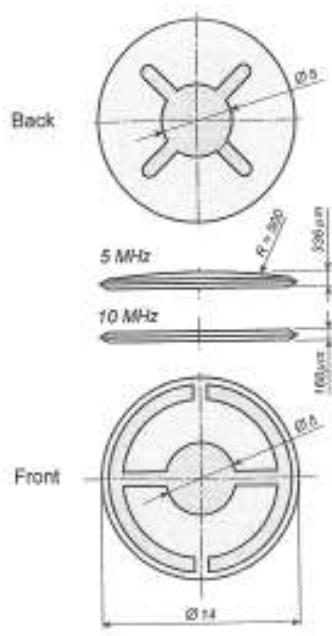


Figure 4. At-cut quartz crystal resonator.

Figure 4: Scheme of a gold-coated quartz crystal for EQCM; only the anchor-like side is facing the solution

variations in their viscosity or density during the experiment. Moreover, polymeric film could be viscoelastic, thus making the theoretical description of the system more complicated. Even the microscopic roughness of the resonator surface could be problematic, in the case that the cavities entrap some liquid, which increases the mass on the surface of the resonator; to minimize this effect, it is possible to operate with polished quartz crystals.

Concerning the instrumentation⁴¹, the EQCM is composed essentially by a holder for the quartz crystal, that is actually the working electrode, connected to a controller device, which is in turn connected to a PC and to a potentiostat, and, obviously, to the electrochemical cell, including a reference electrode and a counter electrode. The crystal, schematically depicted in Figure 4, is very thin; the most common quartz crystals employed for this technique have 5 MHz or 10 MHz resonance frequency.

⁴¹ W. Kutner, A. Ardasiewicz, A. Kochman, *Electrochemical Quartz Crystal Microbalance type EQCM 5710, User Manual*

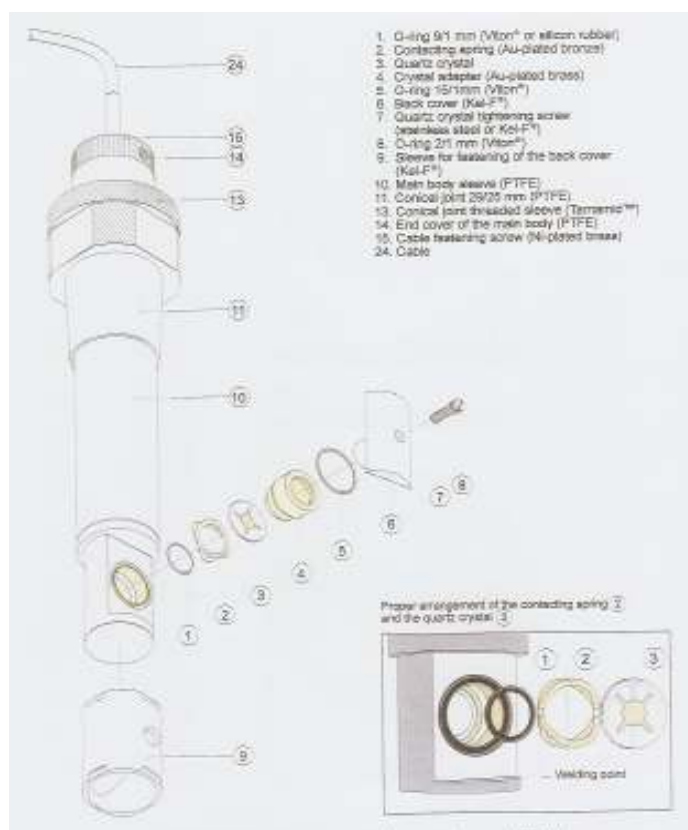


Figure 5: Expanded view of the quartz crystal holder, produced by the Polish Academy of Sciences

Both the crystal sides are covered by a layer of *sputtered* metal, typically gold or platinum, but it is possible to employ different metals. The most difficult phase in preparing the experimental setup is the insertion of the crystal in the holder, because of its extreme fragility: the crystal is inserted in the holder cavity, and is closed by a small screw: the closure has to be tightened enough to ensure the electrical contacts, and to avoid working solution leakage in the holder, but not too much, to avoid to break the quartz crystals. The minimum working solution volume of the electrochemical cell is 14 cm³ but it is possible to operate with small quantity of sample, in few microliters of working solution, keeping the holder in horizontal position.

Since the EQCM is a very sensitive instrument, an accurate maintenance

is necessary: every piece should be carefully rinsed and dried before and after use, to avoid that residuals of solvent, supporting electrolyte, or previous samples may interfere with the measurement.

The gold-coated pieces can be eventually rinsed with H₃PO₄ 0.1 M and then with deionized water, to remove possible oxidized residuals on the gold surface. Some solvents may cause a swelling of the o-rings used for tightening the holder closure: in such a case they should be replaced and let outside the solution in order to recover their original shape. An o-ring swelling may cause a non optimized electrical contact between the holder and the quartz, resulting in an increased resistance in the measured signal or in the quartz break.

The EQCM calibration is a necessary operation to exactly know the sensibility constant C_f (Hz·g⁻¹) of the Sauerbrey equation, and consists in repeated cycles of electrodeposition/electrodissolution of silver by cyclic voltammetry. The electrochemical cell is filled with a 0.001 M AgNO₃ in HClO₄ 0.1 M. At every cycle it is possible to observe a decrease in frequency corresponding to the deposition of a silver layer on the crystal, and a successive increase due to its anodic removal. By repeating the electrodeposition/electrodissolution cycles, it is possible to obtain C_f as average of the values obtained at every single cycle, according to the *Sauerbrey equation*: Δf is known from experimental data, Δm can be calculated from the charge passed during the experiment,

ΔQ , knowing that $m_{Ag} = \frac{M_{Ag} \cdot \Delta Q}{zF}$, where M_{Ag} is the atomic mass of silver, z the number of electrons involved in the reaction and F is the Faraday constant.

The great utility of the EQCM consists in the possibility of measuring simultaneously and in situ the electrochemical charge (and, thus, the current), and mass variations with extraordinary sensitivity, *e.g.*, a 5 MHz device can detect 10 ng·cm⁻².

In ideal conditions, the measured Δf is proportional to the electrochemical charge and related to the apparent molar mass MW (g·mol⁻¹) by the equation $\Delta f = \frac{MW \cdot C_f \cdot \Delta Q}{zF}$. The

slope of the line obtained by plotting Δf vs ΔQ , gives the value of MW/ z , F being known. However, the interpretation of this datum can be a really hard task, since the exact number of exchanged electrons is not always known, and the MW value can be different from the stoichiometric value, *e.g.* on account of interactions with other species in solution (solvent, adsorbed species,...). Moreover, deviations from linearity generally point to non-ideal situations (roughness, viscoelasticity,...)

In the present PhD thesis, EQCM has been used for the characterization of conducting polymer films, and also in one particular case of a poly(cyclopentadithiophene) chains regularly intercalating Re(I) complexes acting as chromophore pendants: this example, reported in Chapter 5, can be considered at the same time a conducting and redox polymer.

Redox polymers are, in fact, polymers containing electroactive groups, discrete and localized. Such groups act independently from the main chain, and the charge transport is ensured by an hopping mechanism, involving sequential self-exchanges between adjacent oxidized and reduced groups of the redox couple. A very interesting study concerns the changes in frequency associated to ion transport, necessary to ensure the electroneutrality, and the quantity of solvent accompanying such transport: in order to maintain the electroneutrality, the electron transfer in/from the film to the interphase polymer/electrode has to be equilibrated by an equivalent ion transfer at the interphase polymer/solution. The transferred ion should be the counter ion (*i.e.*, anion for a positively charged polymers, cation for a negatively charged polymer). However, in case of high ionic strength, the activity coefficients show that even the coion plays an important role, together with an equivalent amount of its counterion (*i.e.*, salt, as defined in the literature concerning ionic exchanges). The consequence is that it is not possible to define a single mechanism that satisfies the electroneutrality requirement: for example, to compensate the positive charge in an oxidized film, both entrance of anions and expulsion of cations are possible. EQCM measurements allow to distinguish which is the prevalent mechanism: first of all, movements of anions or cations have opposite directions, *i.e.* there will be an opposite sign in Δm . A more refined analysis of Δf could point to the fluxes of ions involved as a function of the applied potential and of the film charge.

Differently from the redox polymers, the conducting polymers are characterized by a delocalization of the charge along the conjugated backbone of the polymer. The electroactive functionality is therefore delocalized over the entire chain, and conducting polymers feature a high and highly controllable conductivity. In this class of molecules, the ionic dynamics are strongly dependent on the nature of the counter ions, which is in

turn very important with the aim of developing energy storage devices, concerning the weight, the power and energy density, as a lower mass of the transporting species allows greater energy densities. The EQCM investigation of conducting polymers shows interesting properties and peculiarities: first of all the injection of a charge is strongly correlated to the ion dynamics, because of the corresponding concurrent injection/removal of a dopant; secondly, both the electronic movement along the conducting backbone and the ionic movement on the polymer matrix are function of the dynamics of the polymer, which can assume an internal planar conformation for the π delocalization, creating enough room for the ion movements, with a characteristic rate. The effect of ions in the conducting polymers doping/undoping are often difficult to be interpreted, and the EQCM answer is strongly affected by the potential scan rate, by the possible preconditioning of the films, and by the electrolyte concentration. For example, K.Naoi and coworkers reported the preparation of polypyrrole systems in the presence of various supporting electrolytes, differing for the anion dimensions⁴². In the films prepared with the smaller anions (ClO_4^- , BF_4^-) the oxidation involves the intercalation of the anions in the film network, while in the presence of bulkier anions (polystyrenesulfonate, polyvinylsulfonate), they are entrapped in the film at every doping state of the polypyrrole, and, as a consequence, the polypyrrole chemistry is characterized by the movement of the cations. If intermediate-sized anions were used (*e.g.*, *p*-TS), both anions and cations are involved.

In the present PhD work, EQCM studies were performed either in our laboratory in Milan, using a EQCM 5710 (Polish Academy of Sciences, Poland) run by AUTOLAB PGSTAT12 (Metrohm, Switzerland) and 5 MHz gold-coated quartz crystals, or in the laboratories of Prof. Kutner and Dr. Noworyta at the Institute of Physical Chemistry of the Polish Academy of Sciences, using a EQCM 5710 and 10 MHz gold-coated quartz crystals. In both cases, a 14 cm³ cell was employed, and the reference electrodes were a SCE (in Milan) or Ag|AgCl or an Ag pseudoreference (Warsaw)

⁴² K.Naoi, M. Lien, W. H. Smyrl, *J.Electrochem. Soc.*, **1991**, 138, 440

2.3 Circular dichroism

2.3.1 An introduction to CD spectroscopy⁴³

One of the most useful techniques for the investigation of chiral systems is circular dichroism spectroscopy, which is based on the difference of absorption of left and right circularly polarized light by optically active chiral molecules. Circular dichroism (CD) spectroscopy has a wide range of applications in many different fields, *e.g.*, UV CD is used to investigate the secondary structure of proteins, UV-Vis CD to investigate charge-transfer transitions, NIR CD to study geometric and electronic structure by probing metal $d \rightarrow d$ transitions. Vibrational circular dichroism, which uses light from the infrared energy region, is employed for structural studies of small organic molecules, and most recently proteins and DNA. In particular, in our case, circular dichroism was applied in combination with cyclic voltammetry in an unconventional experimental setup (as described in Chapter 2.3.2) in order to investigate the chiral properties and behaviour of our *inherently chiral* polymer films upon polarization.

Electromagnetic radiation consists of an electric E and magnetic B field that oscillate at right angles to one another and to the propagation direction k . Light may be described as a transverse wave, whose polarization is defined by the direction of its electric field, so the polarization is perpendicular to the wave direction of travel. The electric field may be oriented in a single direction (*linear polarization*: all the photons have their electric field oscillating in the same plane), or it may rotate (*circular or elliptical polarization*: the electric field vector traces out a circle or helix about the propagation direction). In the latter case,

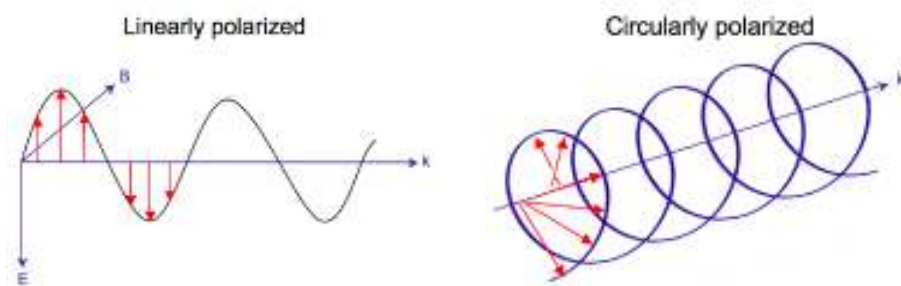


Figure 1: Linearly and circularly polarized light: the arrows indicate the direction of the electric field.

the field may rotate in either direction, determining the wave *chirality* or *handedness*.

The Figure 1 shows the electric vectors of linearly and circularly polarized light, at one moment of time, for a range of positions; the

plot of the circularly polarized electric vector forms a helix along the direction of propagation k . For left circularly polarized light with propagation towards the observer,

⁴³ A. Roger, B. Nordén, *Circular dichroism and Linear Dichroism*, Oxford Chemistry Masters, Oxford University Press, 1997, ISBN 0-19-855897-X

http://en.wikipedia.org/wiki/Circular_dichroism

<http://www.enzim.hu/~szia/cddemo/edemo2.htm>

N. Kobayashi, A. Muranaka, J. Mack, *Circular dichroism and magnetic circular dichroism spectroscopy for organic chemists*, RSC, Cambridge, 2011, ISBN 978-1-84755-869-5

the electric vector rotates counterclockwise. For right circularly polarized light, the electric vector rotates clockwise.

In summary, two perpendicular plane polarized lights having a 90° phase shift, generate a circularly polarized light (left, *lcp*, or right, *rcp*). Interestingly, the combination of a *lcp* light and a *rcp* light, having equal amplitudes, phases and wavelengths, generates a plane polarized light.

When circularly polarized light passes through an optically active medium, the speeds between right and left polarizations differ ($v_L \neq v_R$) as well as their wavelength ($\lambda_L \neq \lambda_R$), so the linearly polarized light plane (obtained as combination of a *lcp* light and a *rcp* light) is rotated (as in polarimetry), as shown in Figure 2.

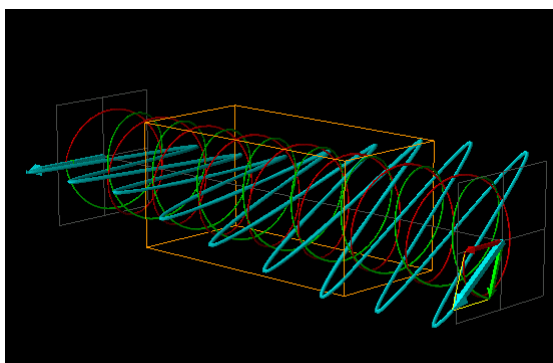


Figure 2: Rotation of the linearly polarized light plane after interaction with a chiral optically active sample.

Furthermore, in this case, also the extent to which *rcp* and *lcp* lights are absorbed differ ($\epsilon_L \neq \epsilon_R$). Circular dichroism is actually the difference $\Delta\epsilon = \epsilon_L - \epsilon_R$. At the wavelength where the absorption takes place, the two types of circularly polarized light are absorbed to different extents, so, considering a linearly polarized incident light, the outcome will be elliptically polarized. In a CD experiment, equal amounts of left and right circularly polarized light of a selected wavelength are alternately radiated into a chiral sample. One of the two polarizations is absorbed more than the other one, and this wavelength-dependent difference of absorption is measured, yielding the CD spectrum of the sample. Due to the interaction with the molecule, the electric field vector of the light traces out an elliptical path after passing through the sample.

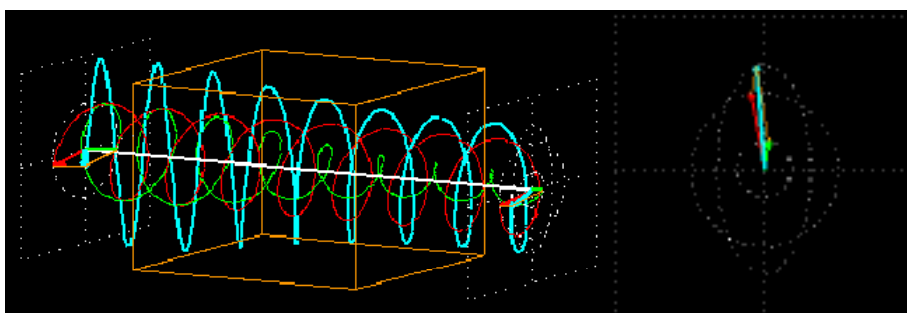


Figure 3: When a plane polarized light (superimposition of symmetrical *lcp* and a *rcp* lights) passes through an optically active sample, the amplitude of the most strongly absorbed component will be smaller than the less strongly absorbed one, resulting in an ellipse.

Generally, intensities of CD signals can be reported in different ways: either as the differential absorbance of left and right circularly polarized light, $\Delta A = A_L - A_R$, that can be easily converted in $\Delta \epsilon$ according to the Lambert-Beer's law: $\Delta \epsilon = \Delta A / c \cdot l$ (where c is the molar concentration of the sample and l is the cell pathlength), or in terms of degrees of ellipticity θ .

As mentioned above, plane polarized light can be viewed as a superimposition of a *lcp* and a *rcp* light of equal amplitude and phase; when this linear polarized beam passes through an optically active sample, the amplitude of the most strongly absorbed component will be smaller than the less strongly absorbed one, resulting in an ellipse, when the amplitudes of the components are combined. The degree of ellipticity is defined as the tangent ratio of the minor to major elliptical axes. Linearly polarized light has 0° of ellipticity, while fully *lcp* and *rcp* light have $+45^\circ$ and -45° , respectively. The interconversion between θ and ΔA is given by $\Delta A = \frac{4\pi\theta(\text{deg})}{180 \ln 10} = \frac{\theta(\text{m deg})}{32,982}$

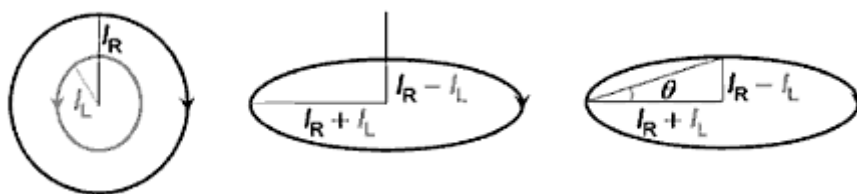


Figure 4: When *lcp* and *rcp* have different intensities (I_L and I_R) they combine to form an elliptically rather than linearly polarized light. The ellipticity θ is defined as the angle between the long and short axes of the ellipse.

Interestingly, the intensity and the shape of the CD signal increases with increasing order of the structure under investigation. For example, a random coil gives only a small and not well defined signal, while an α -helix arrangement leads to sharp and bisignate signals (Cotton effect).

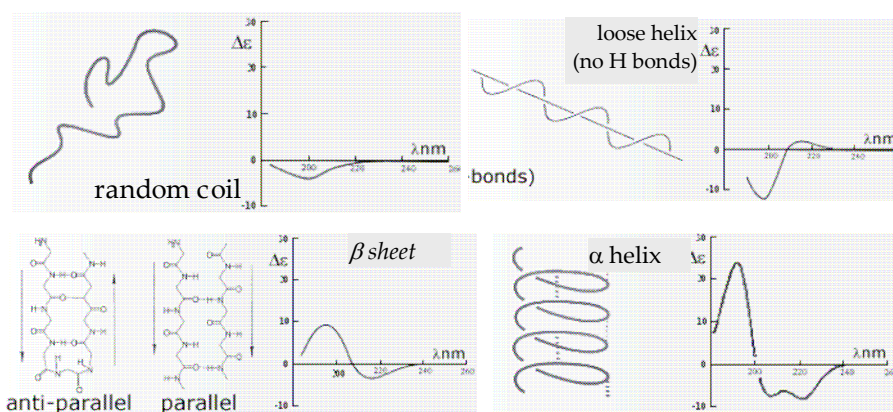


Figure 5: Examples of CD signals in case of structures with differently ordered structures.

2.3.2 The experimental setup and the analysis protocol

The circular dichroism experiments were conducted in the laboratories of Prof. S. Abbate, G. Longhi and with the collaboration of E. Castiglioni at the Università degli Studi di Brescia. Our aim was to investigate the chiral properties and behaviour of our *inherently chiral* polymer films upon polarization, thus a particular apparatus was set up to perform circular dichroism *in situ* with cyclic voltammetry.

This kind of experiment was performed only on T4-BT2 enantiopure films, because it was the only inherently chiral monomer available quantitatively separated in its enantiomers.

The samples were prepared previously according to the following protocol⁴⁴:

The background solution was prepared ($\text{CH}_3\text{CN} + \text{TBAPF}_6$ 0.1 M), deaerated, and tested by performing a voltammetric scan on a GC electrode (with a Pt wire as the counterelectrode and a SCE as reference electrode in a double bridge filled with the same working solution) to check its purity and the absence of oxygen traces.

Two 4 cm³ electrochemical cells were prepared, and filled with the working solution.

(*R*)-T4-BT2 enantiomer was added to the first cell, and (*S*)-T4-BT2 was added to the second cell, the quantity weighed was such to obtain a $5 \cdot 10^{-4}$ M concentration of each enantiomer in the 4 cm³ cell. Their concentration were tested to be equal by performing one anodic scan of each enantiomer and overlaying them.

Once the concentration was found to be the same for the two enantiomers, the polymerization was performed on an ITO coated glass slide, including both the anodic peaks characteristic of the T4-BT2 monomer (as shown in Chapter 3.2.2), generally for 24, 36, or 48 cycles (the number of scan cycles was taken as a reference of the film thickness, and it is indicated in every polymerization plot).

Few cycles of stability tests in monomer-free solution ($\text{CH}_3\text{CN} + \text{TBAPF}_6$ 0.1 M) allowed to check also that the thicknesses of the electrodeposited enantiopure films were equal.

The CD-CV set up was composed by a quartz spectroscopy cuvette with 1 cm pathlength, filled with the working solution, where the electrodes were inserted. The electrodes (ITO, as the working electrode, a thin Pt wire as the counterelectrode and a 6 mm-diameter SCE as the reference electrode), were connected to the potentiostat (PGSTAT 101, Metrohm), and the cuvette was inserted in the sample compartment of the spectropolarimeter (JASCO 815SE). A spectrometer equipped with a photomultiplier extended to the NIR range was employed.

A blank was first recorded, on a new and clean ITO glass in the cuvette filled with the working solution.

Then the ITO covered with the enantiopure sample was inserted in the cuvette, paying particular attention not to make contact with the other electrodes, and fixed at the cuvette wall with an alligator clip and few voltammetric anodic cycles were recorded to check its electroactivity and the presence of possible electrical interferences.

⁴⁴ T. Benincori, V. Bonometti, R. Cirilli, L. Dunsch, W. Kutner, G. Longhi, P. R. Mussini, M. Panigati, M. Pierini, S. Rizzo, F. Sannicolò, *Inherently Chiral Electroactive Polythiophenes: the Breathing Chirality*, submitted, 2012

Absorption and CD spectra have been recorded on films of poly-(+)-(S) and poly-(-)-(R)-T4-BT2 deposited on an ITO electrode dipped into the working solution ($\text{CH}_3\text{CN} + \text{TBAPF}_6$ 0.1 M) contained in the quartz cuvette: different potentials have been applied, each for about 60 s, starting from the neutral state to the heavily p-doped state, corresponding to the maximum of the voltammetric peak, and the CD spectrum was recorded at each potential. The spectra for each potential value were obtained with 1 scan at 1000 nm/min scan speed, 0.25 sec response time, slit width 300 μm .

Before applying a new potential, a voltammetric scan restored the polymer film to the neutral state, and was useful to check that the electroactivity was not lost during the polarization. After the first increasing ramp, a decreasing potential ramp was applied, applying the same potential as in the first one.

A couple of potentials were chosen also in the cathodic region, but generally the CD spectra were the same as in the neutral state (as expected on the basis of UV-Vis spectroelectrochemistry performed previously).

2.4 Electrochemical Impedance Spectroscopy

2.3.1 An introduction to EIS⁴⁵

Electrical Impedance, or simply, impedance, is a vectorial physical quantity, normally indicated by the symbol Z , which can be assumed to be the extension of the concept of resistance to alternated current circuits, describing not only the relative amplitudes of the voltage and current, but also the relative phases: it allows to generalize the Ohm's law to sinusoidal circuits (AC circuits). According to this definition, resistance can be thought as an impedance with zero phase angle.

Mathematically, impedance can be described by a complex number: the real part represents the dissipative phenomena and corresponds to the resistance, R , and the imaginary part, which corresponds to the reactance X , is linked to energy accumulation phenomena (i.e., the presence of capacitances or inductances in the circuit):

$$Z = R + jX, \text{ or, alternatively, } Z(\omega) = Z_{\text{Re}} + jZ_{\text{Im}}$$

where ω is the angular frequency of the sine-wave modulation of the potential or of the current. All of these quantities are measured in ohm.

The variation of the impedance with frequency is often of interest, and can be displayed in different ways. The more common representation is the Nyquist plot, which displays $-Z_{\text{Im}}$ vs Z_{Re} . Unfortunately, the Nyquist plot does not give any information about the frequency at which every point of the curve corresponds to. This is provided by the so-called Bode plots, in which $\log|Z|$ or the phase angle ϕ are both plotted against $\log\omega$.

In the last decades, impedance spectroscopy techniques have received increasing attention, as a powerful method of characterizing many of the electrical properties of materials and their interfaces with the electrodes, and also about possible reactions taking place there. It may be used to investigate the dynamics of bound or mobile charge in the bulk or interfacial regions of any kind of solid or liquid material: ionic, semiconducting, and even insulators.

In most classical experiments, electrode reactions are studied through large perturbation of the system: potential sweeps, potential steps or current steps typically drive the system

⁴⁵ A. J. Bard, L. R. Faulkner, *Electrochemical Methods Fundamentals and Applications*, II edition, Wiley, New York, **2001**, ISBN 13-978-0-471-04372-0

A. Lasia, *Electrochemical Impedance Spectroscopy and its Applications*, in *Modern Aspect of Electrochemistry*, edited by B.E. Conway, J. O'M. Bockris, and R.E. White, vol. 32, p.143-248, Kluwer Academic/Plenum Publisher, New York, **1999**, ISBN 978-0-306-45964-1

M. E. Orazem, B. Tribollet, *Electrochemical Impedance Spectroscopy*, Wiley, **2008**, ISBN 978-0-470-04140-6

E. Barsoukov, J. R. Macdonald, *Impedance Spectroscopy Theory, Experiment, and Applications*, II edition, Wiley, Hoboken, **2005**, ISBN 0-471-64749-7

Gamry Instruments, *Electrochemical Impedance Spectroscopy Primer*, www.gamry.com

E. Giussani, M.Sc. Thesis, Università degli Studi di Milano, 2011

M. Musiani, *Electrochimica Acta*, **1990**, 35, 1665

E. Barsoukov, J. R. Macdonald, *Impedance Spectroscopy Theory, Experiment, and Applications*, II edition, Wiley, Hoboken, **2005**, ISBN 0-471-64749-7

far away from the equilibrium and the response is usually a transient signal. Another approach is to perturb the system with a small amplitude signal, and to observe how the system follows the perturbation at steady state. This alternative approach is the heart of Impedance Spectroscopy methods. The electrochemical cell is perturbed by a small amplitude sinusoidal voltage, and the current/voltage response is linear, and measured over a wide range of frequencies. Impedance Spectroscopy is becoming a popular analytical tool in materials research and development because it involves a relatively simple electrical measurement, whose results may often be correlated with many complex materials variables: from mass transport, rates of chemical reactions, corrosion, and dielectric properties, to defects, microstructures, and compositional influences on the conductance of solids. Impedance Spectroscopy can predict aspects of the performance of chemical sensors and fuel cells, and it has been used extensively to investigate membrane behaviour in living cells. The disadvantages of Impedance Spectroscopy are primarily associated with possible ambiguities in the interpretation: ideal circuit elements may be inadequate to describe the electrical response, so constant-phase elements (CPEs) have been introduced in the ideal circuits to account for non ideal behaviour (due to the presence of inhomogeneities in the electrode-material system, non-uniform diffusions, current distributions), and aiming to achieve a better fitting between the observed impedance data with the model circuit. In addition, it is important to consider that, theoretically, there are infinite possible equivalent circuits that should be used and that well fit the experimental data.

In particular, Electrochemical Impedance Spectroscopy studies the system response to the application of a periodic small amplitude AC signal. These measurements are carried out at different AC frequencies and, thus, the name impedance spectroscopy was later adopted.

EIS is a very sensitive technique, which is also very complicated from a theoretical and mathematical point of view, and it must be used with great care. It should be stressed that EIS cannot give all the answers, since it is a complementary technique, and other methods must also be used to elucidate the interfacial processes. However, the great diffusion of this technique for the material characterization, and in the study of reaction mechanisms

in electrodepositions, passivation and corrosion phenomena, ion diffusion through membranes, cannot be denied, even if electrochemical systems are not always easy to understand, so the data interpretation could be complicated.

EIS is based on the Transfer Function: generally, the input perturbation is sinusoidal, and the output answer is sinusoidal too, with the same frequency but with different intensity and phase angle.

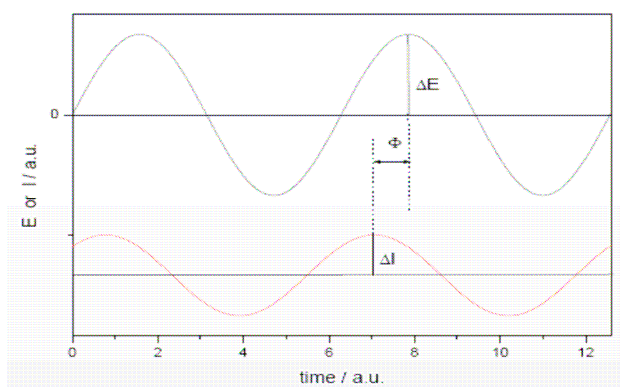


Figure 1: Sinusoidal perturbation of the input signal

The ratio between the system answer and the input perturbing signal is the complex transfer coefficient for a given frequency; in a wide frequency range, the Transfer Function

could describe the properties of the system. In the peculiar case of electrochemical systems, the EIS analysis consists in the measurement of the Transfer Function for a small intensity perturbing signal, in order to be able to consider only the linear part of the response. If the input signal is a current, and the output signal is a potential, the Transfer Function is the impedance Z , while in the opposite case it coincides with the admittance Y , which is the inverse of the impedance Z . When an electrochemical process takes place, mass transport and energy transfer phenomena occur too, which could change the structure and the properties of the system under investigation. Under these circumstances, very frequent in the case of electrochemical analysis, the systems is not linear, not in steady state conditions and characterized by a memory effect.

The impedance derived is valid provided that the following four criteria are met:

- *Linearity*: this condition can be achieved only when the sinusoidal input signal is small, so the system is unchanged. In a linear system, the output signal has the same frequency as the input signal, but the phase angle is shifted, and the response is not dependent on the amplitude. It is easy to verify the linearity of the system: if the obtained impedance is the same when the amplitude of the applied AC signal is halved, then the system is linear.
- *Causality*: One input, one output. The response of the system must be entirely determined by the applied perturbation, that is the output depends only on the present and past input values. The causal system cannot predict what its future input will be. Causal systems are also called *physically realizable* systems. No memory effects have to appear. The causality has an important implication in EIS: if it is ensured, the complete description of the system under investigation could be made with only one part (imaginary or real) of the impedance, since these are related together. This relationship is generally known as the Kramers-Kronig relation, and is widely employed to verify the simplification criteria.
- *Stability*: The stability of a system is determined by its response to inputs. A stable system remains stable unless excited by an external source and it should return to its original state once the perturbation is removed and the system cannot supply power to the output irrespective of the input. The system is stable if its response to the impulse excitation approaches zero at long times or when every bounded input produces a bounded output. The impedance measurements must also be stationary, that is the measured impedance must not be time dependent. This condition may be easily checked by repetitive recording of the impedance spectra; then the obtained Bode plots should be identical.
- *Finiteness*: The real and imaginary components of the impedance must be finite-valued over the entire frequency range. In particular, the impedance must tend to a constant real value for $\omega \rightarrow 0$ and $\omega \rightarrow \infty$.

In addition to these four important requirements, it is also important to check that the phenomena which have to be observed are visible in the frequency range chosen for the analysis.

One of the great advantages of EIS is the possibility to separate the kinetics of the various processes that occur in the system under investigation; however, the most complex aspect of EIS is the possibility to “extract” information from the experimental data which, alone,

do not suggest any information about the electrochemical processes, but need to be inserted into a model able to represent the processes occurring in the system (*i.e.*, an equivalent circuit).

Equivalent circuits may be composed of the “classical” electrical elements (resistors, capacitors, inductors), each of them has its own impedance and gives its typical plots:

<i>Component</i>	<i>Current vs Voltage</i>	<i>Impedance</i>
Resistor, R	$E = IR$	$Z=R$
Inductor, L	$E = L di/dt$	$Z = j\omega L$
Capacitor, C	$I = C dE/dt$	$Z = 1/j\omega C$

For example, a series of a resistor and a capacitor, which may represent the case of an ideally polarizable electrode, like a mercury electrode in a supporting electrolyte solution (or, a more practical example may be that of a metal coated by a non-damaged coating, thus, having very high impedance) will give a characteristic Nyquist plot. The expression of the impedance for these elements in series is the sum of the single impedances reported above in the Table: $Z(j\omega) = R + \frac{1}{j\omega C}$. In this system, the resistor takes into account the resistance of the solution, and the capacitor represents the electrical double layer.

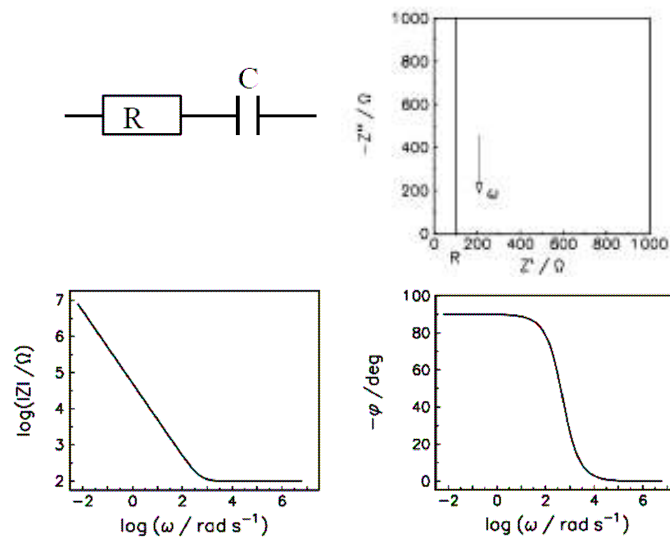


Figure 2: Ideally polarizable electrode: Nyquist and Bode plots in the 100 kHz-1 mHz, frequency range (R = 100Ω, C = 20μF)

At high frequencies, the system tends to the case of the pure resistor, while, for lower frequencies, it approaches to the case of the pure capacitor, as it may be better evidenced from the Bode plots.

When these elements are connected in parallel, the impedance of the system is given by $Z(j\omega) = \frac{1}{1/R + j\omega C}$.

The Nyquist plot shows a semicircle of radius $R/2$, and the frequency at the semicircle maximum is equal to $\omega = \frac{1}{RC}$.

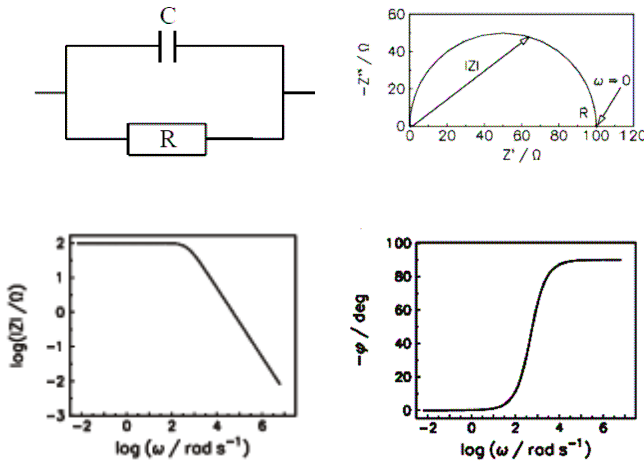


Figure 3: RC in parallel: Nyquist and Bode plots in the 100 kHz-1 MHz frequency range; $R = 100 \Omega$, $C = 20 \mu\text{F}$.

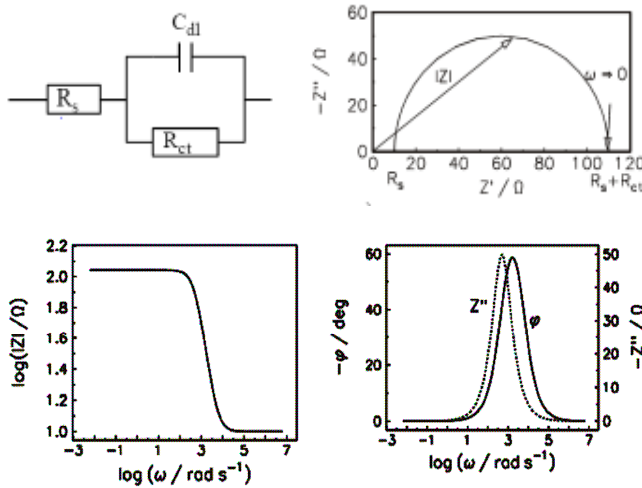


Figure 4: Randles circuit, Nyquist and Bode plots, $R_s=10 \Omega$, $R_{ct}=100 \Omega$, $C_{dl}=20 \mu\text{F}$

A further example of model circuit is the so-called Randles circuit, which is the precursor of the model for an electrochemical cell (also known as Randles model, described more in detail below).

The main difference between the former circuit and this one is connected with the fact that here, at $\omega \rightarrow \infty$, $Z \rightarrow R_s$ and $\phi \rightarrow 0$, due to the presence of R_s , and for $\omega \rightarrow 0$, $Z \rightarrow R_s + R_{ct}$. The dashed line in the Bode phase graphs is actually the plot of Z_{im} vs $\log \omega$, reported to underline that the maximum of the imaginary part of impedance and the maximum of the phase angle do not correspond exactly, since the Z'' maximum corresponds to the maximum of the semicircle at

$$Z' = R_s + R_{ct}/2 \text{ at } \omega = \frac{1}{\tau} = \frac{1}{R_{ct}C_{dl}}, \text{ where}$$

τ is the time constant of the system, while the maximum of the function

$$\phi = \arctan\left(\frac{Z''}{Z'}\right)$$

$$\text{is at } \omega = \frac{1}{R_{ct}C_{dl}} \sqrt{\frac{R_s + R_{ct}}{R_s}}$$

In the case of a generic faradaic process occurring at a working electrode, the total current flowing through the interface between the working electrode and the reaction medium is the sum of a faradaic current (i_f) and a current due to the charging of the double layer (i_c). The capacitance of the double layer is described by a generic capacitance C_d , while the faradaic process itself is represented by the impedance Z_f . The resistance opposed by the electrolyte solution to the current flow has to be taken into account, too (R_s). Very often it happens that the faradaic component is composed by two elements, the resistance to the charge transfer (R_{ct}), and the resistance to the mass transfer (Z_w), which is represented by the so-called Warburg Impedance. The equivalent circuit that depicts a typical electrochemical cell is illustrated in Figure 5a. The Nyquist plot of a simple electrochemical cell is illustrated by the Figure 5b below, where the continuous line represents the total impedance, while the dashed line refers to faradaic impedance. The small green line represents the value of the resistance of the electrolyte solution, R_s : the higher this resistance, the longer this abscissa segment. The diameter of the circle, here indicated by a yellow line, represents the resistance to the charge transfer process R_{ct} . The point indicated in blue on the circle is linked to the capacitance of the double layer, C_d , because in that point is it possible to calculate the time constant τ of the system, being

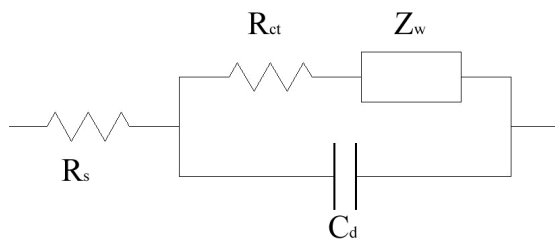


Figure 5a: Electrical circuit representing an electrochemical cell

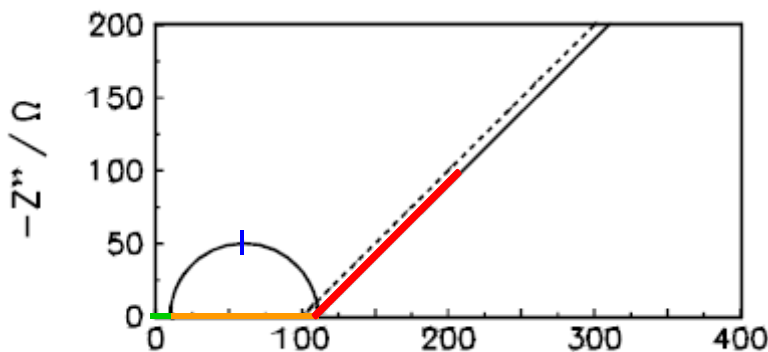


Figure 5b: Nyquist plot corresponding to the equivalent circuit reported in Figure 5a, representing an electrochemical cell

where the continuous line represents the total impedance, while the dashed line refers to faradaic impedance. The small green line represents the value of the resistance of the electrolyte solution, R_s : the higher this resistance, the longer this abscissa segment. The diameter of the circle, here indicated by a yellow line, represents the resistance to the charge transfer process R_{ct} . The point indicated in blue on the circle is linked to the capacitance of the double layer, C_d , because in that point is it possible to calculate the time constant τ of the system, being

$$\omega = \frac{1}{\tau} = \frac{1}{R_{ct} C_{dl}}$$

indicates the Warburg element, which can be recognized as a straight line with a 45° slope, typical of diffusion through infinite-thickness layers. When diffusion occurs in a medium of finite thickness, deviation from linearity at low frequencies can be observed.

The Bode plots for this circuit are here illustrated in Figure 5c:

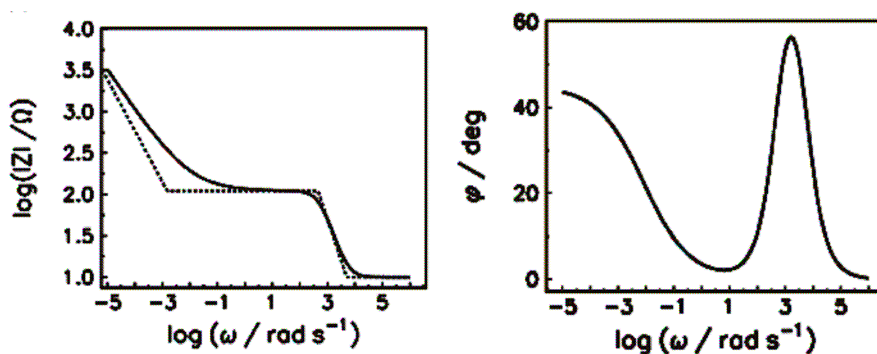


Figure 5c: Bode plots corresponding to the equivalent circuit reported in Figure 5a, representing an electrochemical cell

It is worthwhile spending some words to describe the Warburg element, one of the first introduced to describe diffusion phenomena arising when a redox process occurs at the working electrode. Its impedance is a function of the input potential frequency according to equation $Z_W = \sigma\omega^{-1/2} - i \sigma\omega^{-1/2}$, with

$$\sigma = \sigma_{\text{Ox}} + \sigma_{\text{Red}} = RT/(n^2F^2\sqrt{2}) [(1/(D_{\text{Ox}}^{1/2}C_{\text{Ox}}^*)) + (1/(D_{\text{Red}}^{1/2}C_{\text{Ox}}^*))]$$

Therefore in Warburg impedance the real and imaginary components depend on diffusion coefficients (in particular, they decrease with increasing diffusion coefficients, expressing the difficulty of the mass transfer) and are identical in modulus; accordingly, the phase angle is constant and = -45° . Thus:

- in the Nyquist diagram the Warburg element corresponds to a straight line with 1 slope;
- in the Bode phase diagram, it corresponds to a plateau for $\phi = 45^\circ$;
- in the Bode modulus diagram, it corresponds to a straight line with 1/2 slope.

As the above equation shows, Warburg impedance becomes determining with decreasing frequency, *i.e.* approaching stationary conditions, as in a potentiostatic electrolysis, implying the reagent diffusion to the electrode to become determining, which is accounted for by the Nyquist plot tending to a 45° straight line for $\omega \rightarrow 0$ in Figure 5b. On the contrary, with increasing frequency the reactant diffusion becomes negligible with respect to charge transfer resistance and double layer polarization (half circle); finally at the highest frequencies also these processes are excluded, and the solution ohmic resistance can be observed alone, as the small real segment in proximity to the origin.

This behaviour, typical of *semi infinite diffusion*, is modified in the case of diffusion within a finite boundary (*reflective or transmissive finite diffusion*), as shown in Figure 6.

Practical examples are:

- Semi infinite diffusion: a “bare” electrode involved in ET to/from an electrochemically active molecule diffusing to the electrode from the solution bulk
- Reflective finite diffusion: the same electrode covered by a conducting polymer layer, in the absence of redox active molecules in solution (at the potential considered); In this case, the $R_{ct}C_{dl}$ parallel corresponds to the electrode/polymer interphase and R_{ct} to the ET between electrode and polymer, resulting in the latter charging, with concurrent anion ingress to preserve electroneutrality; this obviously requires electrons and ions to diffuse in opposite directions within the finite polymer thickness (Warburg domain); however with decreasing frequency

capacitive saturation is reached since the amount of sites available for ET is limited and the charge cannot be transmitted beyond the polymeric layer on account of the absence of redox active molecules in solution.

- Transmissive finite diffusion: the same electrode covered by a conducting polymer layer, in the presence of a redox active molecule in solution in this case, the charge can be transmitted beyond the polymer layer, at the interphase between polymer surface and solution.

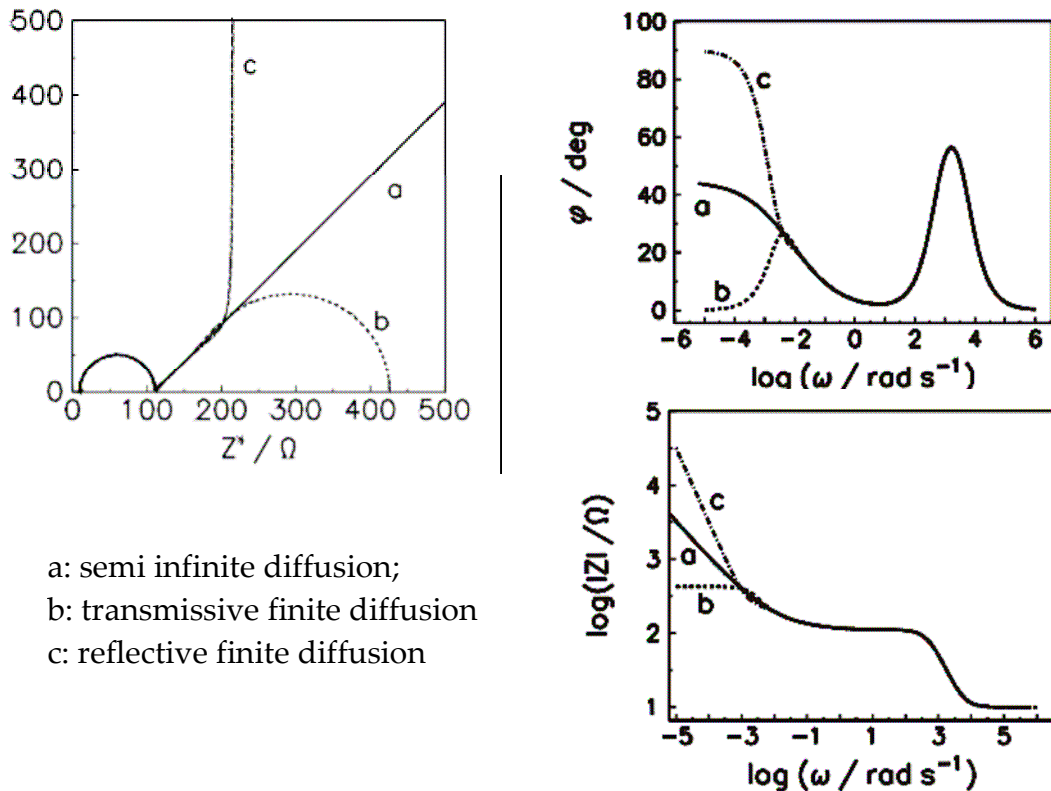


Figure 6: Faradaic (a) and total (b)-(d) impedances for
a) linear semi-infinite
b) finite transmissive
c) finite reflective boundaries,
 $R_s=10 \Omega$, $R_{ct}=100 \Omega$

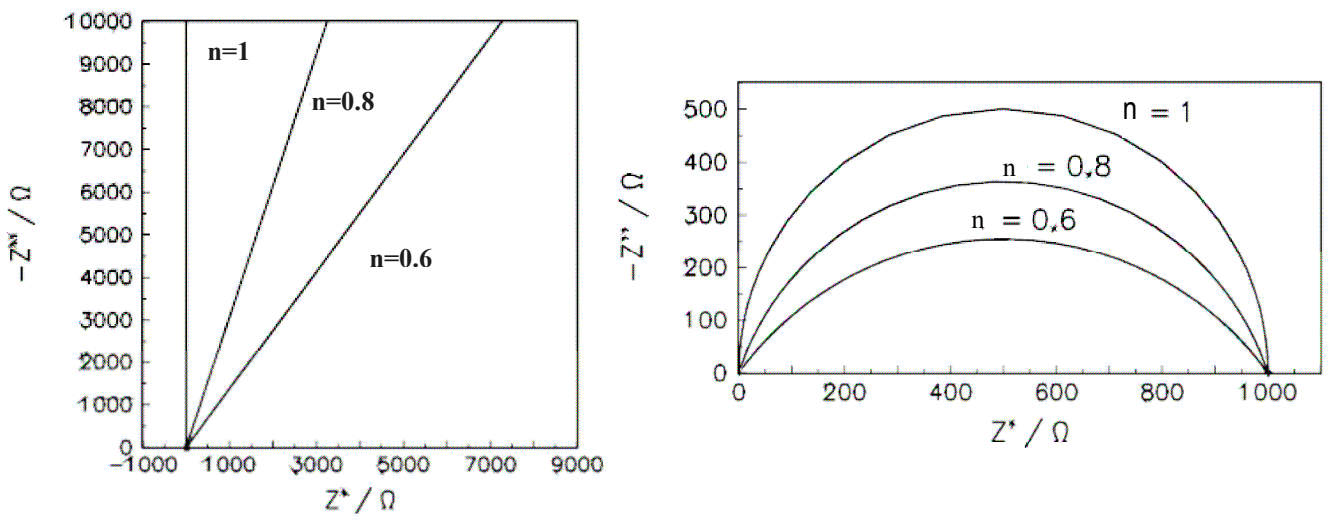
Another important element in EIS is the so-called Constant Phase Element. This element represents an empirical relationship which would take into account the effects of all the inhomogeneities of the surface or of the interfaces: $Z_{CPE}(j\omega) = A^{-1}(j\omega)^n$, where A is a proportionality coefficient, and $0 < n < 1$. The real and the imaginary parts of impedance

can be written as: $Z'_{Re} = \frac{\cos \frac{n\pi}{2}}{A\omega^n}$; $Z''_{Im} = \frac{\sin \frac{n\pi}{2}}{A\omega^n}$

The idea of CPE could be applied to every circuit element where the impedance results to be a function of the frequency by a trend that deviates from linearity; in practice, however, the CPE are normally applied only to capacitors, which act as models for charge separation layers. In fact, the use of capacitors to mimic the behaviour of porous electrode results to be incorrect, *i.e.*, the process under investigation would be too much idealized in this case, and would not consider the possible inhomogeneities and absence of ordered structures that often characterize this kind of electrodes. An ideal capacitor does not consider the possible dispersion of charge at the interface which may change the relationship that links the impedance of the capacitor to the frequency. The use of CPEs greatly helps in making the fitting of experimental data with the model much better, but also creates a debate in literature about the physical basis of the introduction of this element.

It is clear, however, that such an ideal behaviour is very rare, often because of the natural roughness of the electrode surface itself. So, the capacitor has to be replaced by a CPE. In Figure 7, simulated Nyquist diagrams for different values of the exponent n in the expression of the CPE impedance are reported.

Figure 7: Simulated Nyquist diagrams for different values of the exponent n in the expression of the CPE impedance, in the 100 kHz – 1 MHz frequency range, in the case of an ideally polarizable electrode (left) or in the presence of faradaic reactions (right), for different values of n



Both electrode porosity and specific adsorption phenomena deeply affect EIS spectra (examples are provided in the following figures) and require very complex mathematical treatment⁴⁶.

Figure 8: Porous electrodes in stationary conditions; a) intermediate general case, b) limiting case of shallow pores in which current easily reaches the pore base; in this case the electrode behaves as a flat electrode, c) limiting case of very deep pores, in which the penetration length is quite shorter than the pore length.

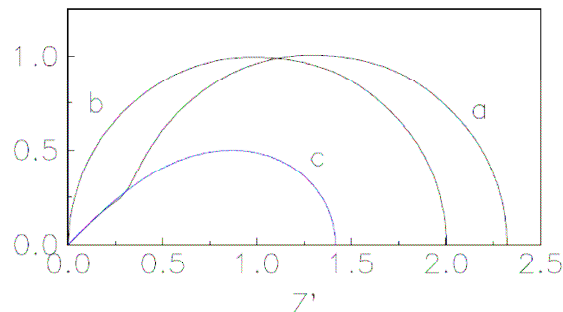


Figure 9: Porous electrodes in the presence of axial diffusion

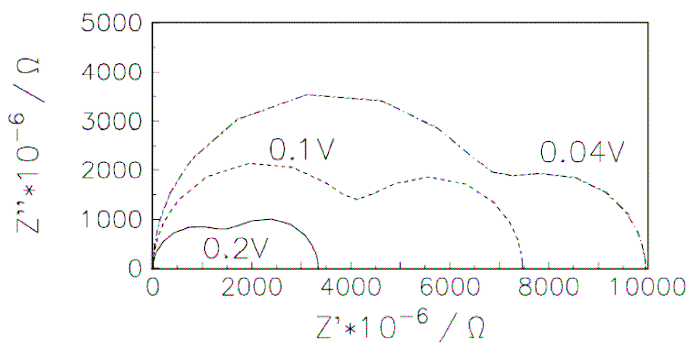
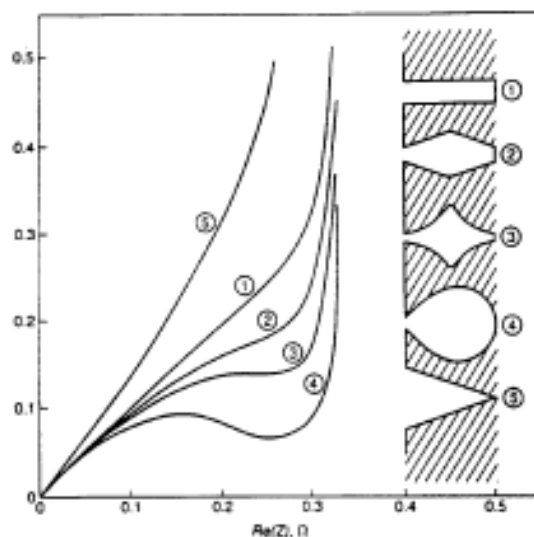


Figure 10: Effect of pore shape



⁴⁶ A.Lasia, Electrochemical Impedance Spectroscopy and its Applications, in Modern Aspect of Electrochemistry, edited by B.E.Conway, J. O'M. Bockris, and R.E. White, vol. 32, p.143-248, Kluwer Academic/Plenum Publisher, New York, 1999, ISBN 978-0-306-45964-1

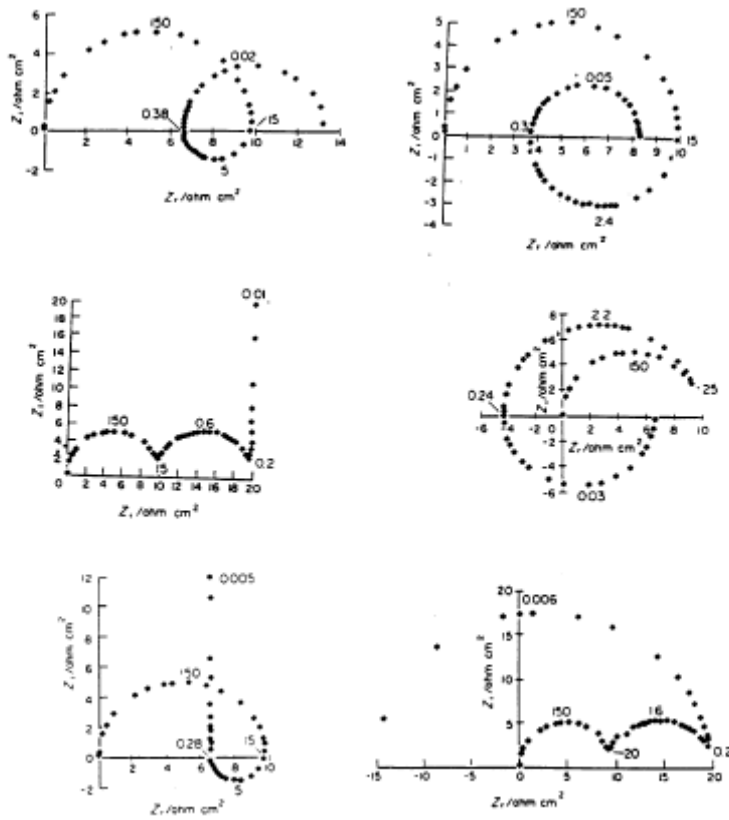


Figure 11: Some examples of the complex plane plots obtained for the case of two adsorbed species

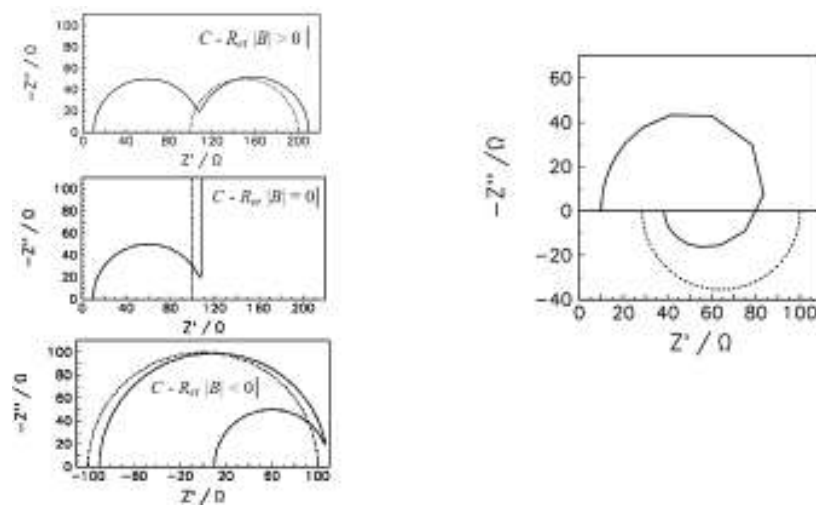


Figure 12: Some examples of the complex plane plots obtained for the case of one adsorbed species

2.4.2 The experimental setup and the analysis protocol

After the electrodeposition by cyclic voltammetry, the polymer films were also studied in monomer-free solution by comparing their electrochemical impedance at different potentials, representative of different possible doping states, in particular in the neutral state, in the onsets of the *p*- and *n*-doped states, and in the heavily *p*- and *n*-doped states. The potentiostat, the electrochemical cell, and the reference electrode (SCE, Amel, Italy, in a double bridge) were the same as described in the Chapter 2.1. The WE was a GC one, embedded in Teflon (0.071 cm², Metrohm, Switzerland), and the CE was a platinum sheet, ensuring a greater geometrical surface. The EIS experiments were performed in our laboratories by M.Sc. Ester Giussani, M.Sc. Mirko Magni and B.Sc. Luca Catalano according to the experimental protocol here described.

2.5 Other experimental techniques

Chiral HPLC and Polarimetry, performed by Dr. Roberto Cirilli, Dipartimento del Farmaco, Istituto Superiore di Sanità, Rome, Italy

HPLC enantioseparations were performed by using the stainless-steel Chiralpak IB-3 (250 mm x 4.6 mm i.d. and 250 x 10 mm i.d.) (Chiral Technologies Europe, Illkirch, France) columns. All chemicals solvents for HPLC, synthesis and spectral grade solvents were purchased from Aldrich (Italy) and used without further purification.

The analytical HPLC apparatus consisted of a Perkin-Elmer (Norwalk, CT, USA) 200 lc pump equipped with a Rheodyne (Cotati, CA, USA) injector, a 20- μ L sample loop, a HPLC Dionex CC-100 oven (Sunnyvale, CA, USA) and a Jasco (Jasco, Tokyo, Japan) Model CD 2095 Plus UV/CD detector. For semipreparative separations a Perkin-Elmer 200 LC pump equipped with a Rheodyne injector, a 500 μ L sample loop, a Perkin-Elmer LC 101 oven and Waters 484 detector (Waters Corporation, Milford, MA, USA) were used. The signal was acquired and processed by Clarity software (DataApex, Prague, The Czech Republic).

Concerning polarimetry, specific rotations were measured at 589 nm by a Perkin-Elmer polarimeter model 241 equipped with a Na/Hg lamp. The volume of the cell was 1 mL and the optical path was 10 cm. The system was set at a temperature of 20 °C

Molecular Modeling Calculations, performed by Prof. Marco Pierini, Dipartimento di Chimica e Tecnologie del Farmaco, Università degli Studi di Roma "La Sapienza", Rome, Italy

Conformational search of compound T4-BT2 has been performed by molecular mechanic calculations based on the MMFF force field, according to the stochastic MonteCarlo algorithm implemented in SPARTAN 08 (Wavefunction Inc. 18401 Von Karman Avenue, Suite 370, Irvine, CA 92612, USA). The two more stable conformations (T4-BT2_conf1 and T4-BT2-conf2), corresponding to 77% of the whole Boltzmann distribution, were further optimized at the HF/3-21G(d) level of theory and eventually refined by the hybrid

Hartree-Fock/Density Functional Theory method B3LYP, employed with the 6-31G(d) CD spectra related to the conformations T4-BT2_conf1 and T4-BT2_conf2 of R configuration have been calculated in vacuum at the BLYP/TZZP large core level of theory, as implemented in the Amsterdam Density Functional (ADF) package v. 2007.01. The set options were: single point calculation; 20 singlet excitations; diagonalization method: Davidson. The average CD spectrum reported in Figure 1b of main text was obtained by weighing the CD profiles of (R)-T4-BT2_conf1 and (R)-T4-BT2_conf2 on the calculated Boltzmann population values of 74% and 26%, respectively. basis set, as implemented within SPARTAN. These latter geometries were also used as starting structures to be optimized in form of cations (T4-BT2_conf1+ and T4-BT2_conf2+), always at the B3LYP/ 6-31G(d) level of theory. Then, relevant UV-visible spectra were calculated (Excited States: 6) for both neutral (*i.e.*, T4-BT2_conf1 and T4-BT2_conf2) and cationic forms (*i.e.*, T4-BT2_conf1+ and T4-BT2_conf2+) of compound T4-BT2, again at the B3LYP/ 6-31G(d) level. For sake of comparison, the same kind of calculations were also carried out on the above two conformations of T4-BT2 in which the dihedral angle between the thianaphthene units was constrained during the optimization at 90° (*i.e.*, T4-BT2_conf1_90°, T4-BT2_conf2_90°, T4-BT2_conf1_90°+, T4-BT2_conf2_90°+) or at 55° (only in the cation, *i.e.*, T4-BT2_conf1_55°+, T4-BT2_conf2_55°+). By both molecular mechanic (force field MM2) and semiempirical (the AM1 and PM3 Hamiltonians) calculations it was assessed that the enantiomerization energy barrier should be comprises between 47.7 and 32.5 kcal mol⁻¹, that is to say, values in any case sufficiently high to guarantee an enantiomerization half-lifetime of several centuries. Nevertheless, the same estimation was carried out by resorting to a different approach, which is based on the simulation of the transition state (TS) connecting the (S) and (R) configurations of T4-BT2. Therefore, the TS geometry of the (S) ⇌ (R) process has been modelled in vacuum at the B3LYP/ 6-31G(d) level of theory starting from the structure of both T4-BT2_conf1 and T4-BT2_conf2. For both the obtained transition states a single imaginary frequency was identified, corresponding to the correct vibration suitable to allow the stereomutation (*i.e.*, the (S) ⇌ (R) enantiomerization). The findings afforded an energy barrier of 35.4 kcal mol⁻¹ from the structure T4-BT2_conf1 and of 43.3 kcal mol⁻¹ from T4-BT2_conf2, in good agreement with previous estimations.

ESR spectroelectrochemistry, performed by Prof. Lothar Dunsch and Dr. Kinga Haubner, Centre of Spectroelectrochemistry, Department of Electrochemistry and Conducting Polymers, Leibniz Institute of Solid State and Materials Research (IFW), Dresden, Germany

In situ ESR/UV-vis-NIR spectroelectrochemical experiments were performed with a EMX X-band CW spectrometer (Bruker, Germany) using an optical ESR cavity ER 4104OR (Bruker Germany). UV-vis-NIR spectra were measured by the Avantes spectrometer AvaSpec-2048x14-USB2 with the CCD detector and AvaSpec-NIR256-2.2 with the InGaAs detector applying the AvaSoft 7.5 software. Both spectrometers were triggered by a HEKA potentiostat PG 390 using the software package PotMaster v2x40 (HEKA Elektronik, Germany). The potentiostat controlled the *in situ* spectroelectrochemical experiments in a special flat cell14 (Quarzglastechnik, Bad Harzburg, Germany) with a PTFE chloride-covered silver wire as the pseudo-reference electrode and a platinum wire as the counter electrode. As a working electrode a laminated platinum mesh was used. Commercially

available dichloromethane puriss. (CH_2Cl_2 , Aldrich) was used without further purification and tetrabutylammonium hexafluorophosphate (TBAPF_6) of puriss. quality (Fluka) dried under reduced pressure at $70\text{ }^\circ\text{C}$ for 24 h were used for the preparation of the solutions in a glove box. The cell was filled in a glove box, sealed and transferred to the ESR cavity.

AFM imaging, performed by Dr. Krzysztof Noworyta, Institute of Physical Chemistry of the Polish Academy of Sciences, Warsaw, Poland

Conducting polymer films were deposited from a $5 \cdot 10^{-4}$ M monomer concentration in the working solution (either acetonitrile or propylene carbonate and 0.1 M tetrabutylammonium hexafluorophosphate) on ITO and gold-coated glass slides electrodes. AFM images were recorded with a Multimode 3D AFM/STM microscope of Veeco.

UV-Vis spectroelectrochemistry, performed together with Dr. Monica Panigati, Università degli Studi di Milano, Milan, Italy

A quartz cuvette for UV-Vis spectroscopy was filled with the working solution; an ITO electrode, covered by a polymer film was the WE and was inserted in the cuvette, pinned to the cuvette wall with an alligator clip; a thin Pt wire was the CE and a small-diameter SCE was the reference electrode. On account of the small dimension of the system, it was not possible to deaerate the working solution. However, this should have not influenced the measurement, since the potential scans concerned mainly the anodic region, *i.e.* not involving the reduction of the molecular oxygen.

SEM imaging, performed together with M.Sc. Benedetta Sacchi, Università degli Studi di Milano, Milan, Italy

ITO or screen-printed electrodes, covered by electrodeposited polymer films, were sputtered with a layer of gold to ensure the necessary electrical conductivity, required by the technique. SEM micrographies have been taken with a scanning electron microscopy SEM-EDS (Energy-Dispersive Spectroscopy).

3. Results and Discussion

We must not forget that when radium was discovered no one knew that it would prove useful in hospitals. The work was one of pure science. And this is a proof that scientific work must not be considered from the point of view of the direct usefulness of it. It must be done for itself, for the beauty of science, and then there is always the chance that a scientific discovery may become like the radium a benefit for humanity.

Marie Curie, *Lecture at Vassar College, Poughkeepsie, New York, 14 May 1921*

3.1 The “genetically-modified” spider-like oligothiophenes⁴⁷

On the way of assembling efficient, light-weight and cheap organic electronic devices, the application of three-dimensional molecules appears to be a smart breakthrough. The isotropic charge-carrier behaviour, owned by branched systems, provides an high-efficiency charge transport into the devices, independently upon molecules orientation, making therefore easier and faster the optimization work.

In this view, all-thiophene macromolecules, presented in the recent literature, show very interesting electronic properties, and examples of preliminary applications of these compounds in the construction of organic devices have been reported⁴⁸.

The optoelectronic properties of these classes of materials are, however, generally unsuitable for applications in other challenging areas like organic photovoltaics, *e.g.*, in bulk-heterojunction solar cells, since they are characterized by a quite large HOMO-LUMO energy gap and, in particular, by energetically too high LUMO levels. For example, our *spider-like* oligothiophenes present a rather modest light harvesting, with absorption maxima at about 480 nm, and, despite the HOMO energy levels display the right values for an effective matching with the LUMO of the PCBM, the LUMO energy levels are hardly reached by electrons excited by sunlight which has an emission maximum at about 650 nm ($\approx 1,9$ eV). Furthermore the energy difference between the LUMOs of the spiders and the LUMO of PCBM is too high ($\approx 1,5$ eV), making easier the recombination of the charges in the donor, a phenomenon which has the same chance to happen as the charge separation when the electron is transferred to the acceptor.

⁴⁷ T. Benincori, M. Capaccio, F. De Angelis, L. Falciola, M. Muccini, P. Mussini, A. Ponti, S. Toffanin, P. Traldi, F. Sannicolò, *Chem. Eur. J.*, **2008**, *14*, 459;

T. Benincori, V. Bonometti, F. De Angelis, L. Falciola, M. Muccini, P. R. Mussini, T. Pilati, G. Rampinini, S. Rizzo, S. Toffanin, F. Sannicolò, *Chem. Eur. J.*, **2010**, *16*, 9086

Valentina Bonometti, M.Sc. Thesis, Università degli Studi di Milano, 2009

Giovanni Rampinini, PhD Thesis, Università degli Studi di Milano, 2010

Cristina Cerqui, M.Sc. Thesis, Università degli Studi di Milano, 2010

Jacopo Bonanomi, M.Sc. Thesis, Università degli Studi di Milano, 2011

Ester Giussani, M.Sc. Thesis, Università degli Studi di Milano, 2011

Renzo Graziosi, M.Sc. Thesis, Università degli Studi di Milano, 2012

⁴⁸ B.L. Rupert, W.J. Mitchell, A.J. Ferguson, M.E. Kose, W.L. Rance, G. Rumbles, D.S. Ginley, S.E. Shaheen, N. Kopidakis, *J. Mater. Chem.*, **2009**, *19*, 5311-5324.

One way to reduce the energy gap could be the increase of the conjugation of the system, *e.g.*, by increasing the length of the conjugative conducting backbone.

However, in *spider-like* oligothiophenes the presence of *nodes*, *i.e.*, distortions from planarity, along the main conjugated chain produces either an outstanding increase in solubility, and an enhancement of the three-dimensional structure of the polymers obtained by electrooxidation but also exerts some influence on the extent of conjugation and consequently onto the optical properties. In these systems, therefore, increasing the length of the α -conjugated chain is a quite ineffective operation in view of reducing the energy gap.

A possible and attracting solution for a more efficient modulation of the optoelectronic properties in the spider-like series, is to introduce into the backbone a central core (the *body* of the spider) endowed with peculiar electronic properties. In order to reduce the energy gap, the common strategy is to alternate a donor unit to an acceptor unit, as reported in many small molecules designed for application in bulk-heterojunction solar cells.

From the electrochemical point of view, this corresponds to differentiate the first oxidation and reduction sites, while in all-thiophene systems both the oxidation and reduction corresponded to the main conjugated chain. Since the LUMO was found to be too high in energy, it should be lowered, *e.g.*, by inserting an electron-withdrawing core in the molecule.

A new series of molecules was then synthesized by the group of Prof. F. Sannicolò from the Università degli Studi di Milano, named *genetically modified spiders*, or, in analogy with the most common vocabulary adopted in organic photovoltaics, *push-pull* spider-like oligothiophenes, characterized by the presence of various electronically different, conjugatively active, central moieties (the *bodies*), decorated with homotopic branched quarterthiophene pendants (the *legs*) (Figure 1)⁴⁹. The name *push-pull* derives from the presence of two donor units, the quarterthiophene legs, which push electrons to the central electron-withdrawing core.

The donor-acceptor (D-A) concept for band gap reduction was proposed by Havinga *et al.* in 1992⁵⁰. The authors conducted an investigation upon the effect of a regular alternation of conjugated strong donor unit, benzodithiazole, and acceptor-like moiety, squaric acid, in a conjugated backbone. Very low band gap (≈ 0.5 eV) and an interesting conductivity upon doping ($1.0 \text{ S}\cdot\text{cm}^{-1}$) have been reported for this polymer.

The band gap is smallest for a combination in which the electronegativity difference between donor and acceptor is greatest.

Six different acceptor bodies have been chosen for this investigation: fluorenone (1), 4H-[3,2-b]-cyclopentadithiophene-4-one (2), acridone (3), thioxantone (4), dibenzothiophene dioxide (5), and 2-bisthienyl-fluorene (6). The fluorenone body was

⁴⁹ G. Rampinini, A. Digennaro, T. Benincori, V. Bonometti, P. R. Mussini, M. Panigati, R. Po', F. Sannicolò, Energy Gap Tuning in Linear and Branched Oligothiophene Semiconductors: Structure-properties relationships in new "push-pull" spider-like oligothiophenes, manuscript in preparation, 2012

⁵⁰ E. E. Havinga, W. ten Hoeve, H. Wynberg, *Polym. Bull.*, 1992, 29, 119

then further modified by inserting an ethylenethioether (7), or an acetyl ester (8) to evaluate the effect of these electronrich substituents.

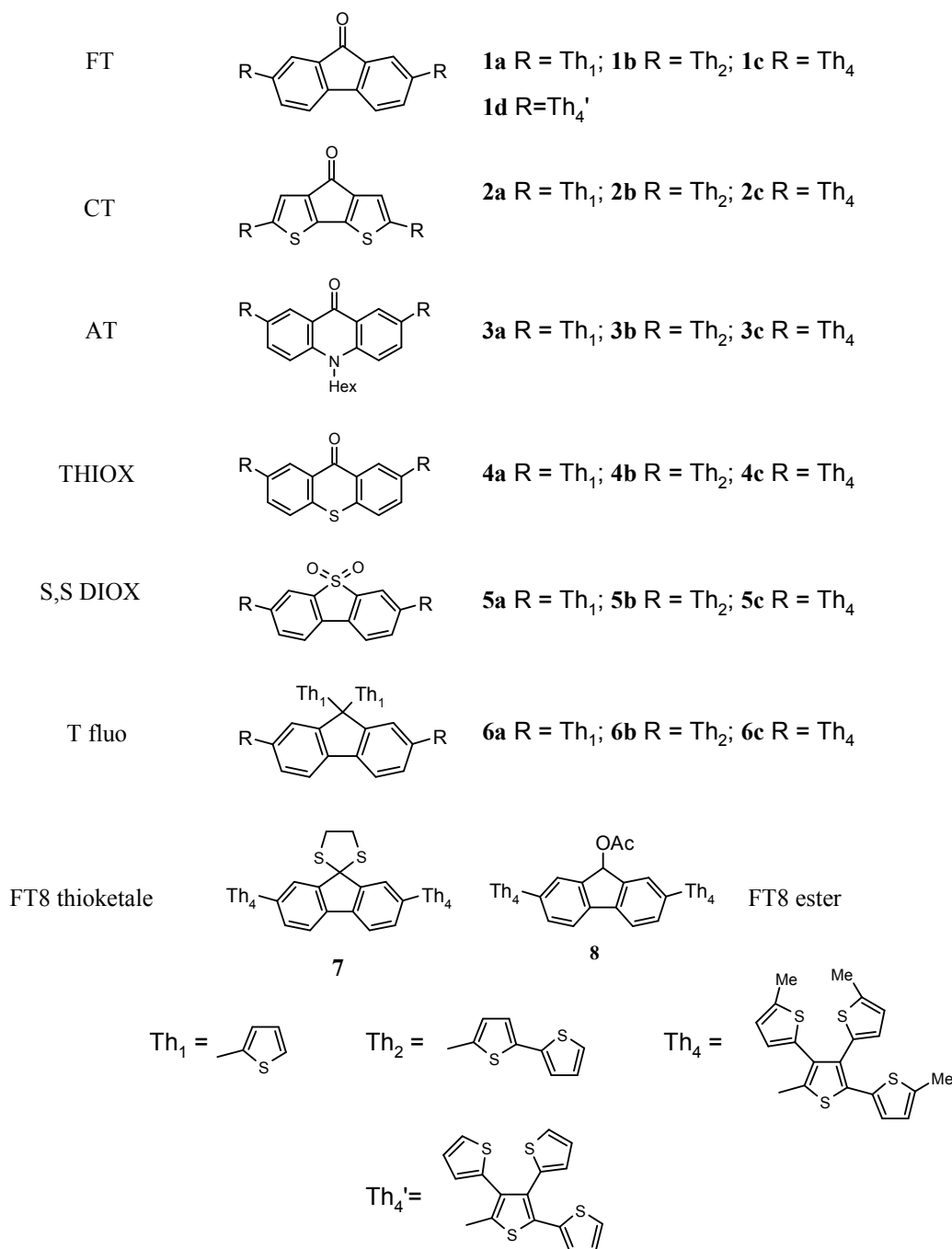


Figure 1: The series of the genetically-modified spider-like oligothiophenes

Another molecule was then synthesized, exploiting the ease of functionalization of the carbonyl group in its precursor, FHexT6 (**10**, Figure 2), to get a fullerene-modified spider-like, FHexT6C₆₀ (**11**, Figure 2), with the α -positions blocked by hexyl groups, that avoid the electropolymerization to occur but allow a good solubility in dichloromethane and an excellent solubility in THF. FHexT6C₆₀ is particularly attractive, bearing the PCBM acceptor, the most widely employed acceptor system in bulk-heterojunction solar cell,

obtained by a quite easy synthetic pathway and featuring good solubility in common organic solvents, an important characteristic for simple industrial processing. These two molecules were characterized by cyclic voltammetry and compared with red-FHexT6 (9, Figure 2), obtained by reduction of the carbonyl function of FHexT6. These molecules will be discussed more in detail in Chapter 3.1.1.

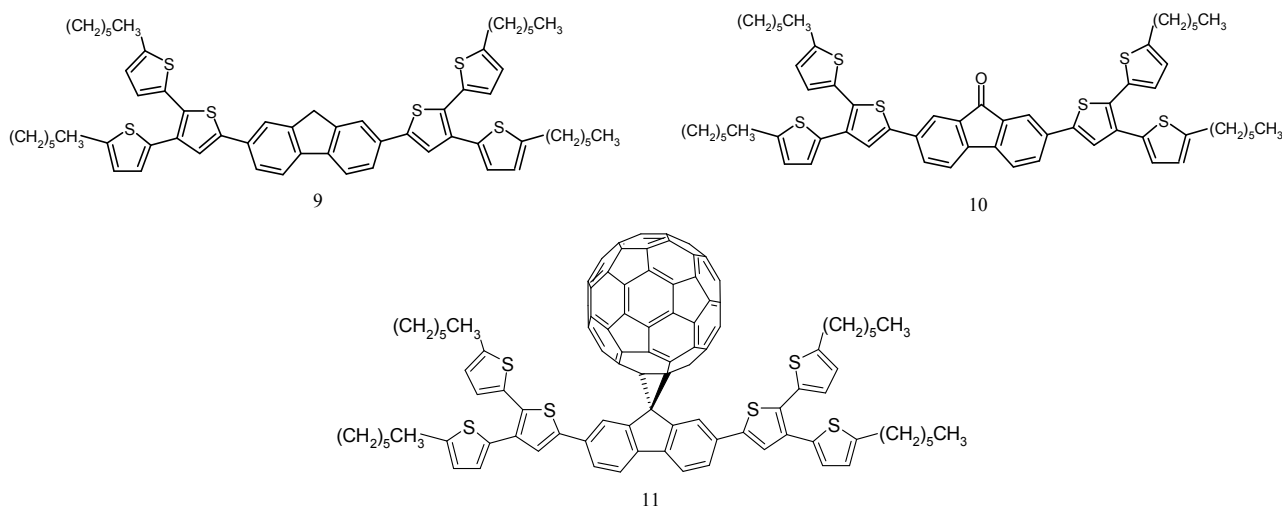


Figure 2: Structures of red-FHexT6, FHexT6 and FHexT6C₆₀

The genetically modified series was investigated by means of cyclic voltammetry and electrochemical impedance spectroscopy⁵¹, considering not only the effect of an increasing ability of the core in stabilizing the negative charge, but also the effect of increasing the conjugation length, having bithienyl side chains instead of monothiophenes (**b** series *vs* **a** series), and the effect of branching (**c** series).

In Figure 3, a synopsis of the voltammetric characteristics of the monomers under investigation is presented.

At a first glance, it can be observed that, increasing the length of the terminal side chains, there is a neat and strong anticipation of the anodic peak: the oxidation becomes much easier thanks to the extended conjugation that allows a better delocalization of the charge. The HOMO and LUMO values, calculated from the first oxidation and first reduction peaks maxima and onsets, as previously explained in Chapter 2.1.3, are then plotted in the graph reported in Figure 4, showing at a first glance the effect of the cores and of the increased conjugation. The missing values were not calculated because the oxidation and/or reduction sites were out of the potential window available in the working medium CH₂Cl₂ + TBAP 0.1 M.

⁵¹ Cristina Cerqui, M.Sc. Thesis, Università degli Studi di Milano, 2010
 Ester Giussani, M.Sc. Thesis, Università degli Studi di Milano, 2011
 Luca Catalano, B.Sc. Thesis, Università degli Studi di Milano, 2011

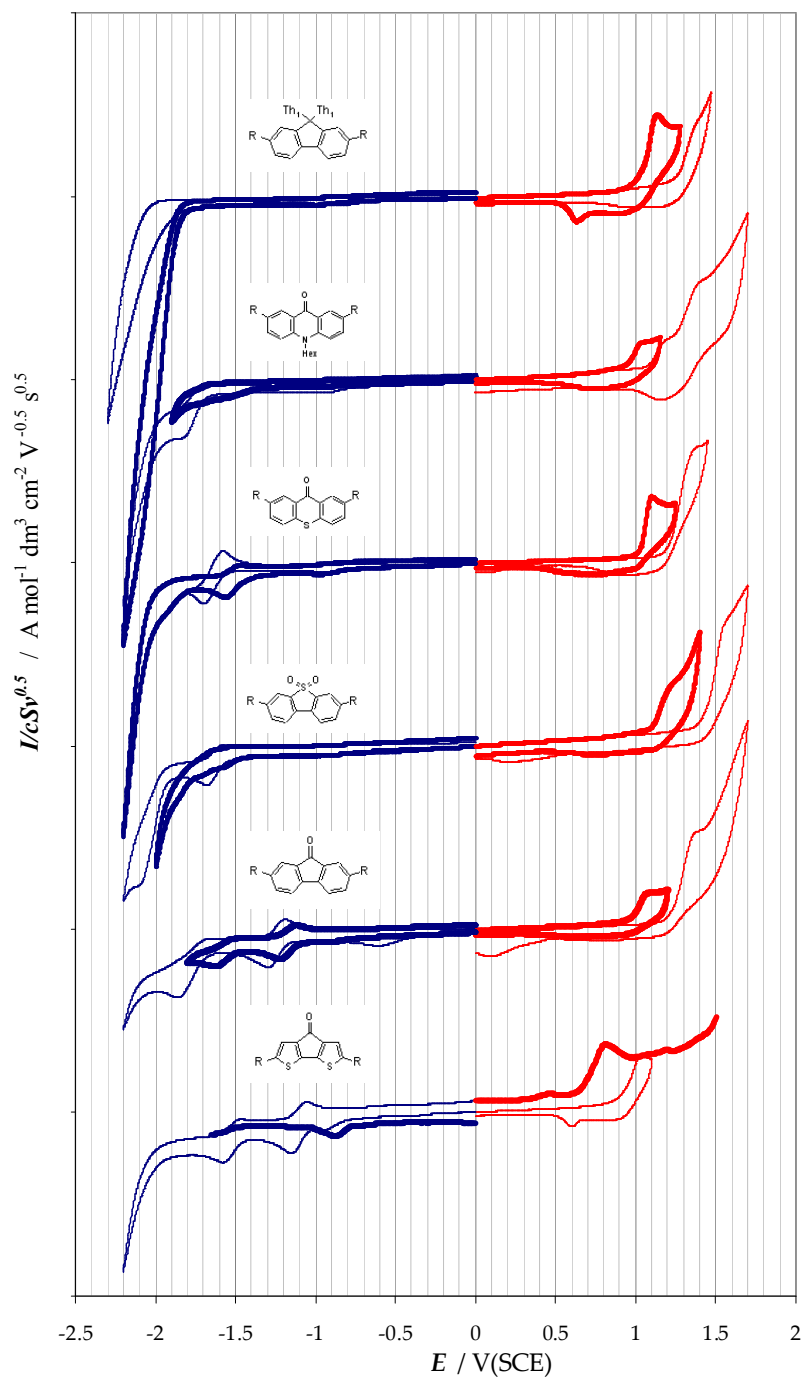


Figure 3: Voltammetric characteristics of the genetically modified spiders, from 1 to 6, *a* series (monothiophene side chains, light line) and *b* series (bithienyl side chains, bold line). CVs were recorded in CH₂Cl₂+TBAP 0.1 M on a GC electrode (S=0.071 cm²). Potentials are referred to SCE. The molecule 2b (CT4) was scarcely soluble in the reaction medium, so a DPV signal was recorded in DMF.

A longer side chain length has, however, negligible effects on the position of the reduction peak, and, consequently, on the LUMO level, which is much more affected by the nature of the core: the more its ability in stabilizing the negative charge, the more stabilized the LUMO. From the voltammetric characteristics, it is possible to observe, where detectable, monoelectronic and reversible reduction peaks.

In this series, interestingly, the molecules CT (**2**), having a cyclopentadithiophene core, have the narrowest energy gap: this could be attributed to the presence of the carbonyl group on the core, that stabilizes the negative charge, and to a more extended conjugation, since the core itself contains two thiophene units, so the conjugation results to be increased with respect to the other similar terms of the family.

In the figure 4, HOMO and LUMO levels for all the genetically-modified spiders were collected; they were calculated from the first anodic and cathodic peak, according to the criterion explained in Chapter 2.1.3, considering both the peaks' maxima (left) and the onsets (right). HOMO and LUMO values of P3HT (orange shadow) and PCBM (light-blue shadow), taken from the literature⁵² and also measured in the same experimental conditions as the genetically-modified molecules⁵³, and averaged, are reported for comparison.

⁵² Sigma Aldrich catalogue *Materials Science Products*

J.T. Blocking, A.T. Higgs, X. Han, J.P. Kastrop, L. Pandey, J.E. Norton, C.Risko, J.L. Brédas, M.D. McGehee, A. Sellinger, *Solution-processed bulk-heterojunction solar cells from non fullerene acceptor molecules*, https://gcep.stanford.edu/pdfs/oH-1g83C3aUMgi1z7Px97Q/JasonBlocking_GCEPposter2011.pdf

⁵³ E.V. Canesi, G. Lerario, R. Sai Santosh Kumar, L. Colella, V. Bonometti, P. R. Mussini, C. Bertarelli, P. E. Keivanidis, submitted, 2012

	$E_{\text{ox, max}}$ V/Fc ⁺ Fc	$E_{\text{red, max}}$ V/Fc ⁺ Fc	$E_{\text{ox, onset}}$ V/Fc ⁺ Fc	$E_{\text{red, onset}}$ V/Fc ⁺ Fc	$E_{\text{gap, max}}$ /eV	$E_{\text{gap, onset}}$ /eV	HOMO max /eV	LUMO max /eV	HOMO onset /eV	LUMO onset /eV
1a	0.90	-1.75	0.73	-1.57	2.64	2.31	-5.70	-3.05	-5.53	-3.23
1b	0.69	-1.73	0.47	-1.53	2.42	2.00	-5.49	-3.07	-5.27	-3.27
1c	0.78	-1.73	0.52	-1.62	2.51	2.13	-6.08	-3.57	-5.81	-3.68
1d	0.81	-1.75	0.63	-1.61	2.56	2.24	-5.61	-3.05	-5.43	-3.38
7	0.75	-2.24	0.51	-2.10	2.99	2.61	-5.55	-2.56	-5.31	-2.70
8	0.80	-2.28	0.59	-2.10	3.07	2.69	-5.60	-2.53	-5.39	-2.70
2a	0.55	-1.61	0.39	-1.47	2.16	1.86	-5.35	-3.19	-5.19	-3.33
2b (DPV)	0.37	-1.40	0.15	-1.31	1.77	1.46	-5.17	-3.40	-4.95	-3.49
2c	0.32	-1.69	0.23	-1.54	2.00	1.76	-5.61	-3.61	-5.52	-3.76
3a	0.79	-2.28	0.68	-2.13	3.07	2.81	-5.59	-2.52	-5.48	-2.67
3b	0.54	-2.20	0.46	-2.08	2.74	2.54	-5.34	-2.60	-5.26	-2.72
3c	0.56	-2.30	0.41	-2.18	2.86	2.60	-5.60	-2.74	-5.46	-2.87
4a	0.87	-2.19	0.66	-2.03	3.06	2.68	-5.67	-2.61	-5.46	-2.78
4b	0.61	-2.06	0.51	-1.91	2.67	2.41	-5.41	-2.74	-5.31	-2.90
4c	0.77	-2.09	0.64	-1.97	2.86	2.61	-6.06	-3.20	-5.94	-3.33
5a	1.06	-2.17	0.91	-2.00	3.23	2.91	-5.86	-2.63	-5.71	-2.80
5b	0.68	-2.08	0.54	-1.91	2.76	2.45	-5.48	-2.72	-5.34	-2.89
5c	0.81	-2.17	0.63	-2.05	2.98	2.68	-6.11	-3.13	-5.93	-3.24
6a	0.87	-2.66	0.78	-2.33	3.54	3.12	-5.67	-2.14	-5.58	-2.47
6b	0.64	-2.51	0.52	-2.35	3.15	2.87	-5.44	-2.29	-5.32	-2.45
6c	0.81	-2.56	0.54	-2.30	3.37	2.84	-5.61	-2.24	-5.34	-2.50
9	0.59	-2.47	0.49	-2.40	3.06	2.89	-5.39	-2.33	-5.29	-2.40
10	0.76	-1.65	0.53	-1.54	2.41	2.07	-5.56	-3.15	-5.33	-3.26
11	0.71	-1.09	0.46	-0.97	1.80	1.43	-5.51	-3.71	-5.26	-3.83

Table 1: Voltammetric data of all the genetically-modified spiders, and calculated HOMO and LUMO levels and gaps.

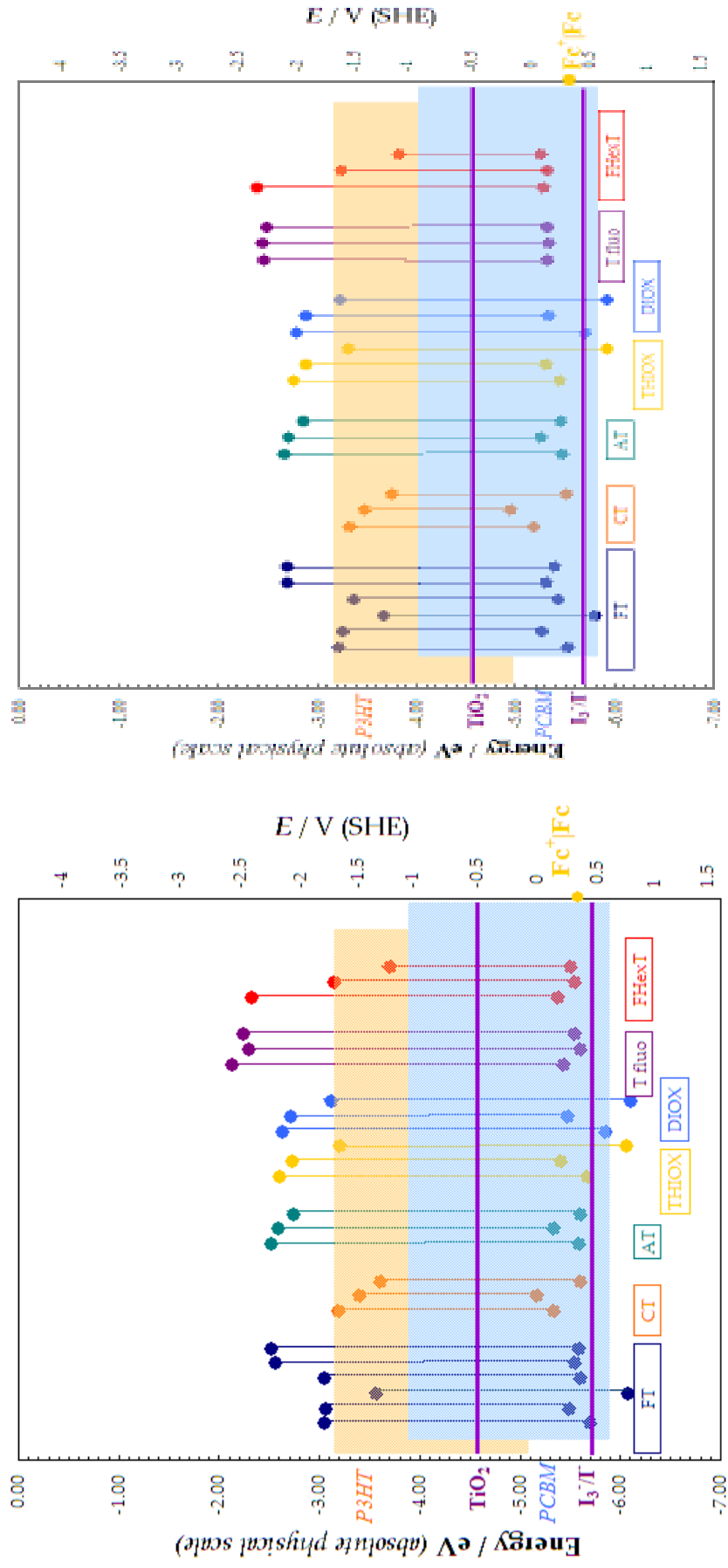


Figure 4: Plot of the HOMO and LUMO levels, for the molecules in the series 1-6, according to the following order (from left to right): In dark blue, FT group: FT2, FT4, Met-FT8, FT8, FT8-thioetale and FT8-ester. In orange: CT2, CT4, Met-CT8; In dark green: AT2, AT4, Met-AT8; In yellow: THIOX2, THIOX4, Met-THIOX8 In light blue: S,S-DIOX2, S,S-DIOX4, Met-S,S-DIOX8, In red: Tflu02, Tflu04, Met-Tflu08, FHexT6, FHexT6 and FHexT6C₆₀. On the left y axis, the potential scale is referred to the standard hydrogen electrode; this scale was adopted by Graetzel albeit with reference to the discarded NHE convention, approximately corresponding to the current SHE one. P3HT, PCBM levels and gaps are reported as orange and light-blue shadows for comparison. TiO₂ and I₃/I⁻ levels are reported as violet lines for comparison.

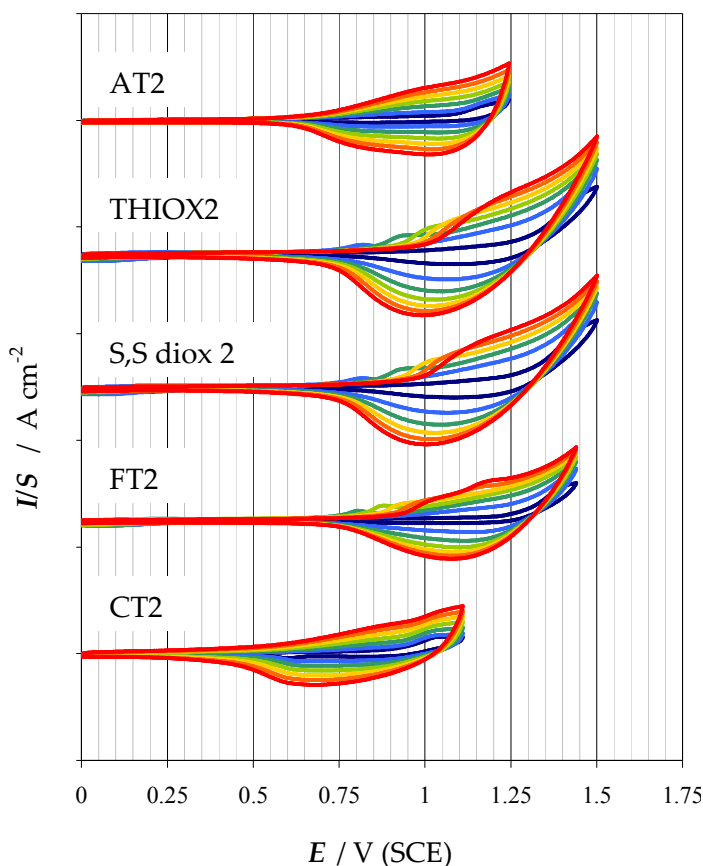


Figure 5: Attitude towards polymerization for monomers belonging to the *a* series (monothiophene side chains). Data recorded in $\text{CH}_2\text{Cl}_2 + \text{TBAP}$ 0.1 M on a GC electrode ($S=0.071 \text{ cm}^2$). Potentials are referred to SCE.

electrons diffusion within the polymer network: the longer this segment, the more difficult the diffusion. In our case, the length of such a segment is greater for FT2 and THIOX2 than for AT2 and CT2, that show almost immediately a capacitive behaviour at medium and low frequencies, as shown in the Bode phase diagram. This behaviour could be attributed to easier ion and electron diffusion in AT2 and CT2 films, confirming the cyclic voltammetry data, since the molecules that offer a lower resistance to the mass transport (both for electrons and counter-ions from the supporting electrolyte) are the molecules that better polymerize, and, on the other hand, good ion- and electron transport within the polymer network affords fast and regular growth of the film, avoiding the formation of structural defects that could hamper the diffusion inside it.

All the genetically modified monomers belonging to the **a** and **b** series can give polymeric films by cycling the potential around the first oxidation peak.

The electropolymerization of AT2 and CT2, for example, proceeds maybe slower than in the other cases, but in a more regular and efficient way, and at less positive potentials. This behaviour was confirmed by preliminar EIS measurements on the electrodeposited films, in $\text{CH}_2\text{Cl}_2 + \text{TBAP}$ 0.1 M, at the potential where the film is in its *p*-doped state AT2: 1.001 V/SCE ; CT2: 0.884 V/SCE ; FT2: 1.148 V/SCE ; T2: 1.146 V/SCE).

The EIS spectra can be interpreted in terms of a Randles equivalent circuit (see Chapter 2.4)⁵⁴ in absence of any other redox couple in solution, where the Z_w (mass transport impedance) is substituted with Z_{rfw} , *i.e.*, restricted finite Warburg impedance element. In the Nyquist plot in Figure 6, the pink segment corresponds to the ions and

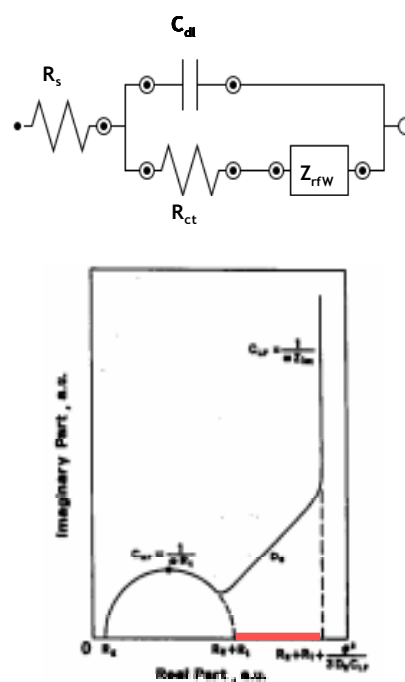


Figure 6: Randles equivalent circuit and corresponding Nyquist plot

⁵⁴ M. Musiani, *Electrochim. Acta*, 1990, 35, 10, 1665

Interestingly AT2 and CT2, in spite of the quite different electronic effects by their cores, are the two terms in the series having their monoelectronic first oxidation peaks at the less positive potentials, corresponding to a maximum efficiency in the radical cation formation (polaron), intermediate in the polymerization process. This can be explained considering that AT2 is electron richer, resulting in negative shift of both the first reduction and first oxidation peaks, while CT2 has an extremely efficient conjugated system, that leads to a strong anticipation of the first monoelectronic peak in spite of the core antagonist effect.

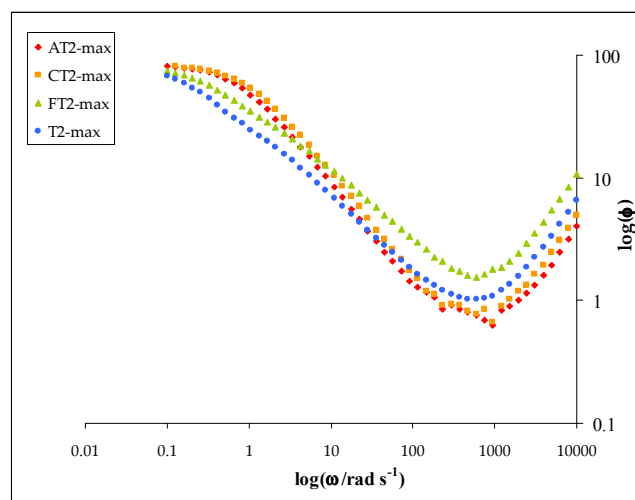
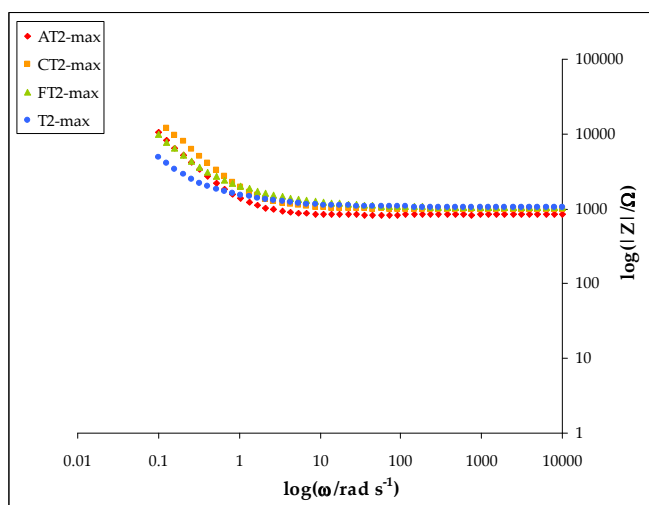
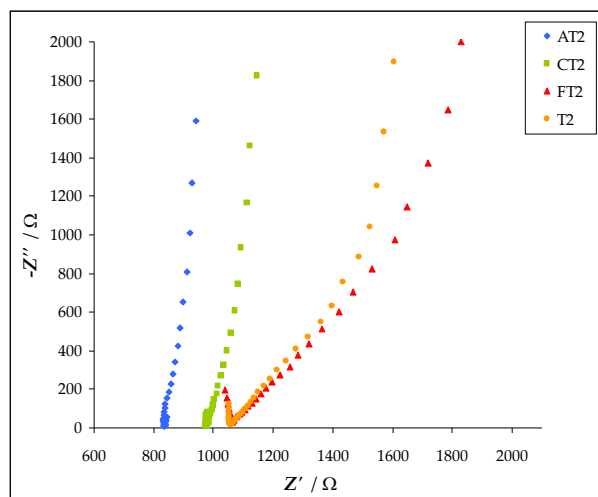


Figure 7: Nyquist, Bode modulus and Bode phase for AT2, CT2, FT2 and THIOX2 films in their *p*-doped states, in CH₂Cl₂+TBAP 0.1 M, on a GC electrode.

The effect of the length of the thiophene side-chains was then investigated by means of cyclic voltammetry, and EIS measurements confirmed the CV data interpretation. As an example, the comparison between THIOX2 and THIOX4 is reported. The shift of the anodic peak towards less positive potentials is evident for THIOX4 (0.264 V). Also its cathodic peak is shifted towards less negative potentials, but the effect is more marked for the oxidation.

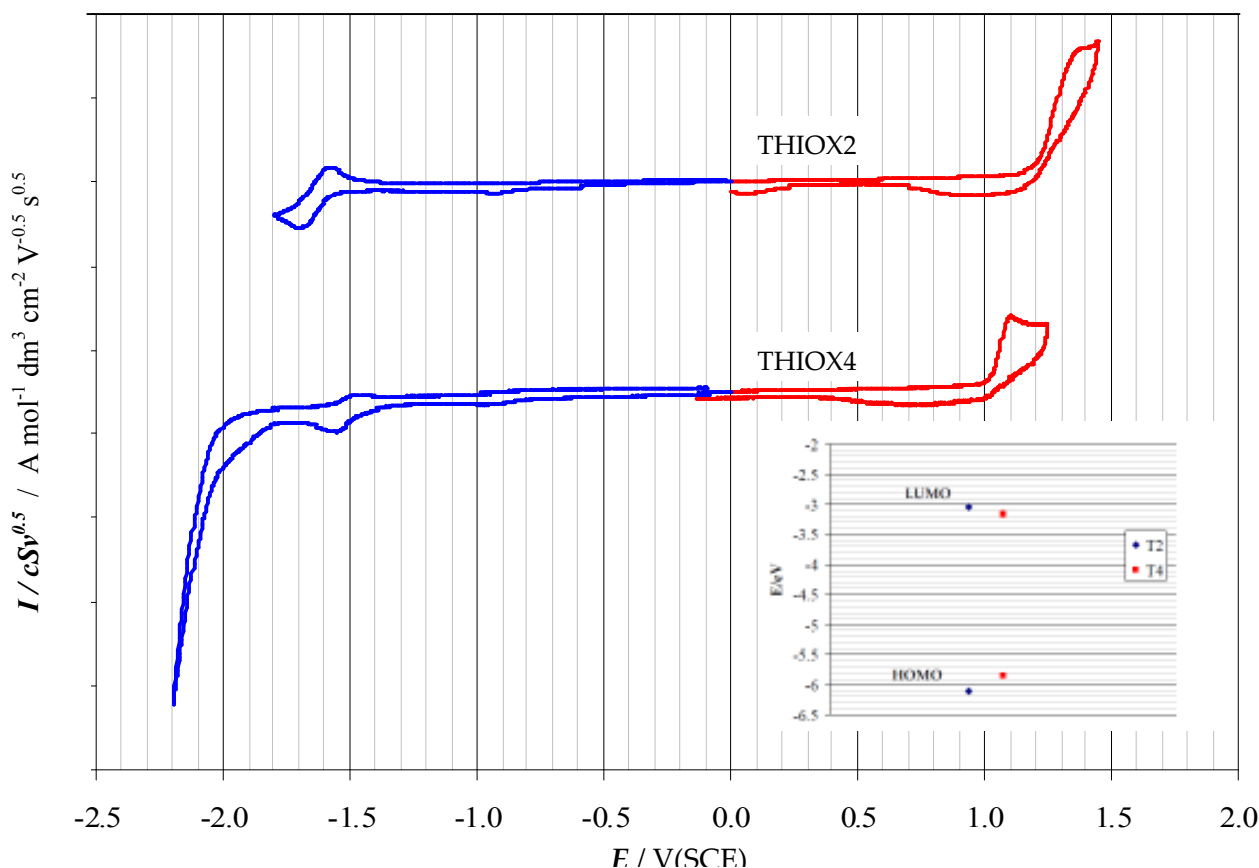


Figure 8: CVs of THIOX2 and THIOX4, $5 \cdot 10^{-4}$ M in $\text{CH}_2\text{Cl}_2 + \text{TBAP}$ 0.1 M, on a GC electrode ($S = 0.071 \text{ cm}^2$), $v = 200 \text{ mV/s}$. Potentials are referred to SCE. Inset: the progressive HOMO-LUMO gap shrinking with increasing length of the side chains.

	$E_{p,a \text{ max}}$ V/Fc ⁺ Fc	$E_{p,c \text{ max}}$ V/Fc ⁺ Fc	$E_{\text{gap max}}$ V	HOMO eV	LUMO eV
THIOX2	0.87	-2.19	3.06	-5.67	-2.61
THIOX4	0.61	-2.06	2.67	-5.41	-2.74

	$E_{p,a \text{ onset}}$ V/Fc ⁺ Fc	$E_{p,c \text{ onset}}$ V/Fc ⁺ Fc	$E_{\text{gap onset}}$ V	HOMO eV	LUMO eV
THIOX2	0.66	-2.03	2.68	-5.46	-2.78
THIOX4	0.51	-1.91	2.41	-5.31	-2.90

So, the HOMO, which is localized on the thiophene chain α terminals, is more affected by the increase of conjugated system length than the LUMO. This is coherent with the π -system increased effective conjugation, that allows a better delocalization of the radical

cation. On the other hand, the cathodic peak shift is only 0.13 V, confirming that the LUMO is mainly localized on the core.

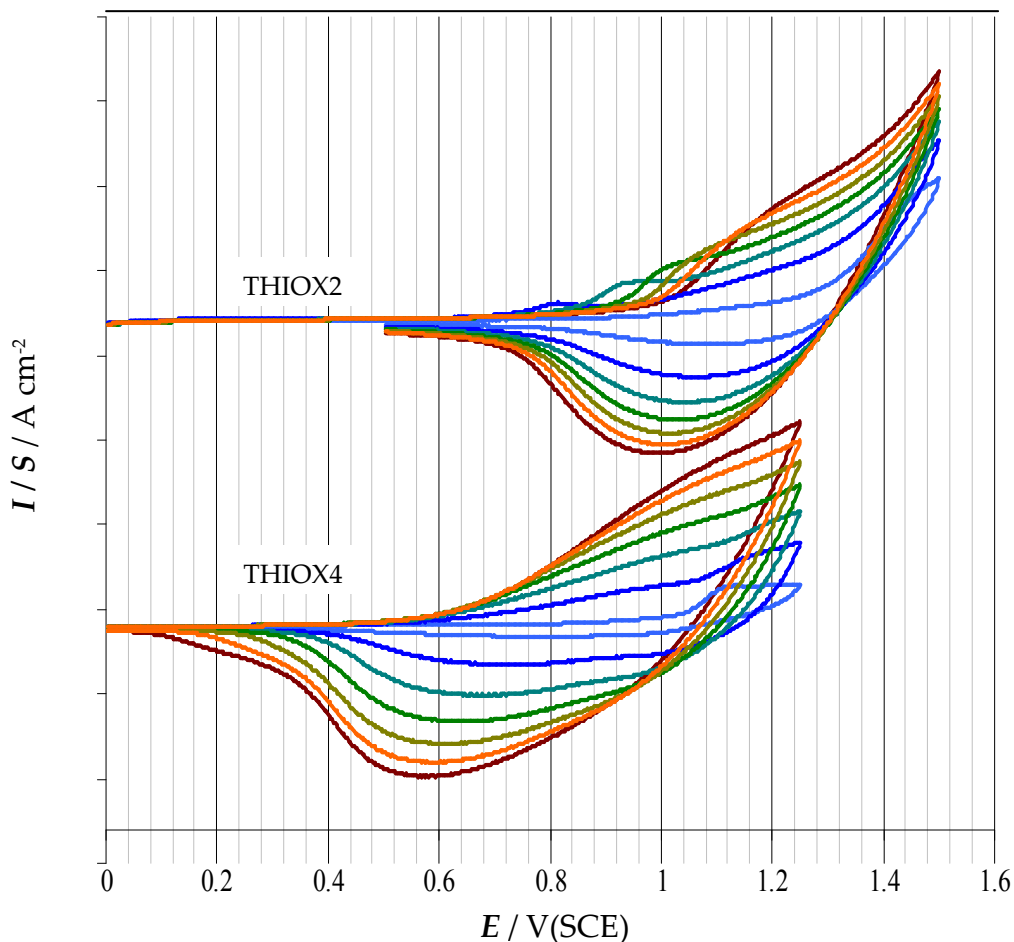


Figure 9: Electropolymerization of THIOX2 and THIOX4 monomers, from a $5 \cdot 10^{-4}$ M solution in $\text{CH}_2\text{Cl}_2 + \text{TBAP}$ 0.1 M, on a GC electrode ($S = 0.071 \text{ cm}^2$), $v = 200 \text{ mV/s}$, 36 cycles. Potentials are referred to SCE.

In addition, as shown in Figure 9, THIOX4 polymerizes even in a more regular way than THIOX2, which shows another peak that is progressively moving towards more positive potentials during the electropolymerization process. Both films were stable upon repeated potential cycling in monomer-free solution, but did not show any *charge trapping* effect.

EIS measurements were performed on the films in the *p*-doped and in the neutral state. In particular, in the *p*-doped state, the potentials corresponded to the maximum of the oxidation peak: 1.146 V/SCE for THIOX2 and 1.157 V/SCE for THIOX4.

THIOX4 shows a lower resistance to mass transport (*i.e.*, electrons and ions from the supporting electrolyte) within the polymer film, and a lower resistance to charge transfer at the interphase electrode/polymer. It is worthwhile underlying that the thickness of the film may influence the length of the Warburg segment, but in this case the thickness of the two films was similar (estimated by comparison of the charge exchanged during the stability cycles). Also in this case, EIS data could be interpreted in terms of an equivalent Randles circuit in absence of other redox couples in solutions, where the Z_w (impedance relative to the mass transport) is substituted with Z_{rFW} (restricted Warburg impedance

element), as shown in Figure 6. The length of the segment corresponding to electron and ion diffusion within the polymer network is lower for THIOX4 (*i.e.*, easier diffusion of electrons and ions), and even the resistance to charge transfer, R_{CT} , is lower, confirming the behaviour shown by cyclic voltammograms.

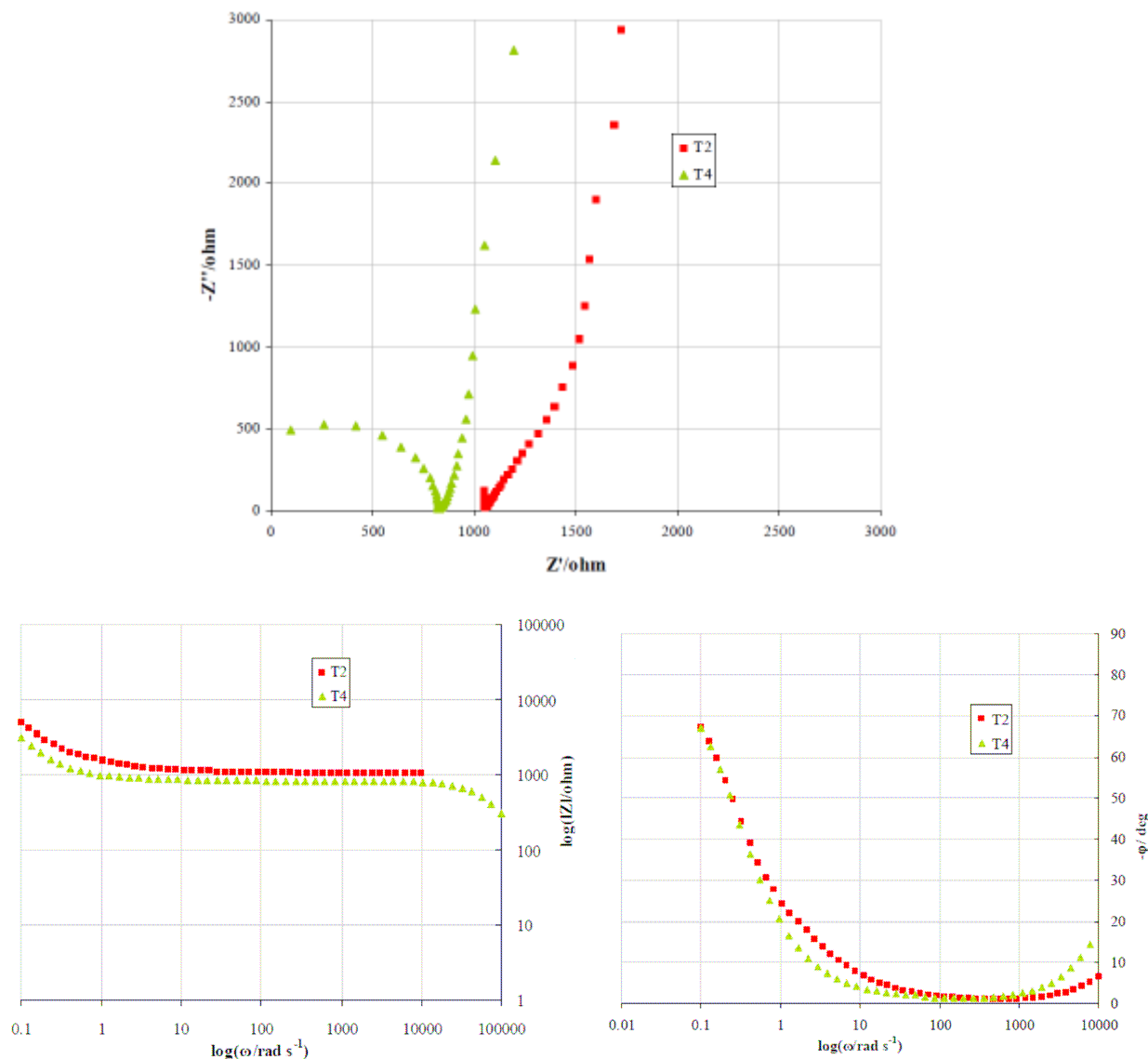


Figure 10: Nyquist, Bode modulus and Bode phase plots for THIOX2 and THIOX4 films, in the p -doped state on a GC electrode ($S=0.071 \text{ cm}^2$), in $\text{CH}_2\text{Cl}_2+\text{TBAP } 0.1 \text{ M}$.

EIS measurements were also carried out in the neutral state of the polymers, *i.e.*, at potentials corresponding to capacitive behaviour in the voltammograms. In particular, two values were chosen for each polymer, in order to verify the reproducibility of the measurements and of the films behaviour: -0.4 V/SCE and $+0.1 \text{ V/SCE}$ for THIOX2 and -0.6 V/SCE and -0.1 V/SCE for THIOX4. EIS measurements were recorded between 10 kHz and 100 mHz, but at lower frequencies THIOX4 showed strong oscillations. The behaviour of the films in the neutral state is completely different than in the p -doped state, since no

faradaic process occurs, and, consequently, no electron transfer, but only the ion transport within the polymeric network is relevant.

The effect of branching was studied by comparison of the molecules FT2 and FT4 with their branched derivative, FT8, whose formula is reported in Figure 11:

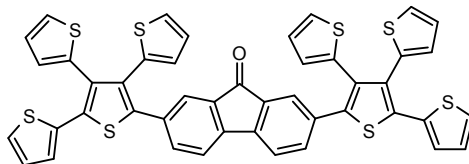


Figure 11: Structure of the *genetically modified spider* FT8

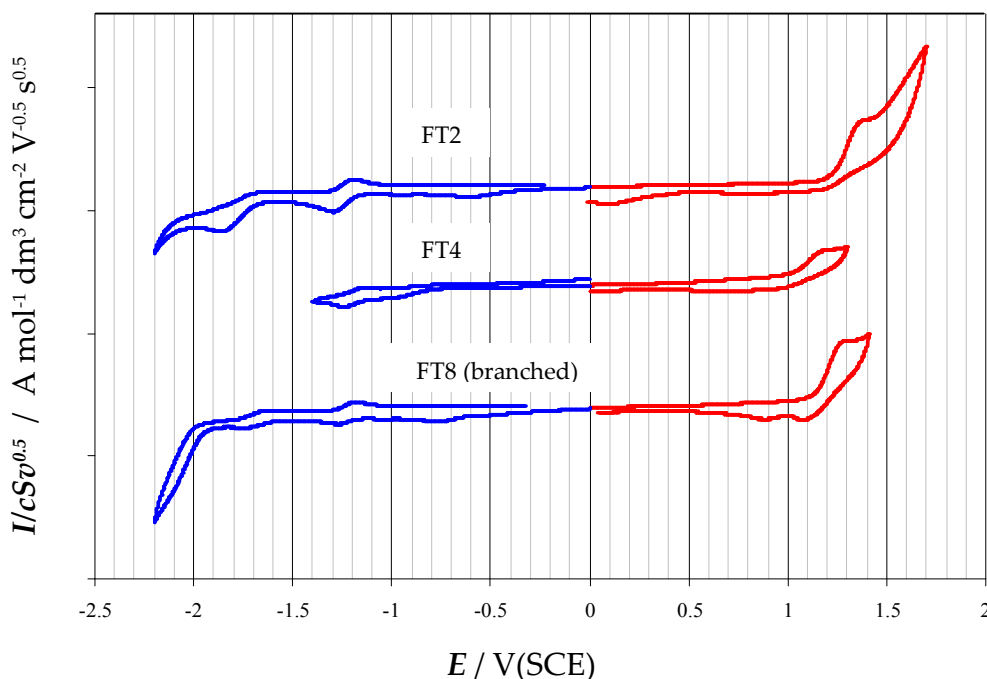


Figure 12: Voltammetric characteristics of FT2, FT4 and FT8, $5 \cdot 10^{-4}$ M in CH_2Cl_2 + TBAP 0.1 M, on a GC electrode ($S=0.071 \text{ cm}^2$), $v=200 \text{ mV/s}$. Potentials are referred to SCE.

It is worthwhile noticing that FT8 shows intermediate characteristics between FT2 and FT4, since branching leads to an enhanced three-dimensional system, but, on the other hand, also leads to the formation of *nodes*, between the core and the terminal tetrathiophene groups. In particular the LUMO is higher in energy than the LUMO of FT4, making the formation of the radical cation less favourable. Concerning the anodic peak, it is at less positive potentials than FT2, thanks to its more extended conjugation, but at more positive potentials than FT4, on account of the distortions from planarity (Figure 12). Interestingly, this is reflected also from the polymerization attitude (Figure 13): FT8 polymerizes at more positive potentials than FT4 because its effective conjugation is hampered by the presence of *nodes*, but the polymerization process appears to be easy and faster, thanks to the enhanced three-dimensional character, allowing more freedom degrees.

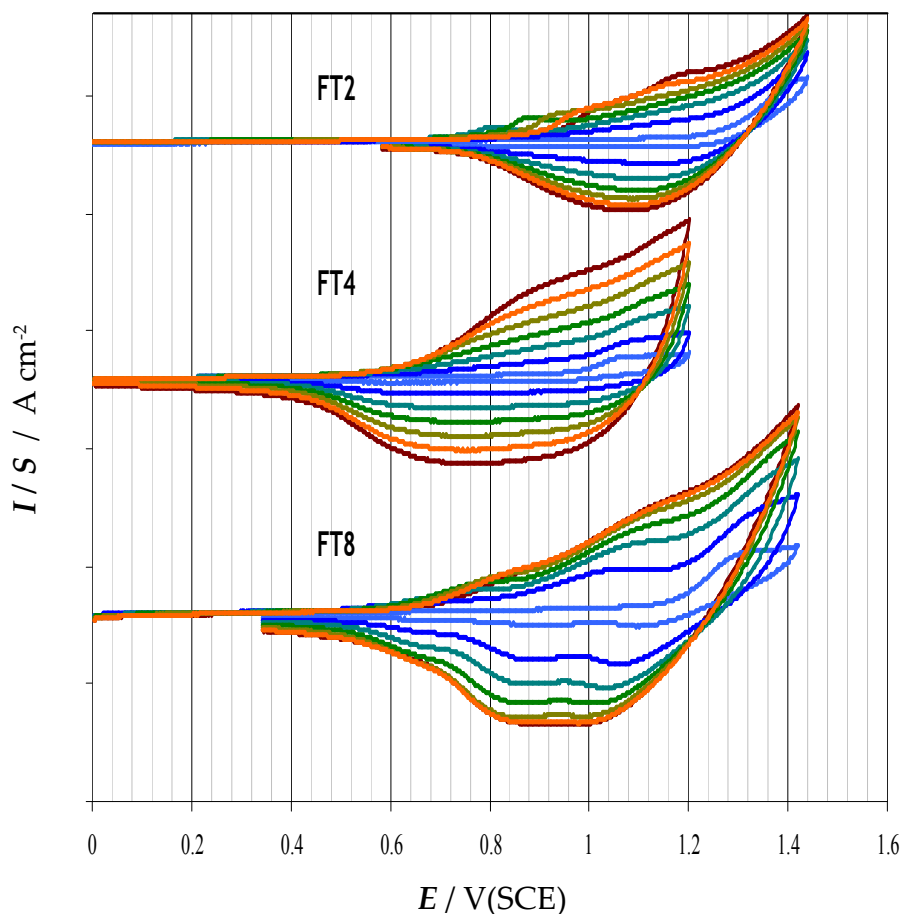


Figure 13: Electropolymerization of FT2, FT4 and FT8, $5 \cdot 10^{-4}$ M in CH_2Cl_2 +TBAP 0.1 M, 36 cycles, $v=200$ mV/s, on a GC electrode ($S=0.071$ cm 2). Potentials are referred to SCE.

The UV-vis spectra of the *genetically modified spiders* (CH_2Cl_2 , 10^{-5} M) showed a recurrent behavior within the investigated families, suggesting a straightforward correlation between optoelectronic properties and structure, and confirming the voltammetric data⁵⁵. It is evident (Figure 14) that the increase in conjugation length (**a-b** series) produces the expected bathochromic shift of the absorption maxima wavelength. The introduction of the thiophene side-chains (**c** series), produces, at the same extent of conjugation (**b** series), an ipsochromic shift which can be interpreted on the basis of steric effects inducing a distortion from coplanarity of the α -interconnected rings, thus reducing their conjugative communication.

⁵⁵ G.Rampinini, A. Digennaro, T. Benincori, V. Bonometti, P. R. Mussini, M. Panigati, R. Po', F. Sannicolò, Energy Gap Tuning in Linear and Branched Oligothiophene Semiconductors: Structure-properties relationships in new "push-pull" spider-like oligothiophenes, manuscript in preparation, 2012

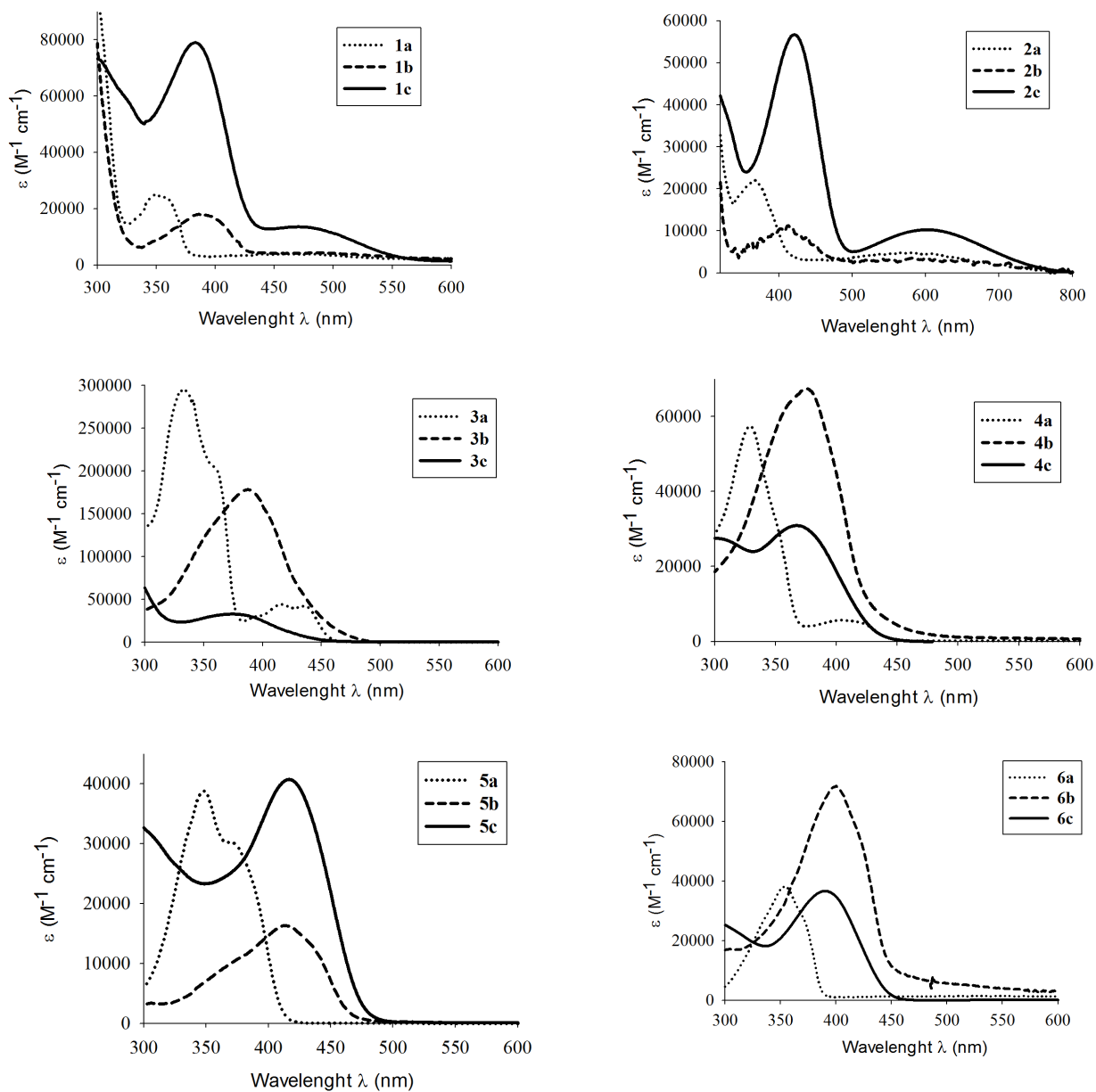


Figure 14: UV-vis spectra of the series 1-6 in 10⁻⁵M dichloromethane solution.

Moreover, all the compounds are characterized by the presence of an inner chromophore (carbonyl group, *S,S*-dioxide function) which gives rise to an internal charge-transfer (ICT) band, which is responsible for a red-shifted broad absorption⁵⁶. Therefore, it is possible to take as a primary assumption that the relative absorption region of each family specifically depends on the selected central core and on its electron-withdrawing capacity.

All the spectra exhibit two more or less resolved absorption bands. The highest energy absorption is attributable to the π - π^* transition of the conjugated backbone. This assignment is confirmed both by the bathochromic shift underwent by this band with the increase of the number of α -conjugated thiophene rings, and by the hypsochromic shift observed by passing from the linear to the branched systems. As reported above, this behavior is attributable to the different *effective conjugation* of linear (*b* series) and branched (*c* series) compounds, where *effective conjugation* means the real extension of the conjugation along the backbone.

It is worth noting that, within each family, the onsets of the curves lay at about the same wavelength, since, as previously reported for the members of the spider-like oligothiophenes family⁵⁷, the maximum absorption wavelength is given by the average absorption of the differently conjugated sequences present in all possible conformers, whereas the onset is related to the absorption of the most conjugated ones. Therefore, the most conjugated conformers of the compounds belonging to the *c* series display two coplanar thiophenes in each *leg*, like in the case of the members of the *b* family. This is the result of the equilibrium between the formal extension and the distortions.

Moreover, the position of this band is significantly red-shifted moving from thioxantone (**4**) to the 4*H*-[3,2-*b*]-cyclopentadithiophene-4-one (**2**), suggesting a correlation between the optical properties and the features of the central body, in particular its electron-withdrawing strength. For example, λ_{max} moves from the 370 nm of **4c**, to the 425 nm of **2c**. These findings suggest a longer five membered conjugated chain for the molecules of the series **2**, in agreement with the involvement of the cyclopentadithiophenone unit in the conjugative sequence of the oligothiophene backbone.

The extension of the conjugation length affords an increase in the HOMO levels as it has been shown also by the electrochemical data.

The lowest energy absorption band, observed in the visible region, is, as anticipated, an ICT transition that occurs between the HOMO, located on the electron-rich oligothiophene segments, and the LUMO levels, which involve the central electron-withdrawing carbonyl group or the *S,S*-dioxide unit. Since the conjugation extent plays a crucial role in determining the HOMO level within the series, as well as the nature of the substituents of the thiophene rings, the position of the CT band is bathochromically shifted in each series moving from *a* to *b*. In the case of compounds **3-5**, the ICT band is clearly visible in the spectra of the shortest oligomers, being covered by the π - π^* transition with increasing the

⁵⁶ H. Sirringhaus, R.H. Friend, C. Wang, J. Leuninger, K. Mullen, *J. Mater. Chem.* **1999**, *9*, 2095

⁵⁷ T. Benincori, M. Capaccio, F. De Angelis, L. Falciola, M. Muccini, P. Mussini, A. Ponti, S. Toffanin, P. Traldi, F. Sannicolò, *Chem. Eur. J.* **2008**, *14*, 459; T. Benincori, V. Bonometti, F. De Angelis, L. Falciola, M. Muccini, P. R. Mussini, T. Pilati, G. Rampinini, S. Rizzo, S. Toffanin, F. Sannicolò. *Chem. Eur. J.* **2010**, *16*, 9086

size of the molecules. Since the energy of the intramolecular charge transfer transition is independent upon the length of the conjugated chain, this band is covered by the main π - π^* transitions band of the thiophene segments in the spectra of longer oligothiophenes **b** and **c**.

The intervention of the electron-withdrawing central moiety in modulating the ICT band is clearly proved by analyzing the behavior of **6**, in which the carbonyl group is substituted by a methylene carbon bearing two thiophene units. The ICT band no longer exists in this family (Figure 15), whereas the highest energy absorption can still be correlated to the π - π^* transition of the conjugated main backbone.

The influence of the thioketal function of **7** on the optical properties is, as expected, very poor, since no conjugative communication occurs between the two sulphur atoms and the backbone (Figure 15).

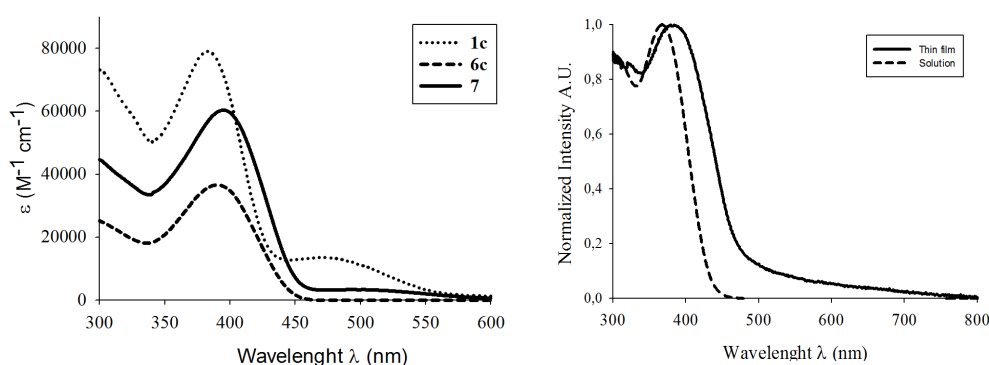


Figure 15: (left) UV-vis spectra of **7, compared with **1c** and **6c**, in 10^{-5} M CH_2Cl_2 solution. (right) Normalized UV-Vis spectra of **4a** in solution (dotted line) and as film (solid line)**

A slight broadening of the absorption band can be explained with a modest positive inductive effect of the sulphur atoms through the methylene carbon. The onset of the absorption (450 nm), however, is not affected by this phenomenon.

The UV-vis properties of thin-films of compounds **1c-6c** and **7** obtained by spin-coating dichloromethane solutions (1mg/0.1mL) on glass substrates have been measured and compared with their behavior in solution (see Figure 15, as an example). In general, the peaks are broader and a red shifting (30-50 nm) of the absorption onsets is achieved, although no enhancement of structuration of the curve is observed, even after thermal annealing.

These results indicate a common tendency to intermolecular interactions in the solid state, *i.e.*, π - π stacking, even if the films have a very amorphous morphology and no local recrystallization occurs after heating.

3.1.1 red-FHexT6, FHexT6 and FHexT6C₆₀

The molecule FHexT6C₆₀ was synthesized in order to complete the series of the *genetically-modified spiders* with a compound that would be suitable for applications in organic photovoltaics, in particular as acceptor component for the bulk-heterojunction solar cells. As explained in the Introduction, analyzing the working mechanism of such solar cells, it appears evident that the energetic levels of the donor-acceptor couple have to be suitably positioned in order to enhance the charge transport mechanism and avoid the charge recombination⁵⁸.

The molecule FHexT6C₆₀ has been designed and synthesized by the group of Prof. Sannicolò, exploiting the ease of functionalization due to the carbonyl group in FHexT6, and the presence of a branched oligothiophene system that acts as the donor group. In particular, the branching level has been reduced with respect to the molecules of the *c* series of the *genetically-modified spiders*, in order to reduce the sterical hindrance of the whole system, and methyl groups have been replaced by hexyl chains in order to increase the solubility of the system in common organic solvents. The design of the molecule was meant to increase the absorbance in the visible region thanks to the thiophene-based side chains, also affording better compatibility with other donor materials possibly present in the blend. The optical and electrochemical characterization were performed in order to evaluate its properties as an acceptor material for applications in bulk-heterojunction solar cells.

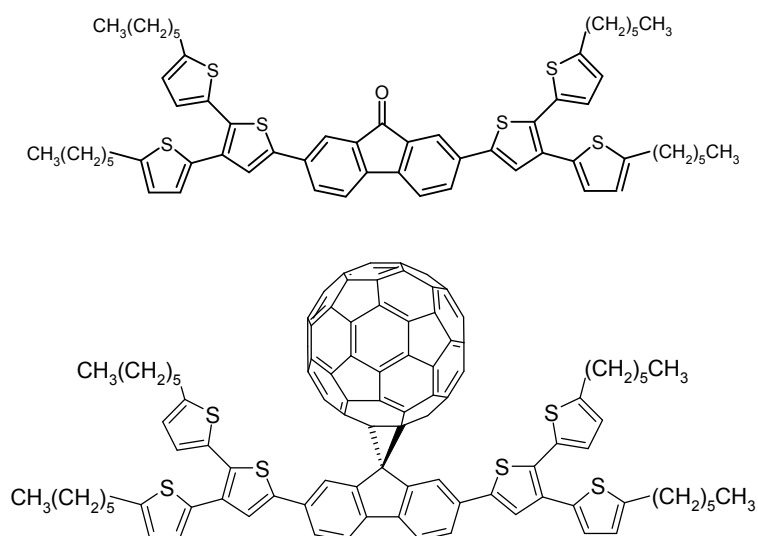


Figure 1: Structures of FHexT6 and FHexT6C₆₀

⁵⁸ Giovanni Rampinini, PhD Thesis, Università degli Studi di Milano, 2010

Renzo Graziosi, M.Sc. Thesis, Università degli Studi di Milano, 2012

C.W. Tang, *Appl. Phys. Lett.*, **1986**, 48,183

C. Deibel, V.Dyakonov, *Rep. Prog. Phys.*, **2010**, 73, 1

Y. He, Y. Li, *Phys. Chem. Chem. Phys.*, **2011**, 13, 1970

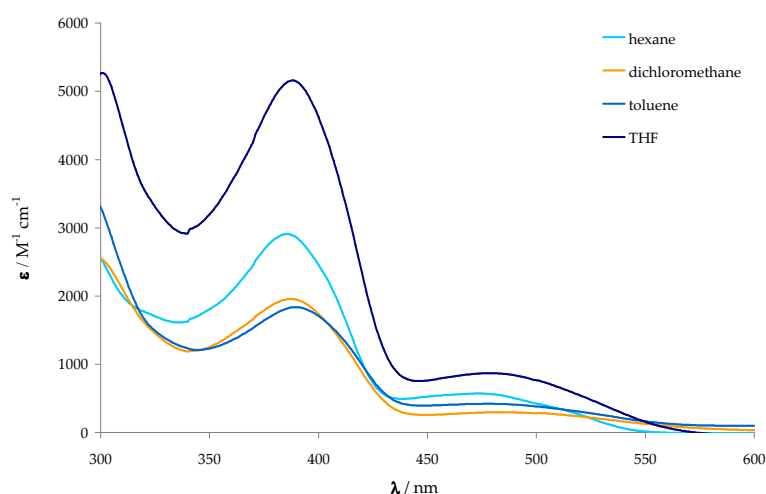


Figure 2: UV-Vis spectra of FHexT6 ($5 \cdot 10^{-5} \text{M}$) in different solvents.

The spectrum shows two absorption maxima, the first one at 385 nm, corresponding to the π - π^* transition of the main conjugated chain, while the second band, characterized by low intensity and red-shifted, could be attributed to an intramolecular charge transfer between the main conjugated chain and the carbonyl group. The spectrum of FHexT6 in dichloromethane was then

compared with the UV-Vis spectra of the *genetically-modified spiders* FT8 and Met-FT8, as shown in Figure 3.

The molecules show a similar behaviour, with λ_{max} at 377, 383 and 387 nm, respectively. The slight red-shift from FT8 to Met-FT8 is attributed to the presence of the methyl groups that make the system electronricher, while, comparing Met-FT8 and FHexT6, the shift at higher wavelengths could be attributed to the absence of a 2-hexylthiophene *leg*, in the β position of the first thiophene of the side chain, that makes the system less distorted, enhancing its conjugation efficiency.

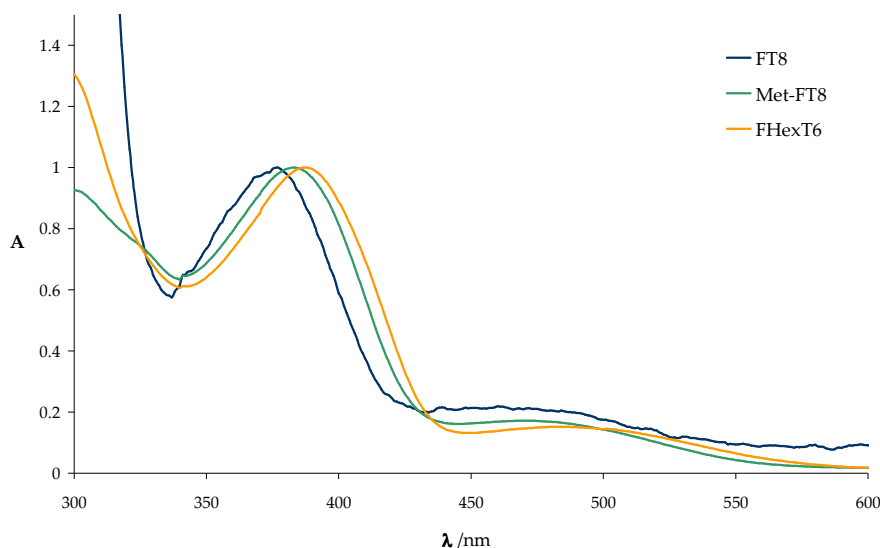


Figure 3: UV-Vis spectra of FHexT6, FT8, Met-FT8 ($5 \cdot 10^{-5} \text{M}$) in CH_2Cl_2

The UV-Vis spectra of FHexT6C₆₀ in dichloromethane and toluene are reported in Figure 4a: in both cases the spectra show a first absorption maximum at 330 nm and a second one at 398 nm; interestingly, comparing these data with the spectra of the PCBM, it is possible to observe that our molecule has a stronger absorption around 400 nm, attributable to the terthiophene pendants (Figure 4b). Unfortunately, in the visible region between 400 and 700 nm, both PCBM and FHexT6C₆₀ have very low absorbancies, as shown in Figure 4c: this feature represents the major drawback in the use of C₆₀ for photovoltaic application, that may be possibly improved by employing the fullerene C₇₀, that has a greater absorbance in the visible region, but it is still too expensive for commercial applications.

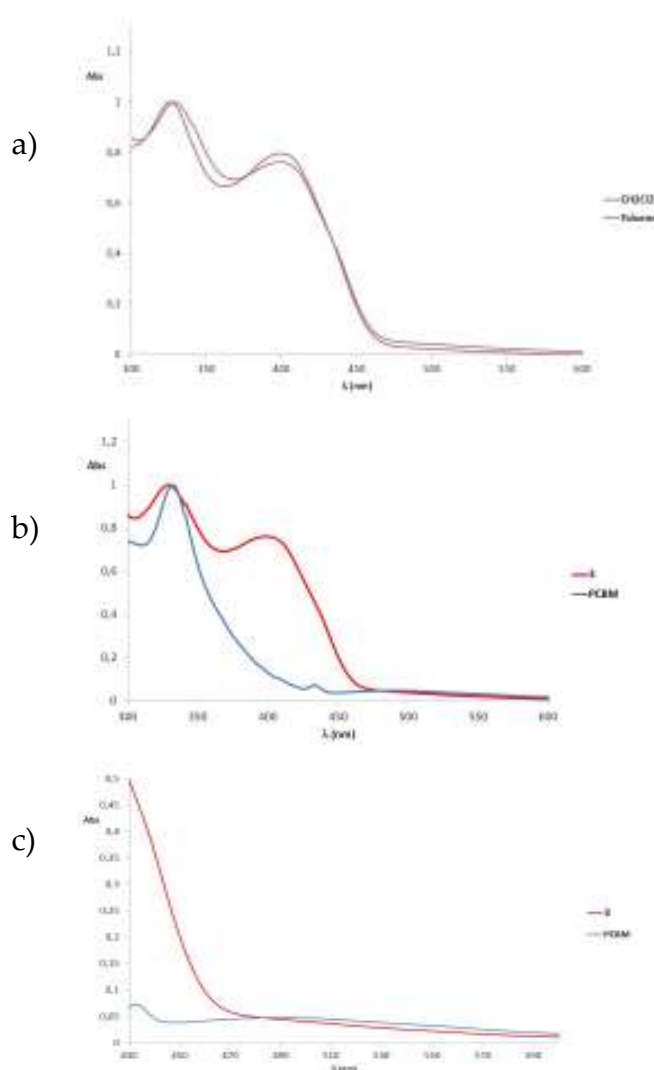


Figure 4:

a) UV-Vis spectra of FHexT6C₆₀ in dichloromethane and toluene;

b) UV-Vis spectrum of FHexT6C₆₀ (in red) compared with the spectrum of PCBM (in light-blue)

c) zoom of the visible region from 400 to 700 nm showing the low absorbancies of FHexT6C₆₀ (in red) and PCBM (in light-blue)

The voltammetric features were studied at $5 \cdot 10^{-4}$ M monomer concentration in CH₂Cl₂ + TBAP 0.1 M, and then compared with the features of the molecule illustrated in Figure 5, analogous of FHexT6 but without the carbonyl function (named red-FHexT6), in order to better evaluate the contribution of the fullerene and fluorene subunits:

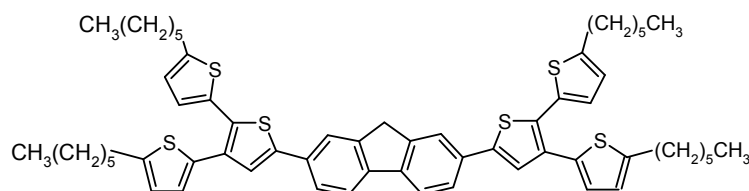


Figure 5: Structure of red-FHexT6

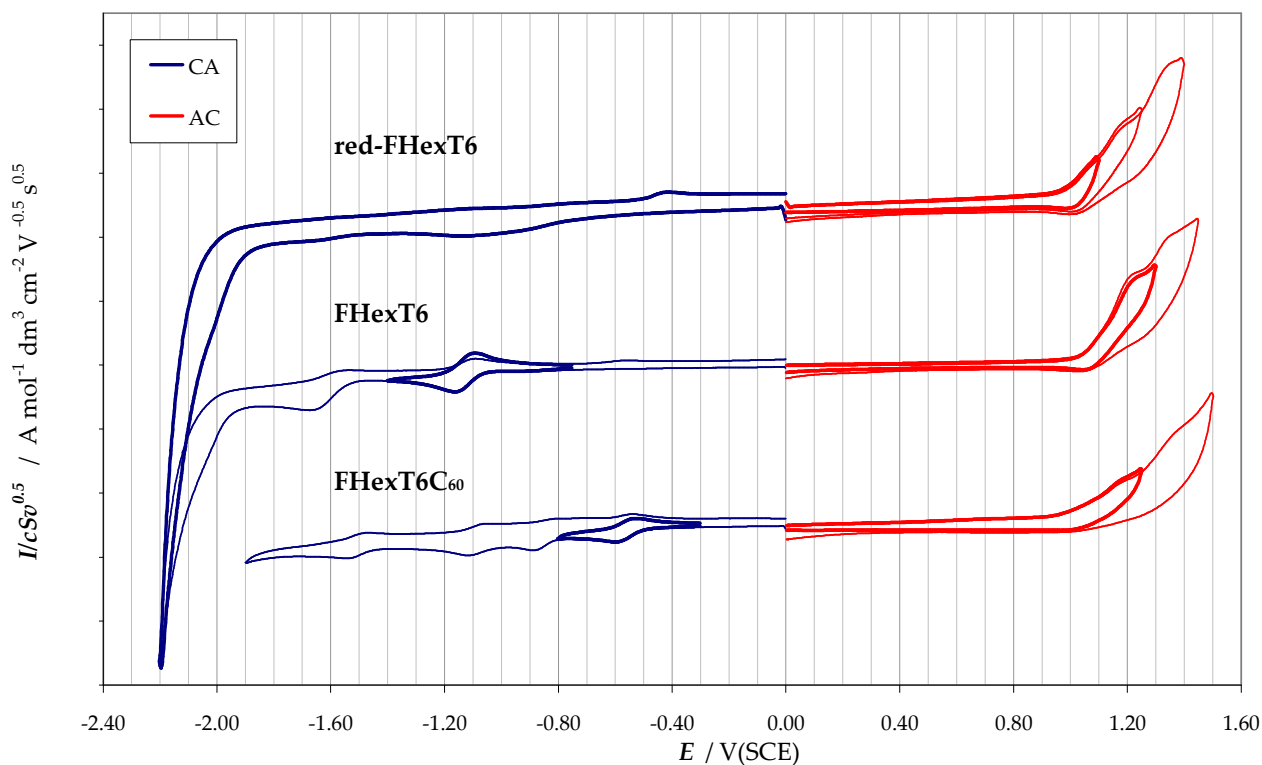


Figure 6: Voltammetric characteristics of red-FHexT6, FHexT6, and FHexT6C₆₀, 5·10⁻⁴ M in CH₂Cl₂+TBAP 0.1 M, on a GC electrode (S=0.071 cm²). v=200mV/s. R=1000 Ω. Potentials referred to SCE (+0.490 V vs Fc⁺|Fc)

From the voltammetric features, reported synoptically in Figure 6, it is possible to observe that:

- in oxidation, there are nearly-equivalent peaks, corresponding to oxidative reactions possibly localized on the thiophene terminals, still interacting through the conjugated core. This process appear to be favoured (*i.e.*, at less positive potentials) in the red-FHexT6 case, where three peaks could be distinguished: the first one is possibly due to an oxidation localized on the core, whose signal is absent in the other two molecules, followed by the two nearly equivalent oxidation peaks typical of the thiophene terminals, shown also by the other two molecules.
- Such split in two nearly equivalent oxidation peaks (rather than one bielectronic peak, that would appear in case of completely independent thiophene terminals) is more evident in the case of the carbonyl-derivative FHexT6, that, as already seen in the case of the *genetically-modified spiders*, enhances the conjugation in the system.
- The features shown in the cathodic region are interesting: FHexT6 shows the monoelectronic, electrochemically and chemically reversible peak typical of the formation of a stable radical anion on the carbonyl system

- This peak is followed another monoelectronic peak, whose reversibility increases with increasing potential scan rate, possibly attributable to a follow-up reaction
- No reductions are observed in the case of red-FHexT6, at least in the available potential window.
- FHexT6C₆₀ shows a sequence of monoelectronic reversible peaks, typical of the fullerene system, unfortunately limited by the non-extended potential window in dichloromethane, and by the acceptable but not complete solubility of the molecule in this solvent. The reversibility of the fullerene peaks may appear in this plot not complete, but cycling around each single peak, the chemical and electrochemical reversibility are recovered.
- In the case of FHexT6C₆₀, cyclic voltammetry alone is not enough to ensure that the fullerene is effectively linked to the molecule core, but it seems likely to be so, as confirmed by NMR spectroscopy.
- The data reported in the tables below show that the attempt to reduce the energy gap is successfully achieved by FHexT6C₆₀, exploiting the electron-withdrawing character of the fullerene system, pointing to the fact that the strategy of linking a fullerene subunit to a branched thiophene system could lead to small band gap materials; possibly, employing C₇₀ (that has a more intense absorption in the visible region) will further reduce the gap.

<i>Maxima criterion</i>	$E_{p,a \max}$ V/SCE	$E_p - E_{p/2}$ V	$E_{p,c \max}$ V/SCE	$E_p - E_{p/2}$ V	$E_{\text{gap} \max}$ V	HOMO eV	LUMO eV
red-FHexT6	1.079 1.194 1.394	0.051	-1.982 ^a	-0.036	3.06	-5.39	-2.33
FHexT6	1.246 1.353	0.099	-1.162 -1.674	-0.056 -0.085	2.41	-5.56	-3.15
FHexT6C ₆₀	1.200 1.406	0.102	-0.596 -0.893 -1.111 -1.542	-0.057 -0.046 -0.053 -0.051	1.80	-5.51	-3.71

<i>Onset criterion</i>	$E_{p,a \text{ onset}}$ V/SCE	$E_{p,c \text{ onset}}$ V/SCE	$E_{\text{gap} \max}$ V	HOMO eV	LUMO eV
red-FHexT6	0.977	-1.910 ^a	2.89	-5.29	-2.40
FHexT6	1.021	-1.050	2.07	-5.33	-3.26
FHexT6C ₆₀	0.953	-0.482	1.43	-5.26	-3.83

a) uncertain attribution (too near to the background)

Potentials are referred to SCE in a double bridge filled with CH₂Cl₂+TBAP 0.1 M (here, + 490.5 mV vs Fc⁺|Fc)

The data in the tables are reported considering both the maxima and onset criterion. The onset criterion appears to be the most convenient in the case of dendrimeric systems, since the onset corresponds to the minimum energy necessary to obtain a minimum intensity in the signal; in other words, it corresponds to the most favourable but less populated

conformation, while the maximum corresponds to the most populated energy levels, that does not mean the most convenient conformation, as it could be expected considering a Gaussian distribution, so the maxima criterion is less suitable for dendrimeric systems. Finally, the HOMO and LUMO levels, and the energy gap were compared with the two most common donor and acceptor molecules employed in bulk-heterojunction solar cells: PCBM and P3HT, measured in the same experimental conditions as FHexT6C₆₀.

<i>Onset criterion</i>	$E_{p,a \text{ onset}}$ V/Fc ⁺ Fc	$E_{p,c \text{ onset}}$ V/ Fc ⁺ Fc	$E_{\text{gap max}}$ V	HOMO eV	LUMO eV
P3HT	0.180	<i>nd</i> ^a	<i>nd</i> ^a	-4.98	<i>nd</i> ^a
PCBM	1.001	-0.965	1.97	-5.80	-3.84
FHexT6C ₆₀	0.462	-0.972	1.43	-5.26	-3.83

*a) nd = not detectable in the available potential window
Potentials are referred to the Fc⁺|Fc redox couple*

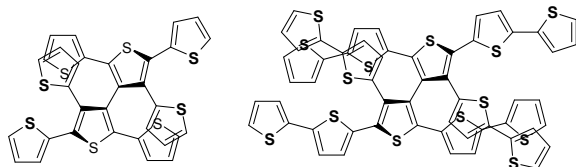
Interestingly, the HOMO of FHexT6C₆₀ is shifted upwards by 0.54 eV with respect to PCBM, making the difference with the donor's HOMO (*e.g.*, for P3HT at -4.98 eV) smaller, but still about 0.3 eV above the donor's HOMO, thus still allowing the exciton dissociation at the interface between donor and acceptor materials.

The LUMO of FHexT6C₆₀ and of PCBM are very similar, confirming the effective nature of the acceptor in FHexT6C₆₀

At the moment, the possibility of application of FHexT6C₆₀ in bulk-heterojunction solar cells, either alone or in blend with another electron donor material, is under investigation.

3.2 The Inherently Chiral molecules

3.2.1 T^*8_3 and T^*14_5 : Inherently Chiral Spider-like oligothiophenes



These molecules appear to be particularly interesting since they belong at the same time to both the molecule families we deal with, *i.e.* the spider-like series⁵⁹, being two branched all-thiophene molecules, and the *inherently chiral* ones, having a 3,3'-bithiophene as central scaffold, the rotation around this link being hindered by thiophene or bithiophene side chains, since in the achiral spider-like series, the central scaffold was made by 2,2'-linked thiophenes, where the sulphur atom in the ortho position was not sufficient to impede the rotation around the interanular link.

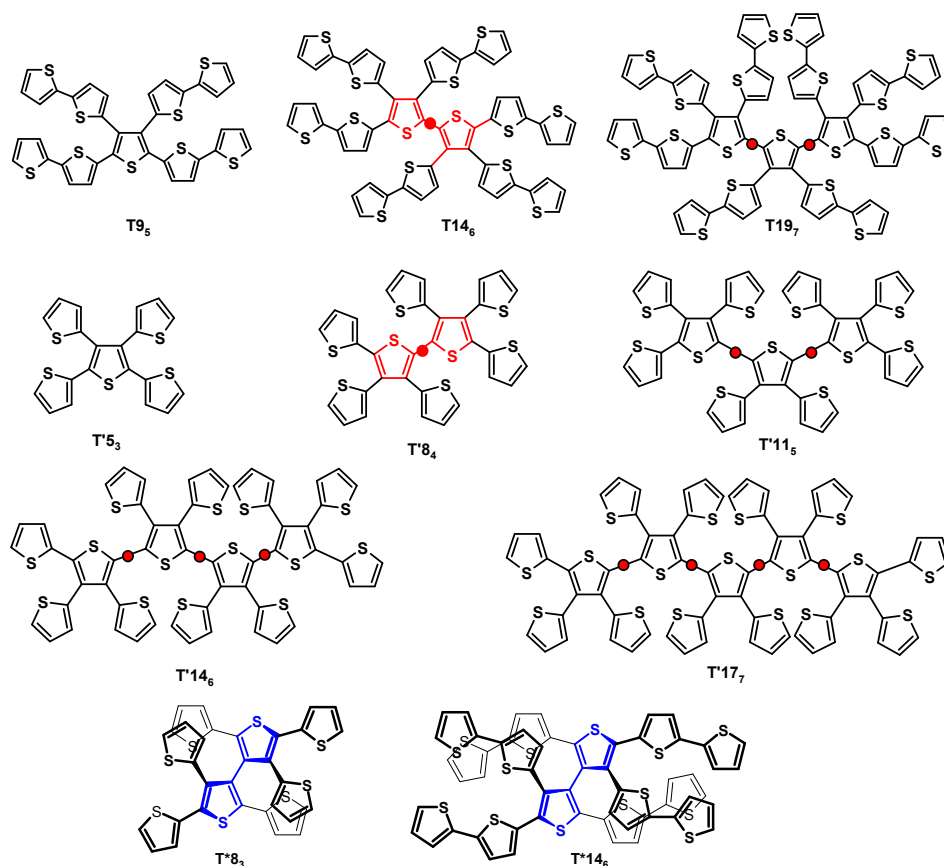


Figure 1: A comparison between the series of the previous spiders and of the two new inherently chiral spiders

⁵⁹ T. Benincori, M. Capaccio, F. De Angelis, L. Falciola, M. Muccini, P. Mussini, A. Ponti, S. Toffanin, P. Traldi, F. Sannicolò, *Chem. Eur. J.*, **2008**, *14*, 459

At a first glance, it could seem obvious to compare the chiral spiders with the spiders having the same overall number of thiophene units (*i.e.*, T*8₃ with T'8₄, and T*14₅ with T14₆), where the central thiophenes are β,β-linked instead of being α,α-linked, while it is more important to compare them with the ones having the same number of α-linked thiophenes, that are responsible of the effective conjugation.

In particular, T*8₃ could be compared with T5₃ and T*14₅ could be compared with T11₅.

The UV-Vis spectra, recorded in CH₂Cl₂, are reported below, together with a table resuming the optical characteristics, calculated according to the Lambert-Beer law.

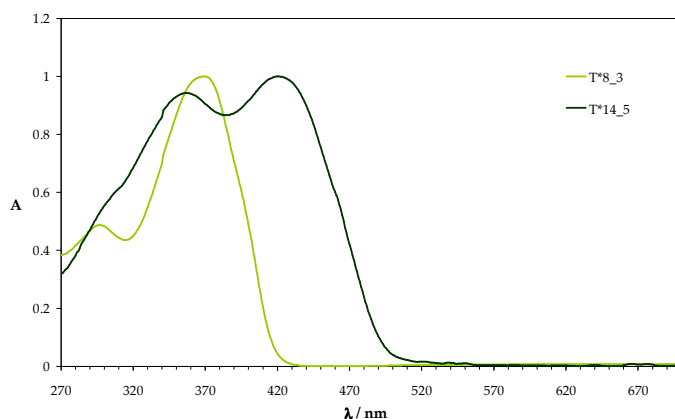


Figure 2: UV-Vis spectra of T*8₃ and T*14₅, 5·10⁻⁵ M in CH₂Cl₂

	λ_{\max} (nm)	ϵ (M ⁻¹ cm ⁻¹)	$E_{g,\max}$ (eV) §	λ_2 (nm)	ϵ_2 (M ⁻¹ cm ⁻¹)	λ_{onset} (nm)	$E_{g,\text{onset}}$ (eV) §
T*8 ₃	370	36000	3.3	297	17500	436	2.8
T*14 ₅	420	39000	2.9	357	37000	514	2.4

$$\S E_g (\text{eV}) = h\nu / \lambda \approx 1240 / \lambda(\text{nm})$$

The spectrum of T*14₆ is red-shifted with respect to T*8₃ one, on account of its increased effective conjugation.

In the case of multithiophene systems, also the wavelength of the curve onset is considered, since the absorbance maximum could be affected by sterical interactions due to non-linear elements on the α,α-linked main chain, and may appear to be blue-shifted with respect to linear oligothiophenes having the same effective conjugation.

The value of T*8₃ λ_{\max} neither corresponds to the one of a linear terthiophene (353 nm) nor to the one of a linear tetrathiophene (390 nm): thus, the conjugation is not limited to the three α-linked thiophenes constituting half of the molecule, but it is more extended, through the atropisomeric link of the central 3,3'-bithiophene scaffold.

On the other hand, for T*14₅, λ_{\max} is similar to the value of a linear pentathiophene (419 nm). This could be attributed to a greater sterical hindrance of bithiophene side chains that leads to a greater distortion around the atropisomeric central link, thus reducing the

communication between the two moieties constituting the molecule. In any case, the energy gap for T*14₆ is lower than the one of T*8₃.

T*8₃ was studied in acetonitrile, while T*14₅ was analyzed in dichloromethane, on account of its poor solubility in acetonitrile. Anyway, in reporting data against ferrocene, we assume to have normalized for the intersolvental junction potential although some residual solvent effect on the redox couple cannot be excluded.

	T5 ₃	T*8 ₃	T8 ₄
$E_{p,a} / V$ vs Fc ⁺ Fc	0.71	0.75	0.63
$E_{p,c} / V$ vs Fc ⁺ Fc	-2.65	-2.56	-2.47
E_{gap} / V	3.36	3.31	3.10

Concerning the voltammetric characteristics of T*8₃, it is possible to observe two nearly-equivalent oxidation peaks, sufficiently distant to suggest that the second oxidation is a more difficult process for the molecule. Even in this case, as observed in other inherently chiral molecules, the two moieties composing the molecule are not completely independent, but still communicating through the β,β -connection node. Cycling around the oxidation peaks leads to the very fast and regular growth of an electroactive film, which resulted to be stable upon repeated potential scans in a monomer-free solution.

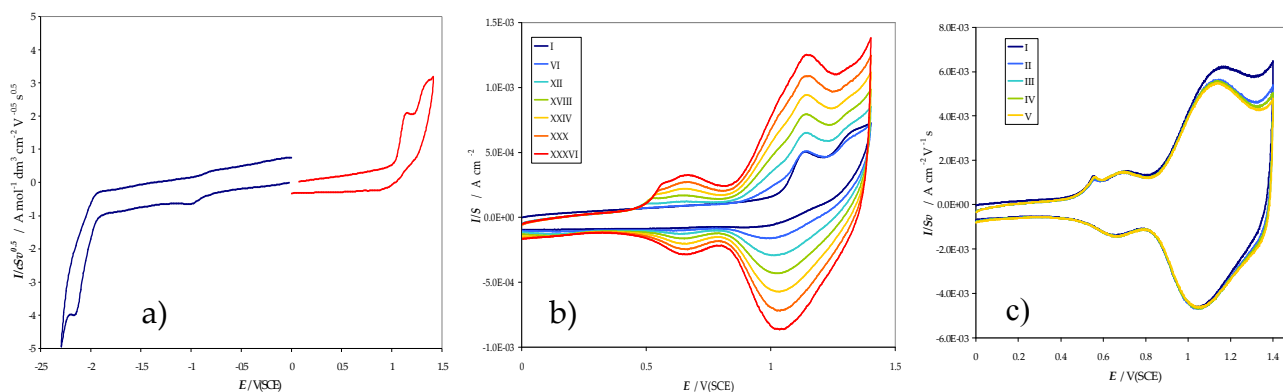
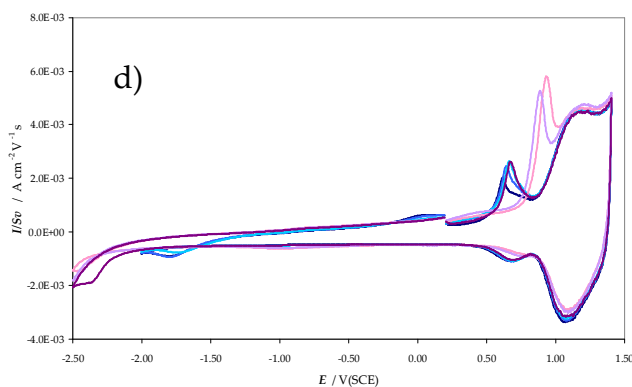


Figure 3: Voltammetric characteristics of T*8₃ a) as a monomer, 5·10⁻⁴ M in CH₃CN+TBAPF₆ 0.1 M, on a GC electrode (S=0.071 cm²) 200 mV/s; b) electropolymerization, 36 cycles, on a GC electrode (S=0.071 cm²), 200 mV/s c) stability test in a monomer-free solution; d) charge trapping effect.



When widening the potential window in the negative direction, a charge trapping effect is observed: the negative charge is then released at a much more positive potential, because

the n-doping process makes the polymer network arrange its structure in order to compensate the charge acquired, and then a greater energy is needed to make it restore its previous structure.

AFM images were also recorded for T*8₃ films deposited in different experimental conditions; all the films revealed a regular and granular structure, as shown in Figure 4.

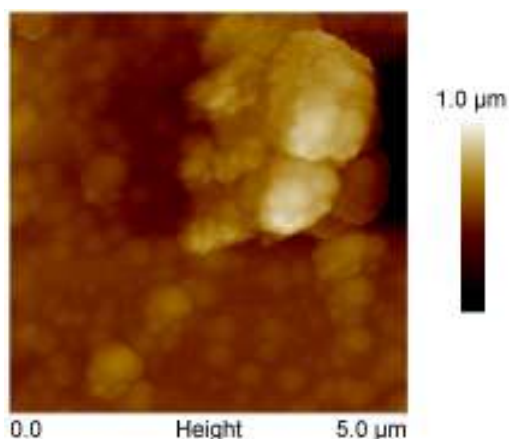


Figure 4: T*8₃ film deposited from a $5 \cdot 10^{-4}$ M monomer solution in CH₃CN+TBAPF₆ 0.1 M on a gold-coated glass slide ($S \sim 1 \text{ cm}^2$), Ag/AgCl reference electrode, scan rate 200 mV/s

T*8₃ was characterized also with electrochemical quartz crystal microbalance, in acetonitrile and tetrabutylammonium hexafluorophosphate, on a 10 MHz AT-cut gold-coated quartz crystal, that confirmed the regular growth, at each cycle, of the electroactive film.

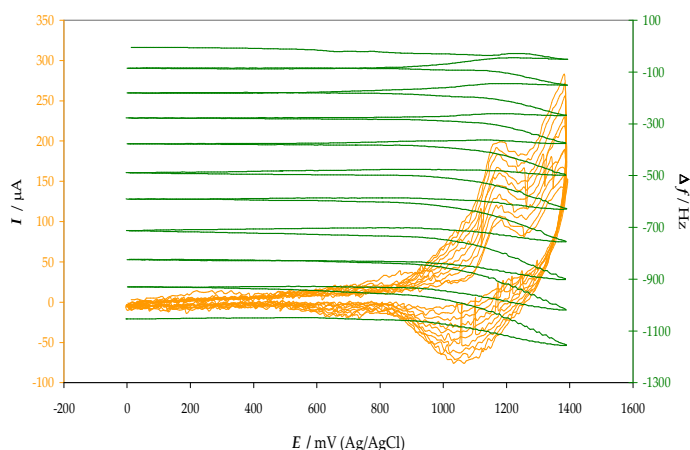


Figure 5: EQCM study of the electropolymerization by cyclic voltammetry of T*8₃, $5 \cdot 10^{-4}$ M in CH₃CN+TBAPF₆ 0.1 M, on a gold-coated AT-cut quartz crystal, $v = 200$ mV/s, potentials referred to Ag|AgCl.

The stability test showed a very thin film, with poor electroactivity: this may be attributed to a possible partial oxidation of the film, which was kept outside the cell for a few days before performing the experiment.

The voltammetric characteristics of T*14₅, instead, are quite different. Also in this case, two peaks were observed in the anodic region, the first one becoming reversible at higher potential scan rates, and the second one more distant from the first. It might be assumed the first electron loss to result in a radical cation delocalized on one of the pentathiophene chains and therefore rather stable, while it is reasonable, considering the presence of two equal moieties, to assume the double positive charge to correspond to one charged site per

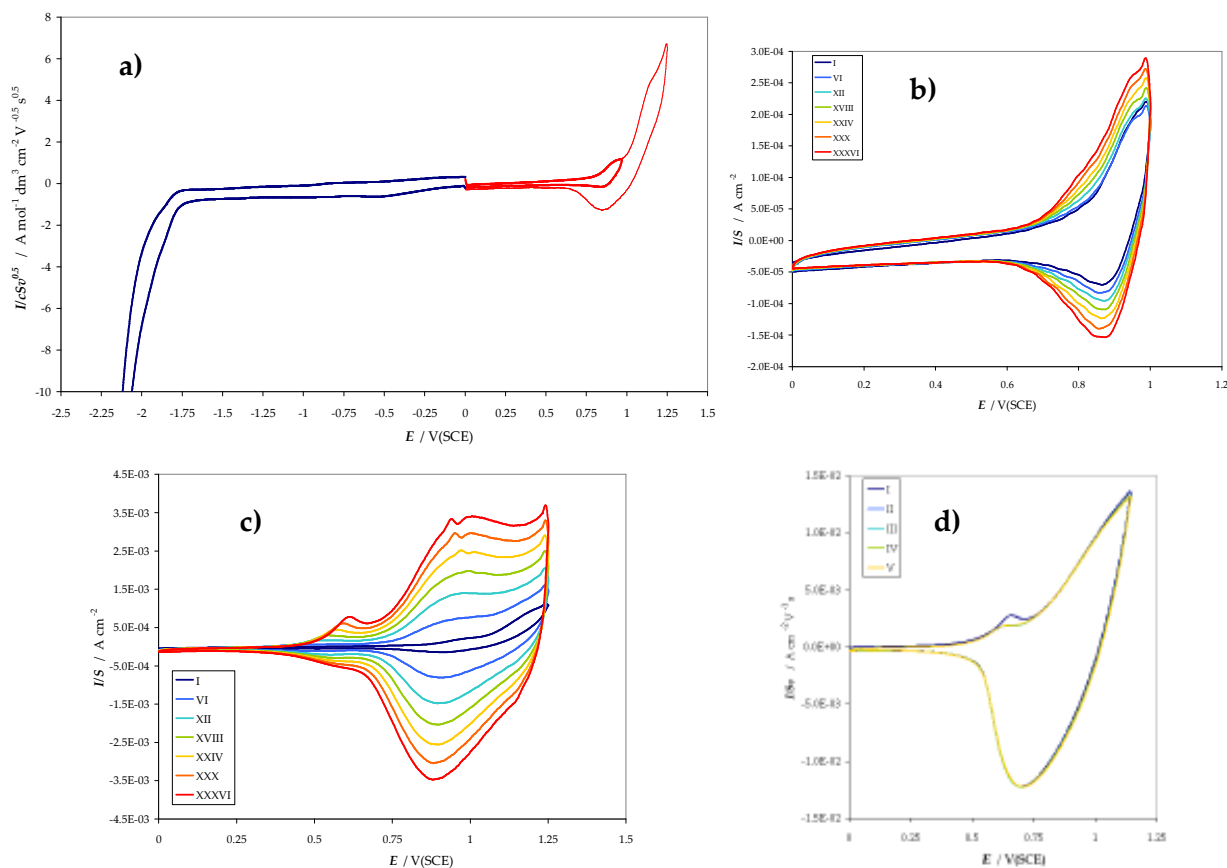


Figure 6: Voltammetric features of T*14₅, 5·10⁻⁴ M in CH₂Cl₂+TBAPF₆ 0.1 M on a GC electrode (S=0.071 cm²), v=200 mV/s; a) monomer characteristics; b) electropolymerization including only the first anodic peak, 36 cycles; c) electropolymerization including both the anodic peaks, 36 cycles; d) stability test in a monomer-free solution of the polymer film deposited in c). Potentials referred to SCE in a double bridge filled with CH₂Cl₂+TBAPF₆ 0.1 M

moiety; in this case, however, to minimize coulombic repulsion the baricenter of the charge should be more peripherally displaced. This is also consistent with the second peak potential resulting in quite higher polymerization rate than the first one. Cycling around the first oxidation peak leads to the deposition of an electroactive film, which resulted to be quite unstable, while including also the second peak, a very fast and regular deposition is observed. This film resulted to be stable upon repeated potential scans in monomer-free solution but did not show any *charge trapping* effect, possibly because of the rigidity of the polymer network, where the subunits composing the monomer are more separated with respect to the case of other *inherently chiral* monomers.

In this case, it is more difficult to make a comparison with the spider-like series:

	T'11₅	T*14₅	T14₆	T'14₆
$E_{p,a} / V$ vs Fc ⁺ Fc	0.612	0.440 0.656	0.582	0.614
$E_{p,c} / V$ vs Fc ⁺ Fc	-2.495	-2.384	-2.155	-2.465
E_{gap} / eV	3.11	2.82	2.74	3.08

The energy gap for T*14₅ was calculated taking into account the first oxidation peak. In this case, T*14₅ shows intermediate characteristics between the benchmark of the previous series: it has higher energy gap than T14₆, which has the same number of *nodes* (only one *node*) and a more extended conjugation, but lower than T'14₆, which has, in turn, a more extended conjugation but three *nodes*. Again, it has lower energy gap than T'11₅, which has the same conjugation extension but two nodes. On the other hand, the second anodic peak corresponds to the oxidation of the α position of terminal thiophenes and is at a higher potential than all the others, maybe because it is more difficult due to the previously acquired positive charge.

The racemates for T*8₃ and T*14₅ have been resolved at analytical level at room temperature on a chiral stationary phase: the chromatograms have been registered by using two detectors, a UV-Vis (in black) and a circular dichroism (in blue). From these previous results it is evident that the two antipodes are stable (absence of a plateau between the two signals).

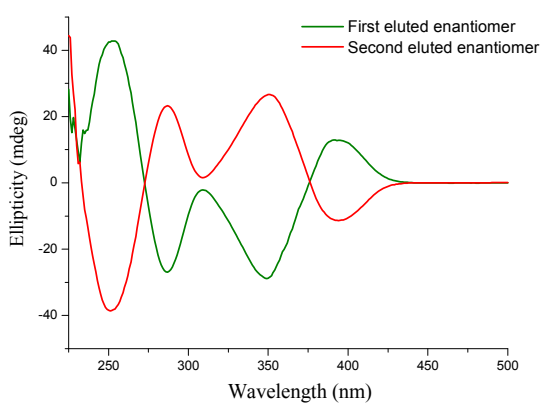
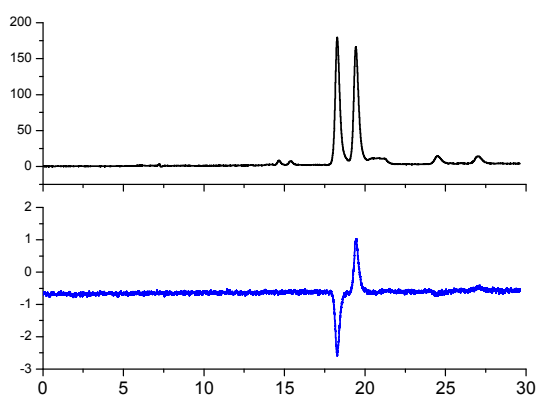


Figure 7: T*8₃, CSP: Chiralpak IB-3 250 x 4.6 mm I.D. + Chiralpak IB-3 250 x 4.6 mm I.D. ; eluent: *n*-hexane-dichloromethane-ethanol 100/5/0.2; flow-rate: 1.0 ml/min; temperature: 25°C; detection: UV (black) and CD (blue) at 350 nm. $k_1 = 1.61$, $\alpha = 1.11$, $R_s = 2.15$. CD in chloroform at 25°C

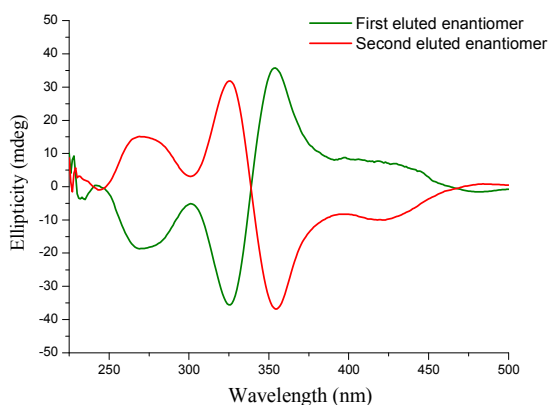
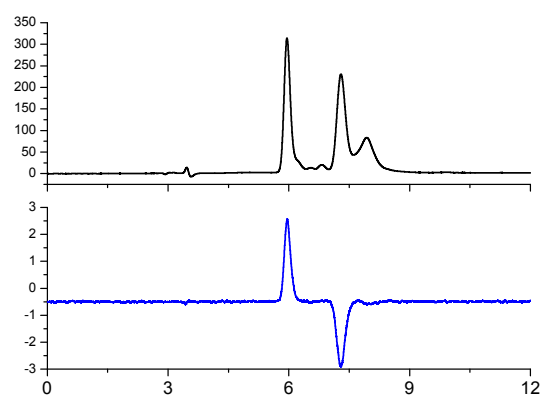
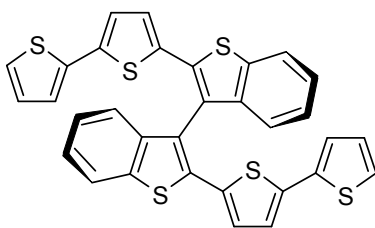


Figure 8: T*14₅, CSP: Chiralpak IA 250 x 4.6 mm I.D.; eluent: *n*-hexane- dichloromethane- 2-propanol 100/5/30; flow-rate: 1.0 ml/min; temperature: 25°C; detection: UV (black) and CD (blue) at 355 nm. $k_1 = 0.98$, $\alpha = 1.46$, $R_s = 3.86$. CD in chloroform at 25°C

3.2.2 T4-BT2



As discussed in the Introduction and in the previous Chapters about *spider-like* and *genetically-modified* oligothiophenes, thiophene-based oligomers are a virtually boundless class of organic semiconductors and starting materials for preparation of electroactive polymer films. Current strategies of molecular design of these oligomers address a trade off between two key requirements, that is branching, to achieve the solubility required for industrial processing, and planarity, for the most efficient conjugation to achieve the highest conductivity. Actually, the *effective conjugation* is a determining factor of the electronic properties of a given molecule, directly accounting for the HOMO–LUMO energy gaps; in this context, the presence of *nodes*, *i.e.*, distortions from planarity, is an undesirable feature, since they reduce the conjugation efficiency and lead to an increase of the HOMO-LUMO gap. However, in some cases the intrinsic 3D character of the nodes could be advantageously exploited, *e.g.* in applications explicitly requiring three-dimensionality. The T4-BT2 molecule⁶⁰ was designed in the frame of a collaboration with Prof. W. Kutner of the Institute of Physical Chemistry of the Polish Academy of Sciences (Warsaw), to act as a *cross-linker* in the development of *Molecularly Imprinted Polymers* (MIP) sensors to form copolymers with bis(dithienyl)methane-based systems, bearing functional groups suitable for sensoristic applications but with poor attitude to polymerization. Beside showing an intrinsically high ability for electropolymerisation, this monomer is an extremely efficient building block for copolymerizations: the atropisomeric *node* and the two homotopic thiophene α -positions free for polymerization confer a three-dimensional and ordered character to the polymer film, and allow to obtain copolymers endowed with functional groups that excellently act as selective piezomicrogravimetric MIP chemosensors for the detection of melamine.

As shown in Figure 1, T4-BT2 is composed by two identical and homotopic moieties, approximately planar (in particular, approximately equivalent to an α -linear terthiophene) and, therefore, of high effective conjugation. The structure of this monomer was purposely designed according to the strategy that leads to the family of the *inherently chiral* monomers:

⁶⁰ F. Sannicolò, S. Rizzo, T. Benincori, W. Kutner, K. Noworyta, J. W. Sobczak, V. Bonometti, L. Falciola, P. R. Mussini, M. Pierini, *Electrochim. Acta*, **2010**, *55*, 8352
A. Pietrzyk, W. Kutner, R. Chitta, M. E. Zandler, F. D'Souza, F. Sannicolò, P. R. Mussini, *Anal. Chem.*, **2009**, *81*, 10061

V. Bonometti, M.Sc. Thesis, Università degli Studi di Milano, 2009

- *Intrinsic 3D character.* Consistently with the typical oligothiophene features described in the Introduction, bulky substituents on both β positions of the thiophene of the thianaphthene ring induce formation of a central *node* between the two moieties. Preliminary molecular mechanics (MM) calculations have also shown that the dihedral angle between the interconnected thianaphthene units is 70° . Therefore, the formation of a tridimensional structure should be expected.
- *Intrinsic regioregularity in polymerisation.* T4-BT2 molecule has only two sites available for polymerisation, *i.e.* one free α position on the terminal thiophene ring of each moiety, separated one from the other, symmetrical, and easily accessible. This structure implies regular polymerisation along the directions of the two planar systems, with a strong 3D character as a consequence of high angle between these planes.
- *Inherent asymmetry.* In spite of the absence of stereogenic centres, the whole molecule is chiral, exhibiting a C_2 symmetry axis. The MM calculations, performed by progressively varying the torsional angle between the thianaphthene units, suggested that the enantiomerisation barrier was comprised between 50 and 65 kcal mol⁻¹ depending on the employed force field. Semiempirical methods, applied in calculations of the conformational potential energy pathway, suggested an even lower barrier value (between 32.5 kcal mol⁻¹ and 38.3 kcal mol⁻¹). In any case, the calculated barriers are sufficiently high to guarantee a racemisation half-lifetime of several centuries. Therefore, stable enantiomers of T4-BT2 can be separated and stored.

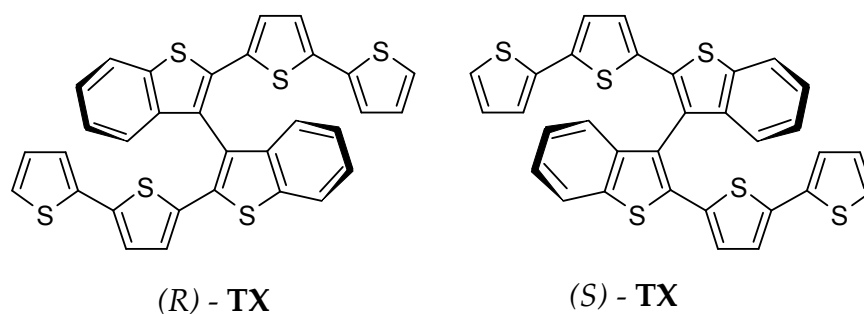


Figure 1: Structure of R- and S- T4-BT2

The characterization of this system was carried on the racemate and also on the separated enantiomers. No differences were expected in solution, but at solid state, *e.g.* between the enantiopure polymers and the racemate one

The voltammetric experiments were performed in different solvents (dichloromethane, acetonitrile, orthodichlorobenzene) and supporting electrolytes (tetrabutylammonium tetrafluoroborate, hexafluorophosphate, perchlorate, *p*-toluenesulfonate, camphorsulfonate) and, finally, in the ionic liquid 1-butyl-3-methyl-imidazolium hexafluorophosphate BMIMPF₆, and the molecule was characterized by means of cyclic voltammetry CV, electrochemical quartz crystal microbalance EQCM, UV-Vis spectroscopy and *in situ* spectroelectrochemistry with electron spin resonance ESR (in collaboration with Prof. L.

Dunsch and Dr. Kinga Haubner, Leibniz Institute for Solid State and Materials Research, Dresden, Germany) or circular dichroism CD (in collaboration with Prof. S. Abbate, G. Longhi and E. Castiglioni, Università degli Studi di Brescia), electrochemical impedance spectroscopy EIS and atomic force and scanning electron microscopies AFM and SEM.

From the voltammetric characteristics it is possible to notice two nearly equivalent oxidation peaks, corresponding to the oxidation of the thiophene α -terminal positions, that are not independent but still communicating through the *node* along the conjugated system. In particular, the first anodic peak width (0.058 V) points to a monoelectronic peak, and, furthermore, the potential of the first anodic peak in the monomer CV pattern is only slightly shifted positively with the increase of the potential scan rate (inset in Figure 2a), slope of the E_p vs $\log v$ dependence being ~ 10 mV. This feature, together with the delayed ill-defined and low cathodic peak, recorded upon potential scan reversal, points to:

- deposition of a solid, electrochemically active product on the electrode surface, (ii)
- a chemically irreversible process initiated by a relatively fast electron transfer and followed by coupling of the cation radical (some trace peak on the potential return, *i.e.*, chemical reversibility, might also be perceived at the higher scan rates).

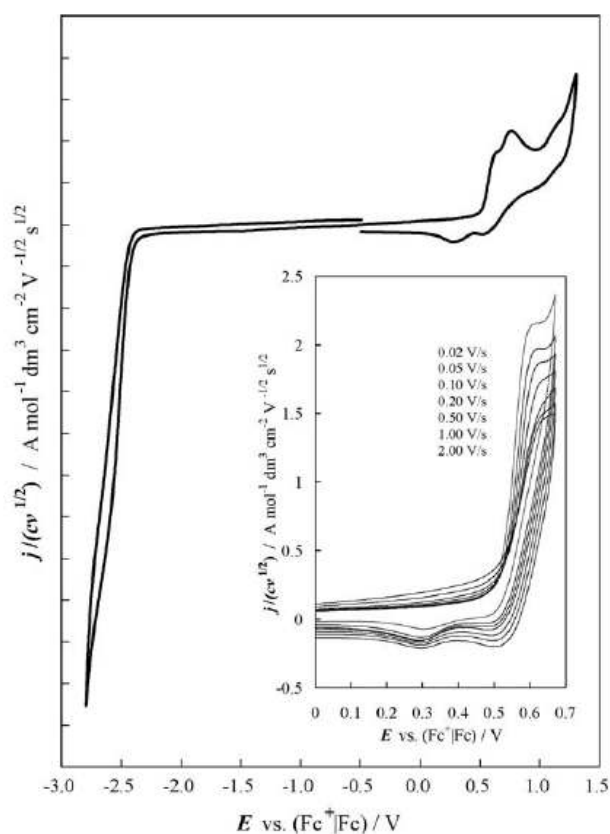


Figure 2a: Voltammetric characteristics for T4-BT2, $5 \cdot 10^{-4}$ M in CH_2Cl_2 + TBAPF₆ 0.1 M on a GC electrode ($S=0.071 \text{ cm}^2$) at 200 mV/s. Inset shows the potential scan rate effect on the first anodic peak, each voltammogram being recorded on a freshly polished electrode surface. Potentials are referred to the Fc^+/Fc redox couple.

The communication of the two thianaphthene units of T4-BT2 through the *node* was demonstrated by comparing the electronic spectrum of the latter with that of the 2-[2-(5,2'-bithienyl)]thianaphthene (BT-T2), corresponding to one half of T4-BT2, prepared by Stille coupling of 2-bromothianaphthene with 2-tributylstannyl-5,2'-bithiophene. The absorption

maximum of T4-BT2, which should be identical to that of BT-T2 if the dihedral angle in the former were 90°, was found slightly red-shifted (λ_{\max} 372 nm *vs* 366 nm for BT-T2 with $\lambda_{\text{onset}} = 430$ and 415 nm for T4-BT2 and BT-T2 respectively, Fig. 1c), indicating that the two homotopic halves were not completely independent but slightly communicating through the *node*. This situation is also inferable from the CV characteristics of T4-BT2, showing two quasi-equivalent monoelectronic peaks, pointing to two equivalent and slightly interacting redox centres, while only one monoelectronic peak is visible in the case of BT-T2. This is by no means inconsistent with the substantial equivalence of the oxidation potentials of T4-BT2 and BT-T2 ($E^{\circ}_a = 1.15$ and 1.14 V *vs* SCE, respectively), since the latter presumably results from a combination of antagonist effects, *i.e.*, the increase in conjugation and the increase in sterical hindrance, favouring and hampering the heterogeneous electron transfer process, respectively.

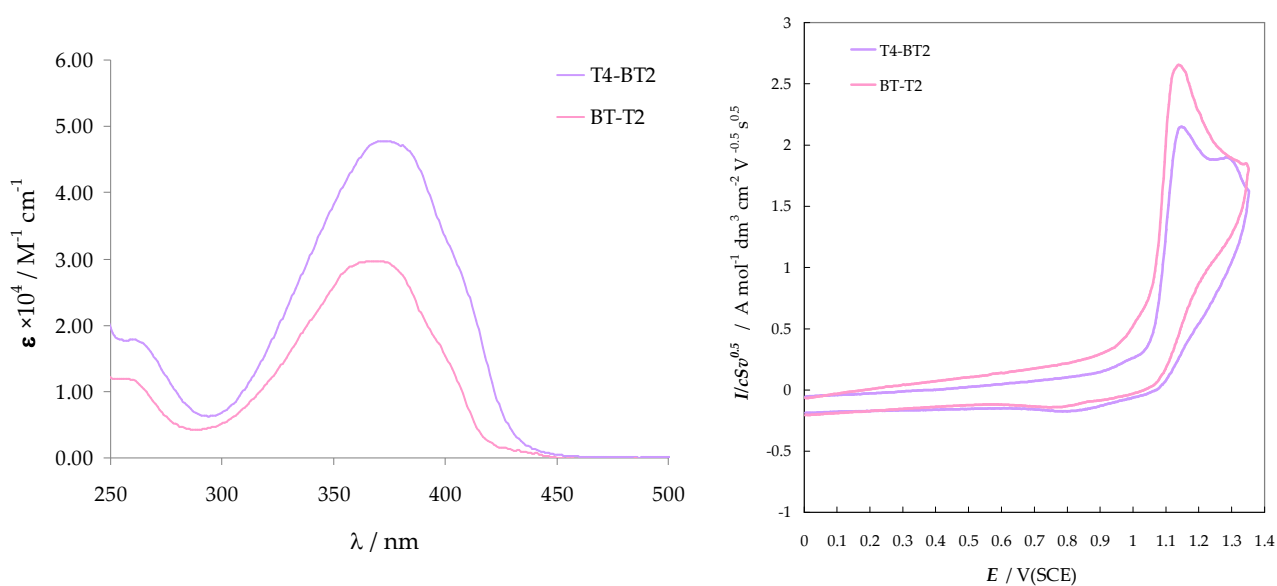


Figure 2b: UV-Vis (in dichloromethane) and cyclic voltammetry characteristics ($5 \cdot 10^{-4}$ M in $\text{CH}_3\text{CN} + \text{TBAPF}_6$ 0.1 M on a GC electrode ($S=0.071$ cm²) at 200 mV/s, potentials are referred to SCE in double bridge filled with $\text{CH}_3\text{CN} + \text{TBAPF}_6$ 0.1 M) for T4-BT2, compared with its *half*, BT-T2.

<i>Maxima criterion</i>	$E_{p,a \max}$ V/SCE	$E_p - E_{p/2}$ V	$E_{p,c \max}$ V/SCE	$E_p - E_{p/2}$ V	$E_{\text{gap} \max}$ eV	HOMO eV	LUMO eV
T4-BT2	1.118	0.058	-2.086 ^a	-0.080	3.20	-5.42	-2.22

<i>Onset criterion</i>	$E_{p,a \text{ onset}}$ V/SCE	$E_{p,c \text{ onset}}$ V/SCE	$E_{\text{gap} \text{ onset}}$ eV	HOMO eV	LUMO eV
T4-BT2	1.002	-1.926 ^a	2.93	-5.03	-2.38

a) uncertain attribution (too near to the background)

The electrochemical energy gaps, determined from either the difference of the first anodic and the first cathodic peak potential ($E_{g,EC \text{ max}} = 3.20 \text{ eV}$) or onsets ($E_{g,EC \text{ onset}} = 2.93 \text{ eV}$) are similar, albeit not coincident, with the spectroscopic gaps, determined from the absorption wavelength maximum ($E_{g,UV-Vis \text{ max}} = 3.32 \text{ eV}$) or onset ($E_{g,UV-Vis \text{ onset}} = 2.79 \text{ eV}$) (Figure 3). The obtained values are intermediate between the literature values⁶¹ for linear α -terthiophene

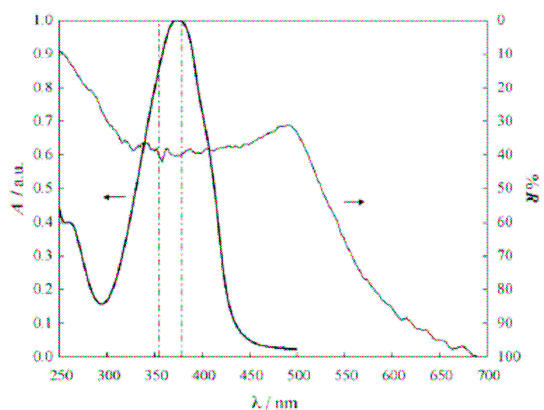


Figure 3: UV-vis spectra for the T4-BT2 monomer (in the absorbance mode, left ordinate) and for the T4-BT2 polymer deposited by electropolymerisation onto the Au-coated glass slide (in the reflectance mode, right ordinate). Values of the absorption wavelength maxima for linear oligothiophenes T3 and T4 are indicated with vertical dash-dot lines, for comparison.

(α -T3; $E_{g,UV-Vis \text{ max}} = 3.50 \text{ eV}$, $E_{g,UV-Vis \text{ onset}} = 3.04 \text{ eV}$, $E_{g,EC} = 3.10 \text{ eV}$) and linear α -tetrathiophene (α -T4; $E_{g,UV-Vis \text{ max}} = 3.28 \text{ eV}$, $E_{g,UV-Vis \text{ onset}} = 2.71 \text{ eV}$, $E_{g,EC} = 2.77 \text{ eV}$).

These data are coherent with the molecule structure, composed by two identical moieties, that can be considered as composed by a linear terthiophene with a condensed benzene ring, thus having an enhanced conjugation with respect to α -T3, that could be attributable either to the benzene ring and/or to some residual interaction with the adjacent twin π -system.

Cycling the potential around the first oxidation peak, leads to the formation of a thin electroactive layer, while including also the second peak a fast and regular growth of the corresponding conducting polymer is

observed. MALDI spectra showed that in our conditions the polymerization process mainly produces dimers and trimers, but could proceed up to the formation of pentamers.

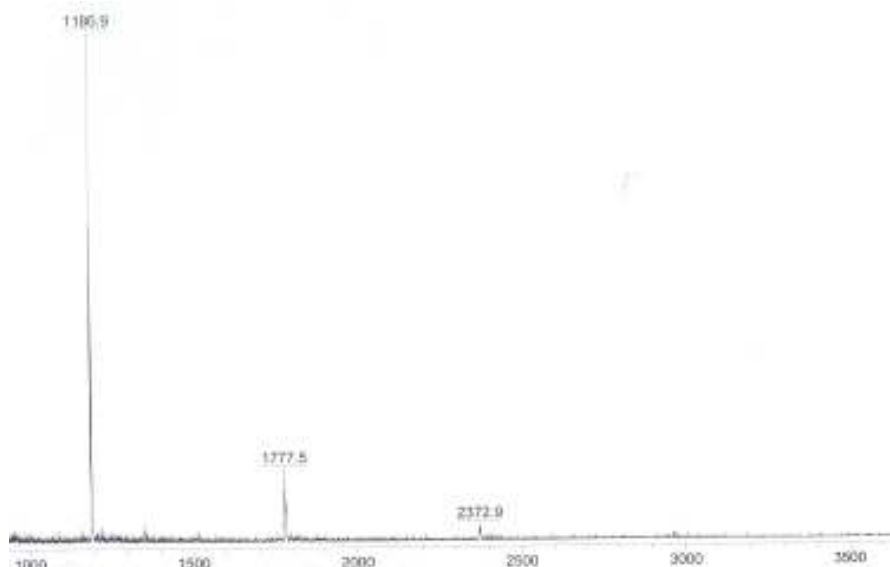


Figure 4: Maldi spectra of poly-T4-BT2. The main products of the oligomerization process are dimers and trimers.

⁶¹ K. Meerholz, J. Henze, *Electrochim. Acta*, **1996**, *41*, 1839
G. Schiavon, S. Sitran, G. Zotti, *Synth. Met.*, **1989**, *32* 209

The regularity of the deposition was confirmed by EQCM measurement, as reported in Figure 5: the mass of the polymer deposited that way increases steadily and regularly (dash-dot line in Figure 4b). The superimposed pulses account for the supporting electrolyte anion ingress and egress thus balancing the cation radical formation and reduction to its neutral form. These regular pulses increase with the increase of the polymer mass, indicating an increasing number of counterions being able to enter the film on the experiment timescale with the increase of the film thickness. Moreover, the pulses feature a fine structure with two maxima indicating multiple subsequent charge-balancing cycles during potential cycling.

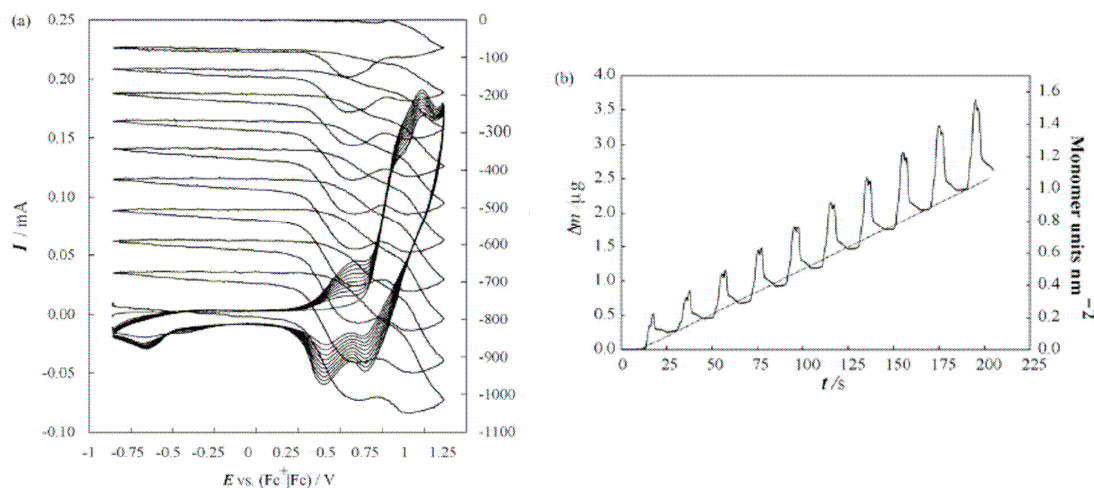


Figure 5: a) Electropolymerisation (10 CV cycles) of 1mM T4-BT2 in $\text{CH}_2\text{Cl}_2 + \text{TBAPF}_6$ 0.1M on the Au/quartz resonator of EQCM, at 200 mV/s. Left hand ordinate: CV curve; right-hand ordinate: frequency changes.

b) Variation with time of the working mass (left-hand ordinate) or monomer units per geometric surface unit (right-hand ordinate).

The film resulted to be stable upon repeated potential scan cycles in a monomer-free solution. Interestingly, stability tests were carried out on in monomer-free solution with different supporting electrolytes and monitored through EQCM (Figure 6). In the same solution used for the deposition of the polymer, *i.e.*, $\text{CH}_2\text{Cl}_2 + \text{TBAPF}_6$, the film results to be stable and the mass *vs* time plot shows a steady ingress and egress of the charge-balancing counterions (Figure 6a). When changing the hexafluorophosphate for tetrafluoroborate counterion (Figure 6b), the film remains still stable. However, it shows a slight tendency to degrade despite that the anion of tetrafluoroborate is even smaller than that of hexafluorophosphate, an effect presumably linked to some *imprinting* of the former in the polymer being formed. Much more retarded is the dynamics at the polymer-solution interface of a much bulkier and very different kind of anion, such as the *p*-toluenesulfonate (pTS). In the presence of this counteranion the first anodic peak is progressively displaced to remarkably higher potentials (Figure 6c). At constant potential window, the pulses corresponding to the anion ingress and egress progressively decrease and the overall polymer mass asymptotically increases, as if the counterion remained trapped in the polymer network. This entrapment may correspond to some irreversible polymer degradation, accounted for by the increasingly more positive oxidation potentials required for the cation radical formation.

Looking for enantioselective features in the *R*-T4-BT2 and *S*-T4-BT2 monomers already at this very early stage, we compared their electropolymerization in a solution of dichloromethane and enantiopure *R*- or *S*-tetrabutylammonium camphorsulfonate (TBACS). In fact, considering that camphor-10-sulfonic acid is reported in the literature as a chiral templating agent⁶², it was expected that polymerization would proceed at different speeds and/or with different features with each enantiomer of the T4-BT2 monomer at constant chiral medium. Unfortunately, in CH₂Cl₂ + TBACS 0.1 M no deposition of electroactive film was observed, but, on the contrary, there was a kind of passivation of the electrode, even when increasing concentration of TBAP was added in order to trigger the polymerization process (increasing the availability of the smaller counter anion). Another approach consisted in depositing conducting polymers from a CH₂Cl₂ + TBAP 0.1 M, and then cycling it in a monomer-free solution of CH₂Cl₂ + TBACS 0.1 M, in order to substitute the perchlorate anions with the chiral anions. Also in this case, however (actually in consistency with the previously illustrated stability tests in Figure 6) the film underwent a degradation process, because of the bulky camphorsulfonate ions.

The great attitude towards polymerization was then exploited in the formation of cross-linked copolymers, combining T4-BT2 as a racemate with bis(bithienylmethane)-based systems, bearing functional groups for applications in sensoristics (*i.e.*, a 1,3,2-dioxaborinane or a benzo-(18-crown-6) ether) but with poor polymerization ability⁶³. By comparing the polymerization voltammograms of the each monomer alone with the polymerization voltammograms of an equimolar mixture of T4-BT2 and the comonomer(s) it is possible to observe the formation of electroactive films of high conductivity and stability, whose patterns are different with respect to the former case, as shown in Figure 7, to be compared with Figure 5 (*i.e.*, homopolymer formations). In particular the comonomer bearing an crown ether as functional group was employed for the development of an highly sensitive and selective micropiezogravimetric chemosensor based on a MIP for the detection of melamine, which was patented and published⁶⁴.

⁶² S. Pleus, M. Schwientek, *Synth. Met.*, **1998**, 95 233

M. Schwientek, S. Pleus, C. Heinz Hamann, *J. Electroanal. Chem.*, **1999**, 461, 94

S. Pleus, B. Schulte, *J. Solid State Electrochem.*, **2001**, 5, 522

G.Y. Han, G.Q. Shi, L.T. Qu, J.Y. Yuan, F.E. Chen, P.Y. Wu, *Polym Int.*, **2004**, 53, 1554

⁶³ F. Sannicolò, S. Rizzo, T. Benincori, W. Kutner, K. Noworyta, J. W. Sobczak, V. Bonometti, L. Falciola, P. R. Mussini, M. Pierini, *Electrochim. Acta*, **2010**, 55, 8352

⁶⁴ A. Pietrzyk, W. Kutner, R. Chitta, M. E. Zandler, F. D'Souza, F. Sannicolò, P. R. Mussini, *Anal. Chem.*, **2009**, 81, 10061

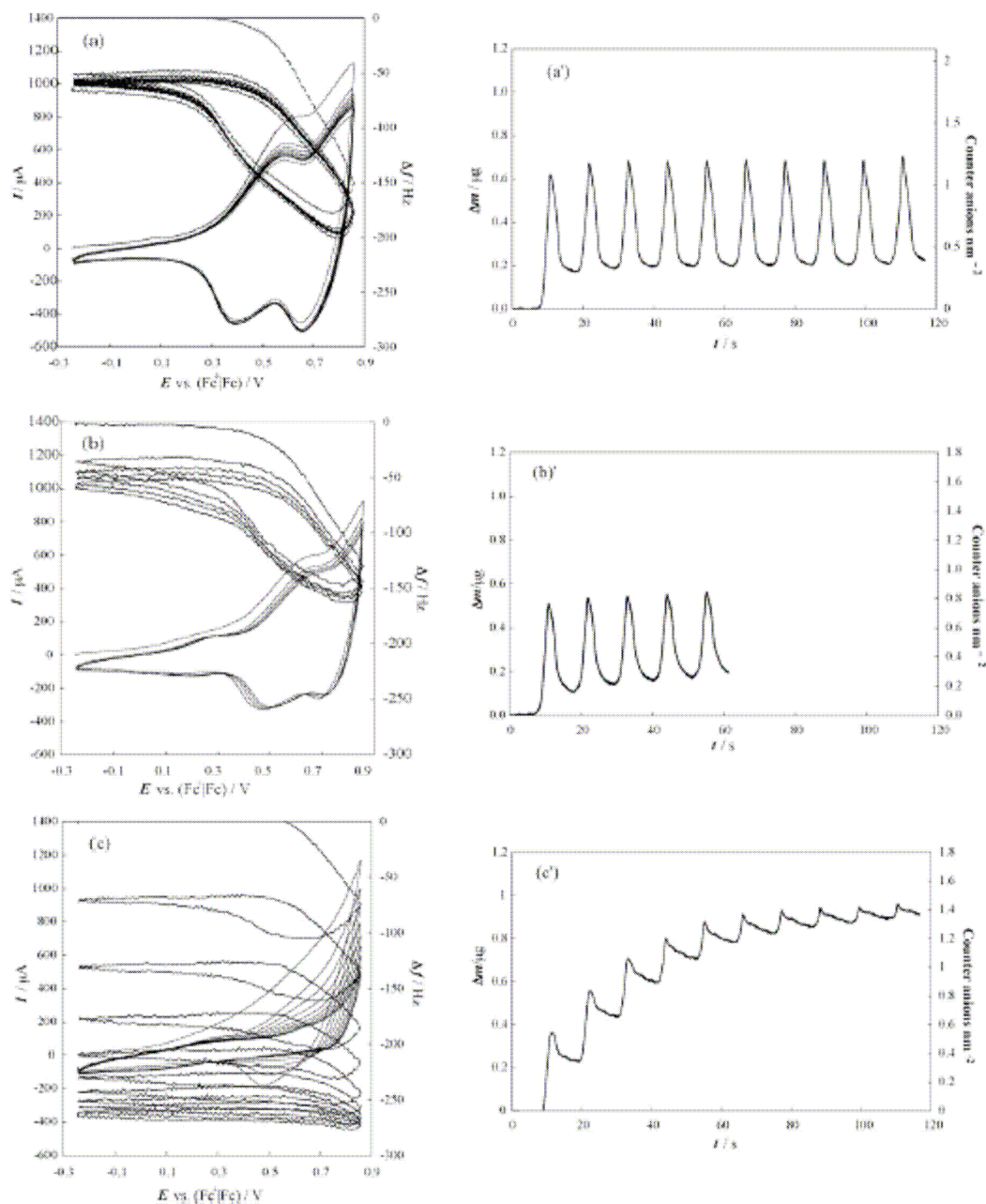


Figure 6: Stability of the T4-BT2 polymer film, electrodeposited on the Au/quartz resonator of EQCM, at 200 mV/s, with respect to anodic CV cycling in the monomer-free CH_2Cl_2 solution, with 0.1M a) TBAPF_6 , b) TBABF_4 , and c) TBAPTS . Left-hand ordinate: CV patterns; Right-hand ordinate: frequency changes. Variation with time of the working electrode mass or counterion units per geometric surface unit for (a') TBAPF_6 , (b') TBABF_4 , and (c') TBAPTS .

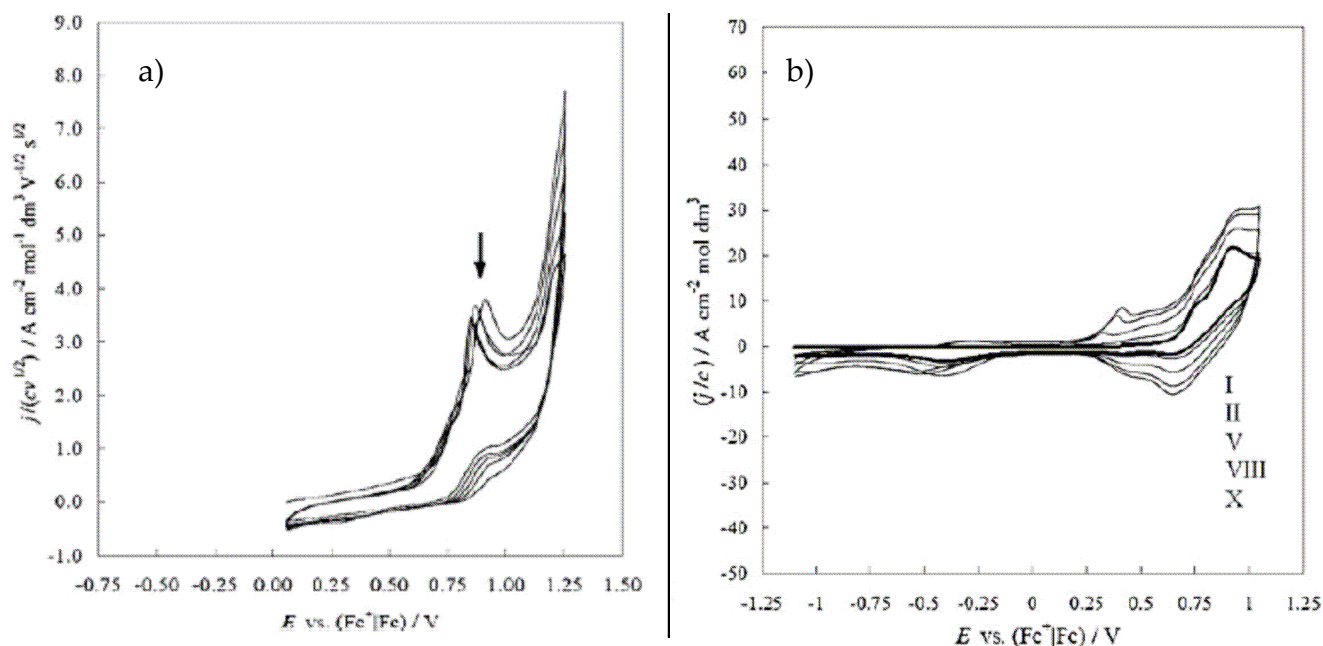


Figure 7: Multiscan CV curves for electropolymerisation of crown-ether based functional monomer (a) 1.22 mM on a Pt disk electrode ($S=0.00785 \text{ cm}^2$), 100 mV/s, in $\text{CH}_3\text{CN}+\text{TBAPF}_6$ and (b) 1 mM, in the presence of 1mM T4-BT2 on a Pt disk electrode ($S=0.00785 \text{ cm}^2$), in $\text{CH}_2\text{Cl}_2 + \text{TBAP } 0.1 \text{ M}$.

After this first promising application of T4-BT2 as a racemate, the research programme continued in the direction of exploiting its most outstanding property, *i.e.*, its *inherent chirality*, for the many possible applications already mentioned in the Introduction, considering not only the enantiopure monomers, but particularly the enantiopure polymers, taking into account also that the 3D structure of the polymeric network is important for amplifying the electro-optical performances of organic semiconductors.

The resolution of racemic (\pm)-T4-BT2, synthetically easy accessible⁶⁵, can be quantitatively achieved by HPLC on the immobilized-type Chiralpak IB-3 chiral stationary phase (CSP), as shown in Figure 8, along a protocol developed by Prof. R. Cirilli from the Istituto Superiore di Sanità in Rome.

Impressively, the absence of a plateau between the two signals confirms the stability at room temperature of the two antipodes, as it was expected on the basis of theoretical calculations mentioned before.

The chiroptical properties of the enantiopure antipodes have been determined and their absolute configuration assigned by comparing the experimental CD spectra with that calculated for the (S)-(+)-T4-BT2 enantiomer (Figure 9)

⁶⁵ F. Sannicolò, S. Rizzo, T. Benincori, W. Kutner, K. Noworyta, J. W. Sobczak, V. Bonometti, L. Falcicola, P. R. Mussini, M. Pierini, *Electrochim. Acta*, **2010**, *55*, 8352

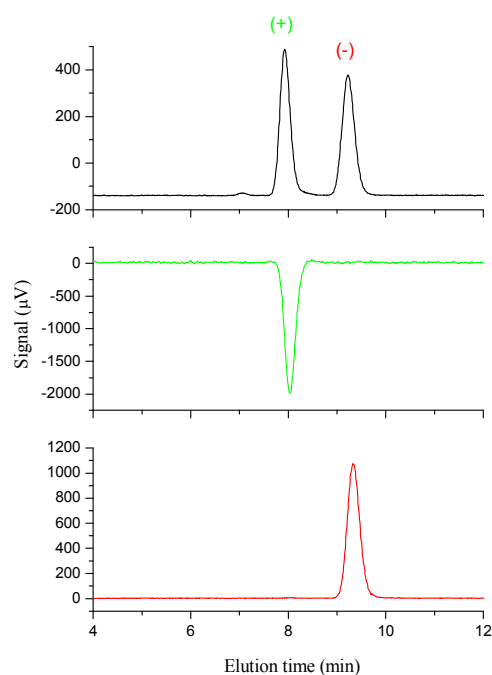


Figure 8: Analytical HPLC resolution of (±)-T4-BT2. Chiralcel OD-H and purity check of the enantiomers isolated on a semi-preparative scale. Column: Chiralcel OD-H (250 x 4.6 mm I.D.); eluent = n-hexane: CH₂Cl₂: EtOH-100: 5: 0.2 (v:v:v); T = 25°C. Black line: (±)-T4-BT2 (detector: UV at 360 nm); green line: first eluted enantiomer (+)-T4-BT2; red line: second eluted enantiomer (-)-T4-BT2 (detector: CD at 360 nm).

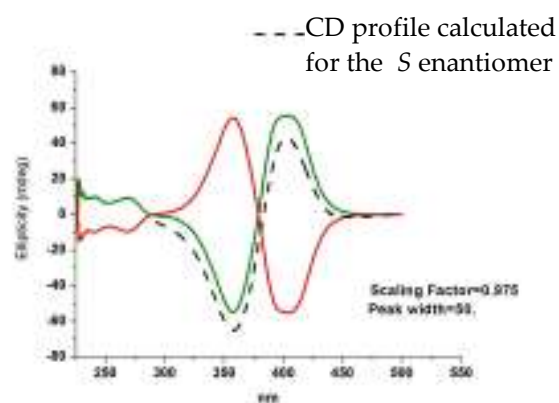


Figure 9: CD spectra (CHCl₃, c = 0.14 mg/ml) of first eluted (S)-(+)-T4-BT2 (green curve) and (R)-(-)-T4-BT2 (red curve) isolated by semi-preparative HPLC. The dotted black curve is the CD spectrum calculated for (S)-(-)-T4-BT2

Impressive is the specific rotation value at 0.1% monomer concentration in chloroform ($[\alpha]_{D^{20}} = +1001^\circ$, $[\alpha]_{D^{20}} = -991^\circ$), in accordance with the presence in the molecule of an inherently dissymmetrical chromophore.

Further information on the properties of T4-BT2 was given by DFT calculations: the favoured dihedral angle was found to be about 80° (angle value computed by averaging those found within the two most representative conformations of T4-BT2, characterized by a relative Boltzmann population of 74% and 26%) and the enantiomerization barrier, related to rotation around the bond connecting the thianaphthene units close to 167 kJmol^{-1} indicating the high configurational stability of the enantiomers even at high temperature⁶⁶. The two more stable conformations (T4-BT2_conf1 and T4-BT2_conf2), corresponding to 77% of the whole Boltzmann distribution, were further optimized. These latter geometries

⁶⁶ T. Benincori, V. Bonometti, R. Cirilli, L. Dunsch, W. Kutner, G. Longhi, P. R. Mussini, M. Panigati, M. Pierini, S. Rizzo, F. Sannicolò, *Inherently Chiral Electroactive Polythiophenes: the Breathing Chirality*, manuscript in preparation, 2012

were also used as starting structures to be optimized in form of cations (T4-BT2_conf1+ and T4-BT2_conf2+). Then, relevant UV-visible spectra were calculated (Excited States: 6) for both neutral (*i.e.*, T4-BT2_conf1 and T4-BT2_conf2) and cationic forms (*i.e.*, T4-BT2_conf1+ and T4-BT2_conf2+) of compound T4-BT2. For sake of comparison, the same kind of calculations were also carried out on the above two conformations of T4-BT2 in which the dihedral angle between the thianaphthene units was constrained during the optimization at 90° (*i.e.*: T4-BT2_conf1_90°, T4-BT2_conf2_90°, T4-BT2_conf1_90°, T4-BT2_conf2_90°+) or at 55° (only in the cation, *i.e.*: T4-BT2_conf1_55°, T4-BT2_conf2_55°+). All the obtained results are shown in Figures 10a and 10b.

CD spectra related to the conformations T4-BT2_conf1 and T4-BT2_conf2 of R configuration have been calculated in vacuum. An estimation of the enantiomerization barrier, related to rotation around the bond connecting the thianaphthene units of T4-BT2 was already calculated, and should be comprises between 47.7 and 32.5 kcal mol⁻¹, that is to say, values in any case sufficiently high to guarantee an enantiomerization half-lifetime of several centuries⁶⁷.

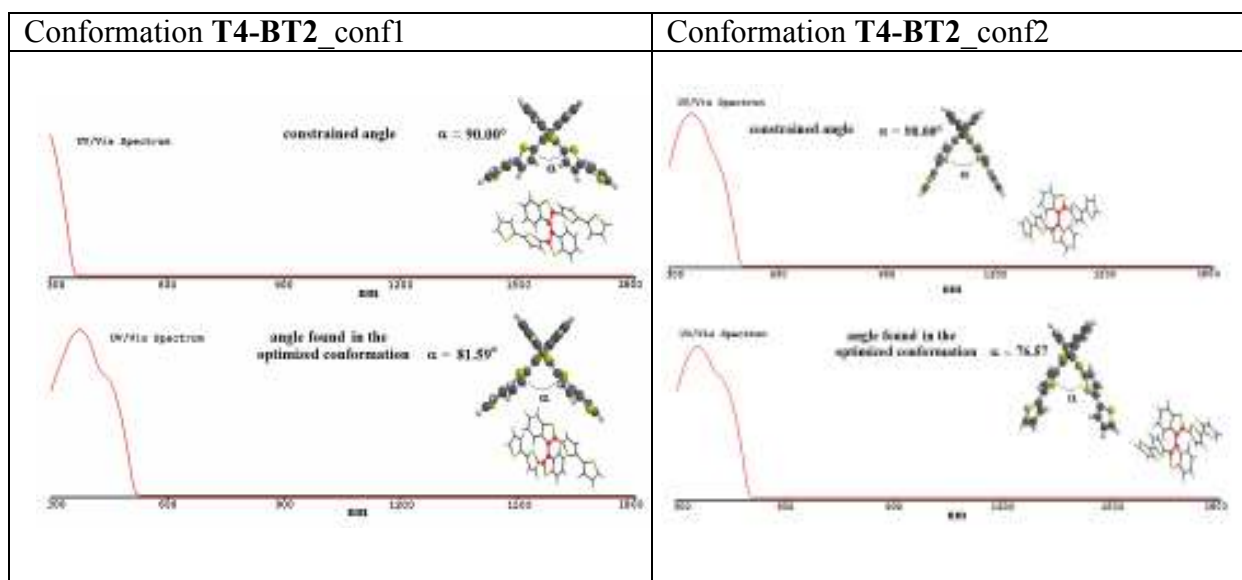


Figure 10a: Calculated UV-visible spectra of the two most representative conformations of T4-BT2 and of those deriving from the optimization performed with the dihedral angle between the thianaphthene units constrained at 90°

⁶⁷ T. Benincori, V. Bonometti, R. Cirilli, L. Dunsch, W. Kutner, G. Longhi, P. R. Mussini, M. Panigati, M. Pierini, S. Rizzo, F. Sannicolò, *Inherently Chiral Electroactive Polythiophenes: the Breathing Chirality*, manuscript in preparation, Supporting Information, 2012

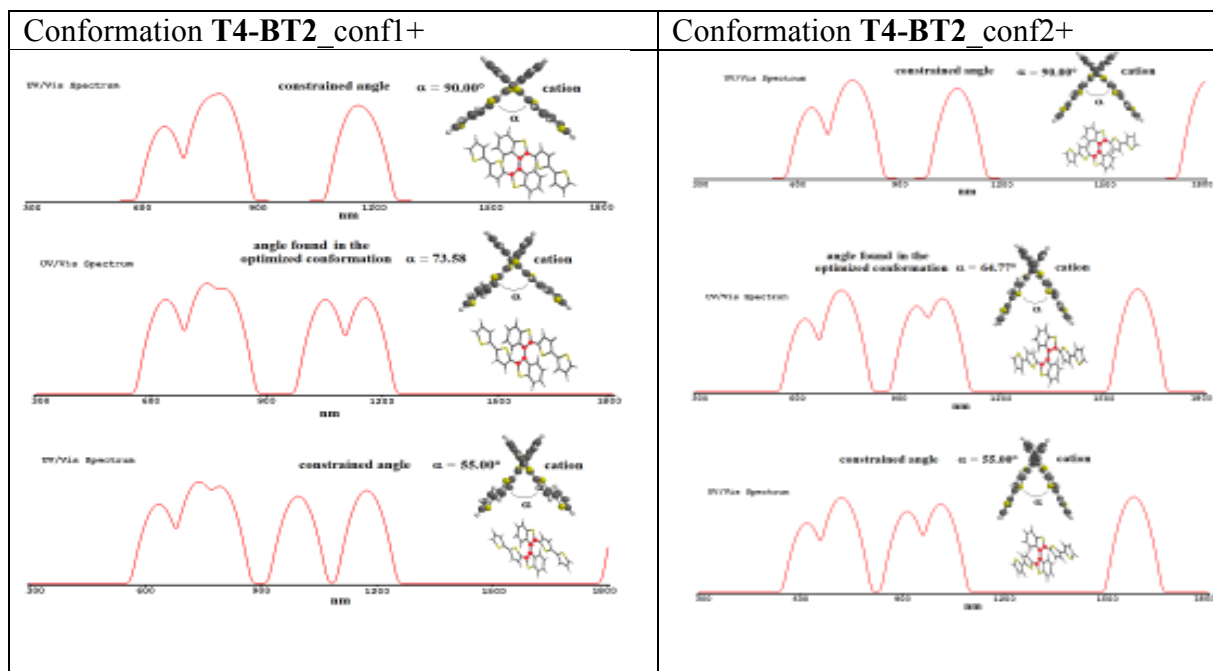


Figure 10b. Calculated UV-visible spectra of the cationic forms of **1** obtained by optimizing the two most representative conformations of T4-BT2 with the dihedral angle between the thianaphthene units free to change or with an imposed constraint of 90° or 55° .

UV-Vis spectroelectrochemistry experiments (Figure 11a) demonstrated that the progressive increase of the anodic potential from 0.55 to 1.15 V(SCE) (in CH_2Cl_2 solvent) produces a strong reduction in intensity of the absorption band at 450 nm and a parallel growth of two less intense new bands at 780 and 1060 nm, attributable to more conjugated polaronic and bipolaronic states respectively. No changes at all were observed when the potential was driven toward negative values (in light blue and blue, Figure 11a). The processes were found fully reversible and repeatable even though some loss of electroactivity was observed after repeated slow cathodic scans.

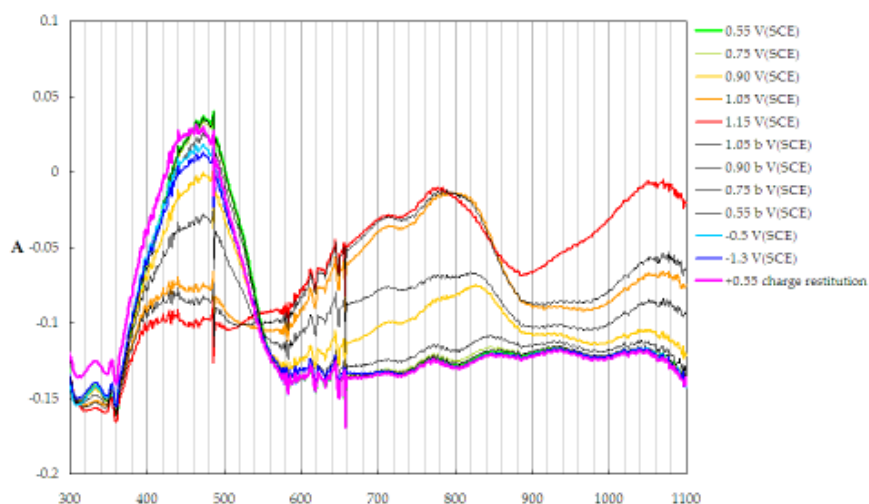


Figure 11a: UV-Vis spectroelectrochemistry on a film of poly-(+)-(S)-T4-BT2 on ITO electrode, under polarization.

The collaboration with Prof. L. Dunsch of the Leibniz Institute for Solid State and Materials Research, Dresden, Germany) allowed to complete this characterization combining UV-Vis spectroelectrochemistry, extended to the near-infrared region, with ESR (Figure 11b), verifying that the stepwise increase of the anodic potential from 0.55 to 1.15V produces a strong reduction in intensity of the absorption band at $\lambda_{\text{onset}} \sim 580$ nm and a parallel growth of two new bands at ~ 800 and ~ 1150 nm attributable to the more conjugated polaronic and bipolaronic states respectively. Accordingly, parallel ESR spectroelectrochemistry showed the progressive formation of a radical state with maximum density signal at 1.1V vs Ag^+/Ag (Figure 11b). This behaviour has been successfully reproduced by calculations on both the two most representative conformations of T4-BT2.

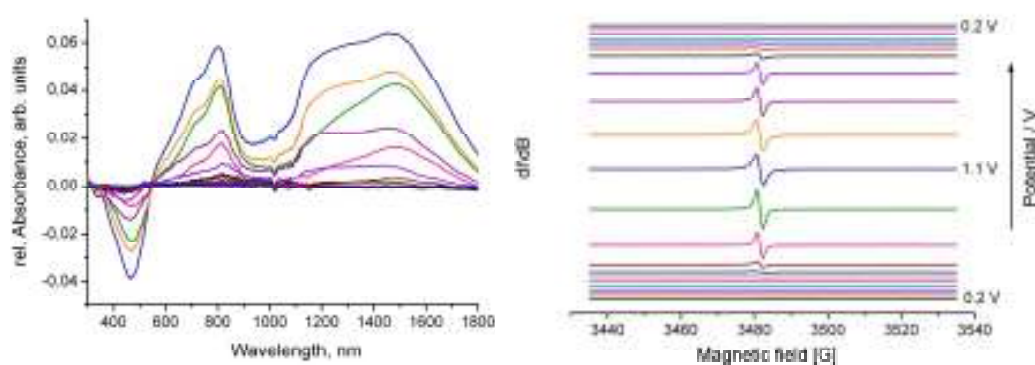


Figure 11b: UV-Vis-NIR spectroelectrochemistry recorded for a sample of poly-T4-BT2 on a Pt grid under increasing polarization (from 0.2 V to 1.1 V vs Ag^+/Ag and backward scan), paralleled by ESR measurement. It is possible to detect the formation of the polaron structure

The most interesting features of these materials are related to their *pseudo-scalar* properties, overall the CD and enantioselection properties. The CD spectra of the films demonstrate that chirality and its CD sign is transferred from monomers to the polymers. The bisignate spectra of the polymers are very similar to those shown by the original monomers, with ellipticity maxima strongly shifted toward higher wavelengths, in accordance with the increased conjugation extent gained with polymerization. This result gives a proof of the great differences existing between these non conventional, inherently chiral polythiophene polymers and the traditional ones, which exhibit CD manifestations only in particular chain aggregation states, but are completely silent under ordinary conditions⁶⁸.

The first observation that chirality is fully retained even at solid state was obtained by comparing the CD signal of the enantiopure monomers in solution with the spectra of electrodeposited enantiopure films on ITO electrodes, as shown in Figure 12.

⁶⁸ B.M.W. Langeveld-Voss, R.A.J. Janssen, E.W. Meijer, *J. Mol. Structure*, 2000, 521, 285

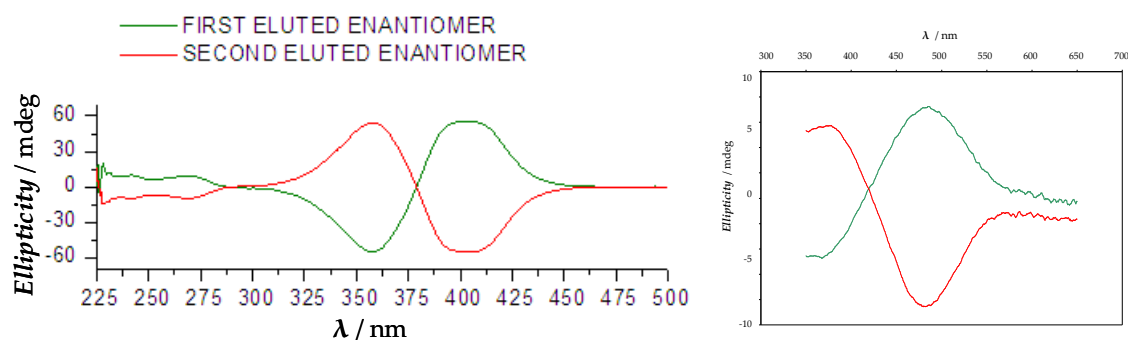


Figure 12: CD spectra for T4-BT2 in chloroform solution (left) and on electrodeposited films (right)

This result, together with the interesting behaviour of T4-BT2 shown by spectroelectrochemical experiments, suggested the extension of our work to the combination of the circular dichroism measurements with cyclic voltammetry. For this purpose a three-electrode cell, with an ITO electrode glass covered by a film of poly(-)-T4-BT2 or poly(+)-T4-BT2 as the working electrode, a thin Pt wire as the counterelectrode and a small saturated calomel reference electrode, was arranged in a standard quartz cuvette and positioned into the cell compartment of a spectropolarimeter. The CD spectra of the polymer, recorded at different potentials, paralleled the UV observations (Figure 13): the original bisignate curve observed in the neutral state was progressively shifted toward higher wavelengths at increasing potentials, as expected on the basis of the UV data. Interestingly this red-shift was accompanied by a considerable decrease in CD signal intensity, indicating a reduction of chirality strength in the *p*-doped state. Hole injection would force the two thianaphthene rings to flatten in order to gain in electronic conjugation with some loss in the stereogenic efficacy of the atropisomeric core. This is also coherent with the fact that the more planar the system, the higher effective conjugation, the narrower the band gap and the higher the conductivity. The two interconnected heteroaromatic units, however, cannot become completely coplanar in the heavily doped state, otherwise chirality would be completely lost, while it is fully recovered when the polymer is switched back to the neutral state. The reversible and repeatable potential-driven variation of the dihedral angle of the atropisomeric backbone, accompanied by fluxional reduction and recovery of the chirality strength, suggested us the image of a *breathing* system (Figure 13 and 13 bis). This breathing mechanism opens up interesting applications, *e.g.* acting as a polarization filter modulable by electric potential modulation.

No influence was exerted instead on the CD behaviour by *n*-doping in accordance with the UV observations. It has to be underlined, however, that we purposely did not go far beyond the reduction onset, to preserve the thin film integrity.

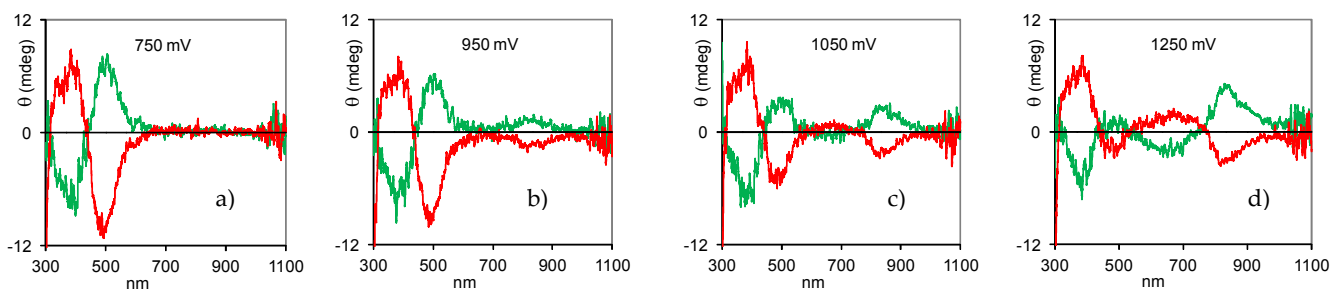


Figure 13: CD spectra of films of poly-(S)-(+)-T4-BT2 (green) and poly-(R)-(-)-T4-BT2 (red) on ITO during an anodic cycle

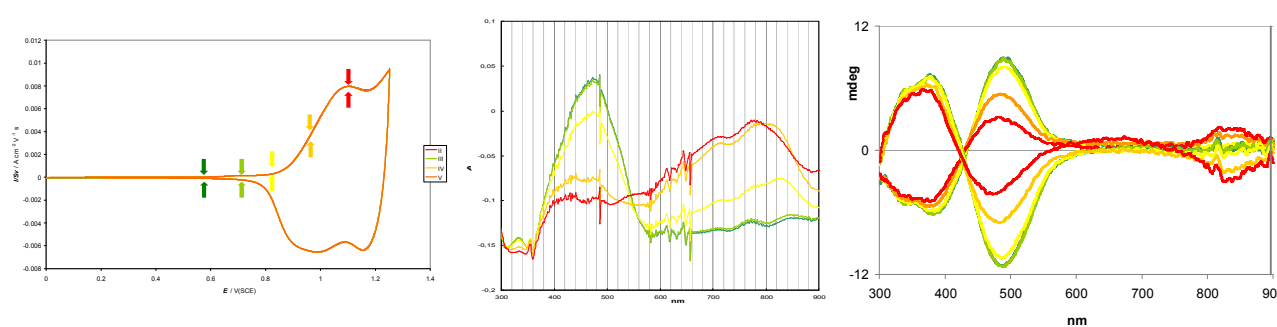


Figure 13 bis: *in situ* CV, UV-Vis and CD at different applied potentials.

As a first test of the enantiorecognition ability of the chiral polymers, in the CV patterns of commercially available (*S*)-(-)- and (*R*)-(+)-*N,N*-dimethyl-1-ferrocenylethylamine, named (*S*)-(Fc*) and (*R*)-(Fc*) (Figure 14), used as chiral probes, recorded on bare gold electrodes and on such electrodes coated with poly-(*R*)-(-)-T4-BT2 and poly-(*S*)-(+)-T4-BT2. The precondition was, of course, to prepare polymer electrode surfaces fully reproducible in size, shape, morphology and thickness. This was achieved by working on screen-printed supports (with a gold working electrode, a platinum counter electrode and a silver pseudo reference electrode) covered by a film electrodeposited from a 0.012 M T4-BT2 solution in the

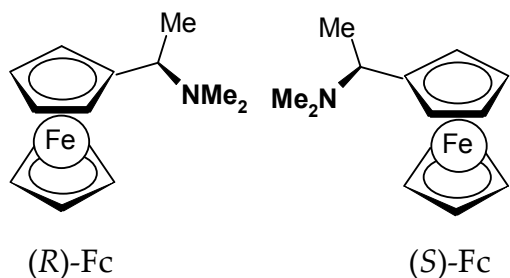


Figure 14: Chiral probes, (*S*)-(-)- and (*R*)-(+)-*N,N*-dimethyl-1-ferrocenylethylamine

ionic liquid 1-butyl-3-methylimidazolium hexafluorophosphate BMIMPF₆ as the working medium. On the bare gold electrode regular diffusive peaks were observed for (*S*)-(Fc*) and (*R*)-(Fc*) with ~60 mV half-peak width and ~60 mV distance between forward and backward peaks, as expected for a reversible one-electron transfer, as shown in Figure 14 b.

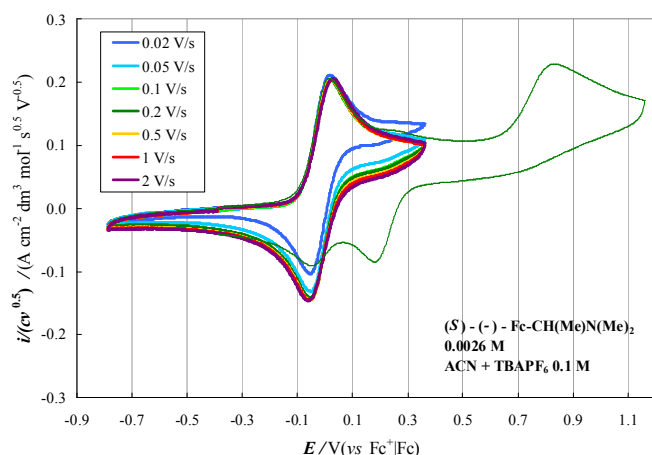


Figure 14 b: Voltammetric characteristics of (S)-Fc*, 0.0026 M in CH₃CN + TBAPF₆ 0.1 M, on a GC electrode (S=0.071 cm²), at different scan rates

On the polymer-coated electrode the same redox peaks remain fully reversible, but they are shifted to much more positive potentials and the distance between forward and backward peaks neatly decreases; both features point to a solid-state process within the

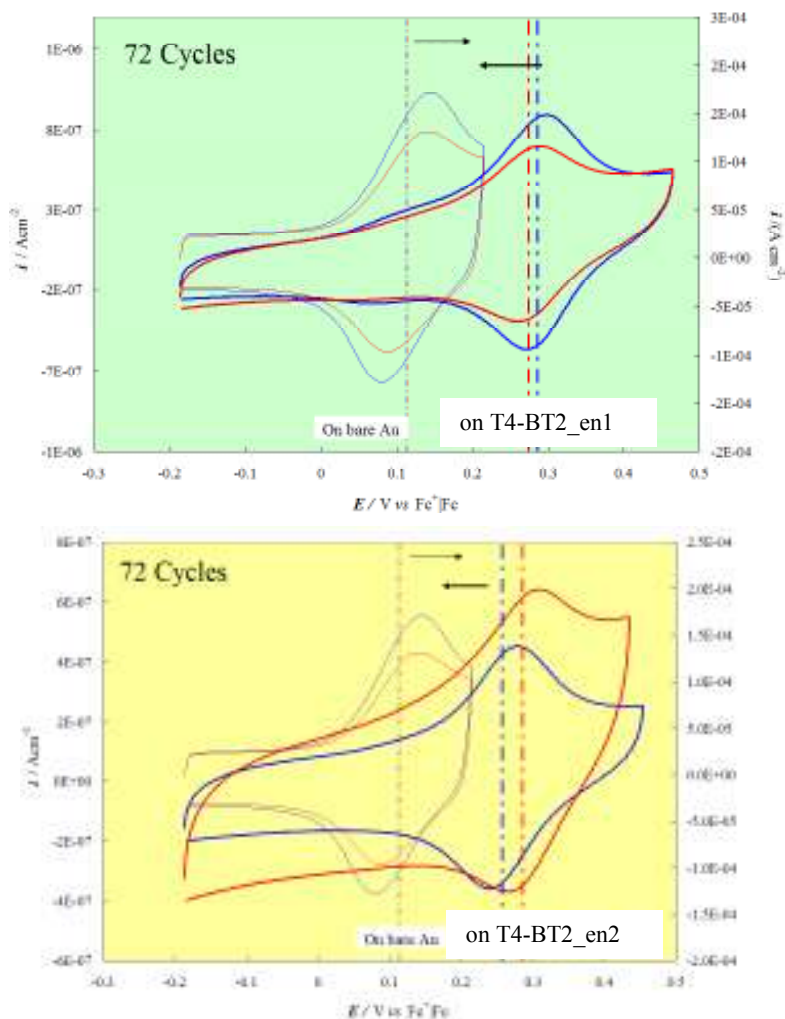


Figure 15: Voltammetric signal of (R)- and (S)-Fc*, in blue and red, respectively, on bare Au screen-printed electrode, and on the Au screen-printed electrode covered by (R)- and (S)- films of T4-BT2.

thin film. Actually, the formal potential of the probe falls in the potential range in which the polymer is neutral; accordingly, the electron transfer process can only take place between the metal electrode and the probe molecule diffusing within the film towards the underlying metal surface.

In these conditions, working with the poly-(-)-(R)-T4-BT2 coated electrode, a different potential shift is observed for (S)-(Fc*) and (R)-(Fc*) (0.27 and 0.29 V, respectively), while the opposite sequence is observed when the film on the electrode is poly-(+)-(S)-T4-BT2. The peak separation increases with increasing the film thickness. Thus, the enantio-selection mechanism should be based on a chromatographic-like process in which the film behaves as a chiral stationary phase.

We also found such diffusion within the film to be reversible (the probe-free film can be easily

recovered by performing a few redox cycles around the first oxidation potential), so that the same film can be used for further subsequent tests. Although such phenomenon could be influenced by some imprinting effect of the first probe entering the film with respect to the second one, it might as well point to some enantioselective effect exerted by the enantiomeric electrode surface towards the antipodes of the probe molecules. A more detailed research is under way, to better elucidate the recognition process.

These preliminar but very promising results were obtained at the end of a three-year work focused on the optimization of the deposition conditions. In fact, as explained in the Introduction, obtaining perfectly equivalent films in terms of thickness, morphology,

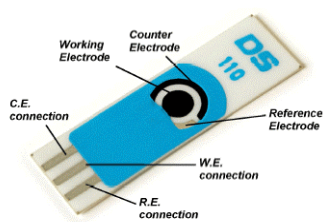


Figure 16: An example of a DropSens® screen printed electrode. On the right, the experimental setup.

physico-chemical properties is probably the hardest task in the field of conducting polymers, since many parameters affect the deposition process. This difficulty was overcome in the last period of the present PhD thesis⁶⁹ when DropSens® screen-printed electrodes have been used: they are perfectly reproducible electrochemical cells, and the geometry of the cell is

perfectly constant, affording high reproducibility of the results. A drawback of these systems is the use of a silver pseudo-reference electrode, but in the experiments performed in the frame of the present work, no potential drift was observed, while the pseudoreference offers, at the same time, the advantage of completely avoiding possible pollution of the working medium by aqueous KCl contained in the SCE or in the double bridge. Furthermore, the screen-printed electrodes have been used in combination with ionic liquids (in particular, BMIMPF₆) that, being non-volatile, solvent and supporting electrolyte at the same time, can assure a constant concentration of the monomer during the experiment, in exactly the same working medium. Unfortunately, ionic liquids are very viscous and sometimes difficult to manage: this problem was overcome by employing either mixture of ionic liquid and traditional organic solvents, and/or by employing small quantities of working medium (few microliters) deposited as drops on the spot containing the electrodes on the screen-printed system.

The characterization was completed with SEM imaging of the morphologies of the electrodeposited films, both on screen-printed electrodes and ITO glass slides, and in different working media (pure CH₃CN, 1:1 CH₃CN:BMIMPF₆, pure BMIMPF₆), by M.Sc. M. Magni and M.Sc. S. Arnaboldi, in collaboration with M.Sc. B. Sacchi from our University. The results are resumed in the following Tables: in the first one, different working electrode materials were compared, and gold screen-printed electrode appeared to be the most interesting one, showing high regularity in the deposition and granulometry, while the platinum substrate showed the formation of a more porous film. In the second Table, the SEM images refer to films deposited on ITO glass slides from

⁶⁹ Mirko Magni, M.Sc. Thesis, Università degli Studi di Milano, 2012

Serena Arnaboldi, Ist year report of PhD course in Chemical Sciences, Università degli Studi di Milano, 2012

different working media, at increasing concentration of ionic liquid in acetonitrile. It is worthwhile noticing the greater homogeneity in the case of the film deposited from pure BMIMPF₆, confirming that ionic liquids are a really advantageous medium for the electropolymerization processes, making them easily reproducible, even on different electrode surfaces, and with a very small amount of working solution (down to 10 μl), affording a wide monomer operating concentration range and minimum reagent consumption. Excellent reproducibility has been obtained as the result of reproducible cell geometry and constant monomer concentration (afforded by the low volatility of the ionic liquid). The use of ionic liquids generally requires a slower scan rate and a higher monomer concentration, but the possibilities to work in few microliters drops and to obtain better quality films overcome these minor drawbacks.

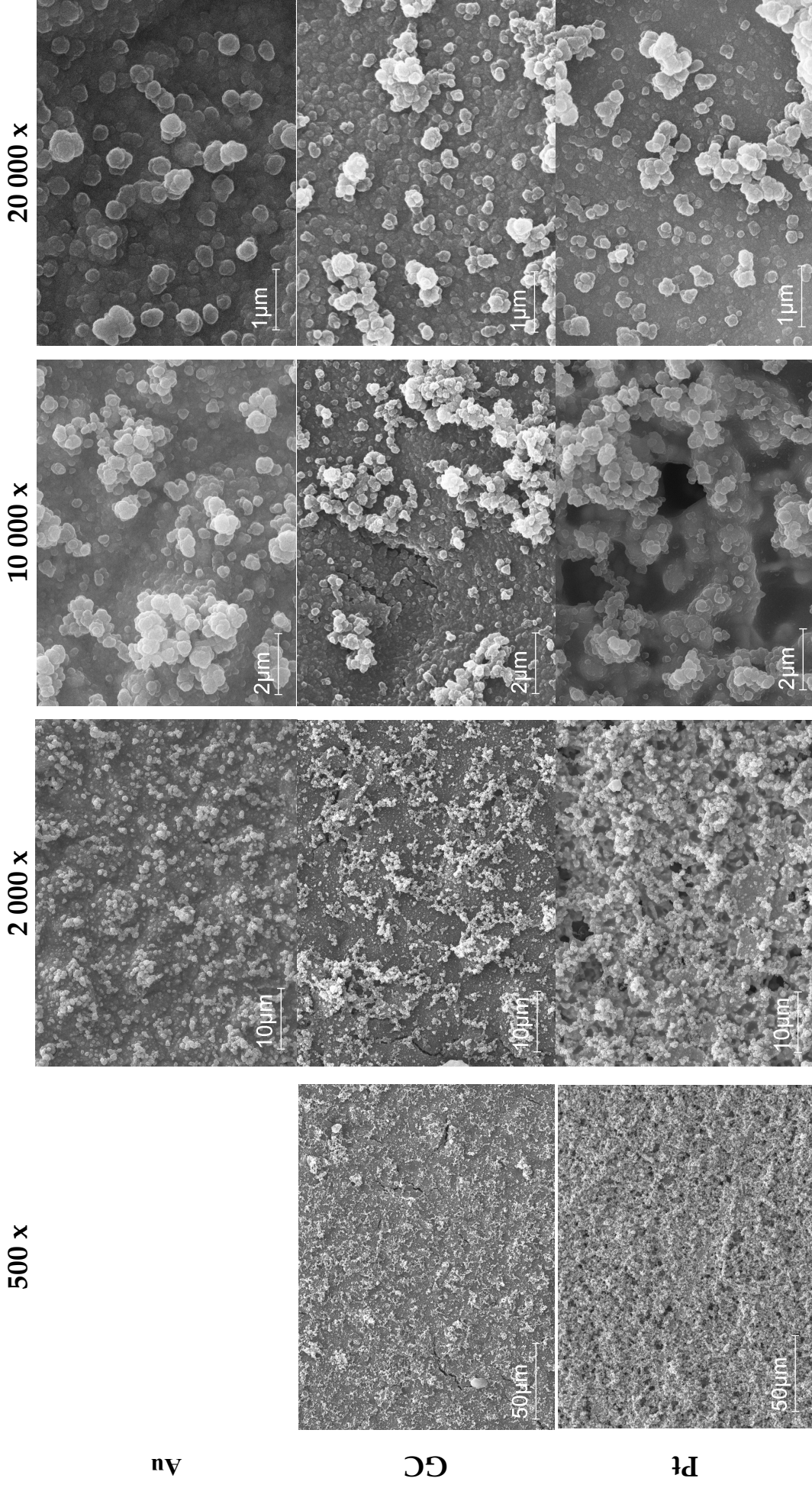


Table 1: SEM micrographies for the morphological study of poly-T4-BT2 films electrodeposited on different electrode materials. Films deposited on DropSens® from a 100% BMIMPF₆ solution with monomer concentration 0.012 M at 20 mV/s.

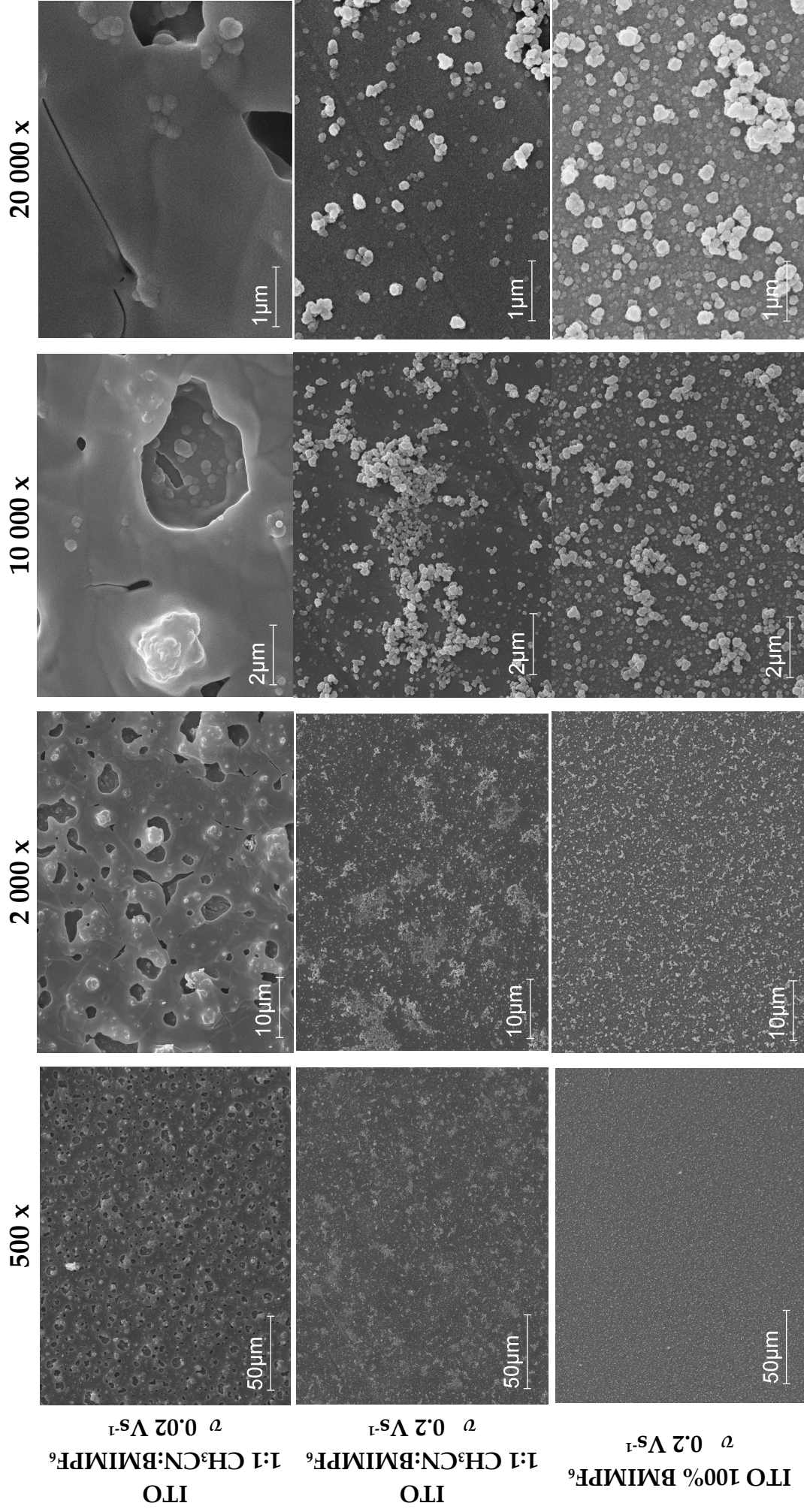
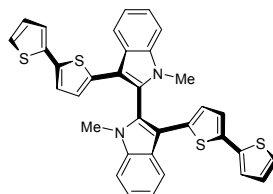


Table 2: Synopsis of SEM micrographies of poly-T4-BT2 films electrodeposited on ITO, showing the effect on the polymer morphology induced by: i) potential scan rate, 20 or 200 mV/s (first and second row); ii) the different percentage of ionic liquid as working medium (second and third row).

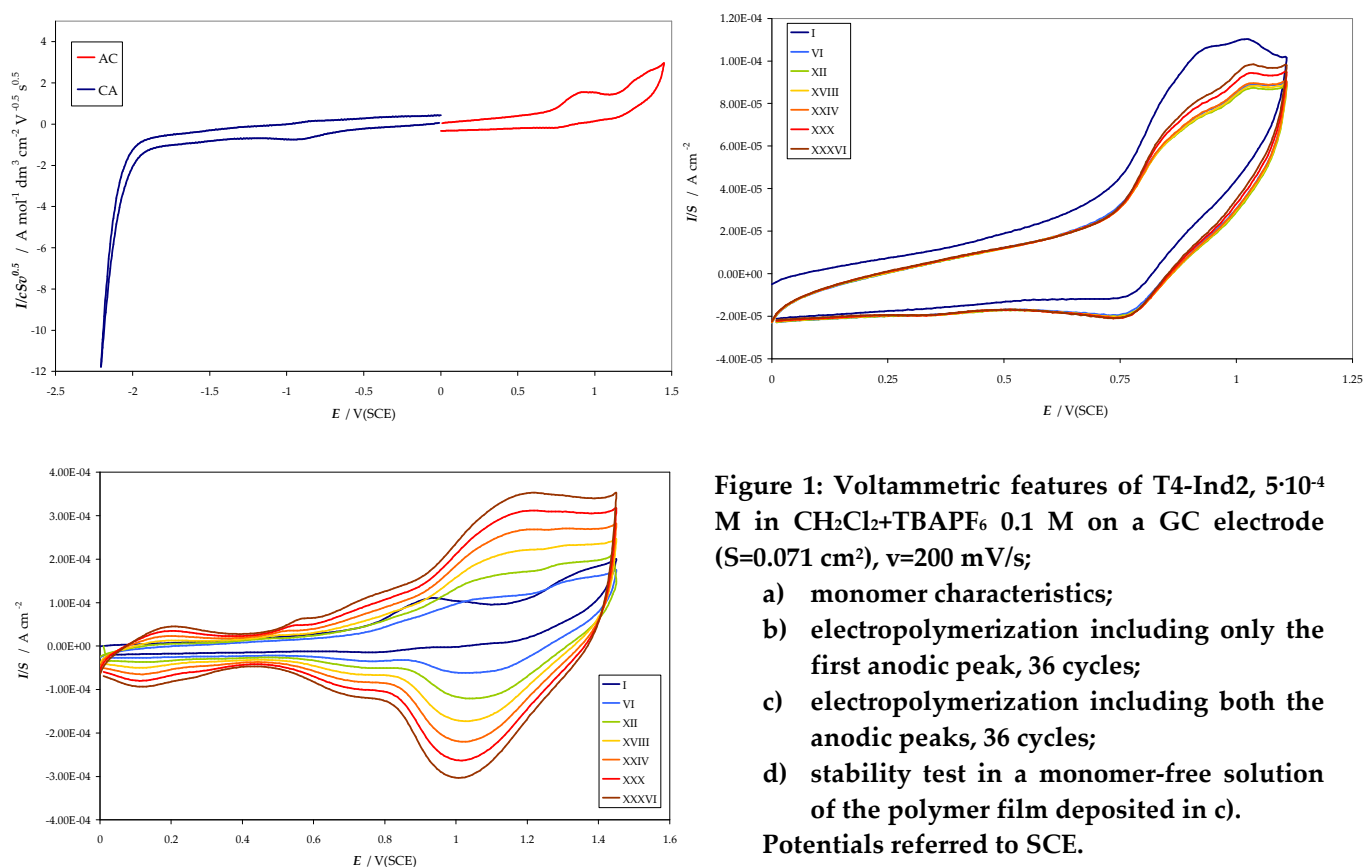
3.2.3 Other cases of inherently chiral molecules

T4-Ind2



T4-Ind2 is a peculiar case of the inherently chiral monomers, having a *N*-methyl indole as central scaffold. The rotation around the atropisomeric torsion is hindered by the presence of the methyl groups on the nitrogen atoms. Its electrochemical characteristics were investigated by means of cyclic voltammetry, and revealed the same behaviour expected for the *inherently chiral* molecules, but with some peculiarities, due to the presence of such an electronrich core as the indolic one.

Interestingly, two oxidation peaks appear in the anodic region: cycling around the first anodic peak, no deposition is observed, while including the second one affords a fast and regular polymerization, while no reduction peak is observed for the monomer, accounting for the electron-richness of the indole core.



It is likely that the first anodic peak corresponds to the formation of a radical cation localized on the indole core, being very electron-rich and without free positions for polymerization, while the second anodic peak corresponds to an oxidation site more displaced towards the terminal thiophene units, allowing the polymerization process to be triggered.

Films of T4-Ind2 show good stability properties, and a significant *charge trapping* effect.

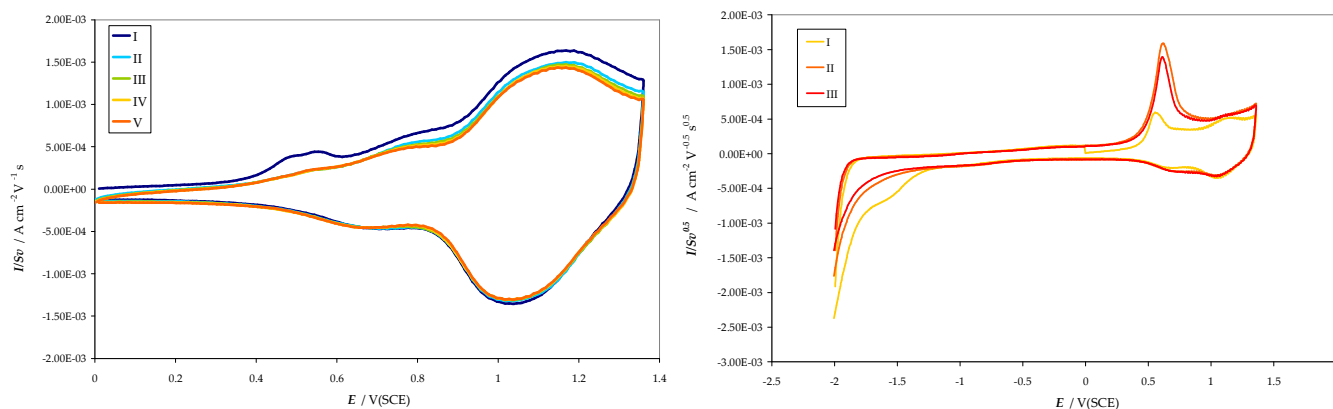


Figure 2: Stability test in a monomer-free solution and charge trapping effect of the T4-Ind2 polymer, electrodeposited according to the conditions described in Figure 1 c). Potentials referred to SCE.

T4-Ind2 racemic films of different thicknesses were also tested as electrode surfaces, in combination with three probe molecules, cobaltocenium hexafluorophosphate, dimethylferrocene and decamethylferrocene, chosen so that their potentials are included in the neutral polymer potential window, and for their different charge and bulkiness. Both the peak current and reversibility decrease with increasing scan rate and increasing bulkiness, indicating a slower diffusion of the probes inside the polymer network. In particular:

- the bulkier decamethylferrocene is discriminated with respect to the other smaller probes (Figure 2).
- also cobaltocenium is discriminated: it has approximately the same dimensions as dimethylferrocene but it is present as a cation and therefore it implies the concurrent entrance of the counteranion hexafluorophosphate in the polymer phase.

This test is particularly significant, since it showed that the polymer films are discriminating other molecules present in the working solution, as a function of their bulkiness and/or charge. With the aim of trying to build a chiral sensor based on an enantiomerically pure polymer film electrodeposited on the electrode surface, this test suggested how to proceed, and helped to get the first enantio-recognition test, as it has been discussed in details in the Chapter 3.2.2 concerning T4-BT2.

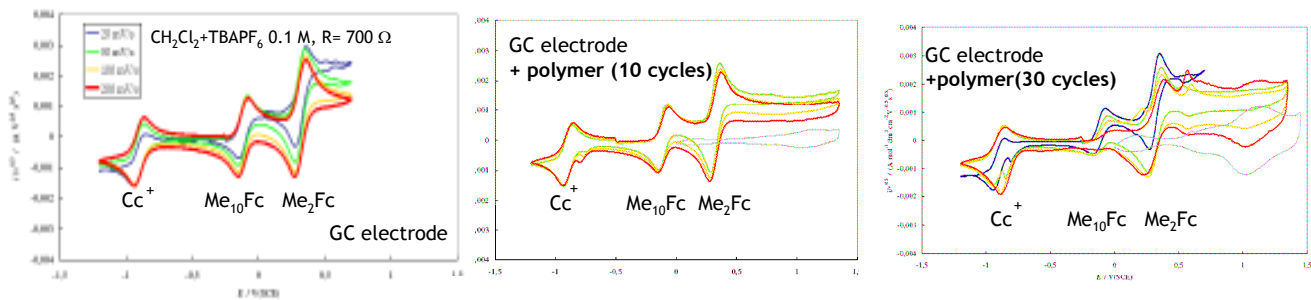
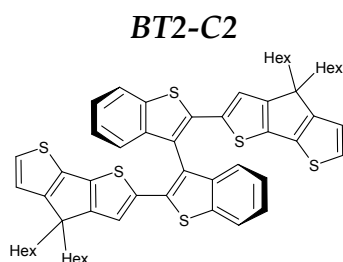


Figure 3: Test of poly-T4-Ind2 as electrode surface, in the presence of three different redox probes, each of them having a 10^{-3} M concentration in the working solution ($\text{CH}_2\text{Cl}_2 + \text{TBAPF}_6$ 0.1 M), and at increasing thickness of the electrodeposited polymer.



In this case, the atropisomeric scaffold 3,3'-bithianaphthene is maintained, while the bithiophene side chains have been substituted by 4,4-hexyl-[2,1-b:3,4-b']-cyclopentadithiophene (CPDT) units, because they could bring several advantages:

- CPDT is actually a planar bithiophene, so it could help in increasing the effective conjugation of the system, as shown by UV-Vis spectra of the monomers in dichloromethane.

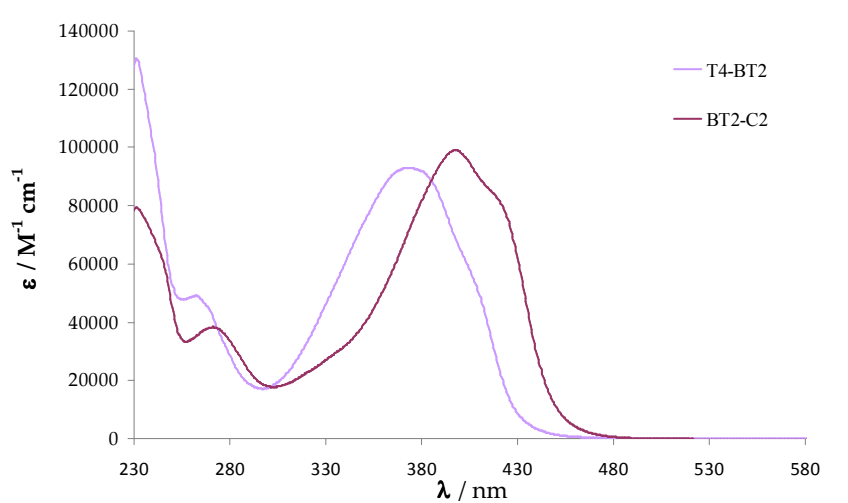


Figure 4: Comparison between UV-Vis spectra of T4-BT2 and BT2-C2, $5 \cdot 10^{-5}$ M in CH_2Cl_2 .

- CPDT can be easily functionalized by choosing appropriate substituents.
- in this case, *n*-hexyl chains were chosen, in order to increase the solubility also for the polymers, that could be more easily processed.
- it would be interesting to study also the effect of other substituents, to allow applications in sensoristics or energetics (for example, by choosing functional groups that could appropriately move the position of the HOMO and LUMO levels).

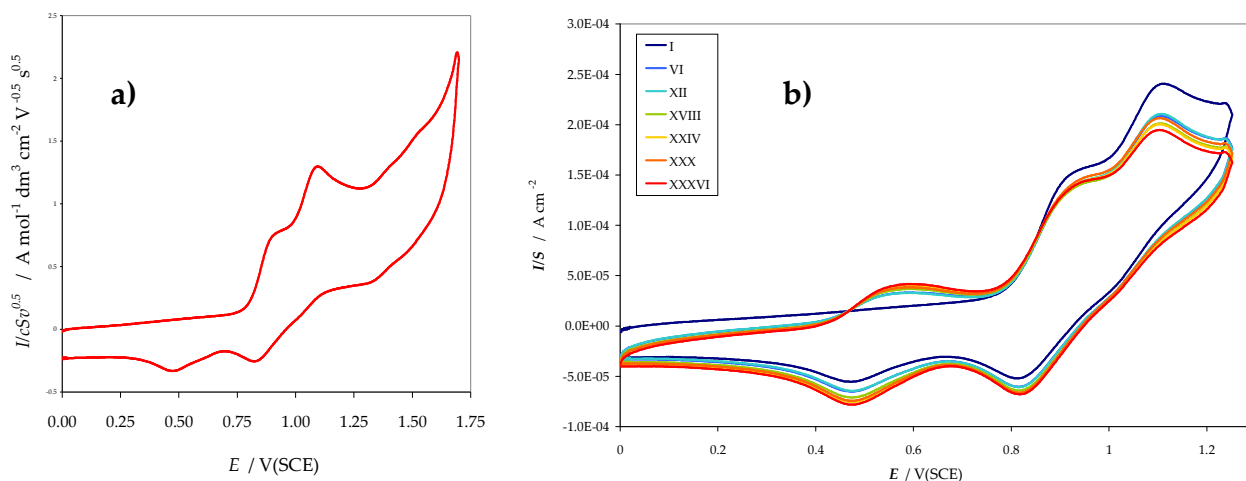


Figure 5: a) Anodic features of BT2-C2, $5 \cdot 10^{-4}$ M in $\text{CH}_2\text{Cl}_2 + \text{TBAPF}_6$ 0.1 M on a GC electrode ($S=0.071 \text{ cm}^2$), $v=200 \text{ mV/s}$; b) polymerization attempt by cycling the potential around the oxidation peaks, 36 cycles. Potentials referred to SCE in a double bridge filled with $\text{CH}_2\text{Cl}_2 + \text{TBAPF}_6$ 0.1 M

Concerning the voltammetric characteristics, also in this case it is possible to observe two nearly equivalent oxidation peaks, corresponding to the oxidation of the two homotopic terminal thiophenes, which are not independent but still slightly communicating through the central node. When cycling the potential around the anodic peaks, the formation of some electroactive product is observed, but it is fairly soluble, and when the electrode is moved to a monomer-free solution to perform the stability test, no signal is detected but the one of a blank electrode. This could be in consistency with the introduction of four hexyl chains resulting in increased solubility, as desired to afford easier processibility, but too much, thus preventing film electrodeposition and further characterization according to our protocol.

For this reason the corresponding polymer (poly-BT2-C2) was obtained by chemical oxidation of the monomer with FeCl_3 , and its characterization was made in solution.

UV-Vis spectra in dichloromethane show a significant bathochromic shift of the maximum of the $\pi-\pi^*$ transition band (from 406 to 516 nm) for the poly-BT2-C2, confirming the formation of a more conjugated product.

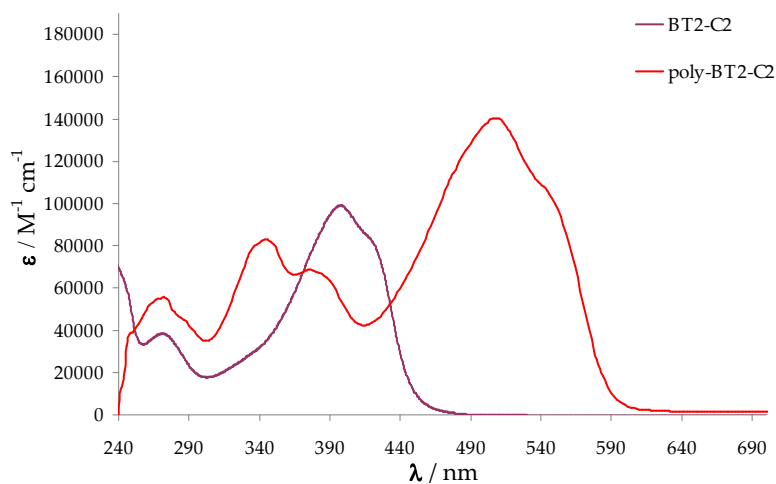
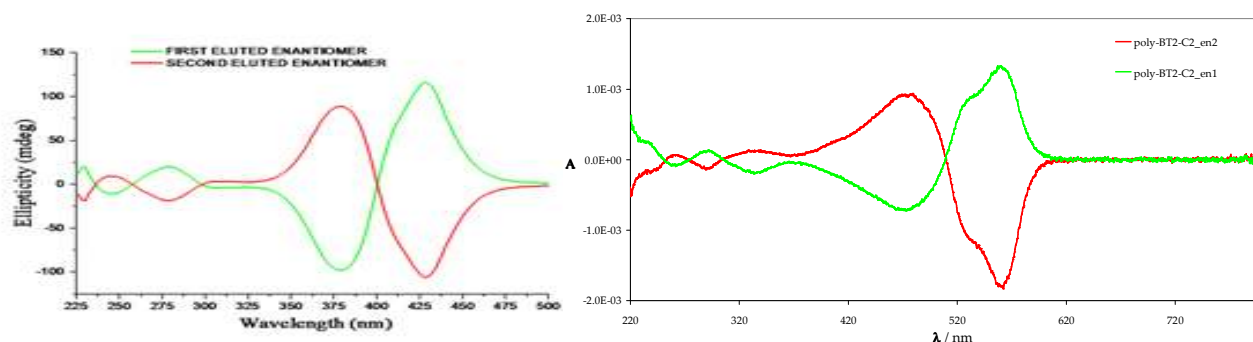


Figure 6: UV-Vis spectra of BT2-C2 and poly-BT2-C2, $5 \cdot 10^{-5}$ M in CH_2Cl_2

This is confirmed also by circular dichroism experiments, which show strong Cotton effects, both for the enantiopure monomers and chemical polymers, that demonstrate that chirality is maintained even for the polymer (as expected, according to design strategy described in the Introduction) and by the measure of the specific rotation, which resulted ten times higher for the polymers than for the monomers.



	<i>monomer</i>	<i>polymer</i>
(+)-BT2-C2	$[\alpha]_{D^{20}} = +883$	$[\alpha]_{D^{20}} = +9956$
(-)-BT2-C2	$[\alpha]_{D^{20}} = -878$	$[\alpha]_{D^{20}} = -9642$

Figure 7: CD spectra of the BT2-C2 enantiomers as monomers (left) and as polymers (right). It is possible to notice the redshift of the signal in the case of poly-BT2-C2. In the Table, the values of the specific rotations are reported.

The polymer, as a racemate, was sent to the group of Prof. L. Torsi at the Università degli Studi di Bari in order to test its performances as a field-effect transistor.

The electrical performance of the polymer was investigated by fabricating the OTFT devices in top contact bottom gate configuration, and then compared with the behaviour of its *leg*, poly-4,4-hexyl-CPTD in the same conditions. The devices were fabricated onto a SiO₂ (300nm)/*n*-doped Si substrate. The polymer was spin coated on the SiO₂/Si substrate and gold electrodes were thermally evaporated on the top using a shadow mask. The first results appear to be promising but still need further investigation.

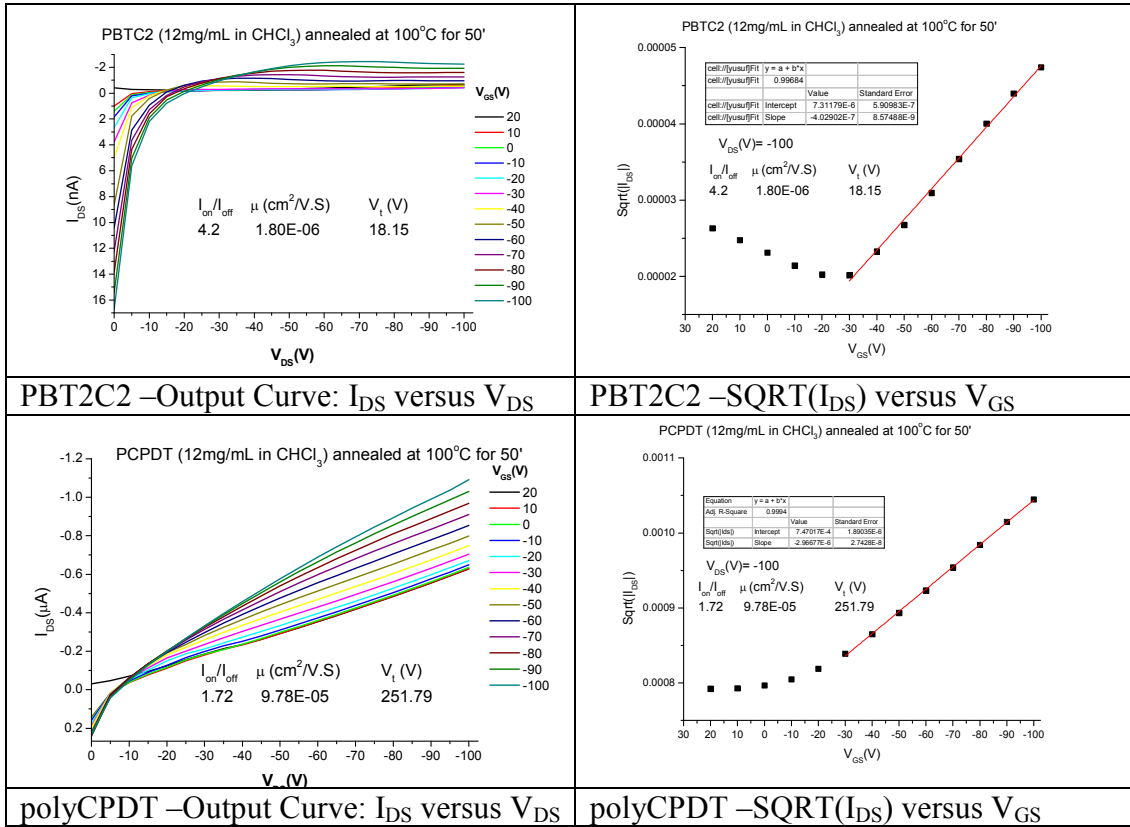
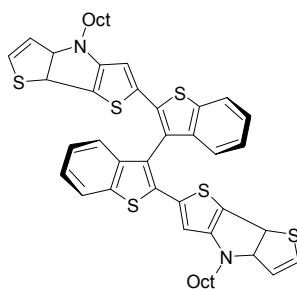


Figure 8: Average values are calculated based on 3 different channels in each device. The channel dimensions are: $W=4\text{mm}$ and $L=200\mu\text{m}$, and $C/A=9\times 10^{-9}\text{F/cm}^2$ is the capacitance per surface of the 300nm SiO_2 dielectric:

	Mobility (μ) ($\text{cm}^2/\text{V.S}$)	Threshold voltage (V_{th}) (V)	I_{on}/I_{off} (@0V)
Poly-BT2C2	$1.49 (\pm 0.28) \times 10^{-6}$	$22.7 (\pm 4.8)$	$3.35 (\pm 0.75)$
Poly-CPDT with Hex chains	$8.56 (\pm 1.10) \times 10^{-5}$	$224.3 (\pm 31.4)$	$1.76 (\pm 0.04)$

BT2-DTP



In this second *inherently chiral* monomer

- the atropisomeric scaffold, 3,3'-bithianaphthene, is maintained, conferring high configurational stability;
- the bithienyl pendants are substituted by dithieno[3,2-*b*:2',3'-*d*]pyrrole DTP units. DTP is a very versatile structure that can be obtained from 3,3'-dibromo-2,2'-bithiophene in one step, by Buchwald-Hartwig reaction with the desired amine. Actually the dithienopyrrole unit is well-known in the literature, as an important building-block for donor-acceptor systems for applications in energetics, optoelectronics and organic photovoltaics⁷⁰.

In our peculiar case the dithienopyrrole unit, being a planar bithienyl system as the cyclopentadithiophene, allows a better delocalization of the charge carriers than the bithiophene units, where free rotation around the 2,2' link is allowed. Moreover, the electronic effects connected to the presence of the pyrrole ring appeared worth to be studied.

- each DTP nitrogen atom is substituted with an *n*-octyl group, added in order to increase the solubility of the resulting polymer, as it was for the *n*-hexyl chains in the case of BT2-C2, albeit each side group, being pyrrole-based, can bear only one alkyl chain instead of two.

On the whole, the benchmark of this *inherently chiral* molecule is still T4-BT2, modified by closing the bithiophene side chains with a nitrogen atom, resulting in a system characterized by a good planarity and strong electron donating ability of nitrogen atoms⁷¹.

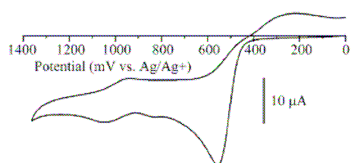


Figure 9: CV of *N*-octyl DTP, from Ref. 56

The electrochemical behaviour of the unit *N*-octyl dithienopyrrole is known in literature⁷². The first oxidation peak potential is at 0.56 V *vs* Ag⁺|Ag in acetonitrile, coherently with our system, where the first oxidation potential is at 0.84 V *vs* SCE in acetonitrile. Thus, the oxidation potential of the *N*-octyl dithienopyrrole does not differ too much from the value of BT2-DTP oxidation. Also in this case, as in the T4-BT2

⁷⁰ X. Hu, M. Shi, L. Zuo, Y. Nan, Y. Liu, L. Fu, H. Chen, *Polymer*, **2011**, 52 (12), 2559

⁷¹ M. M. Shi, D. Deng, L. Chen, J. Ling, L. Fu, X. L. Hu, H. Z. Chen, *J. Polym. Sci., Part A, Polym. Chem.*, **2011**, 49, 6, 1453

⁷² K. Ogawa, S.C. Rasmussen, *J. Org. Chem.*, **2003**, 68, 2921

one, it is possible to observe two nearly equivalent peaks, corresponding to the two active terminal units involved in the electrooxidative process, separated by the central node but still communicating through the conjugated system.

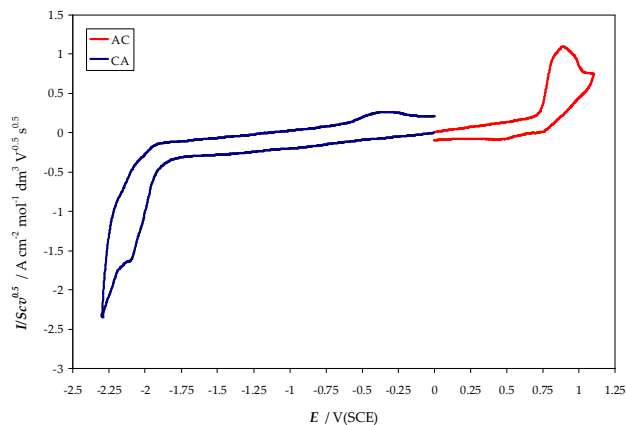


Figure 10: CV features of BT2-DTP, $5 \cdot 10^{-4}$ M in $\text{CH}_3\text{CN} + \text{TBAPF}_6$ 0.1 M, on a GC electrode ($S=0.071 \text{ cm}^2$), potential scan rate 200 mV/s, potentials referred to SCE in double bridge filled with $\text{CH}_3\text{CN} + \text{TBAPF}_6$ 0.1 M

The oxidation potential is strongly anticipated with respect to T4-BT2 because of the presence of *N*-octyl dithienopyrrole groups, electron-richer than the bithiophene groups. BT2-DTP was then compared with BT-DTP, *i.e.*, its *half*, in order to evaluate if the conjugation was effectively maintained through the *node*. From the voltammetric characteristics, it is worthwhile noticing that the value of the potential is almost the same ($E_{p,a} = 0.796 \text{ V vs SCE}$ for BT-DTP, $E_{p,a} = 0.837 \text{ V vs SCE}$ for BT2-DTP), but the shape of the voltammogram becomes the one of a simple monoelectronic peak in BT-DTP ($E_p - E_{p/2} = 0.056 \text{ V}$).

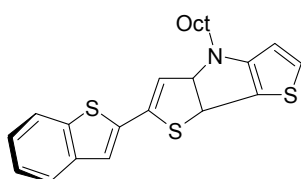


Figure 11: Structure of BT-DTP

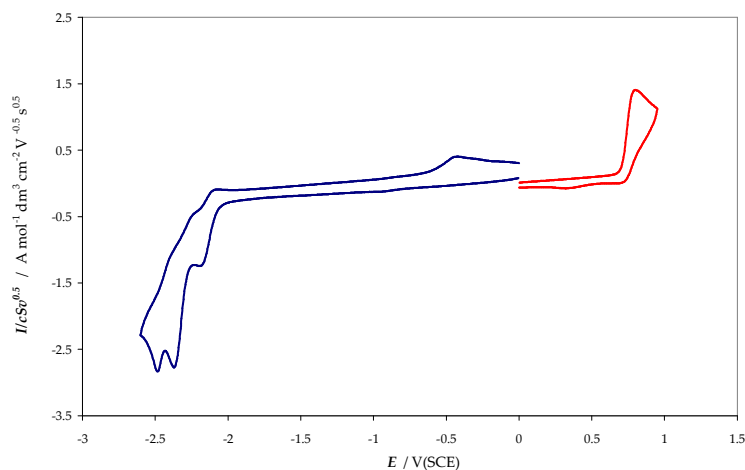


Figure 12: CV features of BT-DTP $5 \cdot 10^{-4}$ M in $\text{CH}_3\text{CN} + \text{TBAPF}_6$ 0.1 M, on a GC electrode ($S=0.071 \text{ cm}^2$), potential scan rate 200 mV/s, potentials referred to SCE in double bridge $\text{CH}_3\text{CN} + \text{TBAPF}_6$ 0.1 M

The UV-Vis spectrum of BT2-DTP, acquired in toluene fluid solution, showed a small but significant bathochromic shift of 10 nm with respect to its *half* BT-DTP (from 370 to 390 nm), confirming the partial communication through the bithiophene 3,3' link.

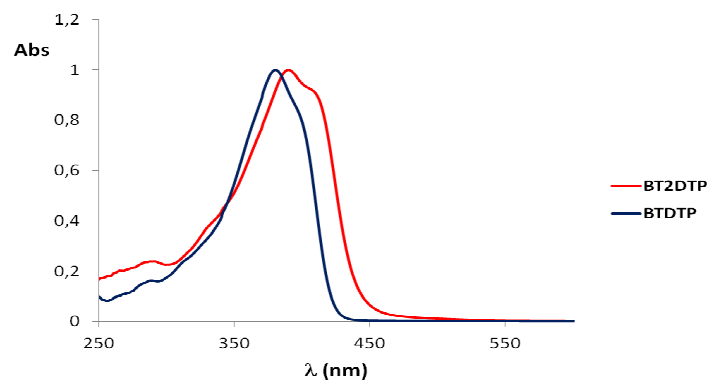


Figure 13: UV-Vis spectra of BT2-DTP and BT-DTP, toluene fluid solution

Concerning the reduction features, the *N*-octyl dithienopyrrole building block does not show any reduction peak in the acetonitrile potential window; in the case of BT-DTP, three peaks can be observed, the first one possibly corresponding to a reduction localized on the benzothiophene core, the other two possibly attributable to follow-up radical reactions. BT2-DTP has one reduction peak at -2.10 V vs SCE; this feature, together with the impressive reversibility of the voltammetric peaks of the polymer, suggests the idea of redox sites localized in parts of the molecule where the charge is well stabilized (*i.e.*, dithienopyrrole and benzothiophene cores), and where follow-up reactions are unlikely. Even the counter-ions dynamics (*i.e.*, income/outcome of the ions from the supporting electrolyte, according to the doping state of the polymer, necessary to ensure the electroneutrality) seems to be an easy and fast process, that suggests the polymer network be very elastic and porous, as also shown by the optical microscope.

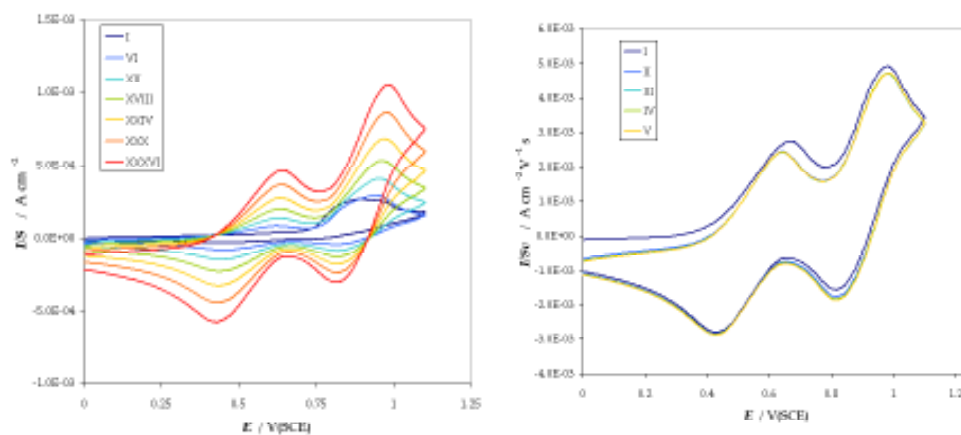


Figure 14: Voltammetric features of BT2-DTP, $5 \cdot 10^{-4}$ M in $\text{CH}_3\text{CN} + \text{TBAPF}_6$ 0.1 M on a GC electrode ($S=0.071 \text{ cm}^2$), $v=200 \text{ mV/s}$: (left) electropolymerization, 36 cycles; (right) its stability test in a monomer-free solution. Potentials referred to SCE in a double bridge filled with $\text{CH}_3\text{CN} + \text{TBAPF}_6$ 0.1 M.



Figure 15: Image at optical microscope of an electrodeposited BT2-DTP film, from a $5 \cdot 10^{-4}$ M monomer solution in $\text{CH}_3\text{CN} + \text{TBAPF}_6$ 0.1 M, on a gold-coated glass slide ($S \sim 1 \text{ cm}^2$), potential scan rate 200 mV/s, potentials referred to Ag/AgCl in double bridge with $\text{CH}_3\text{CN} + \text{TBAPF}_6$ 0.1 M

Furthermore, cycling the potential around the oxidation peaks in a monomer free solution, the film results to be stable, and widening the potential window in cathodic direction, a reduction peak can be observed, with immediate charge release, that supports the hypothesis of the formation of a elastic and porous film that could easily undergo doping/dedoping processes (accompanied by the relative ion dynamics to ensure the electroneutrality), thus suggesting possible applications in the field of batteries.

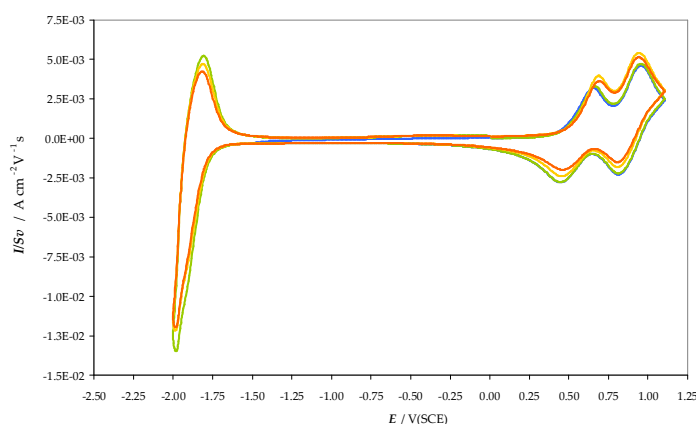


Figure 16: Immediate release of the negative charge acquired by BT2-DTP film when opening the potential window in negative direction; BT2-DTP film deposited in $\text{CH}_3\text{CN} + \text{TBAPF}_6$ 0.1 M, 36 cycles, on a GC electrode ($S=0.071 \text{ cm}^2$), scan rate 200 mV/s, potentials referred to SCE electrode in double bridge $\text{CH}_3\text{CN} + \text{TBAPF}_6$ 0.1 M

This molecule was also characterized by means of electrochemical quartz crystal microbalance, in acetonitrile and TBAPF_6 as supporting electrolyte, on a 10 MHz AT-cut gold-coated quartz crystals. The mechanism of polymerization is still under debate, and does not seem to be so regular as it was thought considering only the voltammograms, since from the EQCM data there seems to be some dissolution of the product at the end of each cycle, especially the first ones, as shown by a slight increase in frequency, and as observed when the quartz crystal was rinsed and put in a monomer-free solution. This phenomenon will be more evident in the case of BT2-DTP-Ph*.

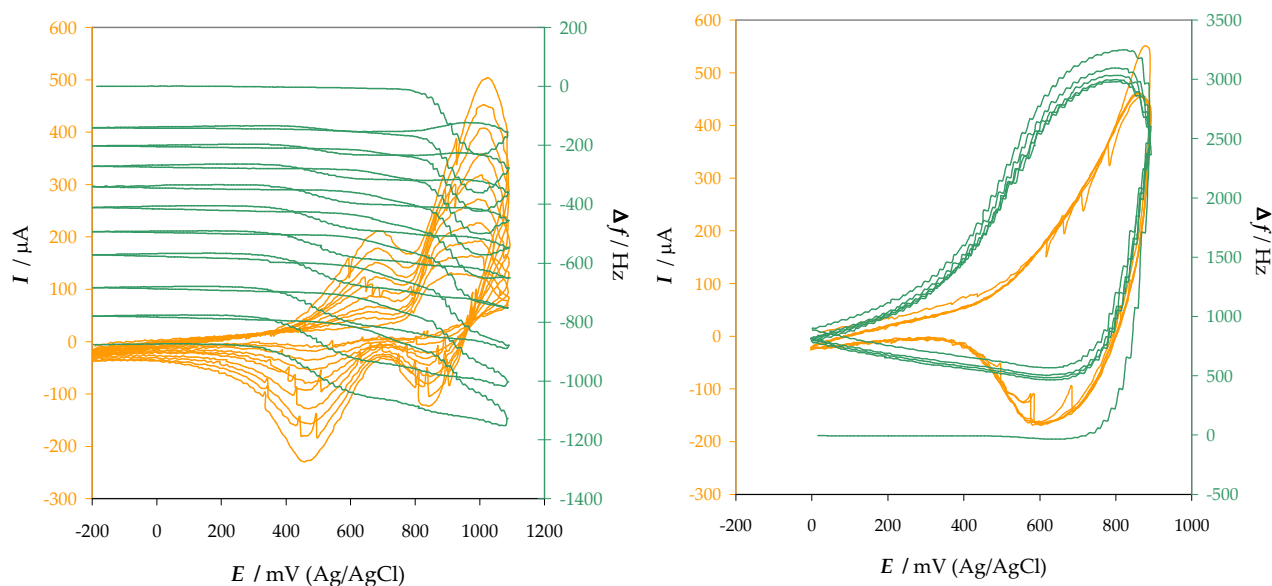


Figure 17: EQCM study of the electropolymerization 10 cycles (left) and stability (right) by cyclic voltammetry of BT2-DTP, $5 \cdot 10^{-4}$ M in $\text{CH}_3\text{CN} + \text{TBAPF}_6$ 0.1 M, on a gold-coated AT-cut quartz crystal, $v = 200$ mV/s, potentials referred to Ag|AgCl.

The enantiopure monomers were obtained by chromatographic separation on a chiral stationary phase, performed by Prof. R. Cirilli from Istituto Superiore di Sanità (Rome).

The impurities were eliminated during the chromatographic process. The chiroptical properties of the enantiomers were evaluated by circular dichroism spectroscopy. The bisignate curves are perfectly specular images; the pattern of this spectrum is similar to the one previously observed for T4-BT2 and BT2-C2, as shown in the Figure 19 below.

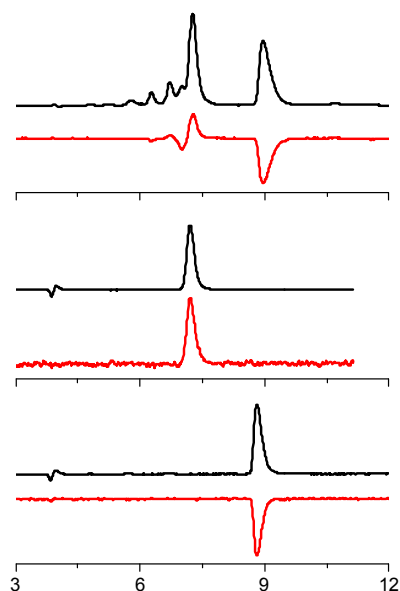


Figure 18: CSP: Chiralpak IA 250 x 4.6 mm I.D.; eluent: n-hexane-dichloromethane-ethanol 100/2/1; flow-rate: 1.0 ml/min; temperature: 40°C; detection: UV (black) and CD (red) at 254 nm.

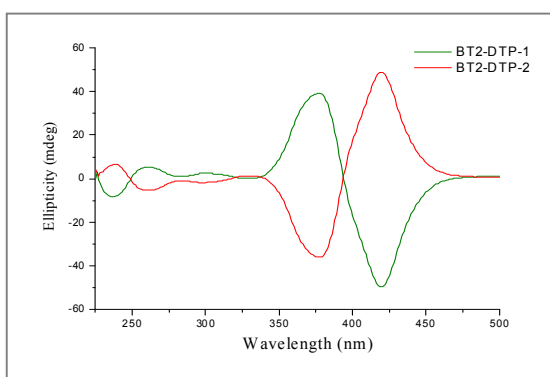


Figure 19: CD spectra of the enantiopure monomers of BT2-DTP, in chloroform.

To understand the polymerization extent, a poly-BT2-DTP was obtained by chemical oxidation with FeCl₃, and the MALDI spectrum revealed that the polymerization process mainly produces dimers, trimers and tetramers, but could proceed up to the hexamers.

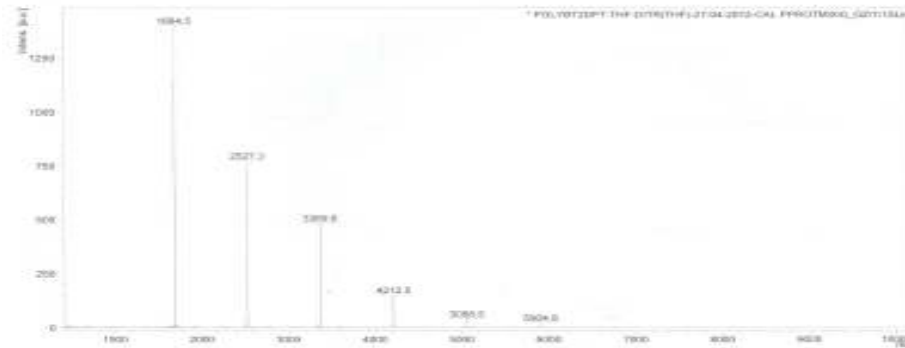
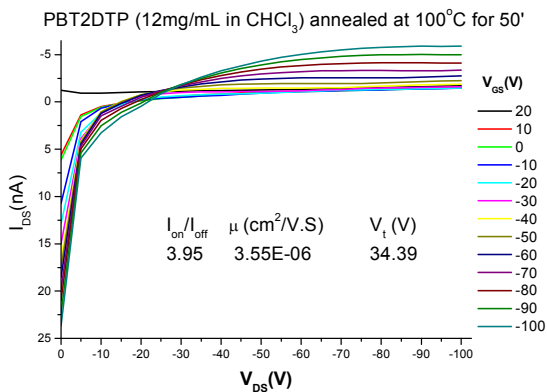


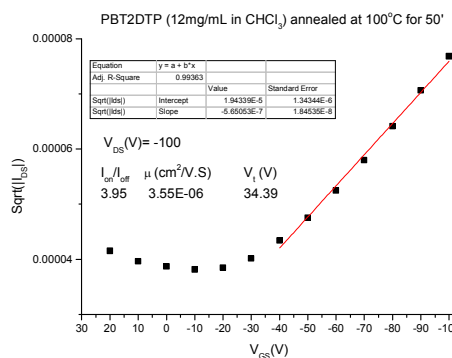
Figure 20: MALDI spectrum of poly-BT2-DTP

The polymer, as a racemate, was sent to the group of Prof. Luisa Torsi at the Università degli Studi di Bari in order to test its performances as a field-effect transistor. The first results appear to be promising but still need further investigations.

The electrical performance of the polymer was investigated by fabricating the OTFT devices in top contact bottom gate configuration. The devices were fabricated onto a SiO₂ (300nm)/*n*-doped Si substrate. The polymer was spin coated on the SiO₂/Si substrate and gold electrodes were thermally evaporated on the top using a shadow mask.



PBT2DTP –Output Curve: I_{DS} versus V_{DS}

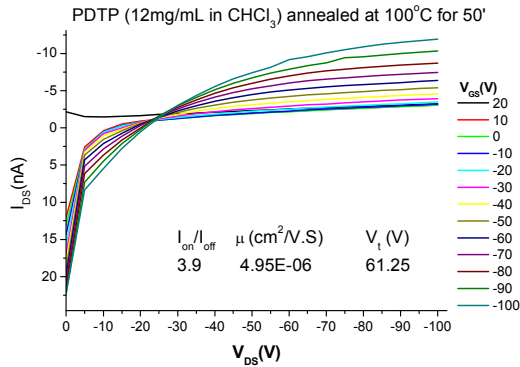


PBT2DTP –SQRT(I_{DS}) versus V_{GS}

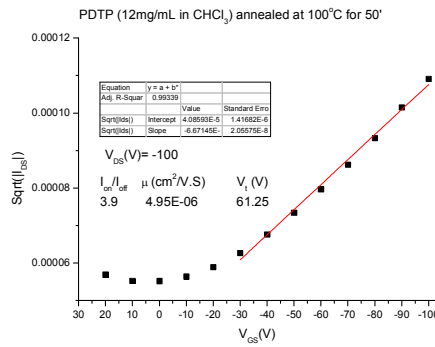
Average values are calculated based on 3 different channels in each device. The channel dimensions are: $W=4\text{mm}$ and $L=200\mu\text{m}$, and $C/A=9 \times 10^{-9} \text{ F/cm}^2$ is the capacitance per surface of the 300nm SiO₂ dielectric.

	Mobility (μ) ($\text{cm}^2/\text{V.S}$)	Threshold voltage (V_{th}) (V)	I_{on}/I_{off} (@ 0V)
<i>Poly-BT2-DTP</i>	$2.94 (\pm 0.54) \times 10^{-6}$	$41.6 (\pm 6.3)$	$3.31 (\pm 0.56)$

These data were then compared also with the electrical performance of the polymer obtained by its *leg*, poly-DTP, investigated by fabricating the OTFT devices in top contact bottom gate configuration, in the same experimental condition as before mentioned.



PDTP –Output Curve: I_{DS} versus V_{DS}

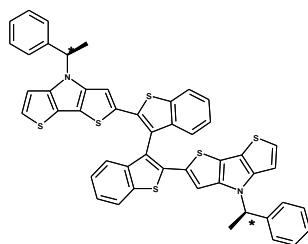


PDTP –SQRT(I_{DS}) versus V_{GS}

Average values are calculated based on 3 different channels in each device. The channel dimensions are: $W=4\text{mm}$ and $L=200\mu\text{m}$, and $C/A=9 \times 10^{-9} \text{ F/cm}^2$ is the capacitance per surface of the 300nm SiO_2 dielectric.

	Mobility (μ) ($\text{cm}^2/\text{V.S}$)	Threshold voltage (V_{th}) (V)	I_{on}/I_{off} (@ 0V)
PDTP	$5.18 (\pm 0.26) \times 10^{-6}$	$59.4 (\pm 1.6)$	$3.93 (\pm 0.05)$

BT2-DTP-Ph*



The design of molecule is derived from the previous BT2-DTP with a different substituent on the nitrogen. In particular, the chiral substituent *R*-phenylethylamine was chosen, its chirality originating from a carbon stereocentre (unlike the inherent chirality of the atropisomeric core). Accordingly, the molecule belongs to the *inherently chiral* monomer family, but unlike the former ones can exist as a mixture of diastereoisomers, on account of the additional carbon stereocentre (in particular, in this case, having used *R*-phenylethylamine, only the two *R,R* and *S,R* diastereoisomers).

This was planned for different purposes:

- having a mixture of diastereoisomers could afford differentiation even in achiral conditions;
- in any case, the isomer separation should be easier;
- the overall chirality should be enhanced, especially in the perspective of building electroanalytical chiral sensors.

The molecule was characterized as racemate, and again showed the expected characteristics of the *inherently chiral* molecules, having two nearly equivalent oxidation peaks, at less positive potentials than the benchmark T4-BT2 on account of the electronrich dithienopyrrole units, corresponding to the α -positions of terminal thiophenes, not completely independent but still communicating through the atropisomeric node.

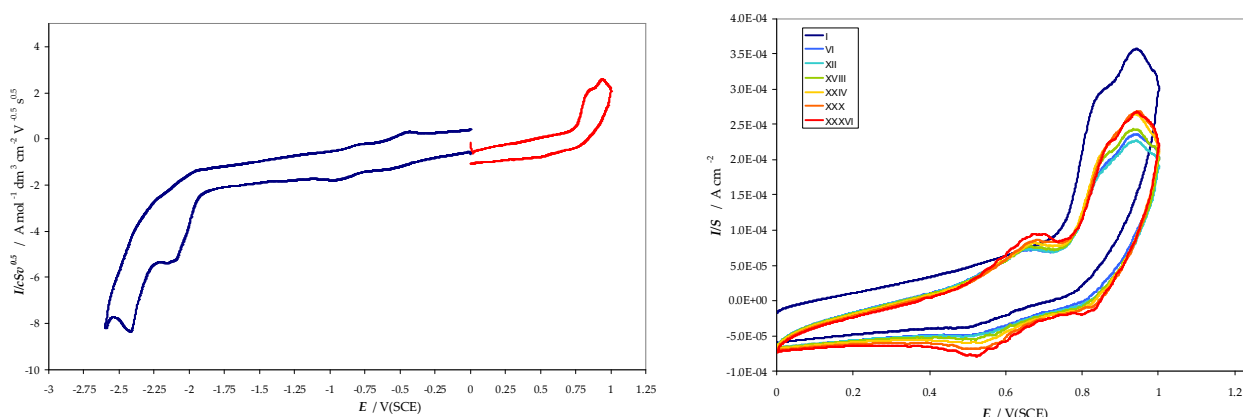


Figure 21: Voltammetric features of BT2-DTP-Ph*, 5·10⁻⁴ M in CH₃CN+TBAPF₆ 0.1 M on a GC electrode (S=0.071 cm²), ν =200 mV/s: (left) monomer characteristics; (right) electropolymerization, 36 cycles. Potentials referred to SCE in a double bridge filled with CH₃CN+TBAPF₆ 0.1 M.

Cycling around the oxidation peaks leads to the formation of a thin electroactive film. This behaviour is confirmed by EQCM analysis, where a significant increase in frequency at the end of each cycle may correspond to some dissolution of product.

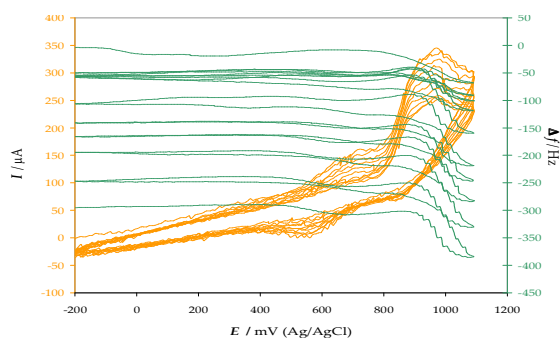


Figure 22: EQCM study of the electropolymerization by cyclic voltammetry of BT2-DT-Ph*, $5 \cdot 10^{-4}$ M in $\text{CH}_3\text{CN} + \text{TBAPF}_6$ 0.1 M, on a gold-coated AT-cut quartz crystal, 10 cycles, $v = 200$ mV/s, potentials referred to Ag|AgCl.

EQCM experiments were performed in acetonitrile and tetrabutylammonium hexafluorophosphate as supporting electrolyte, on a 10 MHz AT-cut gold-coated quartz crystals. The increase in frequency at the end of each cycle may correspond to a different counter-ion dynamics (*i.e.*, outcome of a TBA^+ cation instead of income of a PF_6^- anion) or, probably, to some dissolution of the product as observed when the quartz crystal was rinsed and put in a monomer-free solution. The stability is not excellent: at high scan rate the film seems to be stable and shows a peculiar voltammetric pattern, while at lower scan rate it loses more mass.

The slope of the voltammogram at 50 mV/s could be attributed to a non-perfectly tightened quartz crystal, resulting in additional resistance.

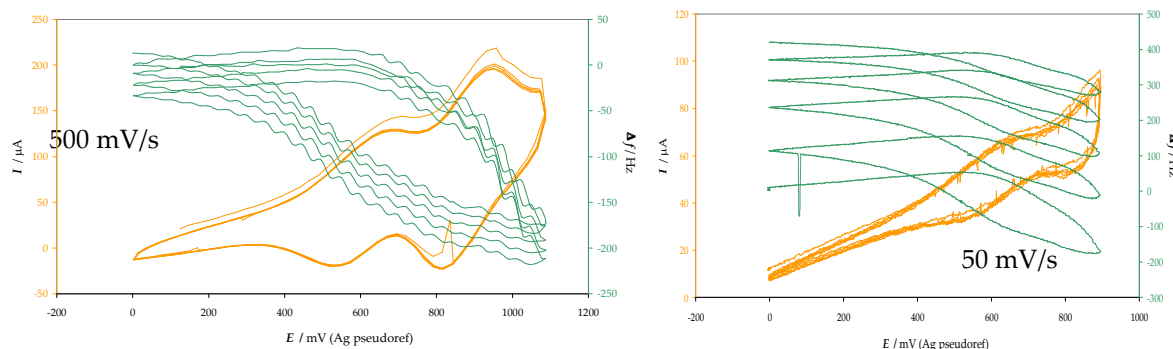


Figure 23: EQCM study of the stability of poly-BT2-DTP-Ph*, $5 \cdot 10^{-4}$ M in $\text{CH}_3\text{CN} + \text{TBAPF}_6$ 0.1 M, on a gold-coated AT-cut quartz crystal, $v = 500$ mV/s (left) or $v = 50$ mV/s (right); potentials referred to Ag|AgCl.

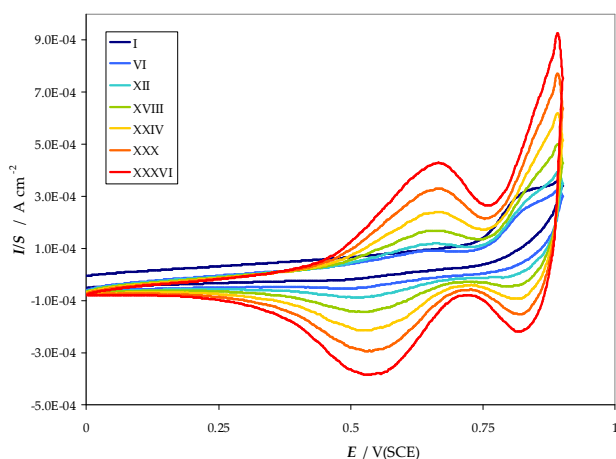

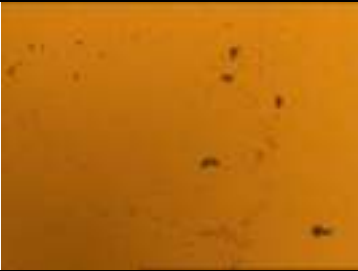
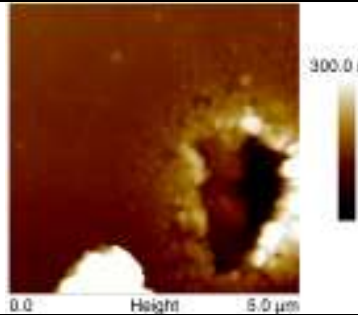
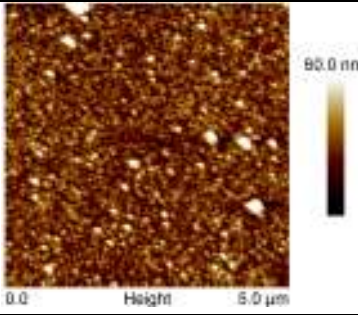
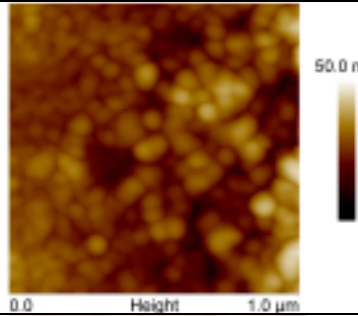
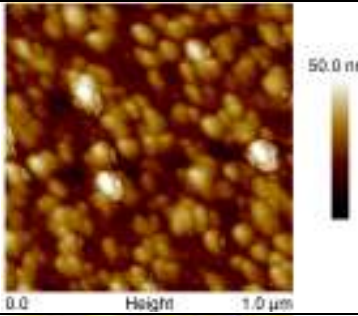
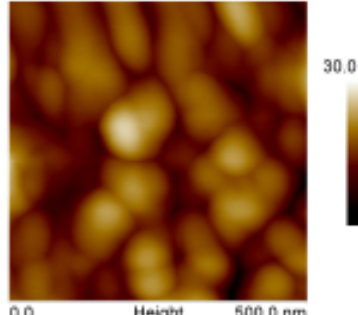
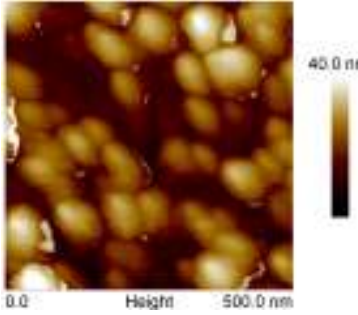


Figure 24: Electropolymerization of BT2-DTP-Ph*, 36 cycles, $5 \cdot 10^{-4}$ M in $\text{CH}_3\text{CN} + \text{TBAPF}_6$ 0.1 M on a GC electrode ($S = 0.071 \text{ cm}^2$), $v = 200$ mV/s, including only the first oxidation peak. Potentials referred to SCE in a double bridge filled with $\text{CH}_3\text{CN} + \text{TBAPF}_6$ 0.1 M.

According to these results, it was tried to perform a polymerization by stopping the potential scan at the first oxidation peak, and a more regular and efficient growth was obtained.

In this frame, the hypothesis of a counter-cation outcome becomes more realistic, since the bulky TBA⁺ ions that are expelled at higher potentials may cause some damage to the polymer network, while stopping at a less positive potential, only the smaller anions may be involved in the process.

Optical microscope and AFM images were then recorded for BT2-DTP-Ph* film deposited in acetonitrile (left) and propylene carbonate (right). It seems that a more viscous solvent favours formation of a more homogeneous film.

Deposition of BT2-DTP_Ph* in...	Acetonitrile + TBAPF ₆	Propylene carbonate + TBAPF ₆
Optical microscope		
AFM 5 μm x 5 μm		
AFM 1 μm x 1 μm		
AFM 500 nm x 500 nm		

A chemical polymer was obtained by oxidation with FeCl_3 , and the MALDI spectra revealed that the polymerization proceeded up to the formation of trimers.

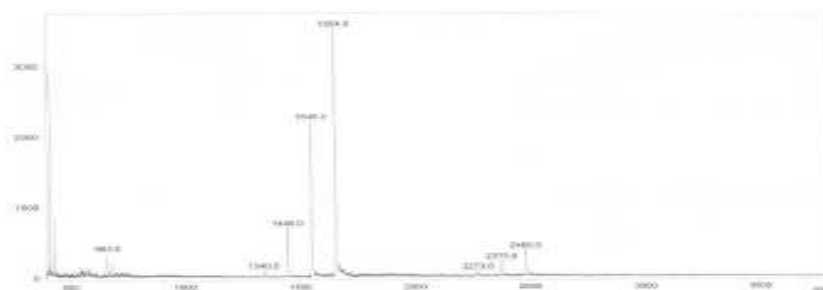
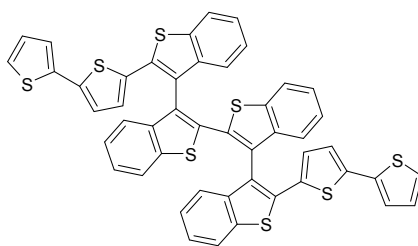


Figure 25: MALDI spectrum of poly-BT2-DTP-Ph* obtained by chemical oxidation with FeCl_3

T4-BT4



T4-BT4 can be considered to be the *double* of T4-BT2, the benchmark of all our *inherently chiral* molecules.

As in the case of BT2-DTP-Ph*, there is another dissymmetry element: however in BT2-DTP-Ph* it was a carbon stereocentre on the nitrogen atom of the dithienopyrrole side chains, while in this case there is a second torsion, also between the benzothiophene scaffolds, so that the molecule exists as two enantiomers plus a mesoform, as shown by the chromatograms registered by using two detectors, a UV-Vis (Figure 26, in black) and a circular dichroism (Figure 26, in orange) one. From these previous results it is evident that the two antipodes are stable (absence of a plateau between the two signals). The circular dichroism spectra show a maximum of intensity at higher wavelength with respect to T4-BT2 (370 nm and 425 nm *vs* 360 nm and 410 nm) on account of its increased effective conjugation.

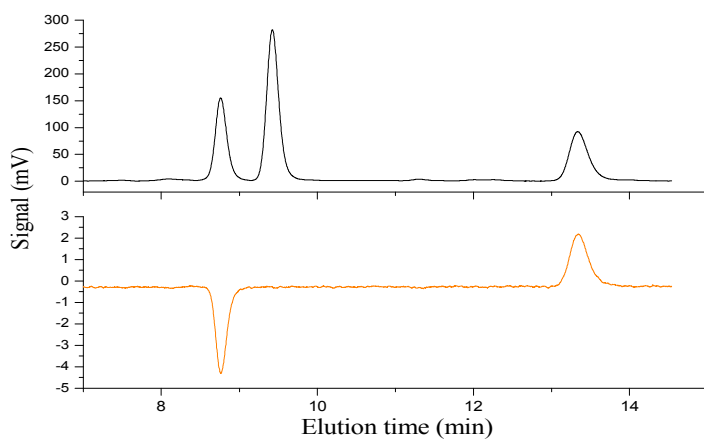


Figure 26: Chromatograms of T4-BT4 separation: the two enantiomers (optically active) and the mesoform can be distinguished

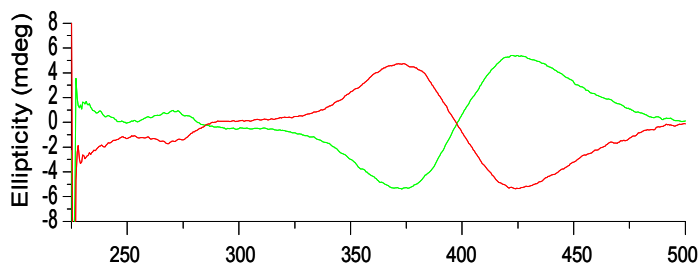


Figure 27: CD spectra of the two T4-BT2 enantiomers, in chloroform

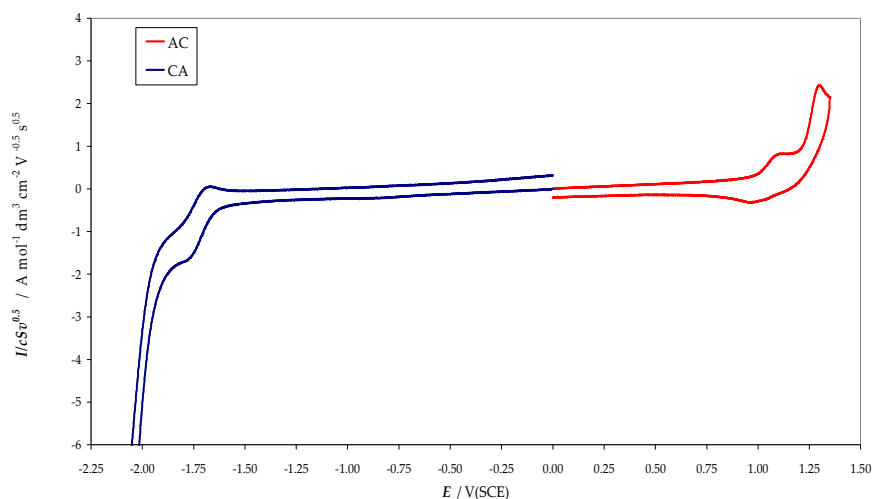


Figure 28: Monomer CV features of T4-BT4 $5 \cdot 10^{-4}$ M in CH_2Cl_2 + TBAP 0.1 M, on a GC electrode ($S=0.071 \text{ cm}^2$), $v= 200 \text{ mV/s}$, potentials referred to SCE.

Cyclic voltammetry shows, in this case, two separate oxidation peaks, the first one possibly corresponding to a radical cation localized in the core of the molecule, while the second one corresponding to the oxidation of the α -position of the terminal thiophenes.

In fact, cycling around the first oxidation peak, which is partially reversible, does not lead to the deposition of any polymer film, while

including also the second one, it is possible to observe the regular growth of an electroactive film, even if slower than T4-BT2, on account of the greater steric hindrance of T4-BT4.

The obtained polymer is stable upon repeated potential scan cycles in a monomer-free solution and shows a significant *charge trapping* effect when opening the potential window in the negative direction.

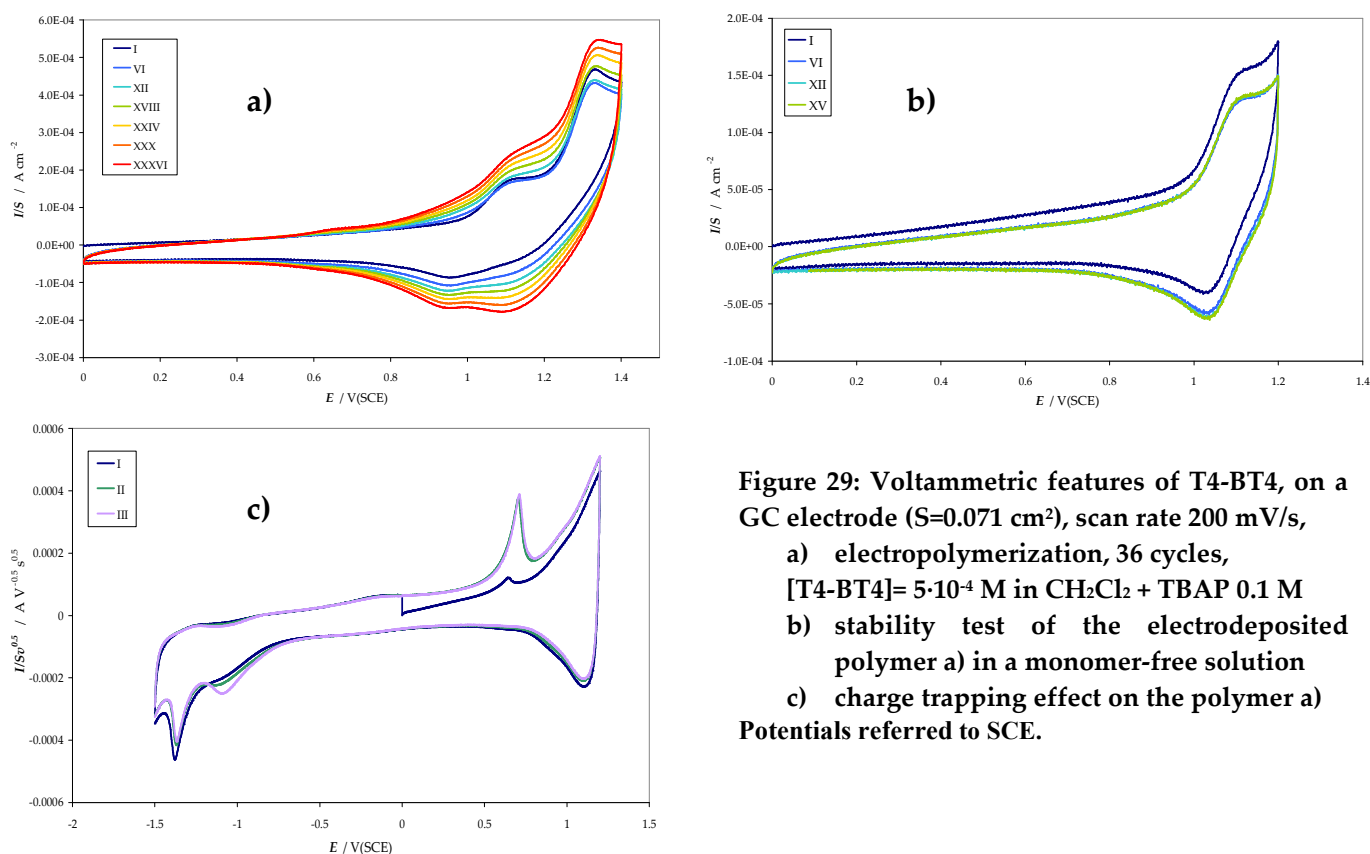


Figure 29: Voltammetric features of T4-BT4, on a GC electrode ($S=0.071 \text{ cm}^2$), scan rate 200 mV/s , a) electropolymerization, 36 cycles, $[\text{T4-BT4}] = 5 \cdot 10^{-4} \text{ M}$ in CH_2Cl_2 + TBAP 0.1 M b) stability test of the electrodeposited polymer a) in a monomer-free solution c) charge trapping effect on the polymer a) Potentials referred to SCE.

4. Conclusions

*If we shadows have offended,
Think but this, and all is mended,
That you have but slumber'd here
While these visions did appear.
And this weak and idle theme,
No more yielding but a dream,
Gentles, do not reprehend:
if you pardon, we will mend:*

*And, as I am an honest Puck,
If we have unearned luck
Now to 'scape the serpent's tongue,
We will make amends ere long;
Else the Puck a liar call;
So, good night unto you all.
Give me your hands, if we be friends,
And Robin shall restore amends.*

William Shakespeare, *A Midsummer Night's Dream*, Act V, Scene I

The present PhD work has been devoted to the extensive application of electrochemistry, as such and in synergy with a series of advanced techniques (EIS, EQCM, *in situ* ESR- and CD- spectroelectrochemistry, AFM and SEM imaging), for the optimized, target-oriented development of two classes of innovative thiophene-based molecular materials, *i.e.*:

- *genetically modified spider-like oligothiophenes* and related conducting polymers, and
- *inherently chiral thiophene-based monomers* and related conducting polymers.

In both classes the exhaustive characterization of electron properties and their rationalization as a function of molecular structure provided important criteria and guidelines for target-oriented molecular design, minimization of the synthetic efforts, and proper selection of the most suitable applications (actually many of the investigated materials can be regarded as multipurpose) in the energy, optoelectronic, and sensor fields.

Genetically modified spider like oligothiophenes can be regarded as an evolution from the previously studied series of all-thiophene spider-like oligomers, aiming to obtain a much smaller energy gap (mainly to improve light harvesting) as a consequence of asymmetric modification of the HOMO and LUMO relative levels by insertion of a suitable non-thiophene core (of which a whole series was characterized), among oligothiophene legs (of which different architectures were compared). The whole class proved to comply with the energy requirements for application in bulk-heterojunction solar cells. The best results were achieved with the cyclopentadithiophenone (CPDT-one) core, affording a remarkably electron poor redox site (and therefore a very small HOMO LUMO gap) together with a conjugated α -linked main thiophene backbone without solution of continuity and of high planarity, involving the two thiophene groups in the CPDT core. An attractive limiting case in this class was the dyad obtained by inserting a fluorene core conjugated to a fullerene group (currently used as electron acceptor in the bulk-heterojunction technology) between branched alkylated oligothiophene wings affording high solubility and processability. On the very efficient CPDT unit, modified with a carboxyl function instead than a carbonyl one, an attractive side study was also pivoted,

resulting in a “charm bracelet/repeating dyad” structure with a conjugated poly-CPDT backbone (on which the HOMO is delocalized) connected, but not conjugated, to periodical pendants consisting of dinuclear rhenium complex with luminescent potentialities (on which the LUMO is localized), that will be reported, as a draft manuscript almost ready for publication, in Chapter 5.

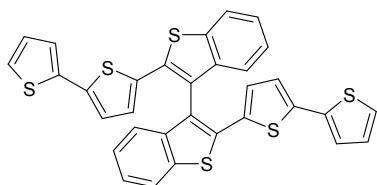


Figure 1: Structure of T4-BT2

The *inherently chiral* thiophene monomer and polymer class is based on the concept of chirality not resulting from "glued" external stereocenters (and therefore of localized character), but intrinsic of the whole conjugated backbone on account of a tailored torsion along it. This class evolved and flourished from the T4-BT2 precursor on which my 5-year degree thesis work was focused, which already showed outstanding polymerization ability and high chirality (being easily and quantitatively separated into very stable enantiomers of high specific rotation, $[\alpha]_{D^{20}} \sim \pm 1000$), entirely retained and even enhanced also after electropolymerization, granting perfectly specular electrode surfaces; *in situ* CD spectroelectrochemistry in the present PhD work showed the chirality of these enantiomer electrode surfaces to be regularly and reversibly modulated by progressively charging/discharging the film (what we termed *breathing chirality*). Molecular structure evolution from T4-BT2 included changes in the atropisomeric scaffold (modulating its electronic properties and polymerization ability) and in the side chains (to improve planarity and solubility and, again, to modulate electronic properties and chirality; it is worthwhile mentioning the paramount $[\alpha]_{D^{20}} \sim \pm 10000$ rotation obtained for poly-BT2-C2); moreover, the addition of a second stereogenic element was also studied, both (a) inserting a "traditional" stereocenter, and (b) inserting a second torsion.

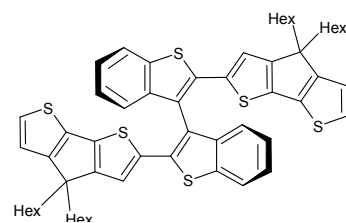


Figure 2: Structure of BT2-C2

Accordingly, both cases yielded diastereoisomers, including, in case (b), a meso form. Concurrently to the structural design evolution a first applicative characterization was started, concerning chiral electrode surfaces with enantio-recognition properties, with promising preliminary results. Also this research line was flanked by an attractive side work focused on a second advanced chirality concept, namely, residual stereoisomerism, in chiral phosphanes and related phosphane oxides with aromatic and heteroaromatic blades; in this case the electrochemical characterization, affording information on the electronic availability of the phosphorus centre, was ancillary to the rationalization of the enantiomer stability.

Acknowledgements



Fondazione Cariplo, project *Inherently Chiral Multifunctional Conducting Polymers*, is gratefully acknowledged for financial support



Nanotechnology, Biomaterials and Alternative
Energy Source for ERA integration
FP7-REGPOT-CT-2011-285949-NOBLESSE



EUROPEAN
UNION

The 7th European Framework Project **Noblesse** *Nanotechnology, Biomaterials and Alternative Energy Source for ERA Integration* is gratefully acknowledged for supporting international exchanges with Prof. Kutner's group, Institute of Physical Chemistry, Polish Academy of Sciences, Warsaw, Poland.

5. Side-works

Electrochromic films of poly-[4H-cyclopenta[3,2-b]dithiophene] charmed with dinuclear Rhenium complexes as smart pendants

Giovanni Rampinini, Elsa Quartapelle Procopio, Monica Panigati,* Valentina Bonometti, Pierluigi Mercandelli, Patrizia Mussini,* Tiziana Benincori, Giuseppe D'Alfonso, Francesco Sannicolò*

Manuscript in preparation, 2012

Introduction

To combine specific recognition properties and electroactivity is a great challenge for modern material research and literature is continuously renewing this area with attractive ideas and smart molecules. A general strategy for designing functional semiconductors involves the association of a conductive polymer backbone to functions responsible for the desired activity. In particular many efforts are devoted to the development of π -conjugated polymers with reversible *p*- and *n*-doping ability and with high stability of the reduced form. Indeed it is well known that the *n*-doping process reduces the stability of the conjugated polymers more than the *p*-doping process. Therefore different groups, having a particular redox behavior can be introduced either as pendants grafted to the electroconductive chain or as constituents of the chain itself.ⁱ

The association of transition metal complexes with the electroactive chain has been widely used in this perspective.^{ii iii iv v vi vii viii ix x xi}. Actually most of the coordinating ligands are redox active and these properties can be modulated by the coordination to the metal centre. Moreover the combination of the redox properties of the ligands with those of the metal can provide a multi-redox hybrid conjugated systems. An incredible number of these new hybrid materials have been prepared endowed with a wide range of tunable electrochemical, photophysical,^{xii} magnetic, or transport properties associated to an ample array of potential uses, like in electrocatalysis, molecular recognition for sensors and biosensors, photoconductivity and molecular electronics; electrochromic materials,^{v,xiii} with colours unique to each metal. Great concern is growing today for the development of applications in the fields of energy conversion and storage.^{ii-ix,xii}

Examples are known of metals hanged by the polymer chain through the coordination to the non-conjugated ligands,^{xiv} while, sometimes, the metal is directly inserted into the conducting skeleton,^{xv} or coordinated to ligands integrated into the skeleton, either devoid of conjugative ability,^{xvi} or conjugatively interacting with the polymer system.^{v,vi,x,xi,xvixviii} Most studies involving polyvinylenes, polyfluorenes, or heterocyclic nitrogen containing polymers are reported, while only few examples are known concerning polythiophenes functionalized with substituents capable of anchoring the metal (usually polypyridines, as ligands for Ru or Pt, and in very few cases Re).^{iii,xi,xix xx xxi xxii xxiii} Regardless of the anchoring method, in many cases, these thiophene systems are difficult to polymerize, or give rise to unstable and poorly defined polymers.^{xxiv}

We report here the results of an investigation on the metallo-polymer thin films obtained by electropolymerization, on different electrodes, of the new dinuclear hydrido-carbonyl rhenium(I) complex $[\text{Re}_2(\mu\text{-H})(\text{CO})_6(\mu\text{-OOC-CPDT})(\mu\text{-3-Me-pydz})]$ (**1**) where 3-Me-pydz indicates 3-methylpyridazine and CPDT the 4H-cyclopenta[2,1-b;3,4-b']dithiophene-4-yl group (Chart 1). To the best of our knowledge there is only another example concerning a metallo-polymer in which the Ru(II) phenanthrolines complexes result hanged to the CPDT backbone.^{xxv}

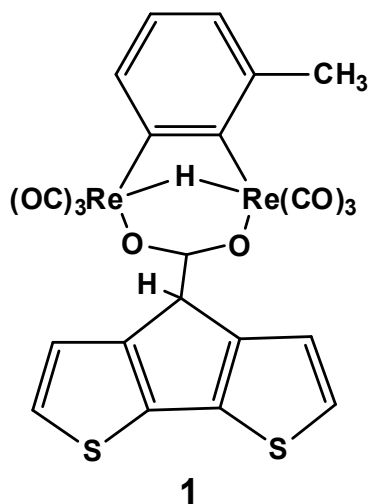


Figure 1 Chemical structure of **1**

The dinuclear rhenium complex belongs to the family of neutral tricarbonyl Re(I) complexes with general formula $[\text{Re}_2(\text{CO})_6(\mu\text{-1,2-diazine})(\mu\text{-X})_2]$, where X can be halogen,^{xxvi} hydride,^{xxvii} alkoxyde or thiophenoxyde.^{xxviii, xxix} Some of them have recently gained interest for their intense yellow/green emission, occurring from triplet metal-to-ligand charge transfer (³MLCT) states,^{xxx} showing the modulation effect of the diazine substituents on energy, lifetimes and quantum yields of the emission. Photoluminescent quantum yields (Φ) up to 0.53 have been measured for the dichloro complexes containing diazines bearing alkyl groups in both the β positions. These properties allowed their successful use as phosphorescent dopants in organic light emitting devices (OLEDs).^{xxxi} However for the bonding with the CPDT unit we have not used the halides derivatives but the much more reactive hydride ones. Indeed, even though, differently from the dichloro derivatives, they are poorly emissive (Φ lower than 1%) these systems can be easily modified and functionalized owing to the reactivity of the hydride centre in particular towards protonation reaction with acidic proton.

Then we have exploited this reactivity to connect the properly functionalized CPDT to the dinuclear rhenium complex with the aim to obtain a monomeric unit already decorated with the organometallic pendant.

The CPDT system was chosen because it is endowed with a very high polymerogenic ability, independently upon the bulkiness of the substituents in position 4, and the resulting polymers are generally highly stable. The resulting monomeric unit **1** was therefore successfully electropolymerized affording an ordered structure in which the hanging Re(I) complexes didn't perturb the electrochemical properties of the poly-CPDT chain, giving a material which has both redox and conductive properties. Moreover, the energy gap of the polymer was expected to be quite low, being the HOMO orbital related

to the poly-CPDT chain and the LUMO orbital essentially localized on the low-lying π^* orbitals of the diazine ligand of the rhenium complexes, expanding the applicative interest for these materials.

Results and Discussion

Synthesis and characterization of the monomer

[omissis]

Photophysical characterization of 1:

[omissis]

Electrochemistry characterization of 1:

Cyclic voltammetry technique was employed to characterize the starting complex/monomer **1**, to oxidatively electropolymerize it, and to characterize the resulting polymer.

The normalized CV pattern of monomer **1**, recorded in MeCN with 0.1 M TBABF₄ as supporting electrolyte, is reported in Figure 2. For comparison, the CV patterns of the corresponding free ligand CPDT-COOH are also reported, as well as that of the analogous dinuclear rhenium complex **1'** containing the same 3-Me-pyridazine chromophore and two chloride anions as ancillary bridging ligands.^{xxvi} The peak and the onset potentials, together with the related HOMO and LUMO energies are collected in Table 1.

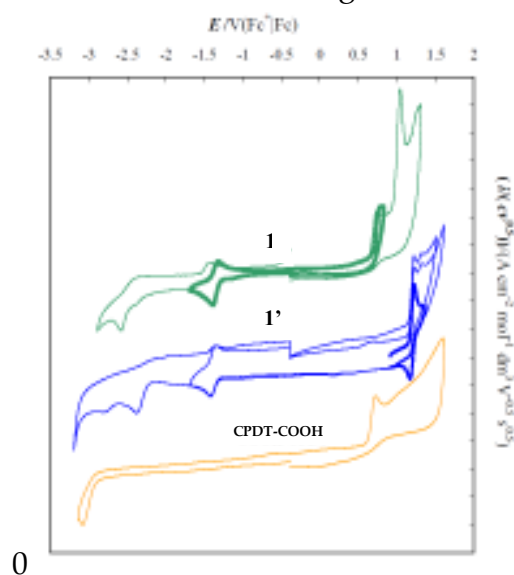


Figure 2: Normalized CV patterns, recorded at 0.2 V s⁻¹ in MeCN + 0.1 M *n*Bu₄BF₄ medium, for complex **1**, for the free ligand CPDT-COOH and for the corresponding complex **1'** having chloride bridging ligands.^{xxvi}

The first oxidation peak of **1** at +0.68 V vs Fc⁺|Fc (chemically irreversible) can be assigned, by comparison with the CV shown by CPDT-COOH, to the formation of a radical cation on the α -position of the thiophene rings, with subsequent fast coupling and oligomerization. The second oxidation peak at +1.05 V vs Fc⁺|Fc, corresponds to the oxidation of the binuclear Re core, by comparison with the behavior of the model complex **1'**. The slight difference of the oxidation potentials between **1** and **1'** is due to the electron-

withdrawing capability of the bridging chlorides making the Re core of complex **1'** significantly electron poorer than that in complex **1**.

On the other hand, the first reduction peak of **1**, located at -1.39 V (Fc⁺|Fc), is nearly coincident with that of **1'**, both in position and in shape, pointing to a monoelectronic, electrochemically and chemically reversible electron transfer centred on the pyridazine ring. This assignment is confirmed by comparison with the electrochemical behaviour of some related dinuclear pyridazine complexes.^{xxix}

Therefore, the CV features of **1** are fully consistent with those shown by its building block molecules, suggesting that there is no direct conjugation between the two interconnected aromatic systems, namely the pyridazine ring and the CPDT moiety. Moreover it is interesting to note that, even if the HOMO level is localized on the CPDT unit, and the LUMO consists essentially in the π^* orbitals of the pyridazine ligand,^{xxvi} no HOMO-LUMO transition can be stimulated by UV-vis absorption. Indeed the lowest energy absorption band involves only the organometallic moiety.

Table 1. Oxidation and reduction peaks and onset potentials, referred to the Fc⁺|Fc couple, and related HOMO and LUMO values, for monomer **1** together with reference molecules **1'** and CPDT-COOH.

	First reduction peak / V (Fc ⁺ Fc)		First oxidation peak / V (Fc ⁺ Fc)		onset criterion			maxima criterion		
	max	onset	onset	max	LUMO /eV	HOMO /eV	E _g /eV	LUMO /eV	HOMO /eV	E _g /eV
CPDT-COOH	-3.07	-2.48	0.62	0.71	-2.32	-5.42	3.10	-1.73	-5.51	3.78
1'	-1.35	-1.23	1.24	1.32	-3.569	-6.04	2.47	-3.46	-6.12	2.66
1	-1.39	-1.29	0.68	0.78	-3.513	-5.48	1.97	-3.41	-5.58	2.17

Electropolymerization:

Very fast and regular oxidative electropolymerization of monomer **1** was achieved by repeated potential cycling between -0.39 and +0.96 V vs Fc⁺|Fc, in acetonitrile (MeCN), with different supporting electrolytes, on Pt, GC, Au and ITO electrodes. Sequential cyclic voltammograms of **1** (Figure 3a), give evidence that the polymer films remain highly electroactive during the polymerization process: indeed oxidative and reductive peak currents regularly grow with no apparent threshold even after 60 cycles. Moreover, the oxidation peak of the monomer **1**, at about 0.68 V vs Fc⁺|Fc, is always present, in agreement with the good conductivity (both electronic and ionic) shown by the polymer.

The sequential cyclic voltammograms of free CPDT-COOH, recorded under similar conditions (Figure 3b), show that the two monomers have a comparable polymerization ability (considering that the concentration of **1** is one half the concentration of CPDT-COOH). Therefore, the connection of the CPDT moiety to the metal complex does not significantly hamper its oxidative coupling, in spite of the bulkiness of the organometallic fragment. The two polymerization patterns appear globally similar (which is reasonable, considering that polymerization involves the same α -positions available in the CPDT unit

comparable in charge at the lowest scan rates, while upon increasing the scan rate, the decrease and the shift to more positive potentials of the first wave, which gradually merges into the second one, is observed (Figures 4a and 4b). This behavior should be indicative of the π -dimerization of the polarons, which affords to a spineless bipolaronic species, stabilized with respect to the two separated polarons. Therefore the further oxidation of the "dimerized polarons" is much more difficult than the oxidation of a single polaron. Moreover the potential separation between the two oxidation peaks is indicative of the stabilization of the π -dimer.^{xxxiii}

These two steps are much more unlighted if we analyzed the CV pattern at different scan rate. The first oxidation peak is clearly observed at low scan rates, indicating that this process is thermodynamically favoured but kinetically hindered due to the difficult exchange of the counterion/solvent between the solution and the coated electrode. This feature is probably due to the fact that the conformational changes required for the neutral-to-polaronic transition and for the formation of the π -dimers, are kinetically slow. This is also confirmed by the analysis of peak currents I , which are linear with v , as expected for surface-controlled charge transfers, in the 0.005 to 0.05 V s⁻¹ interval only, after which they tend to flatten pointing to some kinetic limitation.

Instead the second oxidation peak prevails with increasing the scan rate, suggesting the involvements of sites higher in energy but much more available for the ions diffusion. Moreover on increasing the scan rate the intensity of the first peak progressively decreases and the second oxidation peaks prevails suggesting that, after removing the stabilization of the dimer, the potential of the two oxidations steps, i.e. the formation of the polaron and the bipolaron, are quite similar and therefore only one redox process, affording to the bipolaronic species, can be observed. It also appears to correspond to a higher number of available reaction sites and it features the canonical I vs v linear range at higher scan rates (from 0.05 to 0.5 V s⁻¹), after which, again, the current tends to flatten pointing to some kinetic limitation.

The regularity of the polymerization can be finely appreciated by in situ the weight of the growing film on gold electrodes with the electrochemical quartz microbalance (EQCM) (Figure 5).

The weight of the forming polymer (monitored from the decrease of the frequency of the quartz oscillator supporting the Au electrode, Figure 5a, lower section) increases with time as a straight line (Figure 5b), with a periodic fine structure corresponding to the ingress/egress of ions and solvent within each cycle. In particular the negative variation observed in the first half-cycle (the oxidative one) and the positive variation observed in the second half-cycle (the reductive one) suggests that, during polymer oxidation, the cation egress occurs, rather than the usually observed anion ingress. It is worth noting that the fine structure observed both in the oxidative and in the reductive half-cycle is consistent with the inclusion of more than one electron transfer process.

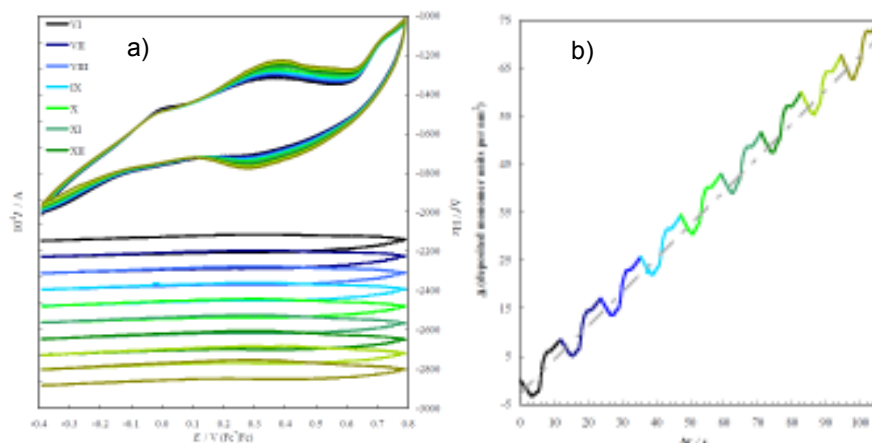


Figure 5. EQCM monitoring (cycles VI-XII) of the electropolymerisation of monomer 1 on Au (0.25 mM in MeCN and 0.1M *n*Bu₄PF₆ at 0.2 V s⁻¹). (a) Upper section, left- hand ordinate: CV curves; (a) Lower section, right-hand ordinate: corresponding frequency changes. (b) Variation with time of the working mass in the same cycles, expressed in monomer units per geometric surface unit.

Charge trapping

After testing the **poly-1** stability at positive potentials, the potential scan range was widened towards more negative values, revealing a broad irreversible reduction peak at -1.4/-1.5 V (Fc⁺|Fc, onset being at -1.1/-1.2 V) (Figure 6). This reduction occurs at the same potential observed for the monomeric unit and therefore the negative charge is confidentially injected on the σ^* orbitals of the diazine units. This means that the lack of electronic communication between the rhenium-diazine moiety and the CPDT unit, observed in the monomer, is maintained affording a polymer film which consists in a linear poly-CPDT conjugated chain regularly decorated with pendant complexes.

This reduction peak is associated to a remarkably delayed sharp return peak of comparable area (i.e. associated charge), appearing just before the first oxidation peak of the neutral polythiophene chain. Restricting the potential scan range to the oxidative region of the polythiophene, this peak progressively disappears after a couple of cycles, to be however completely restored extending again the sweep to cathodic values. The same behavior is observed with different supporting electrolytes and on all the electrode surfaces tested. These features are consistent with a solid-state charge trapping phenomenon, implying that the negative charge, injected at a given cathodic potential, is recovered, at least in part, at much higher potentials in the reverse scan. This property is characteristic for electroactive materials bearing an electron-rich and an electron-poor moiety and different causes could be taken into account for explaining this phenomenon, depending on the molecular structure and the working conditions. Indeed a strong stabilization of the reduced anion species,^{xxxiv} or some conformational changes of the film components^{xxxv} (with concurrent ion and solvent ingress or egress), resulting in a more stable supramolecular structure, or the formation of some isolated microdomains in their reduced form, which are immobile or too dilute to react with the electrode and can undergo electron transfer only by mediation of the polymer backbone^{xxxvi,xxxvii} could explain an oxidation potential much higher than the expected value.

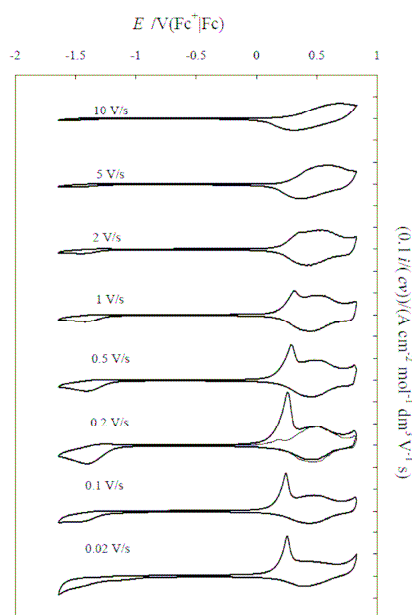


Figure 6. CV cycles including the charge trapping phenomenon, recorded at different scan rates on a film obtained from a 60-cycle electropolymerization of monomer 1 on GC and in MeCN and 0.1 M $n\text{Bu}_4\text{BF}_4$ medium. In the case of 0.2 V s^{-1} scan rate the oxidative cycle of the polymer is also reported as a thinner line, for comparison's sake.

In our case we can exclude some delocalization of the injected charge on the thiophene chain, mainly due to the lack of any π -overlap or conjugative interaction between the diazine moiety and the cyclopentadithiophene backbone, as indicated by the absorption (see above) and electrochemical data. Therefore the charge trapping effect could be reasonably explained by the assumption of a reorganization within the polymer chain, resulting in a more stable supramolecular structure, also mediated by the concurrent ion and solvent ingress or egress and due to the strict regioselectivity of the polymerization process. Actually, such changes could present kinetic barriers to an efficient uptake of these molecules upon reoxidation, leaving some isolated microdomains in the reduced form which could be completely re-oxidized at potentials close to the onset of the poly-CPDT oxidation potential.

The assumption of a supramolecular reorganization within the polymer chain assembly is also supported by the observation that the amount of charge associated with the charge trapping process regularly decreases with increasing the scan rates, pointing to a somehow slow process occurring at the first reduction peak (Figure 6).

The charge trapping effect doesn't modify the structure of the polymer which can be p -doped and n -doped for several times suggesting that the reduction of the pendants prevents the reductions of the polymer chain (usually observed at $-2,3 \text{ V}$ (vs $\text{Fc}^+|\text{Fc}$)^{xxxiiib}) and the further degradation due to the scavenging of acidic cyclopentadienic protons by the reduced polyanions.^{xxxiiib} Moreover if the polymer was maintained in solution the negative charge can be trapped for several hours and therefore quantitatively returned in the anodic scan, restoring the initial conditions.

Electrochemical impedance spectroscopy

The film was also studied in monomer-free solution by comparing its electrochemical impedance at different potentials as representative of different possible states. Figure 7 provides a synopsis of the relevant Nyquist, Bode modulus and Bode phase diagrams.

At -0.79 V vs Fc⁺/Fc **poly-1** (as shown in Figure 4) is in its neutral state, far away from both its oxidation and reduction potentials. Accordingly, it exhibits purely capacitive behaviour (corresponding to a nearly vertical line from high to low frequencies in the Nyquist diagram, and a nearly 90° asymptote in the Bode phase diagram).

At potentials sufficiently positive to allow charge transfer from the polymer to the electrode, the polymer behavior, following the treatment described by Musiani,^{xxxviii} can be rationalized in terms of three subsequent rate determining steps (rds) at increasingly lower frequencies.

Therefore, at more positive potentials than -0.79 V the capacitive straight line is replaced in the Nyquist diagram by half-cycles of decreasing diameter, pointing to decreasing charge transfer resistance. Thus, it can be observed that some electron transfer takes place already at -0.29 V (corresponding to the signal observed in CV at very low potential scan rates, i.e. nearly stationary conditions in Figure 6) although it is kinetically very hindered and possibly corresponding to only a few reaction sites per surface unit ($R \approx 8000 \Omega$). Then, shifting to -0.02 V, the electron transfer becomes easier, the half-circle diameter remarkably decreasing ($R \approx 2300 \Omega$) and a small portion of the Warburg straight line with 45° slope, can be perceived at the lowest frequency. This implies the diffusion of charges within the polymer to be kinetically determining. At 0.27 V the charge transfer resistance is dramatically lower ($R \approx 100 \Omega$); furthermore, the contiguous "diffusive" Warburg section is practically unnoticed, pointing to high conductivity (electronic and ionic) within the polymer. As a consequence, after the small RC semicircle, the system in "charge saturation" state turns into capacitive response with no apparent intermediate diffusive regimen. Finally, at 0.51 V the charge transfer resistance is nearly unperceivable and the system soon reaches the capacitive behavior.

This indicates that the main CV oxidation peak corresponds to extremely facile charge transfer combined with very fast diffusion of both electrons and ions within the polymer.

The decreasing charge transfer resistance is also well recognized

- in the Bode modulus diagram, in terms of horizontal plateaux, providing the R values (with respect to the niveau associated to the electrolyte solution resistance); they get lower and shifts to higher frequencies with increasing potential;
- in the Bode phase diagram, in terms of peaks, again shifting to higher frequencies with increasing potential.

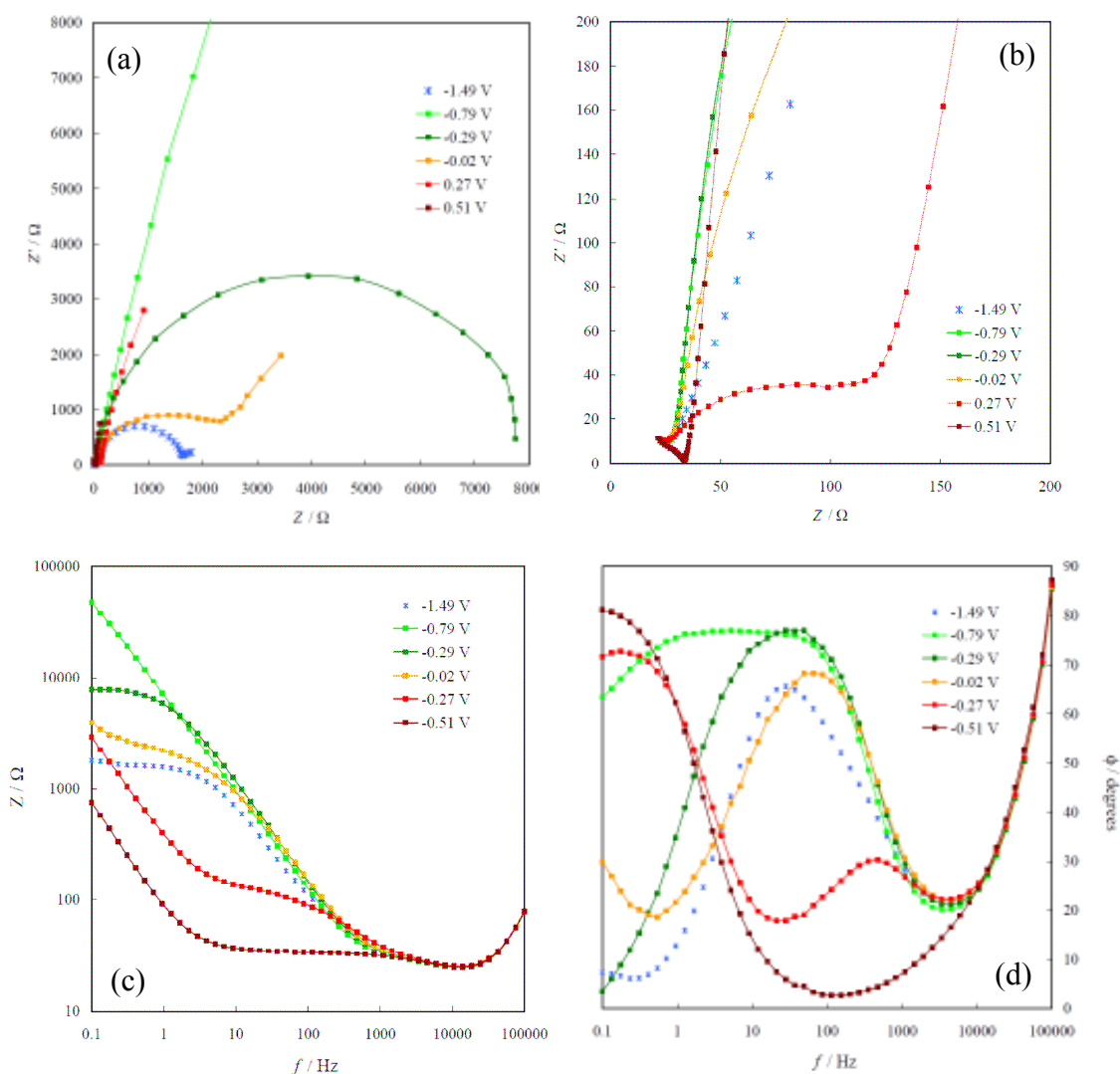


Figure 7. Electrochemical Impedance Spectroscopy (EIS) features of the conducting film obtained by 20-cycle electropolymerization of 0.25 mM monomer 1 on a GC electrode, in MeCN and 0.1 M TBAPF₆ medium, at 0.2 V s⁻¹: (a, b) Nyquist diagrams of the imaginary versus the real components of the impedance Z (focusing on medium and high frequencies, respectively) (c) Bode modulus diagram; (d) Bode phase diagram

On the contrary it is interesting to notice that the impedance recorded at -1.49 V, corresponding to the first reduction peak, is very similar, both qualitatively (RC semicircle followed by the beginning of a Warburg region) and quantitatively ($R \approx 1500 \Omega$) to the one recorded at -0.02 V, corresponding to the onset of the charge trapping peak associated to the reduction one. This suggests that the facile charge transfer could be hampered by the slow diffusion of the ions of the supporting electrolyte within the polymer. However the lack of conjugation between the diazines, which are the isolated sites of the reduction, should be taken into account to explain the observed charge transfer resistance. Indeed we can suppose that the injected electrons can migrate through an hopping process between redox centers without the mediation of the polymer π -electron system. A flow of counterions occurs to compensate the electrical charges in the fixed redox sites. Then the combination of ion and electron motion fix the duality of conduction of our polymer as mixed electronic-ionic conductors whose capacitive behavior is strongly affected to what

extent the solvent or the ions, used to electrostatically compensate the injected charge, really reach the entire bulk of the polymeric film during the doping process, both in reduction and in the oxidation.

Spectroelectrochemistry

The electro-optical properties of the films deposited onto ITO-coated glass electrodes in MeCN solution (0.1 M TBABF₄) have been investigated. At -0.39 V (vs Fc⁺|Fc) the film is neutral. Accordingly, its UV spectrum (Figure 8) shows (almost overlapped) the ¹MLCT transition at 410 nm and the π - π^* transition of the poly-thiophene backbone, at 496 nm. The first band lies at the same energy of the band observed for the monomer **1** (Figure 1), since the diazine ligands are not involved in the polymerization process and are not conjugated to the polymer backbone. On the contrary the band due the π - π^* transition shifts to longer wavelengths, with respect to the corresponding band in monomer **1** and this red-shift increases parallelly with the electropolymerization cycles (from 496 nm for 10 polymerization cycles, as in Figure 12, to 545 nm for 40 cycles), as a consequence of the extension of the π -conjugation.

The increase of the HOMO levels, localized on the thiophene backbone, probably accounts for the lack of emission observed for **poly-1** due to the electron transfer from the backbone to the excited state of the Re-diazine moieties.

The stepwise increase in the electrode potential to 0.36 V makes the absorption band of the polythiophene fragment to slowly disappear and a broad band ascribed to the radical cation emerge at 830 nm, while the ¹MLCT band at 410 nm is still perceivable. This is in agreement with the electrochemical data, indicating that the metal core is not involved in the oxidation of the backbone.

A further increment of the potential to 0.81 V results in a gradual increase of the two absorption bands at 687 and 1050 nm, which could be ascribed to the π -dimer species. Indeed, according to the selection rules the radical cation exhibits two absorption bands (only one in the visible region), while only one is observed for the bipolaron. On the contrary the formation of the π -dimer affords three absorption bands, two of them at higher energy than the corresponding polaronic bands.^{xxxix}

When the potential is settled at negative values, no changes in the UV spectrum of **poly-1** are observed, in agreement with the absence of electronic communication between the thiophene polymer backbone and the redox centres on the pyridazine moieties.

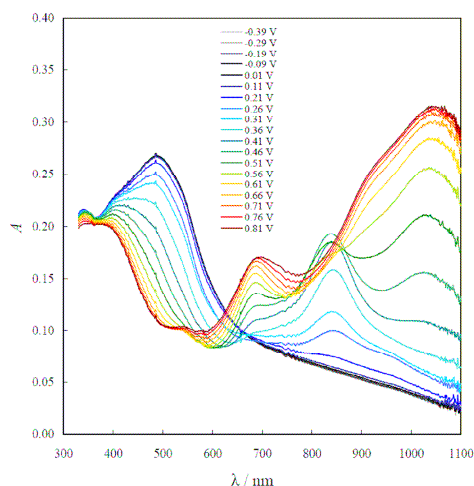


Figure 8. Spectroelectrochemistry of a film (10 polymerization cycles) of poly-1 on ITO-coated glass (MeCN, 0.1 M $n\text{Bu}_4\text{BF}_4$) at applied potentials between -0.39 V and 0.81V (vs $\text{Fc}^+|\text{Fc}$).

Conclusions

A new dinuclear rhenium complex containing a CPDT unit as ancillary ligand is synthesized and characterized by means of UV-vis spectroscopy and cyclic voltammetry. At a molecular level, the spectroscopic and electrochemical properties of both the building blocks, namely the CPDT and the organometallic fragment, are additives, in agreement with the lack of electronic communication in the ground state. In spite of the high steric hindrance of the dinuclear scaffold of the rhenium complex, the electropolymerization of the thiophene easily occurs with high efficiency, on different electrodes, affording a more regular polymer, than that obtained with the un-functionalized CPDT-COOH.

The presence of the electron-withdrawing substituents, electronically isolated from the chain, increases the stability of the conductive polymer also in the reduced state. Moreover the metallo-polymer exhibits high *p*-doping stability, as usual observed for poly-CPDT, and in the same way a very high *n*-doping ability with interesting stability in the reduced form. This remarkable stability in the *n*-doped state is due to the absence of electronic communication also in the polymer film which consists in a linear poly-CPDT conjugated chain regularly decorated with pendant complexes. Moreover the negatively charged carries result firmly trapped and easily removed in the subsequent *p*-doping process with the charge associated to the reduction peak which is comparable to the charge associated to the charge trapping peak. The charge trapping is reversible upon repeated cycling, *e.g.* the polymer network results undamaged by this process and the charge release is observed even if the negatively charged electrode is removed from the solution and stored overnight at room temperature.

The metallo-polymer here presented provide an interesting example of double-cable polymer in which the conductive properties of the π -conjugated system is added to the redox behavior of the pendants isolated complex. Structural features of the polymer, namely a good ordering of the polymer chains imposed by the steric demand of the rhenium fragment, result in highest mixed-valence conductivities so far reported for a polymer with pendant redox groups.

- ⁱ C. Arbizzani, M. Mastragostino, *Curr. Trends Polym. Sci.* 1997, 2, 217; b) M. D. Levi, A. S. Fisyuk, R. Demadrille, E. Markevich, Y. Gofer, D. Aurbach, A. Pron, *Chem. Commun.* 2006, 3299.
- ⁱⁱ S. J. Higgins, *Chem. Soc. Rev.* 1997, 26, 247, and references therein. (b) T Hirao “Conjugated systems composed of transition metals and redox-active pi-conjugated ligands” *Coord. Chem. Rev.* 2002, 226, 81
- ⁱⁱⁱ S. Zhu, P. J. Carroll T. M. Swager, *J. Am. Chem. Soc.* 1996, 118, 8713.
- ^{iv} B. Wang, M. R. Wasielewski, *J. Am. Chem. Soc.* 1996, 119, 12.
- ^v J. L. Reddinger, J. R. Reynolds, *Macromolecules* 1997, 30, 673; J. L. Reddinger, J. R. Reynolds, *Chem. Mater.* 1998, 10, 1236.
- ^{vi} T. Yamamoto, Y. Yoneda, T. Maruyama, *J. Chem. Soc. Chem. Commun.* 1992, 1652; T. Yamamoto, T. Maruyama, Z. Zhou, T. Ito, T. Fukuda, Y. Yoneda, F. Begum, T. Ikeda, S. Sasaki, H. Takezoe, A. Fukuda, K. Kubota, *J. Am. Chem. Soc.* 1994, 116, 4832; T. Maruyama, T. Yamamoto, *Inorg. Chim. Acta* 1995, 238, 9.
- ^{vii} P. G. Pickup, *J. Mater. Chem.* 1999, 9, 1641.
- ^{viii} N. Hayashida, T. Yamamoto, *Bull. Chem. Soc. Jpn.* 1999, 72, 1153.
- ^{ix} G. Zotti, S. Zecchin, G. Schiavon, A. Berlin, G. Pagani, A. Canavesi, *Chem. Mater.* 1995, 7, 2309.
- ^x C. G. Cameron, P. G. Pickup, *Chem. Commun.* 1997, 303; C. G. Cameron, P. G. Pickup, *J. Am. Chem. Soc.* 1999, 121, 11773
- ^{xi} S. S. Zhu, T. M. Swager, *J. Am. Chem. Soc.* 1997, 119, 12568; R. P. Kingsborough, T. M. Swager, *Adv. Mater.* 1998, 10, 1100
- ^{xii} W. K. Chan, *Coord. Chem. Rev.*, 251, 2007, 2104-2118;
- ^{xiii} see *Electrochim. Acta* 1999, 44 (special issue devoted to electrochromic materials)
- ^{xiv} S. J. Higgins, *Chem. Soc. Rev.*, 1997, 26, 247; M. Schmittel, H. Lin, *J. Mater. Chem.* 2008, 18, 333.
- ^{xv} P. T. Wu, T. Bull, F. S. Kim, C. K. Luscombe, S. A. Jenekhe, *Macromolecules* 2009, 42, 671.
- ^{xvi} L. Trouillet, A. De Nicola, S. Guillerez, *Chem. Mater.* 2000, 12, 1611.
- ^{xvii} C. Mangeney, J. C. Lacroix, K. I. Chane-Ching, M. Jouini, F. Villain, S. Ammar, N. Jouini, P. C. Lacaze, *Chem. Eur. J.* 2001, 7, 5029.
- ^{xviii}, M. O. Wolf “Transition-metal-polythiophene hybrid materials” *Adv. Mater.* 2001, 13, 545.
- ^{xix} S. S. Zhu, T. M. Swager, *Adv. Mater.* 1996, 8, 497;
- ^{xx} R. Mirzaei, D. Parker, H. S. Munro, *Synth. Met.* 1989, 30, 263.
- ^{xxi} J. Wang, F. R. Keene, *J. Electroanal. Chem.* 1996, 405, 71.
- ^{xxii} J. Crayston, A. Iraqi, J. J. Morrison, J. C. Walton, *Synth. Met.* 1997, 84, 441
- ^{xxiii} I. H. Jenkins, N. G. Rees, P. G. Pickup, *Chem. Mater.* 1997, 10, 1589; J. Papillon, E. Schulz, S. Ge’linas, J. Lessard, M. Lemaire, *Synth. Met.* 1998, 96, 155;; S. S. Zu, R. P. Kingsborough, T. M. Swager, *J. Mater. Chem.* 1999, 9, 2123.
- ^{xxiv} B. Jousset, P. Blanchard, M. Oçafraïn, M. Allain, E. Levillaina, J. Roncali, *J. Mater. Chem.*, 2004, 14, 421.
- ^{xxv} M. Schmittel, H. Lin, *J. Mater. Chem.* 2008, 18, 333-343
- ^{xxvi} D. Donghi, G. D’Alfonso, M. Mauro, M. Panigati, P. Mercandelli, A. Sironi, P. Mussini, L. D’Alfonso, *Inorg. Chem.* 47 (2008) 4243
- ^{xxvii} M. Panigati, D. Donghi, G. D’Alfonso, P. Mercandelli, A. Sironi, L. D’Alfonso, *Inorg. Chem.* 45 (2006) 10909.
- ^{xxviii} A. Raimondi, M. Panigati, D. Maggioni, L. D’Alfonso, P. Mercandelli, P. Mussini, G. D’Alfonso, *Inorg. Chem.*, 2012
- ^{xxix} M. Panigati, M. Mauro, D. Donghi, P. Mercandelli, P. Mussini, L. De Cola, G. D’Alfonso, *Coord. Chem. Rev.* 2012, **256**, 1621-1643.
- ^{xxx} M. Mauro, E. Quartapelle Procopio, Y. Sun, C.-H. Chien, D. Donghi, M. Panigati, P. Mercandelli, P. Mussini, G. D’Alfonso, L. De Cola, *Adv. Funct. Mater.* 19 (2009) 2607.
- ^{xxxi} M. Mauro, C.-H. Yang, C.-Y. Shin, M. Panigati, C.-H. Chang, G. D’Alfonso, L. De Cola, *Adv. Mater.* 2012,
- ^{xxxii} a) G. Zotti, A. Berlin, G. Pagani, G. Schiavon, S. Zecchin, *Adv. Mater.* 1995, 7, 48-52; b) G. Zotti, G. Schiavon, A. Berlin, G. Fontana, G. Pagani, *Macromolecules*, 1994, 27, 1938-1942; c) N. Camaioni, G. Casalbore-Miceli, G. Beggiano, M. Cristiani, C. Summonte, *Thin Solid Films*, 2000, 366, 211-215.
- ^{xxxiii} a) M.G. Hil, J. F. Penneau, B. Zinger, K. R. Mann, L.L. Miller, *Chem. Mater.* 1992, 4, 1106-xxx; b) Y. Yu, E. Gunic, B. Zinger, L. L. Miller, *J. Am. Chem. Soc.* 1996, 118, 1013-1018; c) M. G. Hill, K. R. Mann, L. L. Miller, J-F. Penneau, *J. Am. Chem. Soc.* 1992, 114, 2728-2730.
- ^{xxxiv} G. Casalbore-Miceli, N. Camaioni, A. Geri, G. Ridolfi, A. Zanelli, M. C. Gallazzi, M. Maggini, T. Bennicori, *J. Electroanal. Chem.* 2007, 603, 227-234, and references therein cited.
- ^{xxxv} G. Zotti, G. Schiavon, S. Zecchin, *Synth. Met.* 1995, 72, 275-281.
- ^{xxxvi} P. Denisevich, K. W. Willmann, R. W. Murray, *J. Am. Chem. Soc.* 1981, 103, 4727-4737.
- ^{xxxvii} P. Denisevich, H.D. Abruna, C. R. Leidner, T. J. Meyer, R. W. Murray, *Inorg. Chem.* 1982, 21, 2153-2161.
- ^{xxxviii} M. Musiani, *Electrochim. Acta* 1990, 35, 1665-1670.
- ^{xxxix} J. Conil, J. L. Brédas, *Adv. Mater.* 1995, 7, 295-297; b) T. Sakai, T. Satou, T. Kaikawa, K. Takimiya, T. Otsubo, Y. Aso, *J. Am. Chem. Soc.* 2005, 127, 8082-8089; c) S. Klod, K. Haubner, E. Jähne, L. Dunsch, *Chem. Sci.* 2010, 1, 743-750.